

Thermally and  
mechanically responsive  
platforms for functional  
polymeric materials

Thesis by  
Brooke Ann Versaw

In Partial Fulfillment of the Requirements for  
the degree of  
Doctor of Philosophy

CALIFORNIA INSTITUTE OF TECHNOLOGY  
Pasadena, California

2023  
(Defended April 24, 2023)

© 2023

Brooke Ann Versaw  
ORCID: 0000-0002-6200-7203

## ACKNOWLEDGEMENTS

This thesis has only one author but reflects the contributions and support of many.

My decision to pursue graduate studies was shaped by my overwhelmingly positive experiences as an undergraduate researcher. Karen Wooley and Craig Hawker were wonderful mentors during my time in their groups—their enthusiasm for polymer science informed and inspired my own. Suma Datta has been a voice of reason and sound professional advice throughout my career. Lastly, I owe a tremendous debt of gratitude to the Arnold and Mabel Beckman Foundation. From the Beckman Scholars Program at Texas A&M to instrumentation and facilities at Caltech, the Beckmans supported my research training from beginning to end.

Caltech, and the division of Chemistry and Chemical Engineering in particular, provided a positive environment for me to grow as a scientist. While Caltech has state-of-the-art research facilities, a beautiful campus, and possibly the largest localized turtle population in the greater Los Angeles area, its greatest asset by far is its people.

I would first like to thank my advisor, Maxwell Robb. I became a more effective chemist and communicator while under his direction. I'm particularly thankful for the relative freedom Max gave me to pursue research questions I was excited to ask and answer. His willingness to find the overlap in our academic interests made my work enjoyable during its many ups and downs.

I also want to thank my committee, Professors Bob Grubbs, Brian Stoltz, Sarah Reisman, and Theo Agapie. They provided feedback and encouragement in equal measures, pushing me to consider my chemistry in depth and in context. Bob's time as my committee chair was cut short with his passing in 2021, but his clever, practical approach to science and thoughtful attitude towards mentorship made lasting impressions. I'm grateful for the chance to learn from him and grateful to Brian for stepping in as my committee chair for the remainder of my degree.

The Division of Chemistry and Chemical Engineering has incredible staff supporting its research and administration. Dave Vander Velde and Mona Shagholi spent considerable time and effort walking me through the most challenging characterization problems I faced in my PhD. Scott Virgil's encyclopedic knowledge of Agilent instruments was indispensable in helping me maintain and repair the Robb group's GPCs. Alison Ross kept the department and the Chemistry Graduate Studies Committee running seamlessly, even during a global health crisis.

Over the last five years, I worked formally or informally with nearly every member of the Robb group and am a better scientist for it—I owe thanks to all of them. I would especially like to acknowledge Ross Barber for improving my efficiency as a synthetic chemist, and the members of my cohort (Anna Overholts, Corey Husic, and Tian Zeng) for making research both easier and a great deal more fun.

I've also benefited from the collective wisdom and collegiality of the Reisman, Stoltz, Grubbs, Fu, and Nelson groups. Always willing to lend a chemical or a second pair of eyes to an idea, they created a community that enabled me to grow as a scientist. Thanks especially to Alex Shimozono, Jeff Kerkovius, JK Ko, Ray Turro, and Travis Delano for many, many helpful discussions.

My friends both at Caltech and beyond were a wonderful source of levity throughout my degree. Anna Overholts, Gabby Lessen, Gracie Zhang, Isabel Klein, and Karli Holman deserve special mention for being first-rate scientists and first-rate friends. Samantha Kristufek regularly sent me encouraging notes over two continents, two states, and a new professor's schedule. Lastly, my fellow Texpats—Caitlin Lacker, Emily Miaou, and Sara Dibrell—made Southern California feel like home.

My family's unfailing love and support has been a constant throughout my life, and graduate school was no exception. My parents, Wayne and Lori, my brother, Miles, and the entire extended Gann and Miller families kept my life balanced. Even when I questioned the trajectory of my career, I never doubted that I was loved.

My last and most important acknowledgement is for my fiancé, Nathan Coonrod. Your support of my career means more than I could possibly describe. You are the first person I want to commiserate with when an experiment goes badly, and the first person I want to celebrate with when an experiment goes well. I am a better scientist, a better engineer, and a better person by your side.

## ABSTRACT

Connecting a polymer's reactivity or properties to its working environment is a grand challenge in polymer chemistry. Research towards this goal is driven both by a fundamental interest in mimicking nature's ability to create surfaces that adapt to their surroundings and a practical desire to tailor the properties of materials to the wide-ranging contexts where they find use. This thesis investigates the development of polymers that exhibit productive changes in physical properties or chemical reactivity under an applied environmental stimulus.

Section I explores polymers responsive to external force. In Chapter 1, we describe the development of substituted naphthopyran mechanophores that exhibit highly tunable coloration and thermal electrocyclization kinetics following mechanical activation. Structure-mechanochemical activity relationships are first established, then applied to create elastomeric materials capable of complex multicolor or multimodal stress-sensing responses. In Chapter 2, we summarize recent developments in the rapidly growing research area of mechanically triggered molecular release. We highlight advances in both specialized and general mechanophore platforms for mechanically triggered release, introduce potential applications, and outline the knowledge gaps that will define the future of this emerging field.

In Section II, we focus on polymers responsive to applied heat. Chapter 3 examines the use of masked furfuryl esters as thermally latent protecting groups for carboxylic acid-functionalized polymers. Judiciously designed masked furfuryl esters were incorporated into poly(methyl acrylate)s as functional initiators or comonomers. Subsequent thermal deprotection proceeded efficiently to afford  $\alpha,\omega$ -telechelic poly(methyl acrylate) and poly(methyl acrylate-*co*-acrylic acid). The relatively mild conditions required for post-polymerization modification are particularly appealing for systems that contain other labile groups and will improve the synthetic accessibility of these functional materials.

## PUBLISHED CONTENT AND CONTRIBUTIONS

1. Versaw, B. A.; McFadden, M. E.; Husic, C. C.; Robb, M. J. Designing naphthopyran mechanophores with tunable mechanochromic behavior. *Chem. Sci.* **2020**, *11*, 4545. <https://doi.org/10.1039/D0SC01359E>  
B.A.V. performed experiments, analyzed data, and wrote the manuscript.
2. Versaw, B. A.; Zeng, T.; Hu, X.; Robb, M. J. Harnessing the Power of Force: Development of Mechanophores for Molecular Release. *J. Am. Chem. Soc.* **2021**, *143*, 21461. <https://doi.org/10.1021/jacs.1c11868>.  
B.A.V. helped write the manuscript.

## TABLE OF CONTENTS

Acknowledgements.....	iii
Abstract .....	vi
Published Content and Contributions.....	vii
Table of Contents.....	viii
Nomenclature.....	ix
<b>Section I: Chemical Probes for Force-responsive Polymers.....</b>	<b>1</b>
Chapter I: Designing Naphthopyran Mechanophores with Tunable Mechanochromic Behavior.....	3
1.1 Introduction .....	4
1.2 Results and Discussion .....	5
1.3 Conclusions .....	14
Chapter II: Harnessing the Power of Force: Development of Mechanophores for Molecular Release .....	16
2.1 Introduction .....	17
2.2 Mechanically Triggered Molecular Release from Specialized Mechanophores.....	21
2.3 Mechanically Gated Reactivity.....	27
2.4 Mechanically Gated Cascade Reactions for Molecular Release.....	30
2.5 Outlook .....	34
<b>Section II: A Functional Platform for Heat-responsive Polymers.....</b>	<b>37</b>
Chapter III: Thermal Unmasking of Latent Furfuryl Esters Accesses Acid-functional Polymers .....	38
3.1 Introduction .....	39
3.2 Results and Discussion .....	40
3.3 Conclusions .....	52
Bibliography .....	53
Appendix A: Supplementary Information for Chapter I .....	65
Appendix B: Supplementary Information for Chapter III.....	130

## NOMENCLATURE

$\alpha$	adjacent to <i>or</i> at the initiating end of a polymer chain
Å	angstrom(s)
<i>anti-</i>	from opposite sides
aq	aqueous
br	broad
°C	degrees Celsius
calc'd	calculated
<i>cis</i>	on the same side
CoGEF	Constrained Geometries simulate External Force
$\Delta$	heat <i>or</i> difference
$\delta$	chemical shift in ppm
Đ	dispersity
d	doublet
DCM	dichloromethane
DFT	density functional theory
DMAP	4-(dimethylamino)pyridine
DMF	<i>N,N</i> -dimethylformamide
e.g.	for example (Latin: <i>exempli gratia</i> )
<i>endo</i>	bridged ring stereoisomer with the substituent <i>syn</i> to the bridge
equiv.	equivalent(s)

ESI	electrospray ionization
<i>et al.</i>	and others (Latin: <i>et alii</i> )
EtOAc	ethyl acetate
FAB	fast atom bombardment
F <sub>max</sub>	maximum force at rupture
g	gram(s)
GPC	gel permeation chromatography
h	hours
H <sub>2</sub> O	water
HPLC	high-performance liquid chromatography
HRMS	high-resolution mass spectrometry
Hz	hertz
i.e.	that is (Latin: <i>id est</i> )
<i>J</i>	coupling constant in Hz
m	multiplet <i>or</i> meter(s)
μ	micro
MALDI	matrix-assisted laser desorption-ionization
Me	methyl
MeCN	acetonitrile
MeOH	methanol
mg	milligram(s)
MHz	megahertz

min	minute(s)
mL	milliliter(s)
$M_n$	number-average molecular weight
mol	mole(s)
$m/z$	mass-to-charge ratio
<i>n</i> -	normal
NMR	nuclear magnetic resonance
<i>o</i> -	<i>ortho</i> -
<i>p</i> -	<i>para</i>
PDMS	poly(dimethyl siloxane)
PMA	poly(methyl acrylate)
q	quartet
quant.	quantitative
$R_f$	retention factor
rt	room temperature
s	singlet <i>or</i> seconds
sat.	saturated
SEC	size-exclusion chromatography
<i>syn</i> -	from the same side
t	triplet <i>or</i> time
<i>t</i> -	<i>tert</i> -
T	temperature

THF	tetrahydrofuran
TLC	thin-layer chromatography
TOF	time-of-flight
<i>trans</i>	on the opposite side
UV	ultraviolet
$\omega$	at the terminating end of a polymer chain
vis	visible (e.g., UV-vis spectroscopy)

## SECTION I

### CHEMICAL PROBES FOR FORCE-RESPONSIVE POLYMERS

Over the last century, polymers have become a >\$500 billion/year industry with inroads in nearly every economic sector, from consumer goods to construction materials.<sup>1</sup> Mechanical properties are a key contributor to this valuation: commodity plastics can be both tough and flexible, both lightweight and durable. Consequently, the mechanical properties of polymers and the effects of applied force on those properties are a longstanding area of research. In the 1930s, Staudinger observed that polymers decrease in molecular weight upon mastication.<sup>2-4</sup> These foundational studies prompted decades of research interest and informed the prevailing understanding that force applied to polymeric materials results in destructive outcomes, from microscopic chain scission to macroscopic failure.

This paradigm has changed in recent years with the emergence of polymer mechanochemistry, a growing field that harnesses the privileged reactivity of force-responsive small molecules termed mechanophores to access selective and productive reactions under mechanical force.<sup>5</sup> In a seminal 2005 study, Moore and coworkers reported site-selective chain scission following ultrasonication of polymers containing a mechanically labile azo group at the chain center.<sup>6</sup> This initial discovery prompted a massive surge in interest, with over 100 mechanophores reported in the years since.<sup>7</sup> Mechanophores have been leveraged to gain fundamental insights into fracture mechanics and advance a wide variety of applications ranging from stress sensing to drug delivery and damage repair. This section of the thesis contributes to that diverse and growing body of knowledge.

In Chapter 1, we establish structure-mechanochemical activity relationships for substituted naphthopyran mechanophores and demonstrate the utility of those relationships in stress-sensing elastomers.<sup>8</sup> Strategic structural modifications of the naphthopyran scaffold provide a range of visible absorption properties and thermal reversion kinetics in the corresponding ring-opened merocyanines. These diverse properties extend the functional

range of naphthopyran mechanophores and can be used to create materials with complex multicolor or multi-stimuli responsive behavior.

In Chapter 2, we review the development of mechanochemical approaches to molecular release, an application that has recently attracted significant research interest.<sup>9</sup> We discuss general strategies for mechanically triggered release before focusing on the two major subclasses of mechanophores intended for molecular release: specialized molecules designed for the release of a specific cargo, and more modular platforms compatible with a wide range of payloads. We also outline potential applications and address important technical hurdles that must be overcome for these mechanophores to achieve their full translational potential.

*Chapter 1*DESIGNING NAPHTHOPYRAN MECHANOPHORES WITH  
TUNABLE MECHANOCROMIC BEHAVIOR

Mechanochromic molecular force probes conveniently report on stress and strain in polymeric materials through straightforward visual cues. We capitalize on the versatility of the naphthopyran framework to design a series of mechanochromic mechanophores that exhibit highly tunable color and fading kinetics after mechanochemical activation. Structurally diverse naphthopyran crosslinkers are synthesized and covalently incorporated into silicone elastomers, where the mechanochemical ring-opening reactions are achieved under tension to generate the merocyanine dyes. Strategic structural modifications to the naphthopyran mechanophore scaffold produce dramatic differences in the color and thermal electrocyclization behavior of the corresponding merocyanine dyes. The color of the merocyanines varies from orange-yellow to purple upon the introduction of an electron donating pyrrolidine substituent, while the rate of thermal electrocyclization is controlled through electronic and steric factors, enabling access to derivatives that display both fast-fading and persistent coloration after mechanical activation and subsequent stress relaxation. In addition to identifying key structure–property relationships for tuning the behavior of the naphthopyran mechanophore, the modularity of the naphthopyran platform is demonstrated by leveraging blends of structurally distinct mechanophores to create materials with desirable multicolor mechanochromic and complex stimuli-responsive behavior, expanding the scope and accessibility of force-responsive materials for applications such as multimodal sensing.

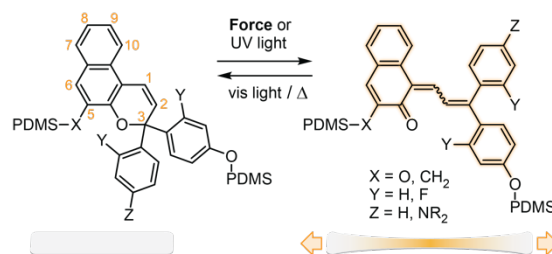
This chapter has been reprinted from Versaw, B. A., McFadden, M. E.; Husic, C. C., Robb, M. J. *Chem. Sci.* **2020**, *11*, 4525.

## 1.1 Introduction

The rapidly growing field of polymer mechanochemistry explores the use of mechanical force to activate chemical transformations in stress-responsive molecules called mechanophores.<sup>5</sup> Mechanical stress is transmitted through polymer chains to covalently attached mechanophores where the transduction of mechanical energy elicits a chemoselective reaction.<sup>10,11</sup> In particular, mechanophores that produce a visible color change in response to mechanical force are of particular interest for stress sensing applications, enabling the straightforward detection of critical stress and/or strain in polymeric materials.<sup>12</sup> Mechanochromic mechanophores have been developed that generate color through a variety of mechanisms. Spiropyran is one of the most widely investigated mechanophores, which undergoes a  $6\pi$  electrocyclic ring-opening reaction under force to generate a highly colored merocyanine species.<sup>13,14</sup> The mechanochromic behavior of other chromene derivatives including naphthopyran<sup>15,16</sup> and spirothiopyran,<sup>17</sup> the ring-opening reaction of a rhodamine-based mechanophore,<sup>18,19</sup> and mechanochemically-induced unzipping of polyladderene<sup>20,21</sup> have also been recently demonstrated. Mechanophores that dissociate homolytically under force to generate a pair of colored stable free radicals in polymers have also been reported.<sup>22-26</sup>

In addition to their recently discovered mechanochemical activity,<sup>15</sup> naphthopyrans have been widely developed for their excellent photochromic properties, which can be extensively modified through chemical substitution to control the color and thermal reversion behavior of the merocyanine.<sup>27</sup> For the 3,3-diaryl-3*H*-naphtho[2,1-*b*]pyran scaffold illustrated in Scheme 1.1, conversion of the colorless naphthopyran to the colored merocyanine form proceeds via a  $6\pi$  electrocyclic ring-opening reaction that is mediated by UV light (or force), while the ring-closing reaction is driven by visible light or heat. Substitution of the aryl rings attached at the 3-position of the naphthopyran has a significant impact on the absorption and electrocyclization behavior of the photochemically generated merocyanine.

**Scheme 1.1** Reaction of naphthopyran in PDMS materials generates colored merocyanine dyes with substituent-dependent mechanochromic properties.



Electron-donating substituents in the *para* position of the phenyl rings cause a bathochromic shift of the merocyanine absorption, which ranges from approximately 30 nm for an alkoxy substituent to greater than 100 nm for a secondary amine.<sup>28,29</sup> Substituents at the *ortho* position dramatically reduce the rate of thermal electrocyclization through putative steric interactions, leading to significantly longer lifetimes of the merocyanine state in solution.<sup>28,30</sup> In addition, substituents on the naphthopyran skeleton have been shown to affect the photochromic properties. Methoxy substitution at the 5-position, for example, results in a hypsochromic shift of approximately 40 nm in the ring-closed form, but does not significantly affect the color of the merocyanine state.<sup>31</sup>

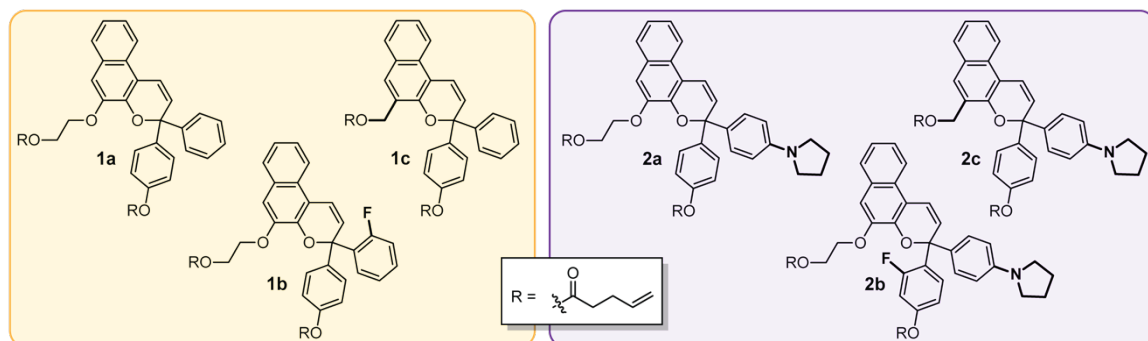
Here we investigate the influence of substitution on the naphthopyran mechanophore framework, establishing a modular platform for accessing polymeric materials with highly tunable mechanochromic properties. Structure–activity relationships for the photochromic and mechanochromic properties of a series of naphthopyran mechanophores are investigated in solution and in crosslinked polydimethylsiloxane (PDMS) materials. Strategic structural modifications to the naphthopyran mechanophore result in significant changes to the visible absorption properties and rates of electrocyclization (i.e., color fading) in solution that translate to the mechanochromic behavior of polymeric materials activated in tension. We leverage the diverse mechanochromic and photochromic properties of the naphthopyran mechanophores to create stimuli-responsive polymers capable of complex reporting functionality including multicolor mechanochromism and visually orthogonal reactivity under photochemical and mechanical stimulation.

## 1.2 Results and Discussion

We designed a series of naphthopyran mechanophores with different substituents tailored to control both the color and fading kinetics of the merocyanine generated under force (Chart 1.1). The regiochemistry of naphthopyran is critical for mechanochemical activity, which is achieved only when mechanical force is effectively transferred across the labile C–O pyran bond.<sup>15</sup> Naphthopyran **1a** with polymer attachment at the 5-position generates an orange-yellow merocyanine dye under mechanical stress in polymeric materials, while regioisomers attached at the 8- and 9-position were previously demonstrated

to be mechanochemically inert due to geometrical incongruity with the direction of applied force (see Scheme 1). Therefore, each naphthopyran in the current study was designed with the same polymer attachment geometry employed for known mechanophore **1a**. Naphthopyrans were synthesized via the acid-catalyzed reaction between appropriately substituted 2-naphthols and propargyl alcohols and appended with vinyl-functional tethers to allow for their incorporation as crosslinkers into elastomeric PDMS networks (see Appendix A for details). A strongly electron-donating pyrrolidine substituent was introduced at the *para* position of one of the phenyl rings on the naphthopyran to bathochromically shift the absorption of the merocyanine relative to **1a**. From these two basic scaffolds with variably colored merocyanines (**1a** and **2a**), we sought to further modulate the thermal reversion kinetics. An *ortho*-fluoro group was incorporated on one of the aromatic rings to reduce the rate of thermal electrocyclization and extend the lifetime of the merocyanine state in mechanochemically activated materials (**1b** and **2b**). Conversely, faster thermal reversion could be useful for achieving materials with rapid switching capabilities. While the influence of alkoxy substituents at the 5-position of naphthopyran on the absorption properties has been characterized,<sup>27</sup> relatively little is known about the impact of substitution at this position on the lifetime of the merocyanine state. As described below, replacing the electron-donating alkoxy group at the 5-position of the naphthopyran with an alkyl tether results in faster electrocyclization (**1c** and **2c**). Encouragingly, density functional theory (DFT) calculations performed using the constrained geometries simulate external force (CoGEF) method<sup>32</sup> predict the desired electrocyclic ring-opening reaction for each naphthopyran derivative upon mechanical elongation (see Appendix A for details).

**Chart 1.1** Naphthopyran mechanophore crosslinkers used in the preparation of PDMS materials with tunable mechanochromic behavior



The absorption properties of the small molecule naphthopyran crosslinkers were first characterized in solution to evaluate the impact of substitution (Figure 1.1). UV-vis absorption spectra were acquired for each compound in THF before and after irradiation with UV light (311 nm for 30 s). The UV-vis absorption properties are summarized in Table 1.1. Each naphthopyran exhibits an absorption peak around 320 nm, while naphthopyrans containing an alkyl tether at the 5-position (**1c** and **2c**) have a second absorption feature at approximately 350 nm, resulting in an overall bathochromic shift relative to the 5-alkoxy derivatives. As expected, substituents on the aryl rings attached at the 3-position of the naphthopyran scaffold do not significantly affect the absorption properties of the ring-closed naphthopyran at wavelengths longer than ~320 nm due to connectivity through the  $sp^3$ -hybridized carbon. Irradiation of the naphthopyran solutions with UV light results

in new absorption peaks in the visible region corresponding to the ring-opened merocyanine state. For compounds **1a–1c**, the associated merocyanine species exhibit absorption peaks between 422 and 435 nm and the solutions appear orange-yellow in color. In contrast to the ring-closed naphthopyrans, the pyrrolidine substituents on compounds **2a–2c** result in a substantial bathochromic shift in the absorption of the merocyanine dyes with peaks at 530–553 nm, producing solutions that appear purple in color. For naphthopyrans **1b** and **2b**, the

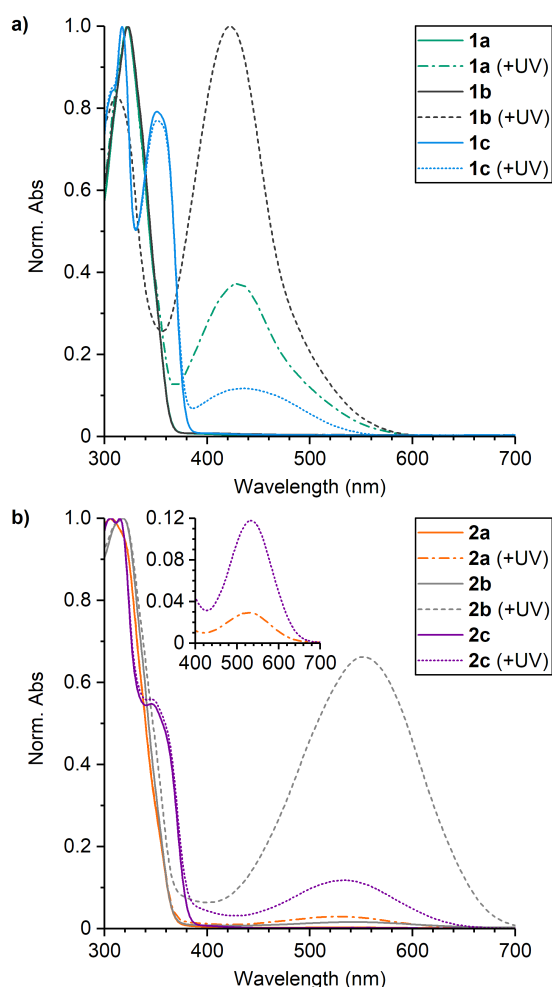


**Figure 1.1** UV-vis absorption spectra acquired for solutions of (a) naphthopyrans **1a–1c**, and (b) pyrrolidine-substituted naphthopyrans **2a–2c** (0.1 mM in THF) before and after irradiation with UV light ( $\lambda = 311$  nm, 30 s). The introduction of a pyrrolidine substituent results in a significant bathochromic shift of the merocyanine absorption.

*ortho*-fluoro group results in greater absorbance in the visible region of the spectra after UV irradiation, consistent with a significantly longer-lived merocyanine state.

**Table 1.1** Summary of absorption properties and thermal reversion kinetics for naphthopyran mechanophores

	Absorption properties		Thermal reversion kinetics					
	Before $h\nu$ ,	After $h\nu$ ,	$k_{r,\text{soln}}^b$ ( $\text{s}^{-1}$ )	$t_{1/2,\text{soln}}$ (s)	$k_{r1,\text{solid}}^c$ ( $\text{s}^{-1}$ )	$k_{r2,\text{solid}}^c$ ( $\text{s}^{-1}$ )	$A_{1,\text{solid}}^c$	$A_{2,\text{solid}}^c$
	$\lambda_{\text{max}}$ (nm)	$\lambda_{\text{max}}$ (nm)						
<b>1a</b>	322	430	0.033	21	0.02	—	—	—
<b>1b</b>	323	422	0.0023	300	0.002	0.02	0.2	0.04
<b>1c</b>	317, 351	435	0.075	9	0.02	0.09	0.07	0.03
<b>2a</b>	318	530	0.19	4	0.01	0.1	0.04	0.03
<b>2b</b>	318	553	0.010	69	0.01	0.002	0.2	0.1
<b>2c</b>	315, 346	533	nd <sup>d</sup>	nd <sup>d</sup>	0.02	0.1	0.04	0.02

<sup>a</sup> Absorption maxima measured in THF (0.1 mM) before and after irradiation with UV light ( $\lambda = 311$  nm, 30 s). <sup>b</sup> Average rate constant and half-life ( $t_{1/2}$  from 1<sup>st</sup> order thermal reversion kinetics in THF at room temperature after UV photoactivation). <sup>c</sup> Rate constants and pre-exponential factors from biexponential fitting of thermal reversion kinetics measured by digital color analysis of PDMS films containing 1.5 wt% mechanophore after UV photoactivation. Kinetic data for **1a** were fitted to monoexponential decay. <sup>d</sup> Not determined. See Appendix A for additional details.

The kinetics of thermal electrocyclization for each merocyanine dye were quantified to further characterize the impact of substitution on the color-fading behavior. Solutions of each naphthopyran in THF were initially irradiated with 311 nm UV light, and the absorbance at wavelengths corresponding to the  $\lambda_{\text{max}}$  of each merocyanine was subsequently monitored at room temperature in the dark. Plots of the time-dependent merocyanine absorbance were fit to first-order exponential decay to determine the rate constant ( $k_{r,\text{soln}}$ ) and in Table 1 as averages from three separate trials. Comparing the rates of thermal ring-closure for merocyanines derived from **1a** and **2a**, for example, illustrates the impact of the electron-donating *para*-pyrrolidine substituent. The pyrrolidine substituent increases the rate of electrocyclization approximately six-fold, corresponding to a reduction in  $t_{1/2}$  from 21 s to 4 s. Conversely, the introduction of an *ortho*-fluoro group decreases the value of  $k_{r,\text{soln}}$  by approximately one order of magnitude with measured half-lives of  $t_{1/2} = 300$  s for **1b** and  $t_{1/2} = 69$  s for **2b**. This effect has previously been attributed to a steric interaction that hinders formation of the requisite geometry for ring-closure.<sup>20</sup> Replacing the alkoxy group with an alkyl tether at the 5-position of the naphthopyran approximately doubles the rate of thermal reversion from the merocyanine state, as illustrated for **1a** and **1c**, respectively.

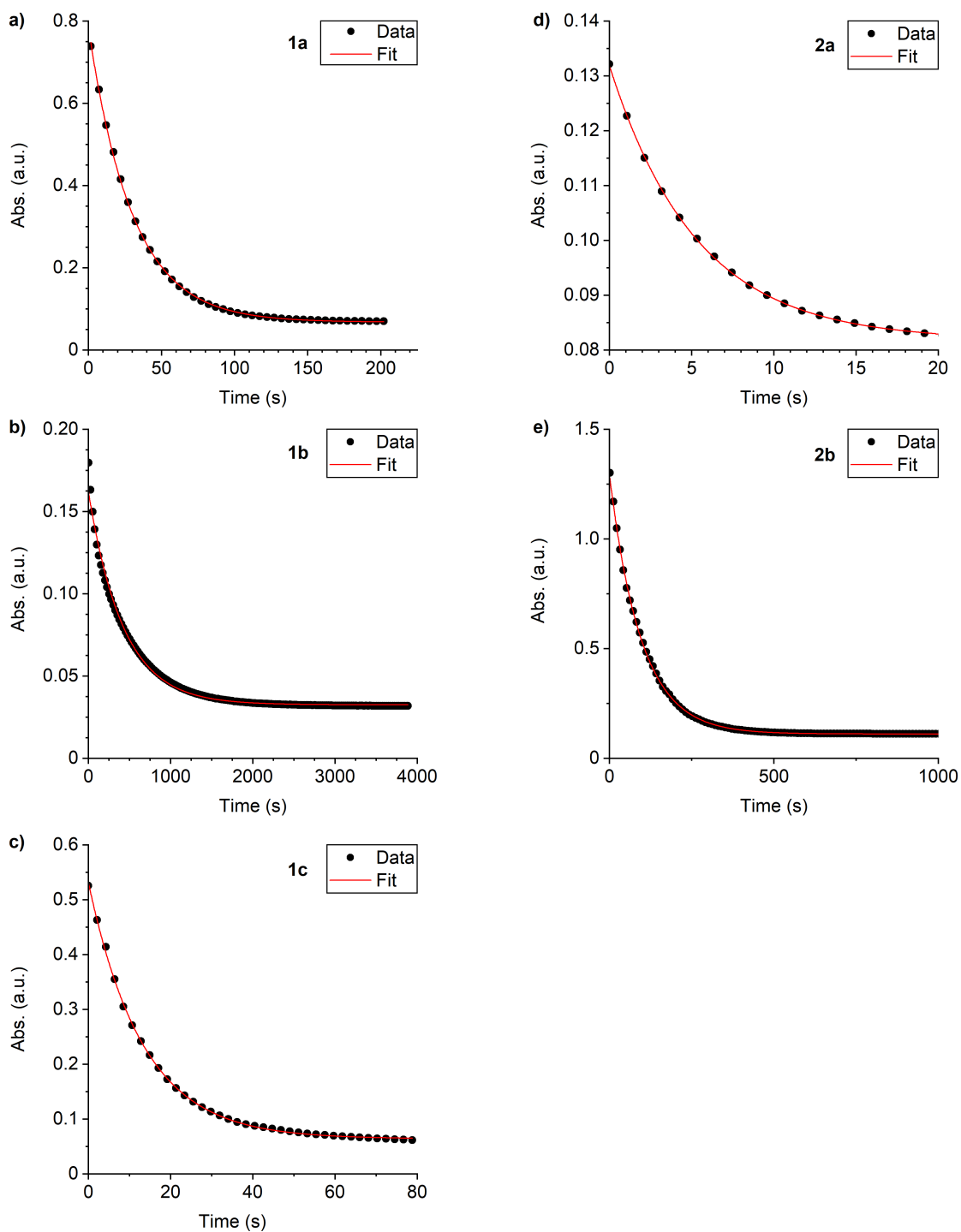


**Figure 1.2** Representative plots for characterizing the kinetics of thermal reversion for the different merocyanines. Solutions of naphthopyrans in THF were irradiated with UV light ( $\lambda = 311$  nm, 30 s) and absorbance was subsequently monitored at the  $\lambda_{\text{max}}$  corresponding to each merocyanine in the dark at room temperature. Data were fit to first-order exponential decay (eq 1) as described in Appendix A to extract the rate constant for electrocyclization. The ring-closing reaction of the merocyanine generated from naphthopyran **2c** was too rapid to characterize effectively (see Section VI for additional details). Solution concentrations were 0.1 mM (**1a**, **1c**, **2b**), 0.01 mM (**1b**), and 0.25 mM (**2a**).

he results are presented Electrocyclization of the merocyanine derived from **2c** was too rapid for the initial fading rate to be effectively characterized, although a persistent merocyanine isomer remains after an extended period of time post-irradiation that is responsible for the visible absorption peak in Fig. 1b. The persistent color observed after UV photoactivation of some naphthopyrans has been attributed to the relative thermal stability of the merocyanine isomer with *trans* configuration of the exocyclic double bond, which isomerizes slowly in the dark to the *cis* isomer prior to ring-closure.<sup>33–35</sup> This isomerization is efficiently promoted with visible light, however, and subsequent irradiation of the above solution with white light results in complete attenuation of the visible absorption peak, indicating full conversion of the merocyanine back to the original ring-closed naphthopyran (see Appendix A for details).

Following evaluation of their solution-phase properties, the mechanochromic behavior of the series of naphthopyran derivatives was investigated in elastomeric PDMS materials. Naphthopyrans were incorporated as crosslinkers (~1.5 wt % loading) into PDMS films via platinum-catalyzed hydrosilylation according to the method reported by Craig and coworkers,<sup>36</sup> which provides an ideal materials testing platform (Figure 1.3a). With the exception of the material containing naphthopyran **2b** that exhibits some background color, the films are

optically clear and nearly colorless. Stretching each naphthopyran-containing PDMS film causes the gauge region of the material to change color, characteristic of the mechanochemical ring-opening reaction to generate the merocyanine dye (Figure 1.3b). After mechanical activation, films containing naphthopyrans **1a–c** are orange-yellow in color, while films containing pyrrolidine-substituted naphthopyrans **2a–c** appear purple, consistent with the photochromic behavior of the molecules in both solution and in the solid-

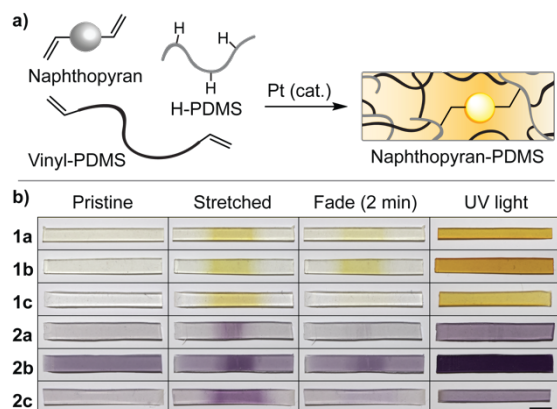


**Figure 1.3** (a) PDMS materials covalently crosslinked with naphthopyran mechanophores are prepared via platinum-catalyzed hydrosilylation. (b) Photographs of PDMS films incorporating naphthopyran mechanophores (1.5 wt%) immediately after mechanical activation (tension) and subsequent stress relaxation (2 min), and after irradiation with UV light ( $\lambda = 311$  nm, 90 s). Scale bar  $\frac{1}{4}$  5 mm.

state after irradiation with UV light. Qualitative differences in thermal reversion kinetics are also evident in the photographs of the films acquired 2 min after initial mechanical activation and subsequent stress relaxation. The color of the merocyanine dye is still apparent in films containing mechanophores **1b** and **2b**, which produce the slowest fading merocyanines due to the *ortho*-fluorophenyl substituents. In contrast, PDMS films incorporating mechanophores **1c** and **2c** that contain the alkyl tether at the 5-position and produce the fastest-fading merocyanines exhibit nearly complete thermal reversion in the same period of time following mechanical activation.

To further characterize the kinetics of thermal ring-closure in the solid-state, PDMS films were uniformly irradiated with UV light and photographs were subsequently acquired at regular time intervals to monitor the disappearance of color associated with the conversion of the merocyanine to the naphthopyran (see Appendix A for details). Time-dependent changes in the ratio of the green and red color channel intensities were extracted from the digital images and fit to models of exponential decay (Figure 1.4).<sup>14</sup> The thermal reversion kinetics for mechanophore **1a** are well described by monoexponential decay; however, a biexponential decay equation was required to accurately model the thermal fading behavior of the other merocyanine dyes in the solid state. Previous studies of naphthopyran–merocyanine systems suggest that the biexponential kinetics originate from multiple merocyanine stereoisomers, each of which exhibits a unique rate of thermal reversion.<sup>33–35</sup> The rate constants determined for thermal reversion of each merocyanine in solid PDMS materials ( $k_{r1,solid}$  and  $k_{r2,solid}$ ) are summarized in Table 1.1, along with the corresponding pre-exponential factors ( $A_{1,solid}$  and  $A_{2,solid}$ ) that express the relative weight of each term (see Appendix A for details). On average, the observed rates of merocyanine reversion are slower in solid PDMS materials than in solution, which we attribute to differences in polarity and conformational constraints imposed by the polymer network.<sup>37–39</sup> The overall trends in fading kinetics, however, reflect the structure–property relationships observed for the small molecules in solution, despite the more complex fading behavior in the solid state that potentially arises from differences in merocyanine isomerization that are more pronounced in solid PDMS materials.



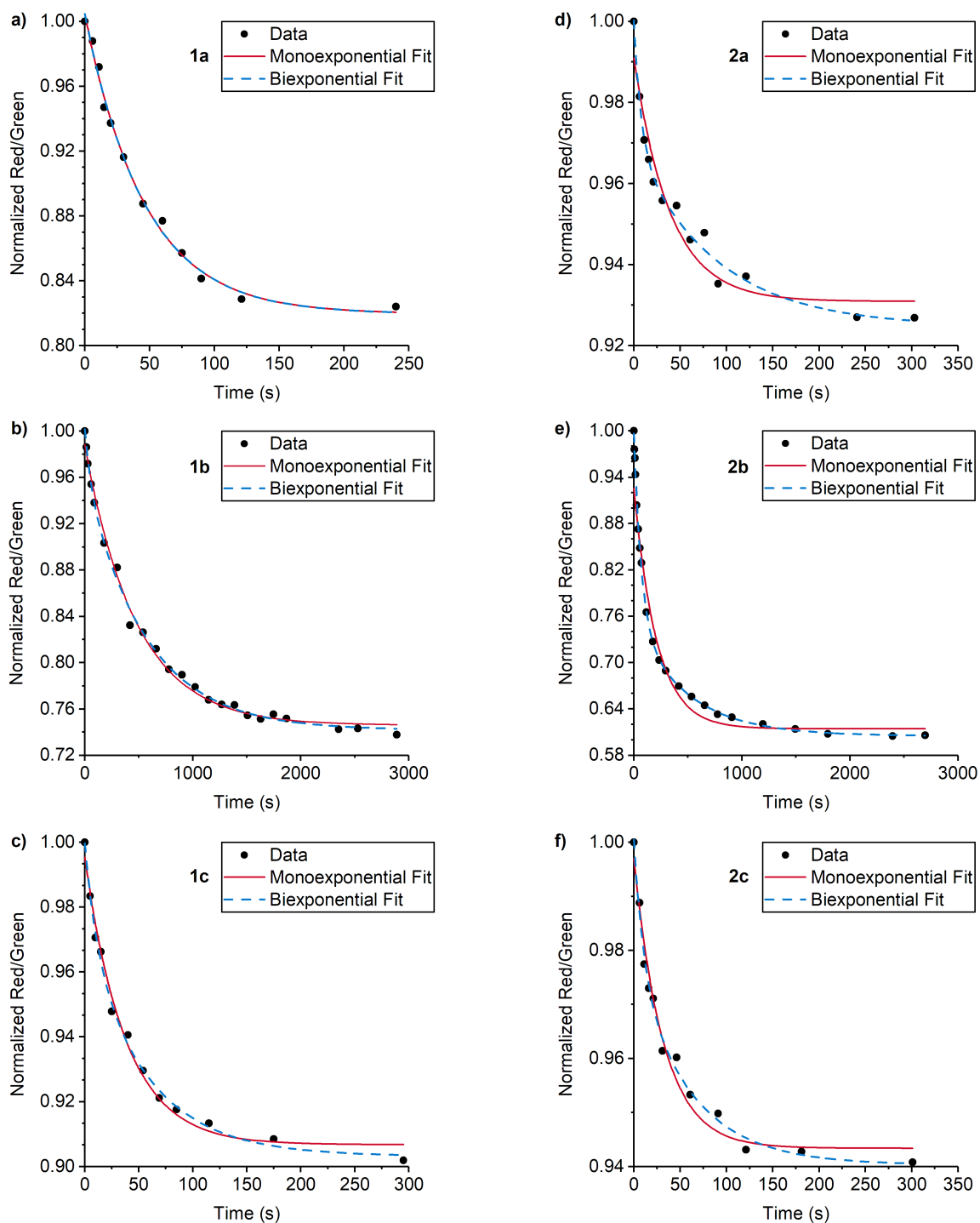


**Figure 1.4** Characterization of thermal reversion kinetics for merocyanines in solid PDMS materials. Digital images of PDMS films containing 1.5 wt % naphthopyran were acquired after uniform irradiation with UV light ( $\lambda = 311$  nm, 90 s). The intensities of the red and green color channels were extracted from each image and the ratio was plotted as a function of time. Data were fit to models of exponential decay to extract the rate constants for electrocyclization, as described in detail in Appendix A. With the exception of **1a**, biexponential decay (eq 2) was required to accurately model the thermal fading behavior of the merocyanine dyes in the solid state.

Beyond the typical binary response of most mechanochromic mechanophores, materials that are capable of reporting on the state of stress or strain through discrete visual signals are desirable targets. Rhodamine<sup>19</sup> and spiropyran<sup>36,40</sup> mechanophores display differences in absorption under active tension and after stress relaxation due to presumed torsional effects and changes in cis–trans isomerization, respectively. We recently developed a bis-naphthopyran mechanophore that exhibits gradient multicolor mechanochromism resulting from force-dependent changes in the distribution of uniquely colored merocyanine products.<sup>16</sup> In addition, the differential activation of distinct mechanophores localized in hard and soft domains of phase-separated polymer and composite materials has been demonstrated using different types of mechanical stimuli (e.g., stretching and grinding).<sup>41,42</sup> Here, the substantial differences in merocyanine absorption and reversion kinetics provided by the library of naphthopyran mechanophores affords opportunities to create materials capable of multicolor mechanochromism and other complex reporting functions. To demonstrate the potential of this approach, a PDMS film was prepared using a blend of mechanophore crosslinkers **1b** and **2c**, which generate a slow-fading orange-yellow and a fast-fading purple-colored merocyanine, respectively (Figure 1.5a). Under active tension the material appears red-orange in

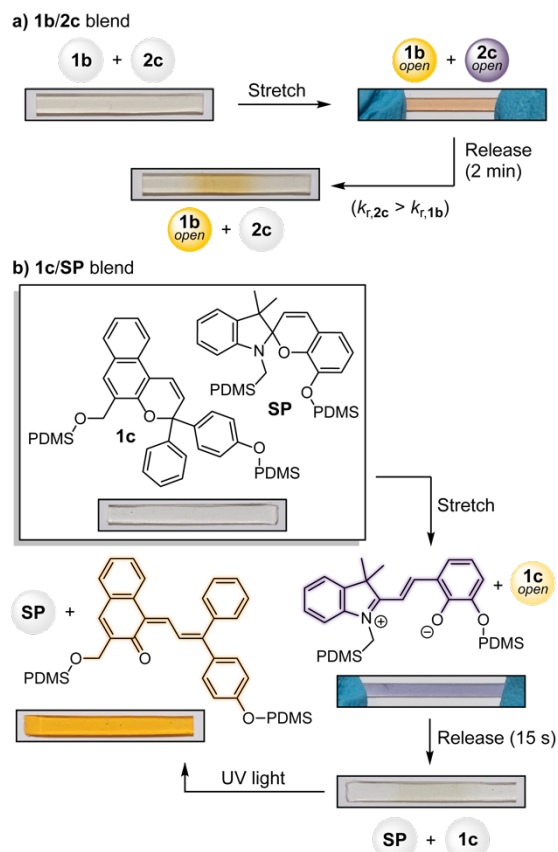


**Figure 1.5** Demonstration of multicolor mechanochromism and photochromism from PDMS materials incorporating blends of different mechanophores. (a) PDMS containing a 4 : 1 mixture (by wt) of naphthopyrans **1b** and **2c**, respectively, exhibits variation in color under tension and after stress relaxation due to pronounced differences in merocyanine absorption and reversion rates. (b) PDMS film containing a 1 : 1 blend (by wt) of naphthopyran **1c** and non-photochromic spiropyran **SP** exhibits distinct responsive behavior when activated mechanochemically in tension or with UV light ( $\lambda = 311 \text{ nm}$ , 90 s). Samples measure 25 mm – 3 mm and contain a total mechanophore loading of 1.5 wt%

color due to the combined contribution of both merocyanines. Upon stress relaxation, the purple component quickly fades to reveal a more persistent orange-yellow color, providing a clear visual response that distinguishes between the different stress states with temporal resolution. A 4:1 ratio (by wt) of **1b/2c** was chosen to optimize the visual contrast between the different stress states.

We further sought to access materials that respond to multiple types of stimuli by taking advantage of the photochromic properties of naphthopyran combined with a photochemically inert spiropyran mechanophore<sup>43</sup> (Figure 1.5b, see Appendix A for details). A PDMS material containing a 1:1 blend (by wt) of naphthopyran **1c** and spiropyran mechanophore **SP** was prepared and activated mechanically in tension, causing the film to turn blue-purple in color due to the dominant appearance of the spiropyran-derived merocyanine. Upon stress relaxation, the color quickly disappears due to the rapid thermal reversion of both merocyanine dyes. The same film was then irradiated with UV light, which selectively activates the ring-opening reaction of naphthopyran **1c** to give a vibrant orange-yellow readout. These examples illustrate the types of stimuli-responsive materials that are accessible for multimodal sensing applications by capitalizing on the highly tunable and modular properties of the naphthopyran platform.

### 1.3 Conclusions

In summary, we have demonstrated the versatility of the naphthopyran scaffold as a modular platform for designing polymeric materials with tunable mechanochromic and stimuli-responsive properties. Diverse naphthopyran mechanophores are accessed through straightforward synthetic methods with strategic structural modifications that provide control over both the color and fading kinetics of the merocyanine dyes generated under photochemical and mechanochemical activation. The rates of thermal reversion are tunable through both steric and electronic factors while the color of the merocyanine dyes is varied from orange-yellow to purple upon the installation of an electron donating pyrrolidine substituent. The absorption and thermal reversion properties of the small molecules in solution translate to the mechanochromic behavior of the naphthopyran mechanophores in crosslinked PDMS elastomers activated in tension. The variation in electrocyclization

kinetics and visible absorption behavior provided by judicious substitution of the naphthopyran scaffold enables the development of polymeric materials that exhibit desirable multicolor mechanochromic and complex stimuli-responsive properties from a simple and modular molecular platform. The structure–activity relationships presented for the naphthopyran mechanophore expand the scope and accessibility of light and force-responsive materials for a number of applications, including multimodal sensing.

*Chapter 2***HARNESSING THE POWER OF FORCE: DEVELOPMENT OF  
MECHANOPHORES FOR MOLECULAR RELEASE**

Polymers that release small molecules in response to mechanical force are promising materials for a variety of applications ranging from sensing and catalysis to targeted drug delivery. Within the rapidly growing field of polymer mechanochemistry, stress sensitive molecules known as mechanophores are particularly attractive for enabling the release of covalently-bound payloads with excellent selectivity and control. Here, we review recent progress in the development of mechanophore-based molecular release platforms and provide an optimistic, yet critical perspective on the fundamental and technological advancements that are still required for this promising research area to achieve significant impact.

This chapter has been reprinted with permission from Versaw, B. A., Zeng, T., Hu, X., Robb, M. J. *J. Am. Chem. Soc.* **2021**, *143*, 21461-21473. Copyright 2021 American Chemical Society.

## 2.1 Introduction

### 2.1.1 Polymer Mechanochemistry: Enabling Productive Reactivity Using Mechanical Force

In the rapidly growing field of polymer mechanochemistry, mechanical force is used to activate the chemical transformations of stress-sensitive molecules termed mechanophores.<sup>10,11</sup> Polymers maintain the important role of transducing mechanical force to the mechanophore via covalent connectivity. In contrast to nonspecific bond scission commonly associated with the mechanical degradation of polymers, mechanophores respond to force chemoselectively to elicit productive chemical changes.<sup>5</sup> Theoretical studies have revealed that the unique mechanochemical activity of mechanophores arises from a distortion of the potential energy surface under large forces, fundamentally changing the reaction landscape.<sup>44-46</sup> Mechanical force has been shown to promote remarkable transformations such as formally forbidden electrocyclic ring-opening reactions of benzocyclobutene and *gem*-dihalocyclopropanes.<sup>47,48</sup> The force-coupled activation of specific covalent bonds in mechanophores has also been harnessed to afford a wide range of productive chemical reactions and responsive materials.<sup>49,50</sup> Examples include, but are certainly not limited to, conductivity switching<sup>20</sup> and the generation of colored,<sup>14-16,18,22,51</sup> fluorescent,<sup>24,52,53</sup> or chemiluminescent species,<sup>54</sup> enabling the visual detection of stress and strain. Mechanochemical reactions have also been used to activate latent catalysts<sup>55,56</sup> and generate reactive functional groups,<sup>17,47,57,58</sup> imbuing polymers with self-healing properties or the ability to strengthen under typically destructive shear forces.<sup>59</sup> Research in the last two decades has produced an impressive library of more than one hundred mechanophores that spans an incredibly diverse range of structure and function.<sup>7</sup>

In a pioneering report from 2005, Moore and coworkers described the site-specific chain scission of polymers containing a mechanically weak azo group near the chain midpoint under the application of force. Mechanochemical fragmentation of the azo-linked polymers was putatively accompanied by the liberation of dinitrogen, which also makes it the first example of mechanically triggered molecular release in polymer mechanochemistry.<sup>6</sup> In the last few years, the topic of mechanically triggered release has gained significant attention. A quickly expanding collection of mechanophores and different mechanochemical reaction strategies are being devised to advance this important research

area, which promises applications ranging from remote controlled drug delivery to catalysis and sensing. Here, we review current progress in the development of mechanophore-based platforms for molecular release with the aim of summarizing notable contributions to the field and providing insight for future development.

### 2.1.2 Strategies for Mechanically Triggered Release from Polymers

In this chapter, we define mechanically triggered release as the selective liberation of a chemical payload under extrinsic force. The development of stimuli-responsive polymers that release functional molecules under stress is an active research area, in large part due to their myriad potential applications in drug delivery, sensing, and damage reporting/repair.<sup>50,60</sup> Compared to other chemical or thermal activation strategies, the use of mechanical force as an external stimulus affords spatiotemporal control over molecular release in force-responsive materials, along with significant opportunities for remote control using technologies such as ultrasound.<sup>61</sup> A variety of different strategies have been developed for achieving molecular release that leverage the innate responsiveness of polymers to mechanically dynamic environments. For instance, the release of cargo molecules physically entrapped within a polymer matrix,<sup>62</sup> self-assembled polymer micelle,<sup>63</sup> or phospholipid liposome<sup>64</sup> has been accomplished through force-induced deformation or disruption of the carrier (Figure 2.1a). Similarly,  $\beta$ -cyclodextrin inclusion complexes,<sup>65</sup> polyaptamers,<sup>66</sup> and metal-organic cages<sup>67</sup> release small molecule guests through mechanical perturbation of the noncovalent interactions that enable complexation. In addition, polymer microcapsules embedded in a material enable the release of a wide variety of liquid payloads, facilitating autonomous healing and visual reporting of mechanical damage.<sup>68</sup> For a more detailed discussion of these strategies involving the release of physically entrapped payloads, we refer the reader to recent reviews.<sup>60,69-71</sup>

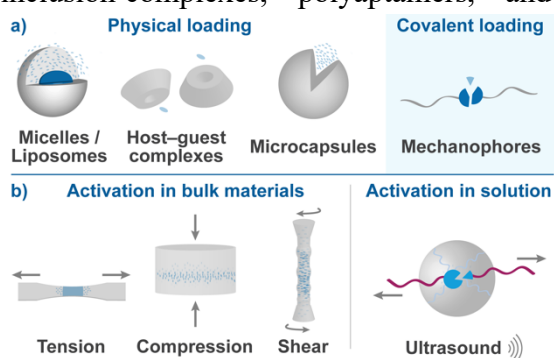


**Figure 2.1** A variety of strategies have been developed enabling the mechanically triggered release of small molecules from polymers. (a) Examples of molecular release platforms based on physically entrapped payloads in comparison to mechanophores that rely on covalent conjugation of the cargo. (b) Common approaches for the mechanochemical activation of mechanophores in bulk materials and in solution via ultrasonication.

Compared to the systems identified above, mechanophore-based release platforms incorporate cargo molecules through covalent linkages (Figure 2.1a). While in many cases these systems are more synthetically demanding, the resulting polymers may be more resistant to nonspecific payload release in the absence of the mechanical triggering event.<sup>72</sup> Perhaps the most significant advantage, however, comes from the ability to precisely modulate the reactivity of mechanophores through molecular structure manipulation, providing the opportunity for unprecedented control over mechanical activation and cargo release. Here, we focus our discussion on these mechanophore-based systems for achieving the mechanically triggered release of small molecules from polymers.

### *2.1.3 Common Techniques for Mechanophore Activation*

The mechanically triggered release of covalently bound molecular payloads is accomplished through the preprogrammed mechanochemical reactions of mechanophores. Force is transduced to mechanophores through attached polymer chains to induce the mechanically selective scission of weak bonds, resulting in a specific functional response. To achieve effective force transfer, mechanophores are covalently incorporated within the backbone of polymers or as crosslinkers in polymer networks.<sup>11</sup> Mechanophore activation in bulk polymeric materials is typically accomplished by mechanical deformation resulting from the application of tension, compression, or shear stress (Figure 2.1b).<sup>49,73</sup> While mechanophore activation in the bulk is successfully achieved via manual deformation of materials, the use of a load frame, hydraulic press, or dynamic mechanical analysis instrument enables more precise control over experimental parameters such as the magnitude and rate of applied force.<sup>74</sup> In addition, ball milling has received increased attention in polymer mechanochemistry recently as a convenient technique for mechanophore activation in polymers,<sup>41,75</sup> adopting the ubiquitous method from the namesake field of powder mechanochemistry also known as trituration chemistry.<sup>76,77</sup> At the single molecule level, atomic force microscopy (AFM) – particularly single molecule force spectroscopy (SMFS) – has been established to uniquely enable quantitative force and rate-dependent characterization of the mechanochemical reactions of mechanophores.<sup>78–80</sup> Nevertheless, the SMFS technique is highly specialized and limited to the study of polymers containing multiple, non-scissile mechanophores in the polymer backbone.<sup>81</sup>

Solution state ultrasonication, on the other hand, provides one of the most general and effective methods for mechanophore activation. High intensity and low frequency ultrasound – typically 20 kHz – is commonly employed to apply mechanical forces to polymers dissolved in solution via acoustic cavitation (Figure 2.1b).<sup>81-85</sup> Polymer chains in the proximity of a collapsing bubble experience rapid elongation due to solvodynamic shear. The force experienced by a polymer under these conditions scales with chain length<sup>86</sup> and is maximized near the chain midpoint, although studies have demonstrated that a significant portion of the total contour length of a polymer is subjected to sufficiently high forces during ultrasound-induced extension to achieve mechanophore activation.<sup>87</sup> Therefore, mechanophores are generally incorporated near the center of a polymer chain or as repeating units distributed along the length of the polymer backbone.<sup>5,81</sup> Solution-phase ultrasonication is readily coupled with conventional characterization techniques such as size-exclusion chromatography and UV-vis, fluorescence, and NMR spectroscopy, making it an indispensable method for the development of new mechanophores and for advancing the fundamental understanding of mechanochemical reactivity. Additionally, experimental variables such as ultrasound frequency, sonication power, temperature, and solvent can be changed to affect reactivity.<sup>87</sup> It is important to note, however, that the influence of these parameters has largely been determined for simple polymer chain scission reactions in studies conducted prior to the conception of the mechanophore hypothesis.<sup>83</sup> The influence of ultrasound frequency on mechanophore activation, in particular, is a critical question for the development of mechanochemical molecular release systems targeting biological applications. The sonication probes typically employed in mechanophore activation experiments are the same as those commonly used for cell lysis and are thus mutually incompatible with mechanophore activation in many biological environments. To begin to address this issue, recent reports have explored the use of biocompatible<sup>88</sup> high-intensity focused ultrasound (HIFU) in the frequency range of 550 kHz to 1.1 MHz.<sup>61,89</sup> While HIFU is still a nascent technique for mechanophore activation, we anticipate that this technology will prove critical for future translational applications in polymer mechanochemistry. We return to a discussion of this topic in the Outlook section.

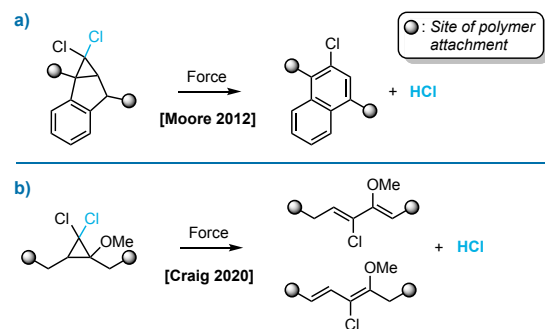
## 2.2 Mechanically Triggered Molecular Release from Specialized Mechanophores

Several different mechanophores have been developed enabling the force-triggered release of small molecules. Unlike the more generalized platforms discussed later, each approach discussed in this section leverages a judiciously designed mechanophore to release a specific compound upon mechanochemical activation. As a result, these mechanophore design strategies are relatively limited in their modularity and the scope of molecules that can be released. Nonetheless, the mechanically triggered release of a small but relatively diverse collection of molecular payloads has been demonstrated through a range of distinct reaction manifolds.

Following their pivotal report on a dinitrogen-evolving azo mechanophore, Moore and coworkers described the mechanically triggered release of another simple diatomic molecule, HCl. As one of the simplest possible reagents and catalysts, the mechanically coupled generation of HCl is promising for the design of stress responsive polymeric materials in which self-healing, degradation, pH-driven optical signals, and other property changes are triggered with acid. The design is based on the mechanically-promoted electrocyclic ring-opening reaction of an indene-derived *gem*-dichlorocyclopropane (gDCC) mechanophore and spontaneous aromatization to drive HCl elimination (Scheme 2.1a).<sup>90</sup> Compression of a poly(methyl acrylate) (PMA) network covalently crosslinked with the gDCC derivative resulted in mechanochemical activation of the mechanophore and HCl generation as demonstrated colorimetrically using a methyl red indicator as well as several other analytical techniques. Control experiments in which the mechanophore was physically

incorporated into a PMA network and subjected to the same compression did not result in the same immediate color change, supporting the mechanochemical origin of the reactivity. More recently, Craig and coworkers also reported the mechanically triggered release of HCl from a methoxy-substituted gDCC (MeO-gDCC) mechanophore (Scheme 2.1b).<sup>91</sup> The gDCC mechanophore scaffold

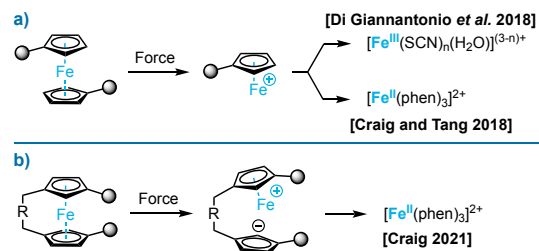
**Scheme 2.1** Mechanically Triggered Release of HCl Is Achieved through Ring Opening and Spontaneous Elimination of Specialized gDCC Mechanophores



popularized by the Craig group has been extensively studied.<sup>92</sup> In the absence of an additional driving force like aromatization in the example above, the electrocyclic ring-opening reaction occurs with chlorine migration to form a stable 2,3-dichloroalkene product. Here, the addition of an electron-donating methoxy group was proposed to stabilize the cationic character that develops during chloride dissociation and ultimately promote the spontaneous elimination of HCl. Consistent with this hypothesis, the ring-opening reaction of the MeO-gDCC mechanophore was found to occur at a force of  $\sim 900$  pN compared to  $\sim 1300$  pN for the unsubstituted analog based on SMFS experiments. In addition, ultrasound-induced mechanochemical activation of polymers containing multiple MeO-gDCC units in the backbone generated, on average, 67 equivalents of HCl per chain scission event. Mechanically triggered release of HCl was also demonstrated in bulk crosslinked polydimethylsiloxane (PDMS) materials under tension and compression. Compared to the earlier indene derivative that exhibits only modest thermal stability, the MeO-gDCC mechanophore is also quite stable with no reaction observed after heating at  $110$  °C for 1 day.

The mechanical activation of metal complexes through force-induced metal–ligand bond dissociation has also received substantial interest, particularly for applications in catalysis.<sup>93</sup> Polymers containing Ag, Co, Cu, Eu, Fe, Pd, Pt, and Ru complexes have all been found to activate selectively at the metal–ligand bond under mechanical force.<sup>55,56,94–107</sup> However, only a few studies performed recently on metallocenes have demonstrated and characterized the complete dissociation of a metal ion from the parent polymer. In 2018, Giannantonio *et al.* sonicated solutions of polymers containing ferrocene units in the backbone and characterized metal ion release by complexation with KSCN and  $K_4[Fe(CN)_6]$ .<sup>102</sup> Formation of the red  $[Fe(SCN)_n(H_2O)_{6-n}]^{(3-n)+}$  complex and Prussian blue from their respective potassium salts suggested that  $Fe^{2+}$  was released upon mechanochemical activation and rapidly oxidized by air to form  $Fe^{3+}$  (Scheme 2.2a). These conclusions were further supported by

**Scheme 2.2** Release of Metal Ions Is Achieved through the Mechanochemical Scission of the Metal–Ligand Bonds in Ferrocene Mechanophores



studies of chain scission kinetics indicating that polymer cleavage occurs selectively at the embedded ferrocene moieties. In close succession, Craig, Tang, and coworkers reported a similar investigation into ferrocene mechanochemistry, successfully trapping the released  $\text{Fe}^{2+}$  ion with phenanthroline to form the stable  $[\text{Fe}(\text{phen})_3]^{2+}$  complex (Scheme 2.2a).<sup>103</sup> In this work and in a subsequent study,<sup>104</sup> the authors characterized the relative mechanical strengths of the Fe–cyclopentadienyl bond in ferrocene as well as the Ru–cyclopentadienyl bond in ruthenocene according to established protocols using the competitive reactivity of a gDCC mechanophore as an internal reference.<sup>108</sup> Interestingly, they found that despite the high thermodynamic stability of ferrocene and ruthenocene, their mechanochemical lability is similar to that of the relatively weak C–N bond of azobisdialkyl nitrile (BDE < 30 kcal/mol) and the C–S bond of a thioether (BDE = 71–74 kcal/mol), respectively.<sup>103,104</sup> Data also suggest that the mechanochemical dissociation of both metallocenes occurs predominately via a heterolytic mechanism.

The mismatch in thermodynamic stability and mechanical susceptibility prompted further investigation into structure–mechanochemical activity relationships for metallocene mechanophores. In 2021, Craig and coworkers demonstrated that the mechanism of ferrocene dissociation under mechanical force could be biased by a distal conformational restraint between the two cyclopentadienyl ligands (Scheme 2.2b).<sup>105</sup> Polymers containing these *ansa*-bridged ferrocene mechanophores were shown to dissociate by peeling, rather than shearing, of the cyclopentadienyl ligands from the metal center. Significantly, this change in mechanism leads to a substantial increase in mechanochemical activity for the *ansa*-bridged ferrocene complex, dissociating at a transition force of ~800 pN compared to the > 1600 pN of force required for reaction of the unbridged ferrocene mechanophore in SMFS experiments. The investigation of metallocene mechanochemistry has also recently been extended to cobaltocenium mechanophores that were demonstrated to react selectively under mechanical force via a peeling-type mechanism that, in this case, is driven by interactions between the metal center and the counterion.<sup>106</sup>

In contrast to the conventional mode of mechanophore activation in which mechanical force is coupled to the scission of a weak bond, small molecule release has also been achieved through a unique “flex activation” manifold where extrinsic force promotes

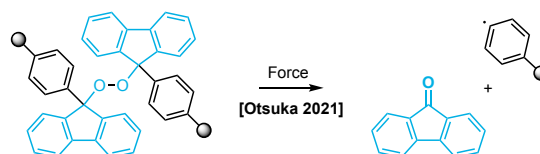


perturbation, likely due to the poor alignment between the direction of applied force and the nearly orthogonal scissile bonds in the mechanophore, which results in weak mechanochemical coupling. While mechanical force decreases the reaction barrier, significant thermal energy is still required under relatively large forces to move along the force modified potential energy surface. In addition to the mechanophore structure, the polymer matrix also contributes to activation efficiency. Recently, Kilian and coworkers investigated the mechanochemical activation of a similar oxanorbornadiene mechanophore in double network hydrogels of polyacrylamide and alginate, achieving ~20% activation upon compression under relatively moderate stress.<sup>112</sup> The improved reactivity is attributed to the enhanced toughness of the material that enables greater deformation prior to failure and adds to other recent insights into mechanophore activation in multinetwork materials.<sup>113-115</sup> Finally, it is notable that the use of solution state ultrasonication methods to probe the reactivity of mechanophores designed for flex activation has not been reported in the literature. Such studies may shed light on whether the low mechanophore activation efficiencies observed for this class of compounds are due primarily to their molecular design, or rather limitations of solid state force transduction.

In addition to the azo mechanophore discussed above, a relatively large collection of diverse mechanophores has been developed that react via homolytic fragmentation pathways.<sup>7</sup> Although not recognized as a mechanophore at the time, the mechanical susceptibility of the peroxide functional group was identified by Encina in 1980 through investigations of the ultrasound-induced chain fragmentation of polyvinylpyrrolidone containing several peroxide linkages distributed throughout the polymer backbone.<sup>116</sup> However, the mechanochemistry of organic peroxides has since received little attention, with a possible exception being the dioxetane mechanophores developed by Sijbesma and coworkers that contain a peroxy linkage within the four-membered ring but exhibit significantly different reactivity.<sup>54</sup> In a recent investigation of peroxide mechanochemistry, Otsuka and coworkers designed a mechanophore based on the bis(9-methylphenyl-9-fluorenyl) peroxide (BMPF) scaffold that undergoes homolytic fragmentation of the O–O bond under mechanical force to ultimately release the fluorescent small molecule 9-fluorenone via  $\beta$ -scission (Scheme 2.4).<sup>117</sup> The BMPF mechanophore was converted into a

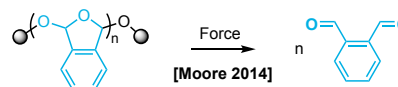
crosslinker and incorporated into both a glassy poly(butyl methacrylate) and rubbery poly(hexyl methacrylate) network via free radical polymerization where mechanical activation was evaluated using ball-milling and compression, respectively. In both cases, a fluorogenic response was observed under UV

**Scheme 2.4** Force-Induced Homolysis of a Mechanically Labile Peroxide Bond Triggers the Release of the Fluorescent Molecule 9-Fluorenone



light and the release of 9-fluorenone was further confirmed through chromatographic and spectroscopic analyses performed on soluble extracts. The BMPF mechanophore was also demonstrated to be thermally stable up to 110 °C. Another peroxy containing mechanophore based on an anthracene–endoperoxide was also recently reported to liberate singlet oxygen in polymers subjected to ball-milling.<sup>118</sup> However, we cautiously note that without control experiments to rule out a thermal activation pathway, additional investigation is warranted to elucidate the reactivity. Further exploration of the mechanochemistry of organic peroxides is certain to contribute to new fundamental understanding of reactivity and enable additional tools for the construction and applications of force-responsive materials. The mechanically triggered release of small molecules has also been accomplished through depolymerization. In 2014, Moore and coworkers demonstrated the ultrasound-induced mechanochemical unzipping reaction of poly(*o*-phthalaldehyde) to produce *o*-phthalaldehyde monomers (Scheme 2.5).<sup>119</sup> The results of trapping experiments and steered molecular dynamics simulations support a mechanism in which mechanochemical chain cleavage via heterolytic fragmentation of a C–O bond in the polymer backbone reveals reactive hemiacetalate and oxocarbenium end groups. At temperatures above the low ceiling temperature of poly(*o*-phthalaldehyde), which is around –40 °C,<sup>120</sup> these polymer chain fragments undergo rapid head-to-tail depolymerization to regenerate monomer. Proof-of-concept experiments were also successfully performed to demonstrate the repolymerization of recovered *o*-phthalaldehyde monomer by treating a sonicated solution of poly(*o*-phthalaldehyde) with an anionic initiator. The molecular weight-dependent kinetics associated with the mechanochemical activation of poly(*o*-phthalaldehyde)

**Scheme 2.5** Mechanical Force Triggers the Heterolytic Chain Scission of Poly(*o*-phthalaldehyde) Resulting in Complete Depolymerization above Its Ceiling Temperature to Regenerate Monomer



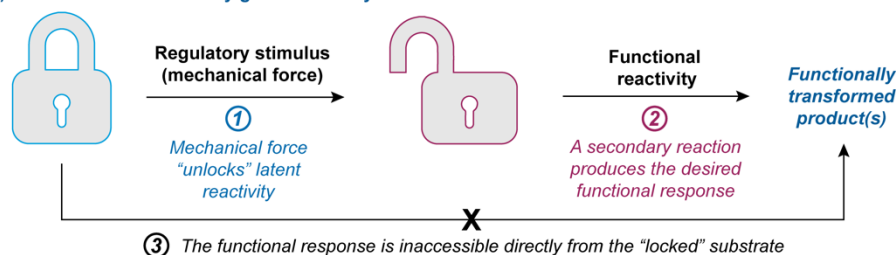
were further investigated by Peterson and Boydston by taking advantage of the rapid depolymerization that occurs following mechanical activation.<sup>121</sup> More broadly, the mechanically triggered degradation of polymers has recently attracted significant research interest because of the opportunities it presents for chemical recycling strategies that address the sustainable end-of-life management of plastics.<sup>122</sup> As discussed briefly in the next section, several reports have leveraged mechanophores to introduce chemically labile functional groups into previously inert polymer backbones;<sup>123-126</sup> however, mechanically triggered end-to-end depolymerization has only been demonstrated for poly(*o*-phthalaldehyde). Expanding mechanically triggered depolymerization strategies to additional self-immolative polymers<sup>127</sup> with greater thermal and chemical stability while ideally also maintaining desirable physical properties for useful materials will be important for advancing these technologies. Beyond polymer degradation, the mechanically triggered depolymerization of self-immolative polymers also presents tremendously exciting opportunities to capitalize on the unique chemical amplification<sup>128</sup> process for stress sensing and other applications.

### 2.3 Mechanically Gated Reactivity

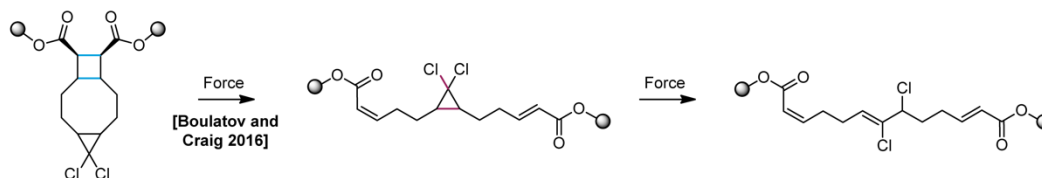
In chemistry, gating generally refers to the use of a specific regulatory stimulus to control a secondary chemical transformation. For example, gated reactivity is an established concept in the context of photoswitching, where a photochemical transformation reveals a new structure with unique reactivity,<sup>129</sup> or alternatively, a photochemically active molecule is produced after a chemical reaction.<sup>130-134</sup> As a pertinent example of the former case of photogated reactivity, Otsuka and coworkers designed an elegant system that uses light to modulate the susceptibility of polymers toward thermal<sup>135</sup> and mechanochemical chain scission.<sup>136</sup> The related concept of mechanically gated reactivity has recently emerged as a powerful approach for the modular design of mechanophores and complex mechanochemically active systems (Figure 2.2a). Here, we briefly introduce this general topic before moving on to discuss its influence on the design of mechanophores for mechanically triggered release.

A formative paper from Craig, Boulatov, and coworkers in 2016 described the mechanochemical reactivity of a unique tricyclic dual mechanophore that possesses two mechanochemically active subunits fused to a central 8-membered ring (Figure 2.2b).<sup>137</sup> A combination of SMFS and ultrasonication experiments revealed that the two subunits react sequentially when force is applied to polymer chains attached to the cyclobutane portion of

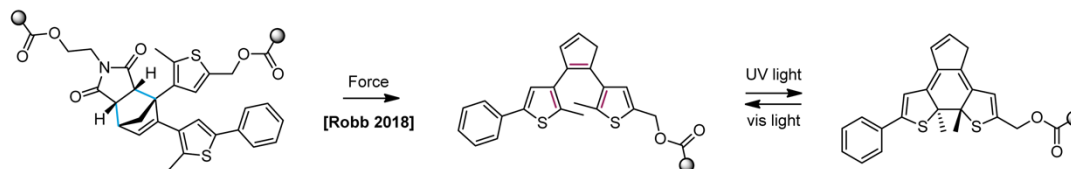
#### a) Overview of mechanically gated reactivity



#### b) Mechanical gating of a mechanochemical reaction



#### c) Mechanically gated photoswitching



#### d) Mechanically gated polymer degradation

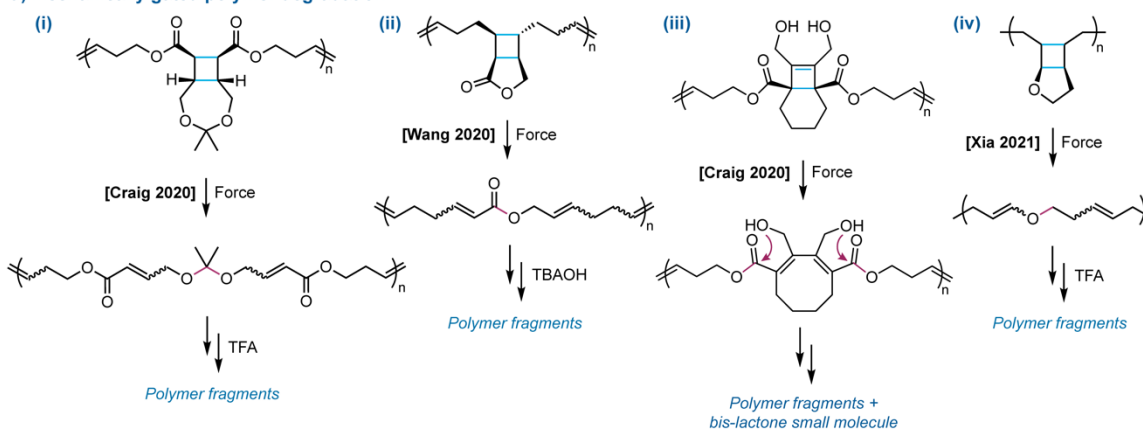


**Figure 2.2** The mechanical gating concept has emerged as a powerful strategy for the design of mechanophores and force-responsive polymers. (a) Mechanically gated reactions use mechanical force to regulate a secondary chemical reaction, effectively decoupling the mechanochemical activation event from the ultimate programmed functional response. Mechanical gating has been used to (b) control the reactivity of a gDCC mechanophore, (c) regulate photochromism, and (d) enable on-demand polymer degradation.

the molecule. The ring-opening reaction of the gDCC subunit in this dual mechanophore was observed at a significantly higher force than that required for the reaction of isolated gDCC mechanophores. Quantum chemistry calculations confirmed that the higher force is required to first activate the less reactive cyclobutane subunit, effectively demonstrating that the cycloelimination reaction gates the ring opening of the more reactive gDCC mechanophore.

Inspired by the idea of gated reactivity, in 2018 our group designed a cyclopentadiene–maleimide Diels–Alder adduct that undergoes a retro-[4+2] cycloaddition reaction upon mechanical activation to reveal a latent diarylethene photoswitch, establishing the concept of mechanically gated photoswitching (Figure 2.2c).<sup>138</sup> Irradiation with UV light subsequently induces a  $6\pi$  electrocyclic ring-closing reaction to produce the conjugated colored isomer, providing a visual indication of the prerequisite mechanochemical transformation. An important feature of this mechanophore design strategy is that mechanical activation is decoupled from the ultimate functional response, which affords a high degree of modularity to the system,<sup>139</sup> and in principle, enables independent control over each component reaction through structural variation.

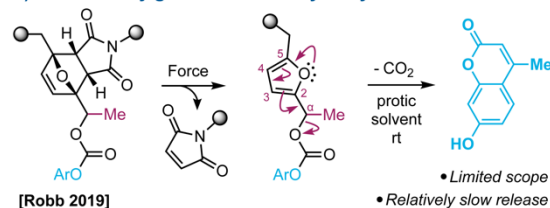
The mechanical gating concept has also recently been applied to the design of polymers that can switch on degradability in response to mechanical force. Polymers incorporating ring-fused cyclobutane mechanophores in the repeating unit structures react under mechanical force to introduce hydrolytically labile acetal,<sup>123</sup> ester,<sup>124</sup> and enol ether<sup>125</sup> linkages along the backbone (Figure 2.2d). While the polymers are initially resistant to degradation, mechanochemical activation “unlocks” their degradability in the presence of acid or base. Craig and coworkers also reported a similar approach with polymers constructed from cyclobutene mechanophores that undergo ring expansion upon mechanochemical activation to reveal a diene structure poised for intramolecular lactonization.<sup>126</sup> Polymer degradation subsequently occurs slowly via the mechanically triggered lactonization cascade with concomitant release of a bis-lactone small molecule. As discussed in the next section, many of these same design concepts derived from mechanically gated reactivity have been successfully implemented in the development of more generalized and highly modular mechanophore platforms for molecular release.

## 2.4 Mechanically Gated Cascade Reactions for Molecular Release

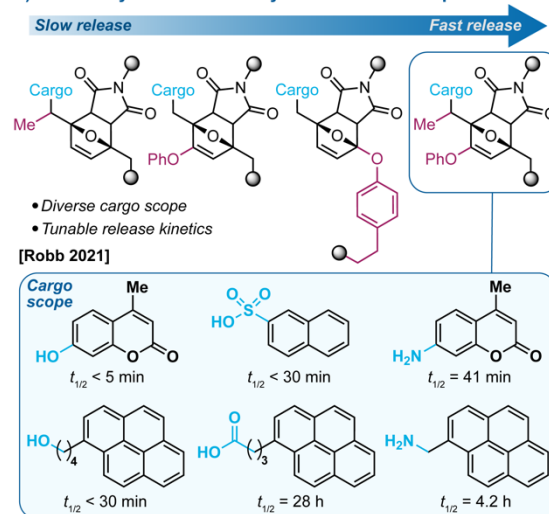
Adapting the design strategy employed in our earlier demonstration of mechanically gated photoswitching, in 2019 our group reported a mechanophore for molecular release that leverages the instability of 2-furylcarbinol derivatives,<sup>140–143</sup> a structural motif that has also been investigated for the design of prodrugs<sup>144</sup> and self-immolative polymers.<sup>145,146</sup> The initial mechanophore design was based on a mechanically triggered cascade reaction in which the mechanochemical retro-[4+2] cycloaddition reaction of a furan–maleimide Diels–Alder adduct unmasks a latent furfuryl carbonate, which subsequently decomposes to release a covalently bound small molecule (Scheme 2.6a).<sup>147</sup> Hydroxycoumarin was

**Scheme 2.6** Mechanically Triggered Molecular Release from Masked 2-Furylcarbinol Derivatives Is Accomplished via a Retro-Diels–Alder/Fragmentation Cascade

### a) Mechanically gated release of hydroxycoumarin



### b) Modularity of masked 2-furylcarbinol mechanophores



used as a model payload due to its fluorogenic properties to facilitate the straightforward characterization of molecular release by photoluminescence spectroscopy in addition to other analytical methods. Judicious substitution of the 2-furylcarbinol scaffold was key to the success of this approach, enabling the decomposition of the furfuryl carbonate to proceed relatively quickly following mechanochemical activation of the Diels–Alder adduct. Density functional theory (DFT) calculations indicated that a combination of alkyl substituents at the 5-position of the furan and at the  $\alpha$ -position significantly suppressed the activation barrier for carbonate fragmentation, reducing  $\Delta G^\ddagger$  from 29.4 kcal/mol for the unsubstituted compound to 22.0 kcal/mol for the dialkyl derivative. In particular, small molecule model experiments confirmed the importance of the  $\alpha$ -methyl substituent, which presumably stabilizes the developing positive charge in the transition state leading to the secondary furfuryl cation intermediate, as depicted by the arrow pushing mechanism in Scheme 2.6. In

a polar protic mixture of acetonitrile and methanol, the furfuryl carbonate decomposes at room temperature with a half-life on the order of ~1 h to cleanly release hydroxycoumarin. Notably, release occurred ~10-fold faster in an aqueous acetonitrile mixture. The mechanically triggered release of hydroxycoumarin was successfully demonstrated by ultrasound-induced mechanochemical activation of a polymer containing a chain-centered furan–maleimide mechanophore, achieving approximately 64% release after 150 min of sonication. By fitting the sonication time-dependent photoluminescence response to an expression of first-order kinetics, the yield of hydroxycoumarin was projected to plateau at a maximum value of ~87%, indicating that mechanophore activation and subsequent payload release occurs efficiently.

While the mechanophore described above offered a promising design platform, molecular release was found to be largely limited to phenols. Kinetic studies performed on small molecule 2-furylcarbinol derivatives with the same substitution pattern demonstrated that the release of a primary alcohol is approximately 100× slower than hydroxycoumarin, with the release of aminocoumarin from the analogous furfuryl carbamate occurring approximately 60× slower than that of the primary alcohol.<sup>148</sup> We envisioned that an additional electron donating substituent on the furan would further suppress the activation barrier for fragmentation through resonance stabilization of the furfuryl cation intermediate, enabling the release of more challenging payloads on reasonable time scales (Scheme 2.6b). DFT calculations were performed to establish structure–activity relationships and further assess the impact of substitution on the reactivity of 2-furylcarbinol derivatives. In particular, the addition of an electron-donating phenoxy group at the 3-position of the furan, in combination with the  $\alpha$ -methyl substituent, was found to significantly lower the activation energy and provide a highly active substrate for molecular release. Mechanochemical activation experiments corroborated the predictions from DFT and demonstrated that release kinetics could be modulated by several orders of magnitude by varying the substitution on the masked 2-furylcarbinol derivatives. Importantly, this tunability allows release rates to be preprogrammed into the mechanophore through independent structural modifications based on the identity of the molecular payload and the desired response. The mechanically triggered release of cargo molecules bearing alcohol, phenol, alkylamine, arylamine, carboxylic acid,

and sulfonic acid functional groups was successfully demonstrated using ultrasonication, illustrating the generality of the molecular design strategy (half-lives for cargo release in 3:1 acetonitrile/methanol are illustrated in Scheme 2.6b). We note, however, that less efficient release of the alkylamine payload was observed compared to the other cargo molecules, which was attributed to a side reaction involving attack of the furfuryl cation intermediate by the liberated nucleophilic amine. These results suggest a potential challenge for achieving the efficient release of cargo molecules possessing strongly nucleophilic functional groups with this mechanophore design.

More recently, our group has also investigated an alternative mechanophore design that incorporates an aryloxy substituent at the 5-position of the masked 2-furylcarbinol scaffold, which serves as both the site of polymer attachment and an electron donating group to accelerate release (Scheme 2.6b).<sup>149</sup> Installation of the aryloxy group at the 5-position of the furan preserves the proximal pulling geometry in the furan–maleimide mechanophore, which leads to greater mechanochemical activity compared to the regioisomer with distal connectivity.<sup>150</sup> This mechanophore is prepared through a considerably more efficient four-step synthesis while still facilitating the mechanically triggered release of both phenol and arylamine payloads with rates that are comparable to those of the phenoxy-substituted mechanophore. Similar to the effects of phenoxy substitution in the prior design, the aryloxy substituent was also demonstrated to significantly improve the thermal stability of the Diels–Alder adduct without adversely affecting mechanochemical activity. Interestingly, small molecule model experiments suggested that decomposition proceeds through a fragmentation mechanism distinct from previously studied 2-furylcarbinol derivatives, involving secondary fragmentation at the aryloxy connection that could be leveraged to provide additional functionality such as dual payload release.

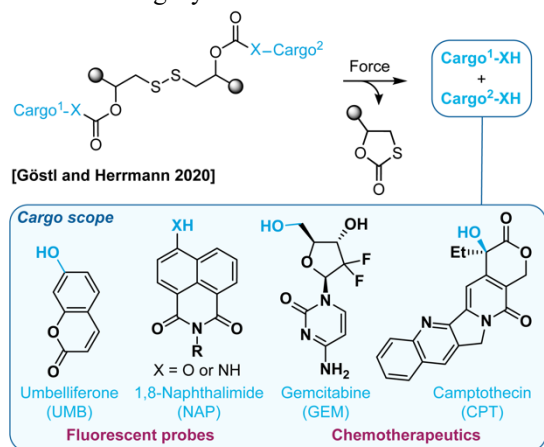
Another system that leverages a mechanically triggered cascade reaction to achieve molecular release was reported by Göstl, Herrmann, and coworkers in 2020.<sup>151</sup> The mechanophore is based on an elegantly designed disulfide motif with payloads attached via  $\beta$ -carbonate linkages. Mechanically activated reduction<sup>152,153</sup> of the disulfide bond is followed by a *5-exo-trig* cyclization to release a pair of alcohol-based cargo molecules (Scheme 2.7). The bifunctional character of this platform enables a theranostic approach with

the concurrent release of a therapeutic compound and a fluorescent reporter molecule for following drug release and biodistribution in real time. Model experiments performed on small molecule disulfide initiators dually conjugated with a reporter/drug combination of umbelliferone (UMB)/gemcitabine (GEM) or *N*-butyl-4-hydroxy-1,8-naphthalimide (NAP)/camptothecin (CPT) exhibited efficient and concomitant release of both

payloads upon chemical reduction. The mechanically triggered release of NAP/CPT payloads from a polymer chain-centered mechanophore was demonstrated using ultrasonication methods. The release of NAP (and by inference, CPT) was characterized by fluorescence spectroscopy, reaching ~56% after 180 min of sonication. In a series of *in vitro* experiments, HeLa cells were treated with samples of the sonicated polymer and characterized by confocal laser scanning microscopy and cell viability assays. Fluorescence from NAP was only observed in cells treated with the polymer that had been subjected to ultrasonication, whereas cells treated with the unsonicated polymer were essentially non-fluorescent, indicating successful release and cellular uptake of NAP. Cell viability studies also confirmed the mechanically triggered release of the CPT small molecule drug from the polymer, with increasing exposure to ultrasonication resulting in progressively lower cell viability. To demonstrate the generality of the platform, the mechanically triggered release of the UMB/GEM fluorophore/drug pair was also investigated, achieving comparable amounts of release to the NAP/CPT system. In this case, however, the release of UMB proceeded at a faster rate than that of GEM. A paper from the same groups that appeared later demonstrated the ultrasound-induced mechanochemical activation of polymers containing symmetrical disulfide mechanophores loaded with two equivalents of UMB or CPT with qualitatively similar results as this earlier study.<sup>66</sup>

A more recent investigation comparing the mechanically triggered release of NAP (X = OH) and the amine analog *N*-alkyl-4-amino-1,8-naphthalimide (X = NH<sub>2</sub>) revealed

**Scheme 2.7** Mechanochemical Reduction of a Disulfide Mechanophore Triggers Cargo Release via a 5-*exo*-trig Cyclization



significantly diminished release efficiency for the amine payload conjugated to the disulfide mechanophore via carbamate linkers (Scheme 2.7).<sup>154</sup> While ~50% release of the hydroxyl-functional payload was released after 240 min of sonication, < 3% release of the amine cargo was observed after being subjected to the same ultrasonication conditions. As for the 2-furylcarbinol platform discussed above, these results highlight the importance of the leaving group on molecular release.<sup>155</sup> Moreover, for the disulfide mechanophore, release is coupled to the equilibrium established between the  $\beta$ -mercapto carbonate/carbamate and the cyclic thiocarbonate, with the more nucleophilic amines expected to shift the equilibrium toward the former state. The susceptibility of the disulfide mechanophore to nonspecific activation via chemical reduction or thiol exchange presents another potential challenge. Studies also confirmed that ultrasound-induced mechanophore activation must occur *ex situ* to avoid loss of viability for mammalian cells,<sup>66</sup> identifying a substantial barrier to translational applications. As discussed in greater detail below, the sonication conditions used here are representative of those employed ubiquitously in polymer mechanochemistry research. Therefore, new remote activation strategies are needed to facilitate the application of mechanophore-based molecular release platforms in biological settings.<sup>156</sup> Interestingly, the same 20 kHz ultrasonication was found to have no considerable effect on the viability of *S. aureus* bacteria.<sup>66</sup>

## 2.5 Outlook

The rapidly growing field of polymer mechanochemistry has captivated the attention of organic chemists and polymer scientists and engineers alike by revealing fundamentally new concepts in chemical reactivity and unprecedented opportunities for the design of stimuli-responsive materials. Over the last decade—and the last several years, in particular—the development of force-sensitive molecules known as mechanophores that enable the mechanically triggered release of covalently bound payloads has attracted significant interest. This research has added new tools to an already active area of investigation into the development of stimuli-responsive polymers that release functional small molecules under stress for a wide variety of applications. Unlike most materials-based approaches, however, mechanophores are constructed with atomic precision and leverage the principles of organic

chemistry to modulate their activity for molecularly programmed responsive behavior. Diverse strategies for harnessing mechanical force to facilitate productive chemical transformations have furnished a quickly expanding library of mechanophores enabling small molecule release. Ongoing efforts to create specialized mechanophores capable of releasing specific cargo molecules are joined by research toward the development of more modular and generalized platforms that take advantage of mechanical gating and mechanically triggered cascade reactions. While the collective intuition of mechanochemical reactivity has advanced substantially in a relatively short period of time, the continued advancement of structure–activity relationships is paramount to establish a thorough understanding of the design rules underpinning mechanically selective bond activation, and to expand the cargo scope and capabilities of mechanophore-based molecular release strategies.

As mechanophore-based molecular release platforms continue to improve and evolve, the desire to seek practical applications in areas like catalysis, autonomous materials, and controlled drug delivery will prompt further innovation. Systems that enable the release of multiple payloads per mechanical activation event by leveraging multicargo designs or multimechanophore polymers are needed to overcome limitations in cargo loading capacity and enhance the utility of mechanophore-based release strategies. Novel approaches are also required to expand beyond small molecule release to develop systems for mechanically triggered depolymerization, a relatively unexplored area of polymer mechanochemistry with substantial promise for the design of adaptable materials with self-repairing or remodeling capabilities as well as emerging chemical recycling and stress sensing technologies. Molecular and materials design concepts for improving the efficiency of mechanically triggered release in bulk materials and in diverse solution environments will also expand the reach of mechanophore-based molecular release chemistry. Lastly, the integration of mechanophores with complementary approaches for achieving force-responsive functionality, such as microcapsule-based methods, will provide new multifaceted platforms for creating complex responsive polymeric materials that operate on multiple size and length scales. Targeted drug delivery is one of the most compelling applications to emerge from research into mechanophore-based molecular release platforms. The ability to activate

mechanophores remotely using ultrasound presents unique opportunities for translational applications of polymer mechanochemistry to benefit human health. From a technological perspective, however, the development of strategies using biomedically relevant ultrasound to activate mechanophores is still a potentially formidable challenge. With few exceptions, the sonication probes routinely employed to study mechanophore activation in the laboratory are the same devices commonly used for cell lysis,<sup>82</sup> illustrating their mutual incompatibility. Some existing clinical applications use ultrasound in this 20 kHz frequency range, but are generally limited to procedures where tissue disruption is desirable due to the strong cavitation effects.<sup>88</sup> On the other hand, many of the paradigms underpinning the current understanding of ultrasound-induced mechanochemical activation are based on models of polymer chain extension induced by cavitation,<sup>85</sup> thus establishing a notable dichotomy between mechanophore activation in the laboratory and physiological constraints. New methodologies will be required, particularly for *in vivo* applications, that effectively couple the mechanical activation of mechanophores with the acoustic energy from ultrasound at higher frequencies where cavitation is suppressed.<sup>83</sup> Fortunately for the field, experiments demonstrating the mechanical activation of mechanophores in micellar systems<sup>89</sup> and bulk elastomers<sup>61</sup> provide a promising example that high intensity focused ultrasound (HIFU) operating within biocompatible frequencies and pressure amplitudes will be an important technology for advancing biomedical applications of polymer mechanochemistry. Future innovations in the technologies that enable remote mechanical activation, together with advances in the design of mechanophores for molecular release, promise to help realize the translational potential of polymer mechanochemistry while further galvanizing important fundamental discoveries in this quickly evolving arena.

## SECTION 2

### A FUNCTIONAL PLATFORM FOR HEAT-RESPONSIVE POLYMERS

Polymers that respond productively to changes in their working environment are desirable for a variety of applications from soft robotics<sup>157</sup> and sensing<sup>158</sup> to diagnostics and drug delivery.<sup>159</sup> While polymers can be designed to respond to a range of chemical<sup>160,161</sup> and physical<sup>162,163</sup> stimuli, heat is particularly attractive for its abundance and opportunities for spatial control.

Thermoresponsive materials can be broadly classified by the type of change triggered under applied heat. The best-studied class of heat-responsive polymers exhibit phase changes above or below a critical solution temperature. Polymers with critical phase behavior at physiologically relevant temperatures have been developed extensively for applications in drug delivery and tissue engineering.<sup>159,164</sup> Recent interest in sustainable materials has spurred the development of additional thermoresponsive polymers that expose reactive functional groups upon heating. These materials include self-immolative polymers that undergo depolymerization when a reactive chain end is deblocked under applied heat,<sup>146,165,166</sup> as well as thermoplastic elastomers<sup>167</sup> that leverage the temperature dependence of dynamic covalent bonding (e.g., transesterification,<sup>168</sup> Diels–Alder cycloadditions<sup>169</sup>) to access materials with thermally reversible crosslinks. Unlike their statically crosslinked counterparts, these networks can be healed when damaged or recycled at end-of-use.

In Chapter 3, we investigate the thermal reactivity of masked furfuryl esters and their applications for the preparation of polymers with synthetically challenging carboxylic acid functional groups. Leveraging the known thermal reversibility of furan-maleimide Diels–Alder adducts,<sup>170</sup> we construct a platform in which a maleimide dienophile “masks” the reactivity of a metastable furfuryl ester. Upon heating, thermal cycloreversion unveils the reactive ester, which quickly decomposes to afford a carboxylic acid. After establishing the kinetics and selectivity of this transformation on a model substrate, we demonstrate its utility for the synthesis of telechelic polar polyacrylates and poly(acrylate-*co*-acrylic acid) copolymers.

*Chapter 3*THERMAL UNMASKING OF LATENT FURFURYL ESTERS  
ACCESSSES ACID-FUNCTIONAL POLYMERS

Heat is a powerful stimulus for controlling polymer reactivity due to its ubiquity, tunability, and ease of use. Here, we describe a mild and selective method for polymer functionalization based on the thermally triggered reactivity of latent furfuryl esters. Thermal cycloreversion of a strategically designed furan–maleimide Diels–Alder adduct unmasks a metastable furfuryl ester, which rapidly decomposes to release a covalently bound alkyl carboxylic acid. Masked furfuryl esters are first incorporated into poly(methyl acrylate)s as functional initiators or comonomers, then cleaved by thermal deprotection to install carboxylic acids as chain-end or pendant functionalities. This thermally gated chemistry proceeds with high efficiency under comparatively mild conditions, improving synthetic access to functional polymers and expanding their applications.

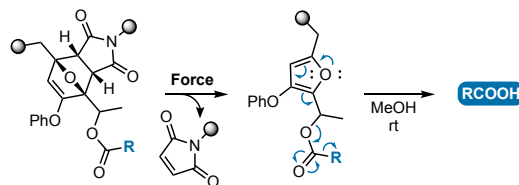
### 3.1 Introduction

External stimuli are valuable components of the polymer chemist's toolbox. Stimuli including light, heat, electrical potential, and mechanical force can be used to mediate a polymer's reactivity during or after synthesis,<sup>171–173</sup> connect its structure and material properties to its working environment,<sup>174,175</sup> or facilitate recycling at the end of its useful life<sup>146,165,166</sup> While a variety of chemical and physical stimuli can be leveraged for these purposes,

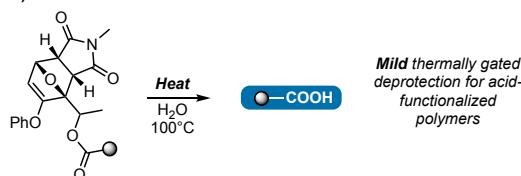
heat is particularly attractive for its spatial tunability and ease of use. Our group recently reported a family of masked 2-furylcarbinol derivatives as a versatile platform for mechanically gated molecular release (Scheme 3.1).<sup>147,148</sup> Our design leverages the known mechanochemical reactivity of furan–maleimide Diels–Alder adducts to trap these reactive motifs as kinetically stable, mechanically labile mechanophore–cargo conjugates. Under applied force, mechanochemical retro-[4+2] cycloaddition of the adduct unveils the 2-furylcarbinol derivative, which decomposes in the presence of a polar protic solvent to release a covalently bound small molecule payload. The kinetics of release can be tuned extensively through strategic structural modification. Installation of a phenyl ether at the furan 3-position and a methyl group  $\alpha$  to the ring generates a highly reactive scaffold that efficiently releases a variety of functional cargos, from alkyl/aryl alcohols and amines to carboxylic acids and sulfonic acids. Importantly, the gated design of this scaffold decouples the initial unmasking step from the cascade elimination that governs release. Consequently, we envisioned that the analogous thermal cycloreversion could be used to give this platform utility beyond the field of polymer mechanochemistry. For example, the ability to selectively unmask functional groups under applied heat could be harnessed as a strategy for post-polymerization modification. Here, we explore the thermal reactivity of masked furfuryl

**Scheme 3.1** Masked furfuryl esters facilitate the release of carboxylic acids using (a) applied force or (b) applied heat.

a) Hu *et al.* 2021:



b) This work:



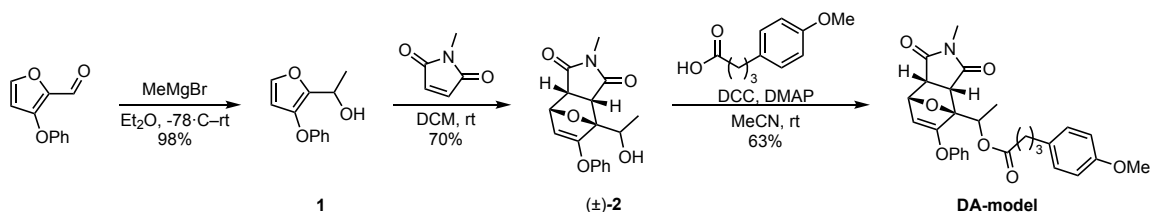
esters, then demonstrate their utility as a mild, tolerant platform for the preparation of polyacrylates with carboxylic acids as pendant or chain-end functionalities.

### 3.2 Results and Discussion

Our design for this platform harnesses strategic molecular design to maximize efficiency and selectivity of the thermally triggered reaction cascade. We have previously shown that incorporation of a methyl group  $\alpha$  to the furan ring substantially improves the kinetics of release by stabilizing the putative cationic intermediate.<sup>147</sup> Adding an electron donating 3-phenoxy group further accelerates decomposition and imparts additional thermal stability to the Diels–Alder adduct.<sup>176</sup> Judicious dienophile choice also dictates the thermal properties of the adduct. For this study, we anticipated that *N*-methyl maleimide would confer sufficient stability to avoid nonspecific activation. Similarly substituted adducts have remained stable for >100 days at room temperature.<sup>148</sup>

With these design principles in hand, we synthesized small molecule masked furfuryl ester **DA-model** (Scheme 3.2) to evaluate its reactivity under applied heat. 3-phenoxyfurfural was subjected to Grignard addition to afford substituted furfuryl alcohol **1**.<sup>148</sup> Subsequent [4+2] cycloaddition with *N*-methyl maleimide furnished an isomeric mixture of Diels–Alder adducts, which was separated by silica gel chromatography to isolate *endo* adduct ( $\pm$ )-**2** bearing a secondary alcohol for cargo attachment. Esterification with representative cargo 4-(4-methoxyphenyl)butanoic acid then afforded **DA-model**. A complementary thermally inert ester (**hDA-model**) was prepared by hydrogenation of a similar furan-maleimide Diels–Alder adduct prior to esterification (see Appendix B for details). To identify the temperature threshold for efficient thermal unmasking of **DA-model**, we first completed variable-temperature NMR experiments with precursor Diels–Alder adduct ( $\pm$ )-**2** (Figure 3.1). Heating a solution of ( $\pm$ )-**2** in 1,2-dichlorobenzene-*d*<sub>4</sub> at a series of temperatures from 50–

**Scheme 3.2** Synthesis of model masked furfuryl ester **DA-model**.



110°C resulted in the appearance of peaks corresponding to *N*-methyl maleimide, consistent with the desired retro-[4+2] cycloaddition. The onset of reaction was observed at 90°C, with more rapid conversion (~17% in 15 minutes) visible at 100°C.

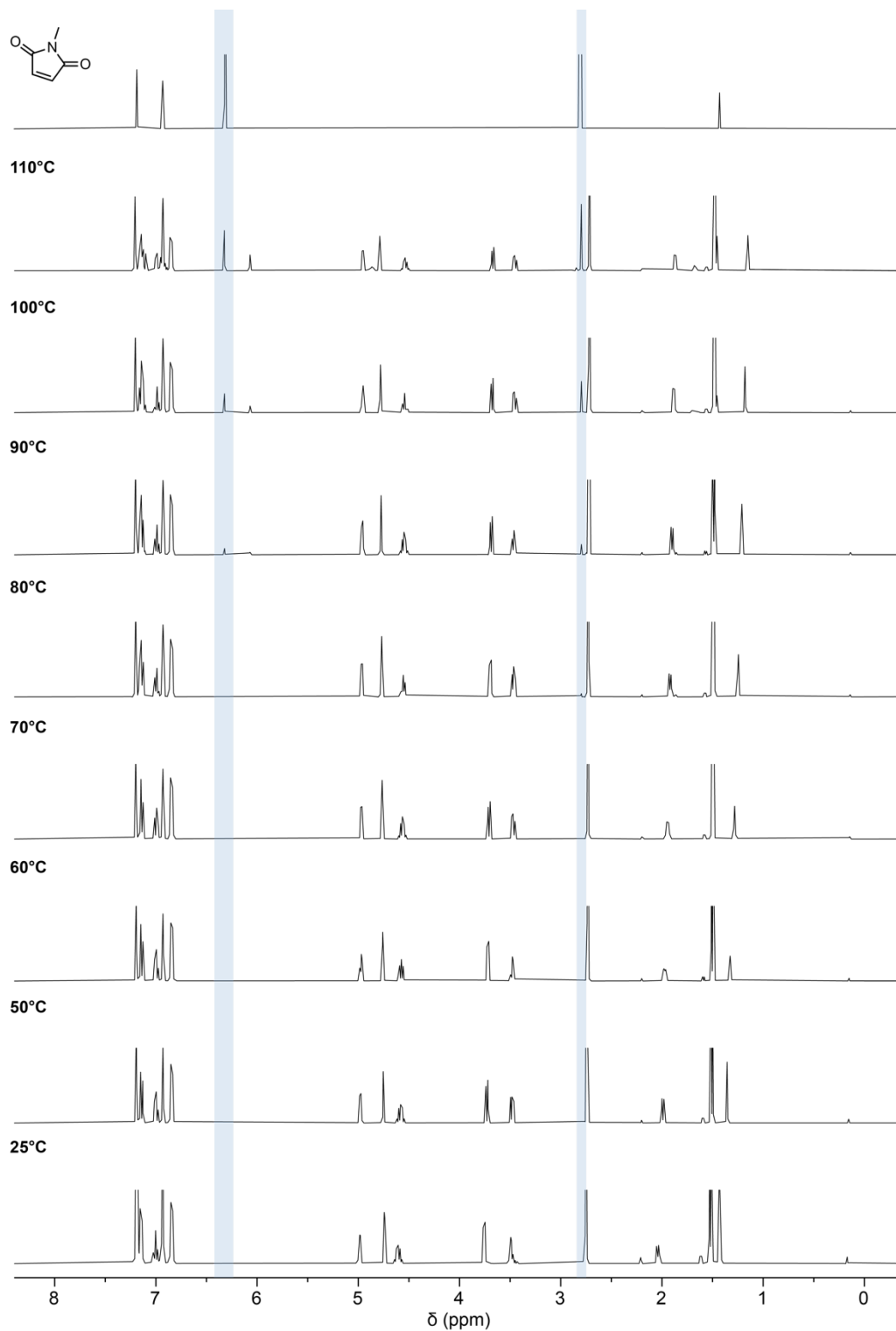


**Figure 3.1** Partial variable-temperature  $^1\text{H}$  NMR spectra (400 MHz) of a solution of ( $\pm$ )-**2** in 1,2-dichlorobenzene- $d_4$ . Spectra were collected for a single sample equilibrated at each set temperature for 15 minutes. Efficient cycloreversion (here defined as >15% conversion over 15 minutes) is observed starting at 100°C, with a new set of peaks emerging that match N-methyl maleimide (top trace).

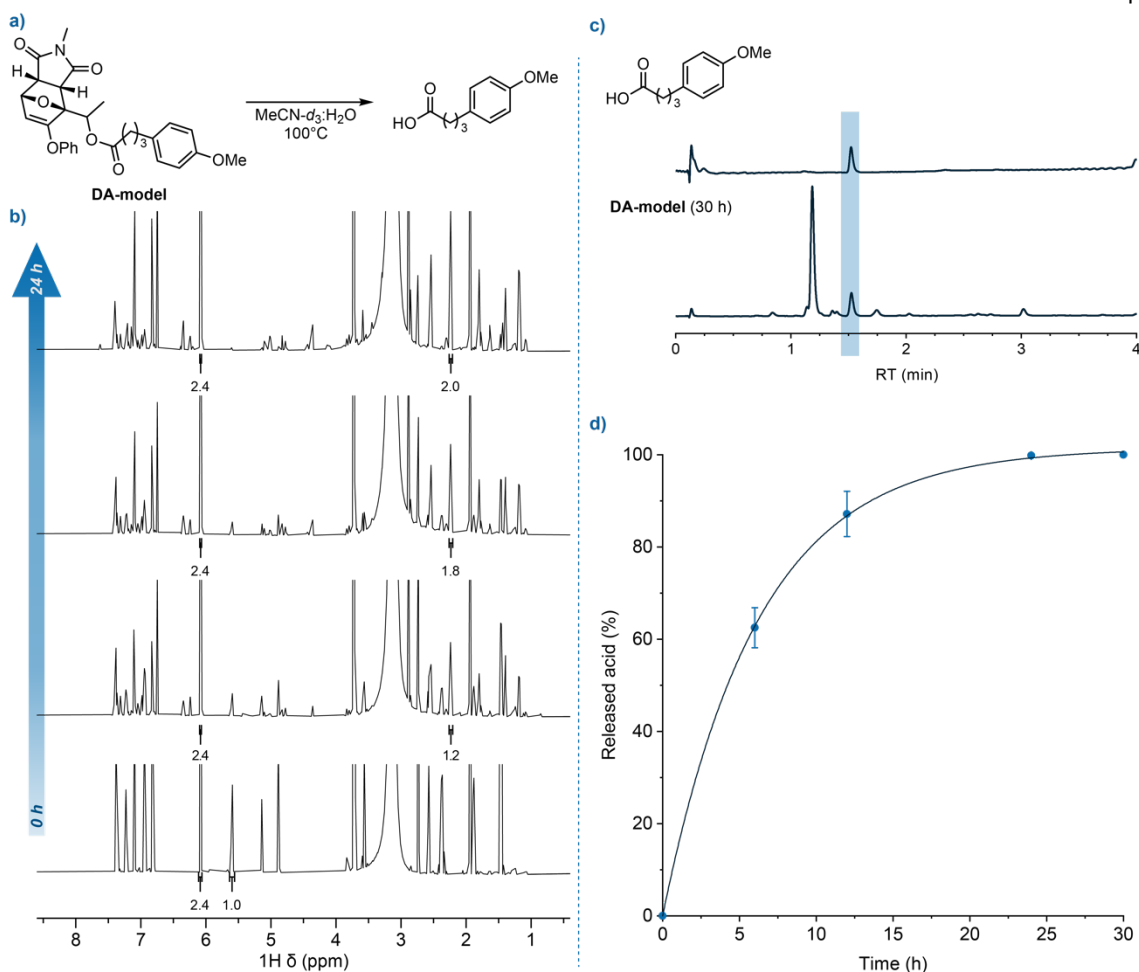


**Figure 3.2** Characterization of thermally triggered unmasking and carboxylic acid release from **DA-model**. (a) Heating **DA-model** in  $\text{MeCN-}d_3\text{:H}_2\text{O}$  (9:1) at  $100^\circ\text{C}$  generates 4-(4-methoxyphenyl)butyric acid; (b) partial  $^1\text{H}$  NMR spectra (600 MHz,  $\text{MeCN-}d_3\text{:H}_2\text{O}$ ) demonstrating full conversion of **DA-model** relative to internal standard 1,2,3-trimethoxybenzene (see SI for details); (c) LCMS chromatograms of **DA-model** after 30 h matching an independent standard of 4-(4-methoxyphenyl)butyric acid; (d) time course experiment tracking the yield of released acid by  $^1\text{H}$  NMR spectroscopy. Data points and error bars represent average values and standard deviation from 3 replicate experiments.

Heating solutions of **DA-model** at  $100^\circ\text{C}$  (10 mM, 9:1  $\text{MeCN-}d_3\text{:H}_2\text{O}$ , closed vial) resulted in complete cycloreversion and quantitative release of the carboxylic acid payload (Figure 3.2a).  $^1\text{H}$  NMR spectroscopy shows the disappearance of signals corresponding to **DA-model** and the emergence of peaks characteristic of the 4-(4-methoxyphenyl)butyric acid cargo (Figure 3.2b). The free acid is also identifiable in LC chromatograms collected after heating (Figure 3.2c). Fitting data from these time course experiments to a first-order rate expression provides an estimated half-life of acid release  $\sim 4.5$  h (Figure 3.2d). Importantly,

thermally inert analogue **hDA-model** remained intact over 24 h (Figure 3.3), confirming that acid release observed from **DA-model** does not result from hydrolysis.

Having identified suitable conditions for thermal unmasking in small molecule models, we next set out to incorporate masked furfuryl esters into polymers and explore their potential as a platform for thermally triggered post-polymerization modification of poly(methyl acrylates). Introducing hydrophilic carboxylic acid end groups to hydrophobic polymers results in substantial changes in viscoelastic properties and surface chemistry due to chain-end aggregation,<sup>177-179</sup> making these materials appealing targets for use as surfactants and dispersion agents.<sup>180</sup> As free carboxylic acids poison the Cu catalysts broadly used for controlled polymerization,<sup>181,182</sup> these groups are typically introduced through post-polymerization deprotection of alkyl ester initiators<sup>182-184</sup> using stoichiometric TFA or high temperatures (>200°C). Here, we envisioned that masked furfuryl esters could be leveraged as protecting groups on polymerization initiators, accessing  $\alpha$ -carboxylic acid functional polyacrylates under significantly milder post-polymerization deprotection conditions.

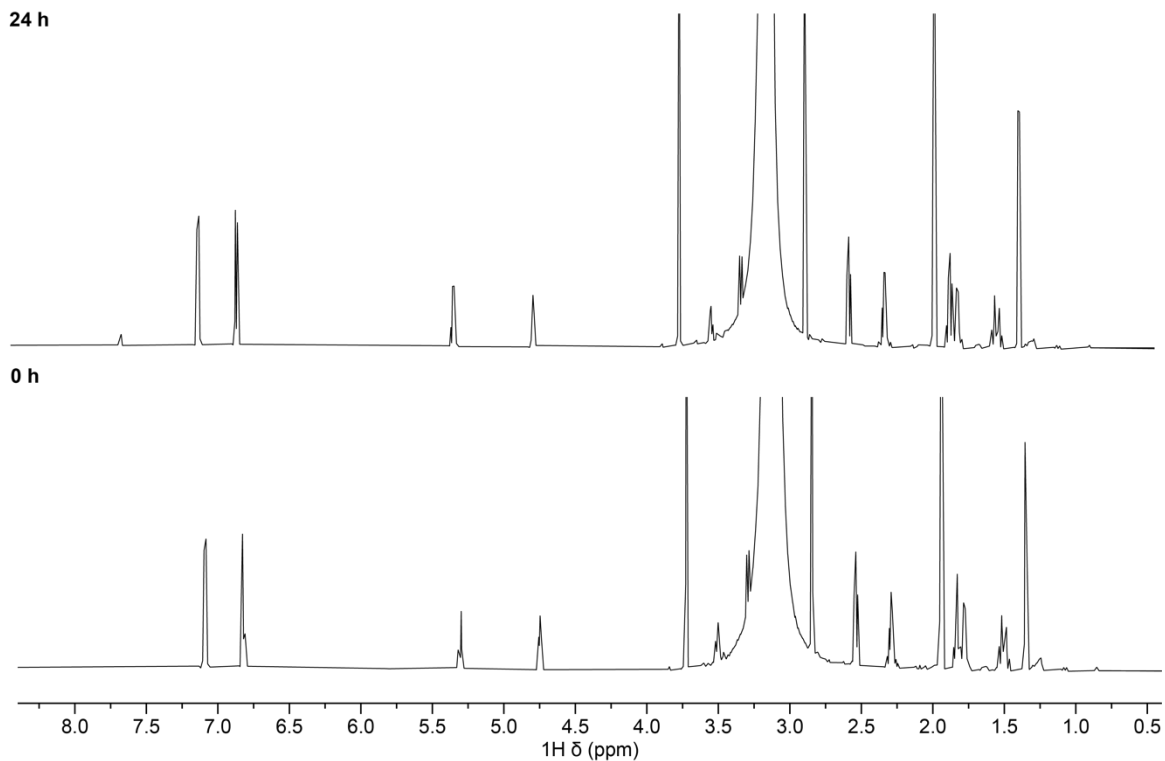


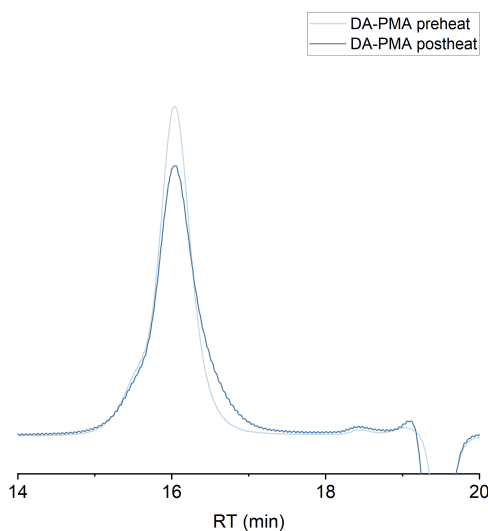
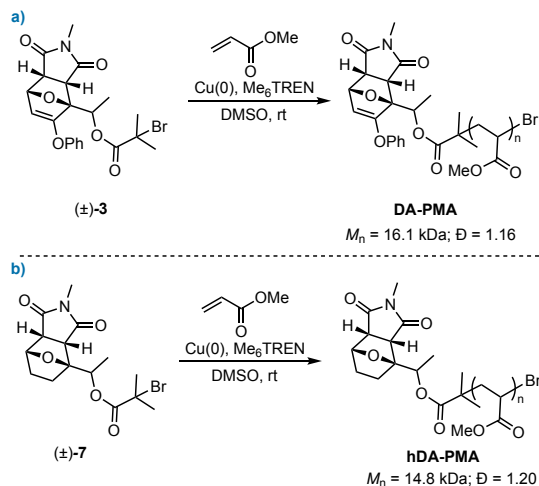
**Figure 3.3** Partial  $^1\text{H}$  NMR spectra (600 MHz) of control model **hDA-model** before and after 24 h of heating at 100°C in  $\text{MeCN-d}_3\text{:H}_2\text{O}$  (10 mM).

A masked furfuryl ester polymerization initiator was accessed in a single step by Steglich esterification of adduct ( $\pm$ )-**2** with  $\alpha$ -bromoisobutyryl bromide, then employed in the controlled radical polymerization of methyl acrylate with Cu wire/ $\text{Me}_6\text{TREN}$  in DMSO<sup>185</sup> to afford  $\alpha$ -masked polymer **DA-PMA** (Scheme 3.3a). An analogous approach was used to prepare thermally inert control **hDA-PMA** (Scheme 3.3b). Polymers with  $M_n \sim 15\text{--}20$  kDa were targeted for this study to demonstrate the

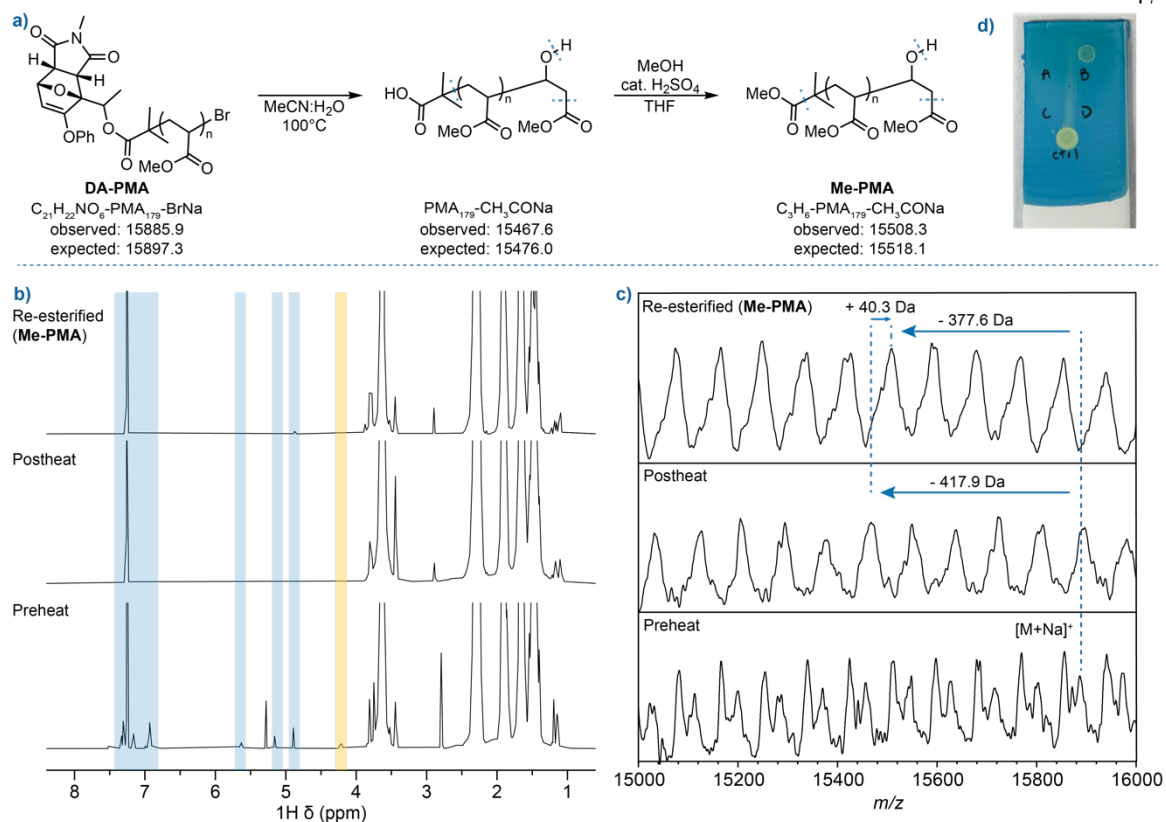
efficiency of end-group modification on high-molecular weight samples. **DA-PMA** was subjected to heating at 100°C in 9:1 MeCN:H<sub>2</sub>O (24 h, 50 mg/mL, Figure 3.5a) then precipitated in MeOH to remove small molecule byproducts from fragmentation of the furfuryl ester. GPC analysis of the purified polymer showed comparable molecular weight distributions before and after heating (Figure 3.4), and <sup>1</sup>H NMR showed the complete disappearance of signals corresponding to the original masked furfuryl ester (Figure 3.5a).

However, we also noted loss of the signal at  $\sim 4.25$  ppm corresponding to the resonance for the terminal methine proton adjacent to bromine, which we hypothesized arose from an elimination-substitution sequence resulting in loss of bromine and incorporation of a hydroxyl group. To model this unexpected reactivity, thermal control **hDA-PMA** was heated either alone or in the presence of 1 equivalent of isobutyric acid, to mimic the presence of the unmasked  $\alpha$  chain end. While NMR spectra acquired after heating appear

**Scheme 3.3** Synthesis of polymers bearing (a) a masked carboxylic acid and (b) a thermally inert hydrogenated Diels–Alder adduct at the  $\alpha$  chain end.



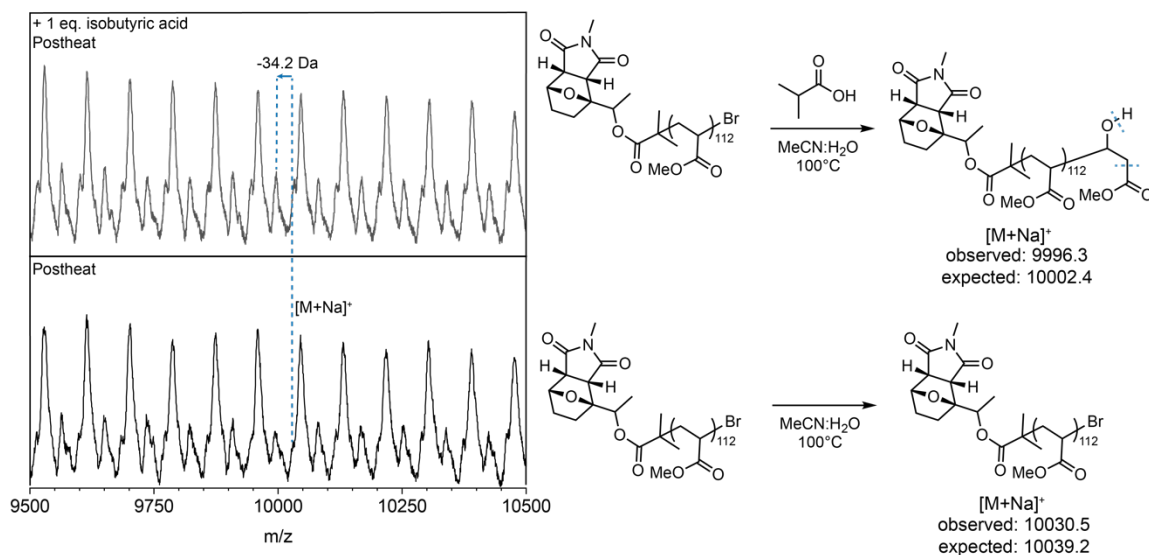
**Figure 3.4** GPC chromatograms (RI response) of DA-PMA before and after heating show minimal changes in molecular weight distribution.



**Figure 3.5** (a) Thermally triggered deprotection of  $\alpha$ -masked polymer **DA-PMA** in 9:1 MeCN:H<sub>2</sub>O (100°C, 24 h 50 mg/mL) and subsequent Fischer esterification to **Me-PMA**; (b) partial <sup>1</sup>H NMR spectra (400 MHz, CDCl<sub>3</sub>) of **DA-PMA** before and after heating and esterification showing removal of masked ester end group (in blue) and substitution of omega chain end (in purple); (c) MALDI-TOF mass spectra of **DA-PMA** with mass shifts corresponding to loss of  $\alpha$  and  $\omega$  endgroup after heating and installation of  $\alpha$  methyl ester following esterification; (d) bromocresol green stain testing of **DA-PMA** before heating (A), after heating (B) and after esterification to **Me-PMA** (C), thermally inert **hDA-PMA** after heating (D), and positive control 4-(4-methoxyphenylbutyric acid) (ctrl). Bromocresol green reacts selectively with carboxylic acids; a yellow spot indicates the presence of carboxylic acid.

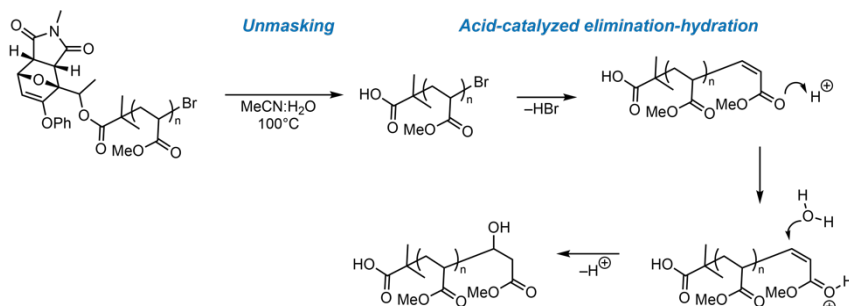
similar under both conditions, MALDI analysis shows additional detail supporting an elimination-substitution sequence. Heating **hDA-PMA** alone left both the hydrogenated Diels–Alder  $\alpha$  and  $\omega$  bromine end groups intact (Figure 3.6). Conversely, heating **hDA-PMA** in the presence of a carboxylic acid produced a peak distribution consistent with mass fragmentation of the hydroxyl end group expected from elimination and hydration (see Scheme 3.4 for additional details). Differential mass analysis of **DA-PMA** reveals a loss of 417.9 Da after heating, which agrees well with the 420 Da difference expected for formation of PMA–CH<sub>3</sub>CONa (Figure 3.5c, Figure 3.7, Figure 3.8). With the  $\omega$  terminal hydroxyl end group identified, we revisited the intended transformation at the  $\alpha$  chain end. While we were unable to observe the putative carboxylic acid end group directly by mass analysis, we

envisioned that re-esterification could furnish a product with greater resistance to end group fragmentation during ionization.



**Figure 3.6** Post-heat MALDI-TOF mass spectra of control polymer **hDA-PMA** show that the inert hDA ester linkage remains intact after heating, confirming the selectivity of the unmasking reaction observed for **DA-PMA**. Adding 1 equivalent of exogenous carboxylic acid during heating leaves the  $\alpha$  chain end intact and produces a mass shift of 34.2 Da. This shift agrees well with the expected 35.9 Da difference between a terminal bromide and the fragmentation pattern produced by  $\beta$ -alcohol substitution at the chain end. Importantly, the  $\alpha$  chain end is preserved during heating with exogenous acid, suggesting that activation and unmasking of **DA-PMA** is not autocatalytic.

**Scheme 3.4** Addition of exogenous carboxylic acid to thermally inert control **hDA-PMA** replicates the reactivity observed at the  $\omega$  chain end of **DA-PMA** after heating. One plausible mechanism is an elimination-hydration cascade of the terminal bromide catalyzed by the newly unveiled  $\alpha$ -carboxylic acid.



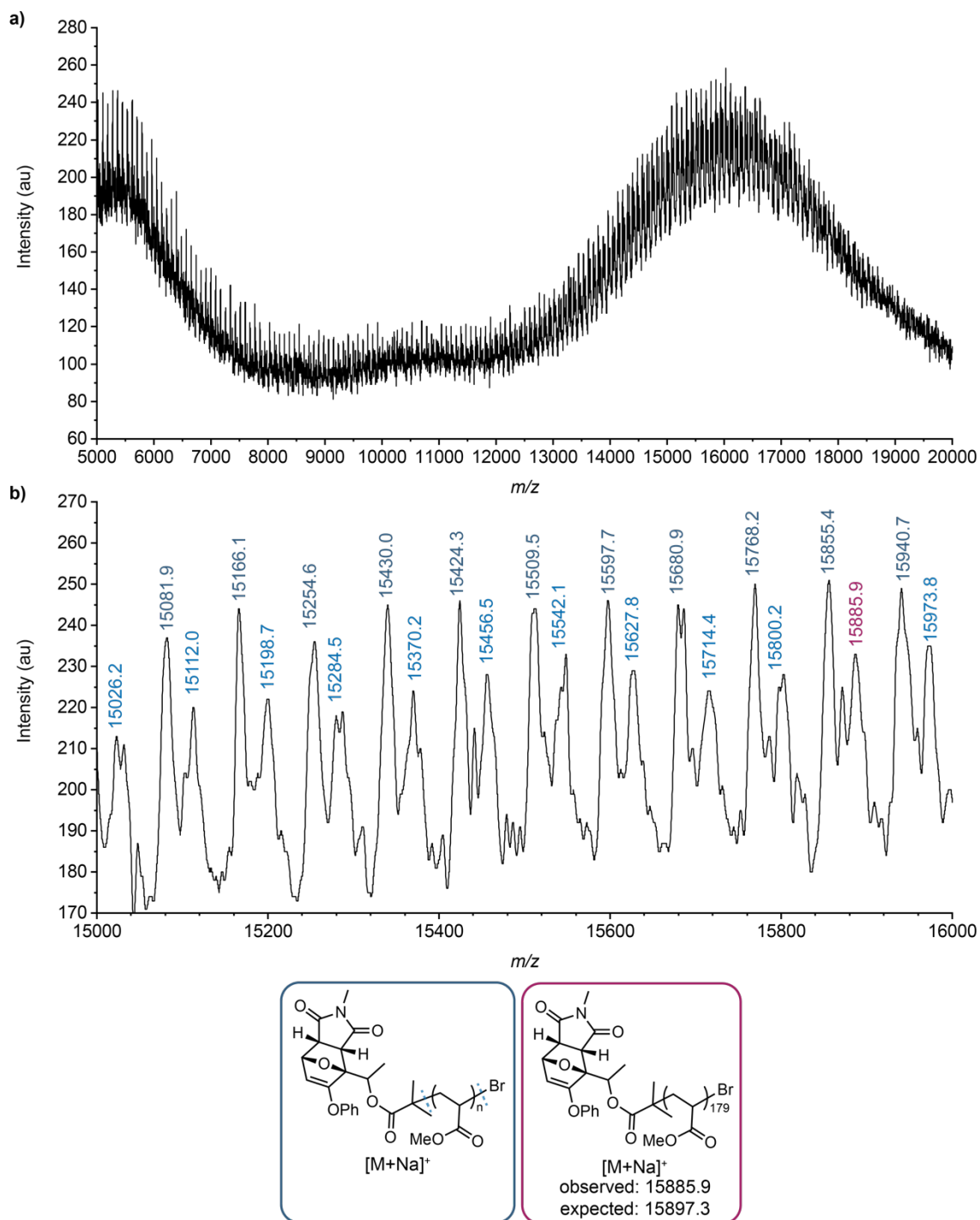


**Figure 3.7** Complete (a) and close-up (b) MALDI-TOF mass spectra of pristine DA-PMA.

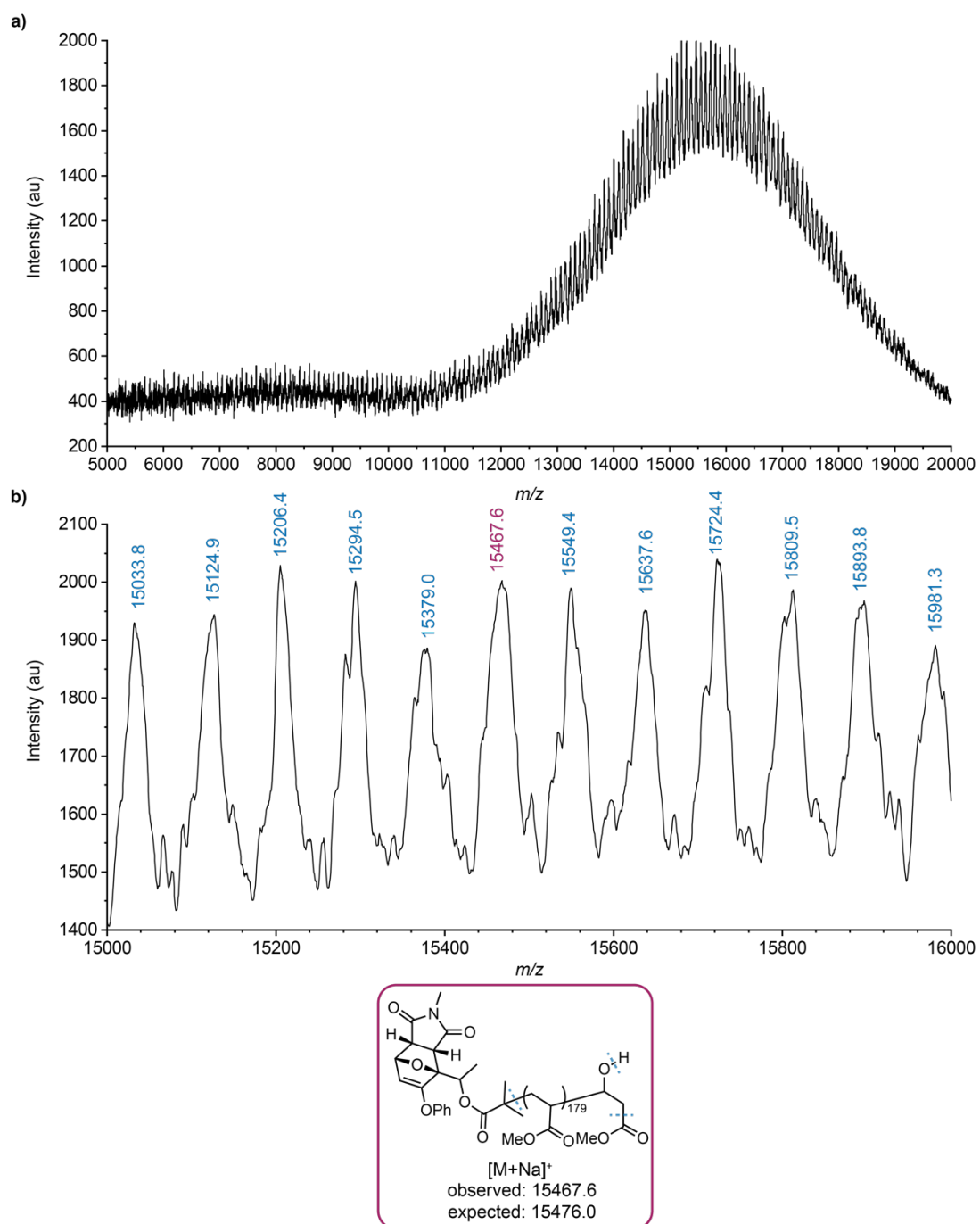


**Figure 3.8** Complete (a) and close-up (b) MALDI-TOF mass spectra of postheat DA-PMA.

**DA-PMA** was first heated to cleave the initial masked furfuryl ester end group, then subjected to Fischer esterification with methanol. MALDI-TOF mass analysis of the high-molecular weight region presented a single major mass population with a loss of 377.6 Da from pre-heat **DA-PMA**, in good agreement with the 378 Da difference expected for  $C_3H_6-PMA-CH_3CONa$  (Figure 3.5c). The lower-mass regions of the spectrum were more conclusive, showing a major mass distribution with the methyl ester intact (Figure 3.9). To further confirm the intended sequence of transformations, **DA-PMA** samples before and after heating and esterification were stained with an ethanolic solution of bromocresol green (Figure 3.5d, A–C). Postheat **hDA-PMA** and free 4-(4-methoxyphenyl)butyric acid were included as negative and positive controls, respectively (Figure 3.5d, D and ctrl). A color change is visible only for postheat **DA-PMA** and the free acid control, visualizing both the thermally triggered deprotection and subsequent re-esterification of an  $\alpha$ -chain-end carboxylic acid.

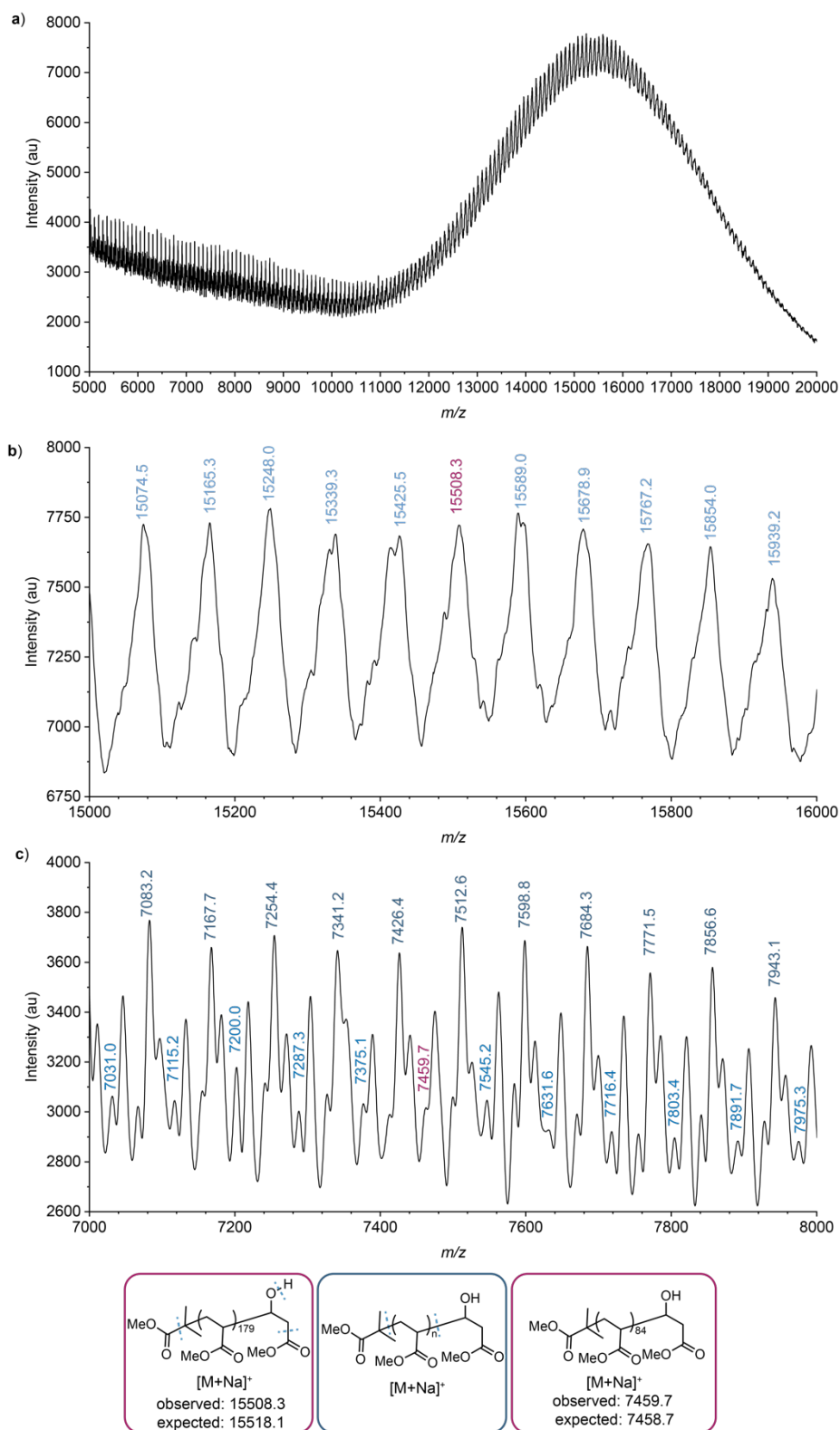


**Figure 3.9** Complete (a) and close-up (b, c) MALDI-TOF mass spectra of Me-PMA synthesized by esterification of postheat DA-PMA.

Having demonstrated the successful postpolymerization modification of chain-end carboxylic acids, we next targeted carboxylic acid pendant groups through the synthesis of masked acrylic acid copolymers. The incorporation of hydrophilic acrylic acid monomers into otherwise hydrophobic polyacrylates is highly desirable as a means to tune the material properties and morphology of the resulting copolymers, especially when paired with controlled polymerizations that enable precise user control over monomer ratios. Masked ester monomer **DAA** was prepared in one step from adduct ( $\pm$ )-**2**, then used directly in the controlled radical copolymerization of methyl acrylate with ethyl  $\alpha$ -bromoisobutyrate and Cu wire/ $\text{Me}_6\text{TREN}$  in DMSO. The resulting copolymer **p(MA-co-DAA)** achieved a calculated 22:1 MA:DAA monomer ratio by  $^1\text{H}$  NMR spectroscopy, in good agreement with the 20:1 ratio targeted. After heating at  $100^\circ\text{C}$  in 9:1 MeCN:H<sub>2</sub>O (50 mg/mL) for 24 h, the putative **p(MA-co-AA)** copolymer was precipitated into cold methanol.  $^1\text{H}$  NMR spectroscopy of the postheat polymer showed disappearance of the signals corresponding to the Diels–Alder-masked comonomer (Figure 3.11b). Substantial changes were observed in GPC traces collected before and after heating,

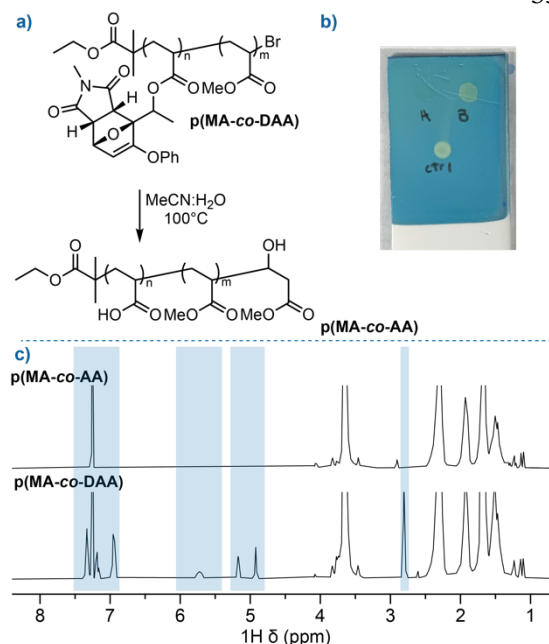


**Figure 3.11** (a) Thermally triggered deprotection of **p(MA-co-DAA)** to reveal **p(MA-co-AA)**; (b) partial  $^1\text{H}$  NMR spectra (400 MHz,  $\text{CDCl}_3$ ) of **p(MA-co-DAA)** and **p(MA-co-AA)** showing removal of the masked furfuryl ester; (c) bromocresol green stain testing **p(MA-co-DAA)** (A), **p(MA-co-AA)** (B) and positive control 4-(4-methoxyphenyl)butyric acid (ctrl).

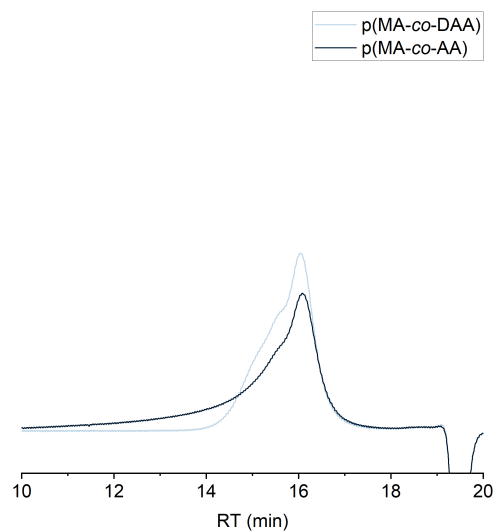


**Figure 3.10** GPC chromatograms (RI response) of pristine **p(MA-co-DAA)** and thermally unmasked **p(MA-co-AA)** demonstrate substantial changes in molecular weight distribution. These changes are consistent with the expected influence of added polar functional groups on  $R_g$ .

consistent with the expected influence of polar functional groups on chain extension (Figure 3.10). Staining with bromocresol green (Figure 3.11c) again provided visual confirmation of carboxylic acid formation and the successful synthesis of **p(MA-co-AA)**.

### 3.3 Conclusions

In summary, we have demonstrated the thermal reactivity of latent furfuryl esters and their applications as a platform for thermally gated post-polymerization modification. Using insights in molecular design gained from our group's prior work on mechanically gated 2-furylcarbinol derivatives, we designed a thermally gated cascade reaction in which the thermal retro-[4+2] cycloaddition of a furan-maleimide Diels–Alder adduct unmasks a latent furfuryl ester intermediate that subsequently decomposes to release a carboxylic acid. Capitalizing on the importance of polar functional groups to polymer properties, we used masked furfuryl ester initiators and monomers to access polyacrylates with chain-end or pendant carboxylic acid functional groups through post-polymerization deprotection. Masked furfuryl esters promote post-polymerization installation of carboxylic acid functionalities at substantially lower temperatures than existing thermolytic deprotections without the need for exogenous reagents. We anticipate that this platform will improve synthetic access to polar-functional polymers and broaden their potential scope of applications.

## BIBLIOGRAPHY

- (1) Cayuela Valencia, R. *The Future of the Chemical Industry by 2050*. Wiley, 2013.
- (2) Staudinger, H.; Bondy, H. F. Über Isopren und Kautschuk, 19. Mitteil.: Über die Molekülgröße des Kautschuks und der Balata. *Ber. Dtsch. Chem. Ges.* **1930**, *63*, 734–736.
- (3) Staudinger, H.; Leupold, E. O. Über Isopren und Kautschuk, 18. Mitteil.: Viscositäts-Untersuchungen an Balata. *Ber. Dtsch. Chem. Ges.* **1930**, *63*, 730–733.
- (4) Staudinger, H.; Heuer, W. Über hochpolymere Verbindungen, 93. Mitteil.: Über das Zerreißen der Faden-Moleküle des Poly-styrols. *Ber. Dtsch. Chem. Ges.* **1934**, *67*, 1159–1164.
- (5) Li, J.; Nagamani, C.; Moore, J. S. Polymer Mechanochemistry: From Destructive to Productive. *Acc. Chem. Res.* **2015**, *48*, 2181–2190.
- (6) Berkowski, K. L.; Potisek, S. L.; Hickenboth, C. R.; Moore, J. S. Ultrasound-Induced Site-Specific Cleavage of Azo-Functionalized Poly(ethylene glycol). *Macromolecules* **2005**, *38*, 8975–8978.
- (7) Klein, I. M.; Husic, C. C.; Kovács, D. P.; Choquette, N. J.; Robb, M. J. Validation of the CoGEF Method as a Predictive Tool for Polymer Mechanochemistry. *J. Am. Chem. Soc.* **2020**, *142*, 16364–16381.
- (8) Versaw, B. A.; McFadden, M. E.; Husic, C. C.; Robb, M. J. Designing naphthopyran mechanophores with tunable mechanochromic behavior. *Chem. Sci.* **2020**, *11*, 4525–4530.
- (9) Versaw, B. A.; Zeng, T.; Hu, X.; Robb, M. J. Harnessing the Power of Force: Development of Mechanophores for Molecular Release. *J. Am. Chem. Soc.* **2021**, *143*, 21461–21473.
- (10) Beyer, M. K.; Clausen-Schaumann, H. Mechanochemistry: The Mechanical Activation of Covalent Bonds. *Chem. Rev.* **2005**, *105*, 2921–2948.
- (11) Caruso, M. M.; Davis, D. A.; Shen, Q.; Odom, S. A.; Sottos, N. R.; White, S. R.; Moore, J. S. Mechanically-Induced Chemical Changes in Polymeric Materials. *Chem. Rev.* **2009**, *109*, 5755–5798.
- (12) Barber, R. W.; McFadden, M. E.; Hu, X.; Robb, M. J. Mechanochemically Gated Photoswitching: Expanding the Scope of Polymer Mechanochromism. *Synlett* **2019**, *30*, 1725–1732.
- (13) Potisek, S. L.; Davis, D. A.; Sottos, N. R.; White, S. R.; Moore, J. S. Mechanophore-Linked Addition Polymers. *J. Am. Chem. Soc.* **2007**, *129*, 13808–13809.
- (14) Davis, D. A.; Hamilton, A.; Yang, J.; Cremar, L. D.; Van Gough, D.; Potisek, S. L.; Ong, M. T.; Braun, P. V.; Martínez, T. J.; White, S. R.; Moore, J. S.; Sottos, N. R. Force-induced activation of covalent bonds in mechanoresponsive polymeric materials. *Nature* **2009**, *459*, 68–72.
- (15) Robb, M. J.; Kim, T. A.; Halmes, A. J.; White, S. R.; Sottos, N. R.; Moore, J. S. Regioisomer-Specific Mechanochromism of Naphthopyran in Polymeric Materials. *J. Am. Chem. Soc.* **2016**, *138*, 12328–12331.

- (16) McFadden, M. E.; Robb, M. J. Force-Dependent Multicolor Mechanochromism from a Single Mechanophore. *J. Am. Chem. Soc.* **2019**, *141*, 11388–11392.
- (17) Zhang, H.; Gao, F.; Cao, X.; Li, Y.; Xu, Y.; Weng, W.; Boulatov, R. Mechanochromism and Mechanical-Force-Triggered Cross-Linking from a Single Reactive Moiety Incorporated into Polymer Chains. *Angew. Chem. Int. Ed.* **2016**, *55*, 3040–3044.
- (18) Wang, Z.; Ma, Z.; Wang, Y.; Xu, Z.; Luo, Y.; Wei, Y.; Jia, X. A Novel Mechanochromic and Photochromic Polymer Film: When Rhodamine Joins Polyurethane. *Adv. Mater.* **2015**, *27*, 6469–6474.
- (19) Wang, T.; Zhang, N.; Dai, J.; Li, Z.; Bai, W.; Bai, R. Novel Reversible Mechanochromic Elastomer with High Sensitivity: Bond Scission and Bending-Induced Multicolor Switching. *ACS Appl. Mater. Interfaces* **2017**, *9*, 11874–11881.
- (20) Chen, Z.; Mercer, J. A. M.; Zhu, X.; Romaniuk, J. A. H.; Pfattner, R.; Cegelski, L.; Martinez, T. J.; Burns, N. Z.; Xia, Y. Mechanochemical unzipping of insulating polyadderene to semiconducting polyacetylene. *Science* **2017**, *357*, 475–479.
- (21) Yang, J.; Horst, M.; Romaniuk, J. A. H.; Jin, Z.; Cegelski, L.; Xia, Y. Benzoladderene Mechanophores: Synthesis, Polymerization, and Mechanochemical Transformation. *J. Am. Chem. Soc.* **2019**, *141*, 6479–6483.
- (22) Imato, K.; Irie, A.; Kosuge, T.; Ohishi, T.; Nishihara, M.; Takahara, A.; Otsuka, H. Mechanophores with a Reversible Radical System and Freezing-Induced Mechanochemistry in Polymer Solutions and Gels. *Angew. Chem. Int. Ed.* **2015**, *54*, 6168–6172.
- (23) Verstraeten, F.; Göstl, R.; Sijbesma, R. P. Stress-induced colouration and crosslinking of polymeric materials by mechanochemical formation of triphenylimidazolyl radicals. *Chem. Commun.* **2016**, *52*, 8608–8611.
- (24) Sumi, T.; Goseki, R.; Otsuka, H. Tetraarylsuccinonitriles as mechanochromophores to generate highly stable luminescent carbon-centered radicals. *Chem. Commun.* **2017**, *53*, 11885–11888.
- (25) Ishizuki, K.; Oka, H.; Aoki, D.; Goseki, R.; Otsuka, H. Mechanochromic Polymers That Turn Green Upon the Dissociation of Diarylbibenzothiophenonyl: The Missing Piece toward Rainbow Mechanochromism. *Chem. – Eur. J.* **2018**, *24*, 3170–3173.
- (26) Sakai, H.; Sumi, T.; Aoki, D.; Goseki, R.; Otsuka, H. Thermally Stable Radical-Type Mechanochromic Polymers Based on Difluorenylsuccinonitrile. *ACS Macro Lett.* **2018**, *7*, 1359–1363.
- (27) Van Gemert, B. Benzo and Naphthopyrans (Chromenes). In *Organic Photochromic and Thermochromic Compounds: Volume 1: Main Photochromic Families*; Crano, J. C., Guglielmetti, R. J., Eds.; Topics in Applied Chemistry; Springer US: Boston, MA, 2002; pp 111–140.
- (28) Gabbutt, C. D.; Heron, B. M.; Instone, A. C. Control of the Fading Properties of Photochromic 3,3-Diaryl-3H-naphthop[2,1-b]pyrans. *Heterocycles* **2003**, *60*, 843–855.
- (29) Gabbutt, C. D.; Heron, B. M.; Instone, A. C.; Horton, P. N.; Hursthouse, M. B. Synthesis and photochromic properties of substituted 3H-naphtho[2,1-b]pyrans. *Tetrahedron* **2005**, *61*, 463–471.
- (30) Van Gemert, B.; Bergomi, M. P. Photochromic naphthopyran compounds. US5066818A, November 19, 1991.
- (31) Van Gemert, B.; Bergomi, M.; Knowles, D. Photochromism of Diarylnaphthopyrans. *Mol. Cryst. Liq. Cryst. A* **1994**, *246*, 67–73.

- (32) Beyer, M. K. The mechanical strength of a covalent bond calculated by density functional theory. *J. Chem. Phys.* **2000**, *112*, 7307–7312.
- (33) Ottavi, G.; Favaro, G.; Malatesta, V. Spectrokinetic study of 2,2-diphenyl-5,6-benzo(2H)chromene: a thermoreversible and photoreversible photochromic system. *J. Photochem. Photobiol. A* **1998**, *115*, 123–128.
- (34) Delbaere, S.; Luccioni-Houze, B.; Bochu, C.; Teral, Y.; Campredon, M.; Vermeersch, G. Kinetic and structural studies of the photochromic process of 3 H -naphthopyrans by UV and NMR spectroscopy. *J. Chem. Soc. Perkin Trans. 2* **1998**, *0*, 1153–1158.
- (35) Delbaere, S.; Micheau, J.-C.; Teral, Y.; Bochu, C.; Campredon, M.; Vermeersch, G. NMR Structural and Kinetic Assignment of Fluoro-3H-naphthopyran Photomerocyanines¶. *Photochem. Photobiol.* **2001**, *74*, 694–699.
- (36) Gossweiler, G. R.; Hewage, G. B.; Soriano, G.; Wang, Q.; Welshofer, G. W.; Zhao, X.; Craig, S. L. Mechanochemical Activation of Covalent Bonds in Polymers with Full and Repeatable Macroscopic Shape Recovery. *ACS Macro Lett.* **2014**, *3*, 216–219.
- (37) Sriprom, W.; Néel, M.; Gabbutt, C. D.; Heron, B. M.; Perrier, S. Tuning the color switching of naphthopyrans via the control of polymeric architectures. *J. Mater. Chem.* **2007**, *17*, 1885–1893.
- (38) Malic, N.; Campbell, J. A.; Evans, R. A. Superior Photochromic Performance of Naphthopyrans in a Rigid Host Matrix Using Polymer Conjugation: Fast, Dark, and Tunable. *Macromolecules* **2008**, *41*, 1206–1214.
- (39) Evans, R. A.; Hanley, T. L.; Skidmore, M. A.; Davis, T. P.; Such, G. K.; Yee, L. H.; Ball, G. E.; Lewis, D. A. The generic enhancement of photochromic dye switching speeds in a rigid polymer matrix. *Nat. Mater.* **2005**, *4*, 249–253.
- (40) Kim, T. A.; Robb, M. J.; Moore, J. S.; White, S. R.; Sottos, N. R. Mechanical Reactivity of Two Different Spiropyran Mechanophores in Polydimethylsiloxane. *Macromolecules* **2018**, *51*, 9177–9183.
- (41) Ishizuki, K.; Aoki, D.; Goseki, R.; Otsuka, H. Multicolor Mechanochromic Polymer Blends That Can Discriminate between Stretching and Grinding. *ACS Macro Lett.* **2018**, *7*, 556–560.
- (42) Kosuge, T.; Zhu, X.; Lau, V. M.; Aoki, D.; Martinez, T. J.; Moore, J. S.; Otsuka, H. Multicolor Mechanochromism of a Polymer/Silica Composite with Dual Distinct Mechanophores. *J. Am. Chem. Soc.* **2019**, *141*, 1898–1902.
- (43) Peterson, G. I.; Larsen, M. B.; Ganter, M. A.; Storti, D. W.; Boydston, A. J. 3D-Printed Mechanochromic Materials. *ACS Appl. Mater. Interfaces* **2015**, *7*, 577–583.
- (44) Ribas-Arino, J.; Shiga, M.; Marx, D. Understanding Covalent Mechanochemistry. *Angew. Chem. Int. Ed.* **2009**, *48*, 4190–4193.
- (45) Stauch, T.; Dreuw, A. Quantum Chemical Strain Analysis For Mechanochemical Processes. *Acc. Chem. Res.* **2017**, *50*, 1041–1048.
- (46) Roessler, A. G.; Zimmerman, P. M. Examining the Ways To Bend and Break Reaction Pathways Using Mechanochemistry. *J. Phys. Chem. C* **2018**, *122*, 6996–7004.
- (47) Hickenboth, C. R.; Moore, J. S.; White, S. R.; Sottos, N. R.; Baudry, J.; Wilson, S. R. Biasing reaction pathways with mechanical force. *Nature* **2007**, *446*, 423–427.
- (48) Wang, J.; Kouznetsova, T. B.; Niu, Z.; Ong, M. T.; Klukovich, H. M.; Rheingold, A. L.; Martinez, T. J.; Craig, S. L. Inducing and quantifying forbidden reactivity with single-molecule polymer mechanochemistry. *Nat. Chem.* **2015**, *7*, 323–327.

- (49) Chen, Y.; Mellot, G.; Luijk, D. van; Creton, C.; Sijbesma, R. P. Mechanochemical tools for polymer materials. *Chem. Soc. Rev.* **2021**, *50*, 4100–4140.
- (50) Ghanem, M. A.; Basu, A.; Behrou, R.; Boechler, N.; Boydston, A. J.; Craig, S. L.; Lin, Y.; Lynde, B. E.; Nelson, A.; Shen, H.; Storti, D. W. The role of polymer mechanochemistry in responsive materials and additive manufacturing. *Nat. Rev. Mater.* **2021**, *6*, 84–98.
- (51) Qian, H.; Purwanto, N. S.; Ivanoff, D. G.; Halmes, A. J.; Sottos, N. R.; Moore, J. S. Fast, reversible mechanochromism of regioisomeric oxazine mechanophores: Developing in situ responsive force probes for polymeric materials. *Chem* **2021**, *7*, 1080–1091.
- (52) Göstl, R.; Sijbesma, R. P.  $\pi$ -extended anthracenes as sensitive probes for mechanical stress. *Chem. Sci.* **2016**, *7*, 370–375.
- (53) Baumann, C.; Stratigaki, M.; Centeno, S. P.; Göstl, R. Multicolor Mechanofluorophores for the Quantitative Detection of Covalent Bond Scission in Polymers. *Angew. Chem. Int. Ed.* **2021**, *60*, 13287–13293.
- (54) Chen, Y.; Spiering, A. J. H.; Karthikeyan, S.; Peters, G. W. M.; Meijer, E. W.; Sijbesma, R. P. Mechanically induced chemiluminescence from polymers incorporating a 1,2-dioxetane unit in the main chain. *Nat. Chem.* **2012**, *4*, 559–562.
- (55) Piermattei, A.; Karthikeyan, S.; Sijbesma, R. P. Activating catalysts with mechanical force. *Nat. Chem.* **2009**, *1*, 133–137.
- (56) Michael, P.; Binder, W. H. A Mechanochemically Triggered “Click” Catalyst. *Angew. Chem. Int. Ed.* **2015**, *54*, 13918–13922.
- (57) Robb, M. J.; Moore, J. S. A Retro-Staudinger Cycloaddition: Mechanochemical Cycloelimination of a  $\beta$ -Lactam Mechanophore. *J. Am. Chem. Soc.* **2015**, *137*, 10946–10949.
- (58) Wang, J.; Piskun, I.; Craig, S. L. Mechanochemical Strengthening of a Multi-mechanophore Benzocyclobutene Polymer. *ACS Macro Lett.* **2015**, *4*, 834–837.
- (59) Ramirez, A. L. B.; Kean, Z. S.; Orlicki, J. A.; Champhekar, M.; Elsagr, S. M.; Krause, W. E.; Craig, S. L. Mechanochemical strengthening of a synthetic polymer in response to typically destructive shear forces. *Nat. Chem.* **2013**, *5*, 757–761.
- (60) Zhang, Y.; Yu, J.; Bomba, H. N.; Zhu, Y.; Gu, Z. Mechanical Force-Triggered Drug Delivery. *Chem. Rev.* **2016**, *116*, 12536–12563.
- (61) Kim, G.; Lau, V. M.; Halmes, A. J.; Oelze, M. L.; Moore, J. S.; Li, K. C. High-intensity focused ultrasound-induced mechanochemical transduction in synthetic elastomers. *Proc. Natl. Acad. Sci. USA* **2019**, *116*, 10214–10222.
- (62) Lee, K. Y.; Peters, M. C.; Mooney, D. J. Controlled Drug Delivery from Polymers by Mechanical Signals. *Adv. Mater.* **2001**, *13*, 837–839.
- (63) Xiao, L.; Zhu, J.; David Londono, J.; J. Pochan, D.; Jia, X. Mechano-responsive hydrogels crosslinked by block copolymer micelles. *Soft Matter* **2012**, *8*, 10233–10237.
- (64) Lin, H.-Y.; Thomas, J. L. PEG–Lipids and Oligo(ethylene glycol) Surfactants Enhance the Ultrasonic Permeabilizability of Liposomes. *Langmuir* **2003**, *19*, 1098–1105.
- (65) Izawa, H.; Kawakami, K.; Sumita, M.; Tateyama, Y.; Hill, J. P.; Ariga, K.  $\beta$ -Cyclodextrin-crosslinked alginate gel for patient-controlled drug delivery systems: regulation of host–guest interactions with mechanical stimuli. *J. Mater. Chem. B* **2013**, *1*, 2155–2161.
- (66) Huo, S.; Zhao, P.; Shi, Z.; Zou, M.; Yang, X.; Warszawik, E.; Loznik, M.; Göstl, R.; Herrmann, A. Mechanochemical bond scission for the activation of drugs. *Nat. Chem.* **2021**, *13*, 131–139.

- (67) Küng, R.; Pausch, T.; Rasch, D.; Göstl, R.; Schmidt, B. M. Mechanochemical Release of Non-Covalently Bound Guests from a Polymer-Decorated Supramolecular Cage. *Angew. Chem. Int. Ed.* **2021**, *60*, 13626–13630.
- (68) White, S. R.; Sottos, N. R.; Geubelle, P. H.; Moore, J. S.; Kessler, M. R.; Sriram, S. R.; Brown, E. N.; Viswanathan, S. Autonomic healing of polymer composites. *Nature* **2001**, *409*, 794–797.
- (69) Esser-Kahn, A. P.; Odom, S. A.; Sottos, N. R.; White, S. R.; Moore, J. S. Triggered Release from Polymer Capsules. *Macromolecules* **2011**, *44*, 5539–5553.
- (70) Patrick, J. F.; Robb, M. J.; Sottos, N. R.; Moore, J. S.; White, S. R. Polymers with autonomous life-cycle control. *Nature* **2016**, *540*, 363–370.
- (71) Wang, J.; Kaplan, J. A.; Colson, Y. L.; Grinstaff, M. W. Mechanoresponsive materials for drug delivery: Harnessing forces for controlled release. *Adv. Drug Deliv. Rev.* **2017**, *108*, 68–82.
- (72) Kaminskas, L. M.; McLeod, V. M.; Porter, C. J. H.; Boyd, B. J. Association of Chemotherapeutic Drugs with Dendrimer Nanocarriers: An Assessment of the Merits of Covalent Conjugation Compared to Noncovalent Encapsulation. *Mol. Pharmaceutics* **2012**, *9*, 355–373.
- (73) Stratigaki, M.; Göstl, R. Methods for Exerting and Sensing Force in Polymer Materials Using Mechanophores. *ChemPlusChem* **2020**, cplu.201900737.
- (74) Wiggins, K. M.; Brantley, J. N.; Bielawski, C. W. Methods for activating and characterizing mechanically responsive polymers. *Chem. Soc. Rev.* **2013**, *42*, 7130–7147.
- (75) Noh, J.; Peterson, G. I.; Choi, T.-L. Mechanochemical Reactivity of Bottlebrush and Dendronized Polymers: Solid vs. Solution States. *Angew. Chem. Int. Ed.* **2021**, *60*, 18651–18659.
- (76) Suslick, K. S. Mechanochemistry and sonochemistry: concluding remarks. *Faraday Discuss.* **2014**, *170*, 411–422.
- (77) O'Neill, R. T.; Boulatov, R. The many flavours of mechanochemistry and its plausible conceptual underpinnings. *Nat. Rev. Chem.* **2021**, *5*, 148–167.
- (78) Liang, J.; Fernández, J. M. Mechanochemistry: One Bond at a Time. *ACS Nano* **2009**, *3*, 1628–1645.
- (79) Gossweiler, G. R.; Kouznetsova, T. B.; Craig, S. L. Force-Rate Characterization of Two Spiropyran-Based Molecular Force Probes. *J. Am. Chem. Soc.* **2015**, *137*, 6148–6151.
- (80) Barbee, M. H.; Kouznetsova, T.; Barrett, S. L.; Gossweiler, G. R.; Lin, Y.; Rastogi, S. K.; Brittain, W. J.; Craig, S. L. Substituent Effects and Mechanism in a Mechanochemical Reaction. *J. Am. Chem. Soc.* **2018**, *140*, 12746–12750.
- (81) Bowser, B. H.; Craig, S. L. Empowering mechanochemistry with multi-mechanophore polymer architectures. *Polym. Chem.* **2018**, *9*, 3583–3593.
- (82) Suslick, K. S. Sonochemistry. *Science* **1990**, *247*, 1439–1445.
- (83) Basedow, A. M.; Ebert, K. H. Ultrasonic degradation of polymers in solution. In *Physical Chemistry; Advances in Polymer Science*; Springer: Berlin, Heidelberg, 1977; pp 83–148.
- (84) Cravotto, G.; Cintas, P. Forcing and Controlling Chemical Reactions with Ultrasound. *Angew. Chem. Int. Ed.* **2007**, *46*, 5476–5478.
- (85) May, P. A.; Moore, J. S. Polymer mechanochemistry: techniques to generate molecular force via elongational flows. *Chem. Soc. Rev.* **2013**, *42*, 7497–7506.
- (86) Odell, J. A.; Keller, A. Flow-induced chain fracture of isolated linear macromolecules in solution. *J. Polym. Sci., Part B: Polym. Phys.* **1986**, *24*, 1889–1916.

- (87) Lenhardt, J. M.; Black Ramirez, A. L.; Lee, B.; Kouznetsova, T. B.; Craig, S. L. Mechanistic Insights into the Sonochemical Activation of Multimechanophore Cyclopropanated Polybutadiene Polymers. *Macromolecules* **2015**, *48*, 6396–6403.
- (88) Mitragotri, S. Healing sound: the use of ultrasound in drug delivery and other therapeutic applications. *Nat. Rev. Drug. Discov.* **2005**, *4*, 255–260.
- (89) Tong, R.; Lu, X.; Xia, H. A facile mechanophore functionalization of an amphiphilic block copolymer towards remote ultrasound and redox dual stimulus responsiveness. *Chem. Commun.* **2014**, *50*, 3575–3578.
- (90) Diesendruck, C. E.; Steinberg, B. D.; Sugai, N.; Silberstein, M. N.; Sottos, N. R.; White, S. R.; Braun, P. V.; Moore, J. S. Proton-Coupled Mechanochemical Transduction: A Mechanogenerated Acid. *J. Am. Chem. Soc.* **2012**, *134*, 12446–12449.
- (91) Lin, Y.; Kouznetsova, T. B.; Craig, S. L. A Latent Mechanoacid for Time-Stamped Mechanochromism and Chemical Signaling in Polymeric Materials. *J. Am. Chem. Soc.* **2020**, *142*, 99–103.
- (92) Lenhardt, J. M.; Black, A. L.; Craig, S. L. gem-Dichlorocyclopropanes as Abundant and Efficient Mechanophores in Polybutadiene Copolymers under Mechanical Stress. *J. Am. Chem. Soc.* **2009**, *131*, 10818–10819.
- (93) Groote, R.; Jakobs, R. T. M.; Sijbesma, R. P. Mechanochemistry: forcing latent catalysts into action. *Polym. Chem.* **2013**, *4*, 4846.
- (94) Paulusse, J. M. J.; Sijbesma, R. P. Reversible Mechanochemistry of a PdII Coordination Polymer. *Angew. Chem. Int. Ed.* **2004**, *43*, 4460–4462.
- (95) Yount, W. C.; Loveless, D. M.; Craig, S. L. Small-Molecule Dynamics and Mechanisms Underlying the Macroscopic Mechanical Properties of Coordinatively Cross-Linked Polymer Networks. *J. Am. Chem. Soc.* **2005**, *127*, 14488–14496.
- (96) Kersey, F. R.; Yount, W. C.; Craig, S. L. Single-Molecule Force Spectroscopy of Bimolecular Reactions: System Homology in the Mechanical Activation of Ligand Substitution Reactions. *J. Am. Chem. Soc.* **2006**, *128*, 3886–3887.
- (97) Paulusse, J. M. J.; Sijbesma, R. P. Selectivity of mechanochemical chain scission in mixed palladium(II) and platinum(II) coordination polymers. *Chem. Commun.* **2008**, No. 37, 4416.
- (98) Karthikeyan, S.; Potisek, S. L.; Piermattei, A.; Sijbesma, R. P. Highly Efficient Mechanochemical Scission of Silver-Carbene Coordination Polymers. *J. Am. Chem. Soc.* **2008**, *130*, 14968–14969.
- (99) Wei, K.; Gao, Z.; Liu, H.; Wu, X.; Wang, F.; Xu, H. Mechanical Activation of Platinum–Acetylide Complex for Olefin Hydrosilylation. *ACS Macro Lett.* **2017**, *6*, 1146–1150.
- (100) Jakobs, R. T. M.; Ma, S.; Sijbesma, R. P. Mechanochemical Polymerization and Cross-Linking in a Polymeric Matrix. *ACS Macro Lett.* **2013**, *2*, 613–616.
- (101) Balkenende, D. W. R.; Coulibaly, S.; Balog, S.; Simon, Y. C.; Fiore, G. L.; Weder, C. Mechanochemistry with Metallosupramolecular Polymers. *J. Am. Chem. Soc.* **2014**, *136*, 10493–10498.
- (102) Di Giannantonio, M.; Ayer, M. A.; Verde-Sesto, E.; Lattuada, M.; Weder, C.; Fromm, K. M. Triggered Metal Ion Release and Oxidation: Ferrocene as a Mechanophore in Polymers. *Angew. Chem. Int. Ed.* **2018**, *57*, 11445–11450.
- (103) Sha, Y.; Zhang, Y.; Xu, E.; Wang, Z.; Zhu, T.; Craig, S. L.; Tang, C. Quantitative and Mechanistic Mechanochemistry in Ferrocene Dissociation. *ACS Macro Lett.* **2018**, *7*, 1174–1179.

- (104) Sha, Y.; Zhang, Y.; Xu, E.; McAlister, C. W.; Zhu, T.; Craig, S. L.; Tang, C. Generalizing metallocene mechanochemistry to ruthenocene mechanophores. *Chem. Sci.* **2019**, *10*, 4959–4965.
- (105) Zhang, Y.; Wang, Z.; Kouznetsova, T. B.; Sha, Y.; Xu, E.; Shannahan, L.; Fermen-Coker, M.; Lin, Y.; Tang, C.; Craig, S. L. Distal conformational locks on ferrocene mechanophores guide reaction pathways for increased mechanochemical reactivity. *Nat. Chem.* **2021**, *13*, 56–62.
- (106) Cha, Y.; Zhu, T.; Sha, Y.; Lin, H.; Hwang, J.; Seraydarian, M.; Craig, S. L.; Tang, C. Mechanochemistry of Cationic Cobaltocenium Mechanophore. *J. Am. Chem. Soc.* **2021**, *143*, 11871–11878.
- (107) Razgoniaev, A. O.; Glasstetter, L. M.; Kouznetsova, T. B.; Hall, K. C.; Horst, M.; Craig, S. L.; Franz, K. J. Single-Molecule Activation and Quantification of Mechanically Triggered Palladium–Carbene Bond Dissociation. *J. Am. Chem. Soc.* **2021**, *143*, 1784–1789.
- (108) Lee, B.; Niu, Z.; Wang, J.; Slebodnick, C.; Craig, S. L. Relative Mechanical Strengths of Weak Bonds in Sonochemical Polymer Mechanochemistry. *J. Am. Chem. Soc.* **2015**, *137*, 10826–10832.
- (109) Larsen, M. B.; Boydston, A. J. “Flex-Activated” Mechanophores: Using Polymer Mechanochemistry To Direct Bond Bending Activation. *J. Am. Chem. Soc.* **2013**, *135*, 8189–8192.
- (110) Larsen, M. B.; Boydston, A. J. Successive Mechanochemical Activation and Small Molecule Release in an Elastomeric Material. *J. Am. Chem. Soc.* **2014**, *136*, 1276–1279.
- (111) Shen, H.; Larsen, M. B.; Roessler, A.; Zimmerman, P.; Boydston, A. J. Mechanochemical Release of N-heterocyclic Carbenes from Flex-Activated Mechanophores. *Angew. Chem. Int. Ed.* **2021**, *60*, 13559–13563.
- (112) Jayathilaka, P. B.; Molley, T. G.; Huang, Y.; Islam, M. S.; Buche, M. R.; Silberstein, M. N.; Kruzic, J. J.; Kilian, K. A. Force-mediated molecule release from double network hydrogels. *Chem. Commun.* **2021**, *57*, 8484–8487.
- (113) Ducrot, E.; Chen, Y.; Bulters, M.; Sijbesma, R. P.; Creton, C. Toughening Elastomers with Sacrificial Bonds and Watching Them Break. *Science* **2014**, *344*, 186–189.
- (114) Qiu, W.; Gurr, P. A.; Qiao, G. G. Regulating Color Activation Energy of Mechanophore-Linked Multinetwork Elastomers. *Macromolecules* **2020**, *53*, 4090–4098.
- (115) Chen, Y.; Sanoja, G.; Creton, C. Mechanochemistry unveils stress transfer during sacrificial bond fracture of tough multiple network elastomers. *Chem. Sci.* **2021**, *12*, 11098–11108.
- (116) Encina, M. V.; Lissi, E.; Sarasúa, M.; Gargallo, L.; Radic, D. Ultrasonic degradation of polyvinylpyrrolidone: Effect of peroxide linkages. *J. Polym. Sci.: Polym. Lett.* **1980**, *18*, 757–760.
- (117) Lu, Y.; Sugita, H.; Mikami, K.; Aoki, D.; Otsuka, H. Mechanochemical Reactions of Bis(9-methylphenyl-9-fluorenyl) Peroxides and Their Applications in Cross-Linked Polymers. *J. Am. Chem. Soc.* **2021**, *143*, 17744–17750.
- (118) Turksoy, A.; Yildiz, D.; Aydonat, S.; Beduk, T.; Canyurt, M.; Baytekin, B.; Akkaya, E. U. Mechanochemical generation of singlet oxygen. *RSC Adv.* **2020**, *10*, 9182–9186.
- (119) Diesendruck, C. E.; Peterson, G. I.; Kulik, H. J.; Kaitz, J. A.; Mar, B. D.; May, P. A.; White, S. R.; Martínez, T. J.; Boydston, A. J.; Moore, J. S. Mechanically triggered heterolytic unzipping of a low-ceiling-temperature polymer. *Nat. Chem.* **2014**, *6*, 623–628.

- (120) Aso, C.; Tagami, S.; Kunitake, T. Polymerization of aromatic aldehydes. II. Cationic cyclopolymerization of phthalaldehyde. *J. Polym. Sci., Part A: Polym. Chem.* **1969**, *7*, 497–511.
- (121) Peterson, G. I.; Boydston, A. J. Kinetic Analysis of Mechanochemical Chain Scission of Linear Poly(phthalaldehyde). *Macromol. Rapid Commun.* **2014**, *35*, 1611–1614.
- (122) Coates, G. W.; Getzler, Y. D. Y. L. Chemical recycling to monomer for an ideal, circular polymer economy. *Nat. Rev. Mater.* **2020**, *5*, 501–516.
- (123) Lin, Y.; Kouznetsova, T. B.; Craig, S. L. Mechanically Gated Degradable Polymers. *J. Am. Chem. Soc.* **2020**, *142*, 2105–2109.
- (124) Hsu, T.-G.; Zhou, J.; Su, H.-W.; Schrage, B. R.; Ziegler, C. J.; Wang, J. A Polymer with “Locked” Degradability: Superior Backbone Stability and Accessible Degradability Enabled by Mechanophore Installation. *J. Am. Chem. Soc.* **2020**, *142*, 2100–2104.
- (125) Yang, J.; Xia, Y. Mechanochemical generation of acid-degradable poly(enol ether)s. *Chem. Sci.* **2021**, *12*, 4389–4394.
- (126) Lin, Y.; Kouznetsova, T. B.; Chang, C.-C.; Craig, S. L. Enhanced polymer mechanical degradation through mechanochemically unveiled lactonization. *Nat. Commun.* **2020**, *11*, 4987.
- (127) Yardley, R. E.; Kenaree, A. R.; Gillies, E. R. Triggering Depolymerization: Progress and Opportunities for Self-Immolative Polymers. *Macromolecules* **2019**, *52*, 6342–6360.
- (128) Roth, M. E.; Green, O.; Gnam, S.; Shabat, D. Dendritic, Oligomeric, and Polymeric Self-Immolative Molecular Amplification. *Chem. Rev.* **2016**, *116*, 1309–1352.
- (129) Kathan, M.; Hecht, S. Photoswitchable molecules as key ingredients to drive systems away from the global thermodynamic minimum. *Chem. Soc. Rev.* **2017**, *46*, 5536–5550.
- (130) Yokoyama, Y.; Yamane, T.; Kurita, Y. Photochromism of a protonated 5-dimethylaminoindolylfulgide: a model of a non-destructive readout for a photon mode optical memory. *J. Chem. Soc., Chem. Commun.* **1991**, No. 24, 1722–1724.
- (131) Lemieux, V.; Branda, N. R. Reactivity-Gated Photochromism of 1,2-Dithienylethenes for Potential Use in Dosimetry Applications. *Org. Lett.* **2005**, *7*, 2969–2972.
- (132) Kühni, J.; Belser, P. Gated Photochromism of 1,2-Diarylethenes. *Org. Lett.* **2007**, *9*, 1915–1918.
- (133) Ohsumi, M.; Fukaminato, T.; Irie, M. Chemical control of the photochromic reactivity of diarylethene derivatives. *Chem. Commun.* **2005**, No. 31, 3921–3923.
- (134) Kawai, S. H.; Gilat, S. L.; Lehn, J.-M. Photochemical pKa-Modulation and Gated Photochromic Properties of a Novel Diarylethene Switch. *Eur. J. Org. Chem.* **1999**, *1999*, 2359–2366.
- (135) Kida, J.; Imato, K.; Goseki, R.; Morimoto, M.; Otsuka, H. Photoregulation of Retro-Diels–Alder Reaction at the Center of Polymer Chains. *Chem. Lett.* **2017**, *46*, 992–994.
- (136) Kida, J.; Imato, K.; Goseki, R.; Aoki, D.; Morimoto, M.; Otsuka, H. The photoregulation of a mechanochemical polymer scission. *Nat. Commun.* **2018**, *9*, 3504.
- (137) Wang, J.; Kouznetsova, T. B.; Boulatov, R.; Craig, S. L. Mechanical gating of a mechanochemical reaction cascade. *Nat. Commun.* **2016**, *7*, 13433.
- (138) Hu, X.; McFadden, M. E.; Barber, R. W.; Robb, M. J. Mechanochemical Regulation of a Photochemical Reaction. *J. Am. Chem. Soc.* **2018**, *140*, 14073–14077.
- (139) Barber, R. W.; Robb, M. J. A modular approach to mechanically gated photoswitching with color-tunable molecular force probes. *Chem. Sci.* **2021**, *12*, 11703–11709.

- (140) v. Braun, J.; Köhler, Z. Ungesättigte Reste in chemischer und pharmakologischer Beziehung. (I. Mitteilung.). *Ber. Dtsch. Chem. Ges.* **1918**, *51*, 79–96.
- (141) Gilman, H.; Vernon, C. C. 2-Chloromethyl-furan from 2-Furancarbinol. *J. Am. Chem. Soc.* **1924**, *46*, 2576–2579.
- (142) Zanetti, J. E. Alpha Furfuryl Iodide (2-Iodomethyl furan). *J. Am. Chem. Soc.* **1927**, *49*, 1061–1065.
- (143) Zanetti, J. E.; Bashour, J. T.  $\alpha$ -Furfuryl Bromide (2-Bromomethyl furan). *J. Am. Chem. Soc.* **1939**, *61*, 2249–2251.
- (144) Berry, J. M.; Watson, C. Y.; Whish, W. J. D.; Threadgill, M. D. 5-Nitrofuran-2-ylmethyl group as a potential bioreductively activated pro-drug system. *J. Chem. Soc., Perkin Trans. 1* **1997**, No. 8, 1147–1156.
- (145) Fan, B.; Trant, J. F.; Hemery, G.; Sandre, O.; Gillies, E. R. Thermo-responsive self-immolative nanoassemblies: direct and indirect triggering. *Chem. Commun.* **2017**, *53*, 12068–12071.
- (146) Nichol, M. F.; Clark, K. D.; Dolinski, N. D.; Alaniz, J. R. de. Multi-stimuli responsive trigger for temporally controlled depolymerization of self-immolative polymers. *Polym. Chem.* **2019**, *10*, 4914–4919.
- (147) Hu, X.; Zeng, T.; Husic, C. C.; Robb, M. J. Mechanically Triggered Small Molecule Release from a Masked Furfuryl Carbonate. *J. Am. Chem. Soc.* **2019**, *141*, 15018–15023.
- (148) Hu, X.; Zeng, T.; Husic, C. C.; Robb, M. J. Mechanically Triggered Release of Functionally Diverse Molecular Payloads from Masked 2-Furylcarbinol Derivatives. *ACS Cent. Sci.* **2021**, *7*, 1216–1224.
- (149) Zeng, T.; Hu, X.; Robb, M. J. 5-Aryloxy substitution enables efficient mechanically triggered release from a synthetically accessible masked 2-furylcarbinol mechanophore. *Chem. Commun.* **2021**, *57*, 11173–11176.
- (150) Stevenson, R.; De Bo, G. Controlling Reactivity by Geometry in Retro-Diels–Alder Reactions under Tension. *J. Am. Chem. Soc.* **2017**, *139*, 16768–16771.
- (151) Shi, Z.; Song, Q.; Göstl, R.; Herrmann, A. Mechanochemical activation of disulfide-based multifunctional polymers for theranostic drug release. *Chem. Sci.* **2021**, *12*, 1668–1674.
- (152) Wiita, A. P.; Ainavarapu, S. R. K.; Huang, H. H.; Fernandez, J. M. Force-dependent chemical kinetics of disulfide bond reduction observed with single-molecule techniques. *Proc. Natl. Acad. Sci. USA* **2006**, *103*, 7222–7227.
- (153) Dopieralski, P.; Ribas–Arino, J.; Anjukandi, P.; Krupicka, M.; Marx, D. Unexpected mechanochemical complexity in the mechanistic scenarios of disulfide bond reduction in alkaline solution. *Nat. Chem.* **2017**, *9*, 164–170.
- (154) Shi, Z.; Song, Q.; Göstl, R.; Herrmann, A. The Mechanochemical Release of Naphthalimide Fluorophores from  $\beta$ -Carbonate and  $\beta$ -Carbamate Disulfide-Centered Polymers. *CCS Chem.* **2021**, *3*, 2333–2344.
- (155) Alouane, A.; Labruère, R.; Le Saux, T.; Schmidt, F.; Jullien, L. Self-Immolative Spacers: Kinetic Aspects, Structure–Property Relationships, and Applications. *Angew. Chem. Int. Ed.* **2015**, *54*, 7492–7509.
- (156) Zhao, P.; Huo, S.; Fan, J.; Chen, J.; Kiessling, F.; Boersma, A. J.; Göstl, R.; Herrmann, A. Activation of the Catalytic Activity of Thrombin for Fibrin Formation by Ultrasound. *Angew. Chem. Int. Ed.* **2021**, *60*, 14707–14714.
- (157) Zhang, Q. M.; Serpe, M. J. Stimuli-Responsive Polymers for Actuation. *ChemPhysChem* **2017**, *18*, 1451–1465.

- (158) Hu, L.; Shu, T.; Wan, Y.; Fang, C.; Gao, F.; Serpe, M. J. Recent advances in stimuli-responsive polymers for sensing and actuation. *Mol. Syst. Des. Eng.* **2021**, *6*, 108–121.
- (159) Badeau, B. A.; DeForest, C. A. Programming Stimuli-Responsive Behavior into Biomaterials. *Annu. Rev. Biomed. Eng.* **2019**, *21*, 241–265.
- (160) Huo, M.; Yuan, J.; Tao, L.; Wei, Y. Redox-responsive polymers for drug delivery: from molecular design to applications. *Polym. Chem.* **2014**, *5*, 1519–1528.
- (161) Kocak, G.; Tuncer, C.; Bütün, V. pH-Responsive polymers. *Polym. Chem.* **2016**, *8*, 144–176.
- (162) Jochum, F. D.; Theato, P. Temperature- and light-responsive smart polymer materials. *Chem. Soc. Rev.* **2013**, *42*, 7468–7483.
- (163) Black, A. L.; Lenhardt, J. M.; Craig, S. L. From molecular mechanochemistry to stress-responsive materials. *J. Mater. Chem.* **2011**, *21*, 1655–1663.
- (164) Schmaljohann, D. Thermo- and pH-responsive polymers in drug delivery. *Adv. Drug Deliv. Rev.* **2006**, *58*, 1655–1670.
- (165) Peterson, G. I.; Church, D. C.; Yakelis, N. A.; Boydston, A. J. 1,2-oxazine linker as a thermal trigger for self-immolative polymers. *Polymer* **2014**, *55*, 5980–5985.
- (166) Fan, B.; Trant, J. F.; Hemery, G.; Sandre, O.; Gillies, E. R. Thermo-responsive self-immolative nanoassemblies: direct and indirect triggering. *Chem. Commun.* **2017**, *53*, 12068–12071.
- (167) Denissen, W.; M. Winne, J.; Prez, F. E. D. Vitrimers: permanent organic networks with glass-like fluidity. *Chem. Sci.* **2016**, *7*, 30–38.
- (168) Montarnal, D.; Capelot, M.; Tournilhac, F.; Leibler, L. Silica-Like Malleable Materials from Permanent Organic Networks. *Science* **2011**, *334*, 965–968.
- (169) Polgar, L. M.; van Duin, M.; Broekhuis, A. A.; Picchioni, F. Use of Diels–Alder Chemistry for Thermoreversible Cross-Linking of Rubbers: The Next Step toward Recycling of Rubber Products? *Macromolecules* **2015**, *48*, 7096–7105.
- (170) Froidevaux, V.; Borne, M.; Laborbe, E.; Auvergne, R.; Gandini, A.; Boutevin, B. Study of the Diels–Alder and retro-Diels–Alder reaction between furan derivatives and maleimide for the creation of new materials. *RSC Adv.* **2015**, *5*, 37742–37754.
- (171) Campos, L. M.; Killops, K. L.; Sakai, R.; Paulusse, J. M. J.; Damiron, D.; Drockenmuller, E.; Messmore, B. W.; Hawker, C. J. Development of Thermal and Photochemical Strategies for Thiol–Ene Click Polymer Functionalization. *Macromolecules* **2008**, *41*, 7063–7070.
- (172) Kost, J.; Bleiziffer, A.; Rusitov, D.; Rühle, J. Thermally Induced Cross-Linking of Polymers via C,H Insertion Cross-Linking (CHic) under Mild Conditions. *J. Am. Chem. Soc.* **2021**, *143*, 10108–10119.
- (173) Pan, X.; Fantin, M.; Yuan, F.; Matyjaszewski, K. Externally controlled atom transfer radical polymerization. *Chem. Soc. Rev.* **2018**, *47*, 5457–5490.
- (174) Guerre, M.; Taplan, C.; Winne, J. M.; Prez, F. E. D. Vitrimers: directing chemical reactivity to control material properties. *Chem. Sci.* **2020**, *11*, 4855–4870.
- (175) Wei, M.; Gao, Y.; Li, X.; Serpe, M. J. Stimuli-responsive polymers and their applications. *Polym. Chem.* **2016**, *8*, 127–143.
- (176) Hu, X.; Zeng, T.; Husic, C. C.; Robb, M. J. Mechanically Triggered Release of Functionally Diverse Molecular Payloads from Masked 2-Furylcarbinol Derivatives. *ACS Cent. Sci.* **2021**, *7*, 1216–1224.

- (177) Fetters, L. J.; Graessley, W. W.; Hadjichristidis, N.; Kiss, A. D.; Pearson, D. S.; Younghouse, L. B. Association behavior of end-functionalized polymers. 2. Melt rheology of polyisoprenes with carboxylate, amine, and zwitterion end groups. *Macromolecules* **1988**, *21*, 1644–1653.
- (178) Broze, G.; Jerome, R.; Teyssie, P.; Marco, C. Halato-telechelic polymers. 6. Viscoelastic properties of solutions of alkaline earth  $\alpha,\omega$ -dicarboxylato polybutadiene. *Macromolecules* **1983**, *16*, 996–1000.
- (179) Yu, X.; Zhong, S.; Li, X.; Tu, Y.; Yang, S.; Van Horn, R. M.; Ni, C.; Pochan, D. J.; Quirk, R. P.; Wesdemiotis, C.; Zhang, W.-B.; Cheng, S. Z. D. A Giant Surfactant of Polystyrene-(Carboxylic Acid-Functionalized Polyhedral Oligomeric Silsesquioxane) Amphiphile with Highly Stretched Polystyrene Tails in Micellar Assemblies. *J. Am. Chem. Soc.* **2010**, *132*, 16741–16744.
- (180) Kim, J.; Jung, H. Y.; Park, M. J. End-Group Chemistry and Junction Chemistry in Polymer Science: Past, Present, and Future. *Macromolecules* **2020**, *53*, 746–763.
- (181) Haddleton, D. M.; Heming, A. M.; Kukulj, D.; Duncalf, D. J.; Shooter, A. J. Atom Transfer Polymerization of Methyl Methacrylate. Effect of Acids and Effect with 2-Bromo-2-Methylpropionic Acid Initiation. *Macromolecules* **1998**, *31*, 2016–2018.
- (182) Zhang, X.; Matyjaszewski, K. Synthesis of Functional Polystyrenes by Atom Transfer Radical Polymerization Using Protected and Unprotected Carboxylic Acid Initiators. *Macromolecules* **1999**, *32*, 7349–7353.
- (183) Telitel, S.; Petit, B. É.; Poyer, S.; Charles, L.; Lutz, J.-F. Sequence-coded ATRP macroinitiators. *Polym. Chem.* **2017**, *8*, 4988–4991.
- (184) Hegewald, J.; Pionteck, J.; Häußler, L.; Komber, H.; Voit, B. End-functionalized polystyrene by ATRP: A facile approach to primary amino and carboxylic acid terminal groups. *J. Polym. Sci., Part A: Polym. Chem.* **2009**, *47*, 3845–3859.
- (185) Nguyen, N. H.; Rosen, B. M.; Lligadas, G.; Percec, V. Surface-Dependent Kinetics of Cu(0)-Wire-Catalyzed Single-Electron Transfer Living Radical Polymerization of Methyl Acrylate in DMSO at 25 °C. *Macromolecules* **2009**, *42*, 2379–2386.

*APPENDIX A:**SUPPLEMENTARY INFORMATION FOR CHAPTER 1***I. General Experimental Methods**

Reagents from commercial sources were used without further purification unless otherwise stated. Dry tetrahydrofuran (THF) and dichloromethane (DCM) were obtained from a Pure Process Technology solvent purification system. All reactions were performed under a N<sub>2</sub> or argon atmosphere unless specified otherwise. Column chromatography was performed on a Biotage Isolera system using SiliCycle SiliaSep HP flash cartridges.

NMR spectra were recorded using a 400 MHz Bruker Avance III HD with Prodigy Cryoprobe, a 400 MHz Bruker Avance Neo, or Varian Inova 500 or 600 MHz spectrometers. All <sup>1</sup>H NMR spectra are reported in δ units, parts per million (ppm), and were measured relative to the signals for residual acetone (2.05 ppm) or chloroform (7.26 ppm) in deuterated solvent. All <sup>13</sup>C NMR spectra were measured in deuterated solvents and are reported in ppm relative to the signals for acetone (206.26 ppm) or chloroform (77.16 ppm).

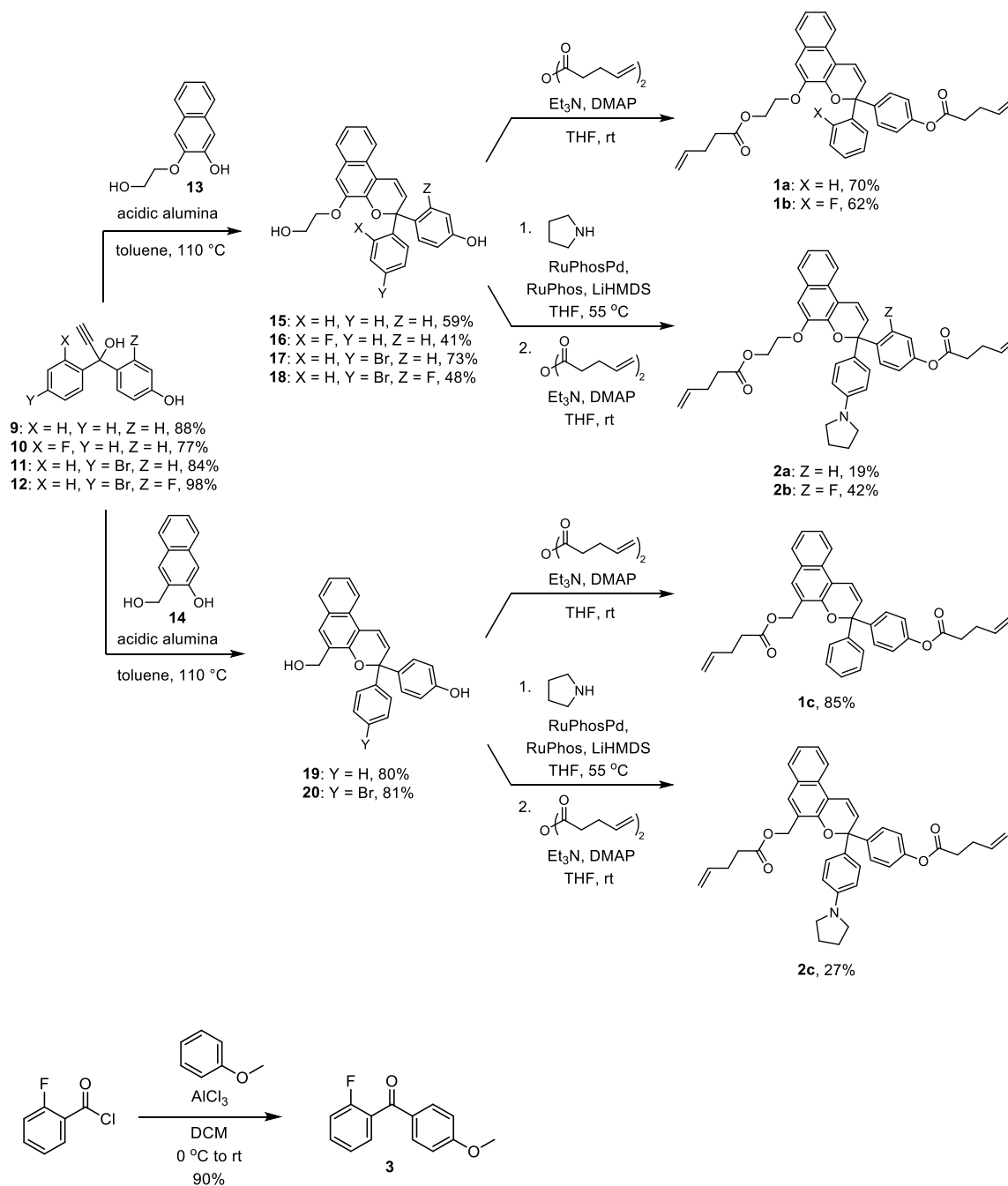
High resolution mass spectra (HRMS) were obtained from an Agilent 6200 series time-of-flight mass spectrometer equipped with an Agilent G1978A multimode source (ESI+ or ESI-) or a JEOL JMS-600H magnetic sector mass spectrometer equipped with a FAB+ probe.

UV-Vis absorption spectra were recorded on a Thermo Scientific Evolution 220 spectrometer. UV irradiation was performed using a Philips PL-S 9W/01/2P UVB bulb with a narrow emission of 305–315 nm and a peak at 311 nm under ambient conditions.

**II. Synthetic Details**

The synthesis of naphthopyran crosslinker **1a**<sup>1</sup> and spiropyran crosslinker **SP**<sup>2</sup> has been described previously.

## Scheme A.1 Synthesis of naphthopyran crosslinkers



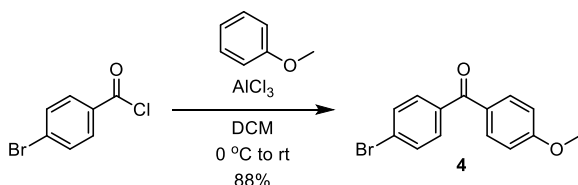
**(2-fluorophenyl)(4-methoxyphenyl)methanone (3).** A round bottom flask equipped with a stir bar and rubber septum was charged with AlCl<sub>3</sub> (4.63 g, 34.7 mmol) and dry DCM (80 mL). The flask was cooled to 0 °C in an ice bath, followed by the slow sequential addition of anisole (17.0 mL, 156 mmol) and 2-fluorobenzoyl chloride (3.8 mL, 32 mmol). The flask was allowed to warm to room temperature and stirred overnight. The mixture was then

poured over ice and partitioned between water and ethyl acetate. The aqueous layer was discarded and the organic phase was washed with water (80 mL) and brine (80 mL), dried over MgSO<sub>4</sub>, filtered, and concentrated under reduced pressure. Trituration with hexanes afforded the title compound as an off-white crystalline solid (6.6 g, 90%).  $R_f = 0.70$  (3:7 EtOAc/hexanes).

$^1\text{H NMR}$  (400 MHz, acetone- $d_6$ )  $\delta$ : 7.83–7.77 (m, 2H), 7.63 (dddd,  $J_{\text{HF}} = 5.3$ ,  $J_{\text{HH}} = 8.4$ , 7.3, 1.8 Hz, 1H), 7.55–7.50 (m, 1H), 7.36 (ddd,  $J_{\text{HF}} = 7.5$  Hz,  $J_{\text{HH}} = 7.5$ , 1.0 Hz, 1H), 7.32–7.25 (m, 1H), 7.09–7.04 (m, 2H), 3.91 (s, 3H) ppm.

$^{13}\text{C}\{^1\text{H}\}$  NMR (101 MHz, CDCl<sub>3</sub>)  $\delta$ : 192.0, 164.0, 159.8 (d,  $J_{\text{CF}} = 251.1$  Hz), 132.7 (d,  $J_{\text{CF}} = 8.1$  Hz), 132.6, 130.5 (d,  $J_{\text{CF}} = 3.2$  Hz), 130.3, 127.6 (d,  $J_{\text{CF}} = 15.5$  Hz), 124.3 (d,  $J_{\text{CF}} = 3.6$  Hz), 116.2 (d,  $J_{\text{CF}} = 21.8$  Hz), 113.8, 55.6 ppm.

HRMS (ESI,  $m/z$ ): calcd for [C<sub>14</sub>H<sub>12</sub>FO<sub>2</sub>]<sup>+</sup> (M+H)<sup>+</sup>, 231.0816; found 231.0810.

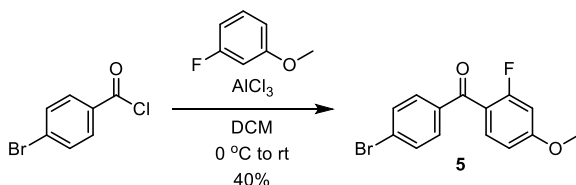


**(4-bromophenyl)(4-methoxyphenyl)methanone (4).** A round bottom flask equipped with a stir bar and rubber septum was charged with AlCl<sub>3</sub> (3.72 g, 27.9 mmol) and dry DCM (80 mL). The flask was cooled to 0 °C in an ice bath, followed by the slow sequential addition of anisole (14.2 mL, 131 mmol) and a solution of 4-bromobenzoyl chloride (6.025 g, 27.46 mmol) dissolved in dry DCM (10 mL). The flask was allowed to warm to room temperature and stirred for 26 h. The mixture was then cooled to 0 °C in an ice bath, quenched with water (40 mL), and diluted with DCM (80 mL). The aqueous layer was discarded and the organic phase was washed with water (2 x 70 mL), saturated aqueous NaHCO<sub>3</sub> (70 mL), and brine (70 mL), dried over Na<sub>2</sub>SO<sub>4</sub>, filtered, and concentrated under reduced pressure. The crude product was dried under vacuum at 60 °C overnight to yield the title compound as a light pink crystalline solid (7.05 g, 88%).  $R_f = 0.34$ . (5:95 EtOAc/hexanes)

$^1\text{H NMR}$  (400 MHz, acetone- $d_6$ )  $\delta$ : 7.83–7.78 (m, 2H), 7.77–7.72 (m, 2H), 7.70–7.66 (m, 2H), 7.11–7.06 (m, 2H), 3.92 (s, 3H) ppm.

$^{13}\text{C}\{^1\text{H}\}$  NMR (101 MHz, acetone- $d_6$ )  $\delta$ : 194.6, 163.6, 137.2, 132.6, 131.6, 131.4, 129.9, 127.0, 113.8, 55.7 ppm.

HRMS (ESI,  $m/z$ ): calcd for  $[C_{14}H_{12}BrO_2]^+$  (M+H) $^+$ , 291.0015; found, 291.0012.

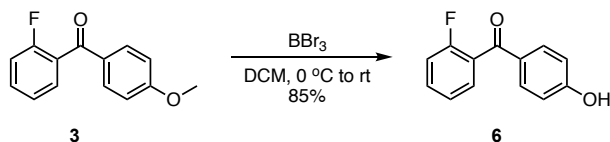


**(4-bromophenyl)(2-fluoro-4-methoxyphenyl)methanone (5).** A round bottom flask equipped with a stir bar and rubber septum was charged with AlCl<sub>3</sub> (6.32 g, 47.4 mmol) and dry DCM (100 mL). The flask was cooled to 0 °C in an ice bath, followed by the slow sequential addition of 3-fluoroanisole (8.0 mL, 70 mmol) and a solution of 4-bromobenzoyl chloride (10.195 g, 46.455 mmol) dissolved in dry DCM (35 mL). After warming to room temperature and stirring overnight, the mixture was cooled to 0 °C in an ice bath, quenched with water (200 mL), and diluted with ethyl acetate (100 mL). The aqueous layer was discarded and the organic phase washed with saturated aqueous NaHCO<sub>3</sub> (75 mL) and brine (75 mL), dried over MgSO<sub>4</sub>, filtered, and concentrated under reduced pressure. Purification by column chromatography (0–20% EtOAc/hexanes) afforded the title compound as a white crystalline solid (5.7 g, 40%).  $R_f = 0.58$  (15:85 EtOAc/hexanes)

<sup>1</sup>H NMR (400 MHz, CDCl<sub>3</sub>)  $\delta$ : 7.71–7.63 (m, 2H), 7.61–7.54 (m, 3H), 6.79 (dd,  $J = 8.7, 2.4$  Hz, 1H), 6.65 (dd,  $J_{HF} = 12.0$  Hz,  $J_{HH} = 2.4$  Hz, 1H), 3.87 (s, 3H) ppm.

<sup>13</sup>C {<sup>1</sup>H} NMR (101 MHz, CDCl<sub>3</sub>)  $\delta$ : 191.8, 164.3 (d,  $J_{CF} = 11.4$  Hz), 162.0 (d,  $J_{CF} = 254.0$  Hz), 137.3, 132.8 (d,  $J_{CF} = 4.3$  Hz), 131.7, 131.2, 128.0, 118.9 (d,  $J_{CF} = 13.7$  Hz), 110.7 (d,  $J_{CF} = 2.9$  Hz), 102.0 (d,  $J_{CF} = 25.7$  Hz), 56.0 ppm.

HRMS (FAB,  $m/z$ ): calcd for  $[C_{14}H_{11}FO_2Br]^+$  (M+H) $^+$ , 308.9926; found, 308.9915.



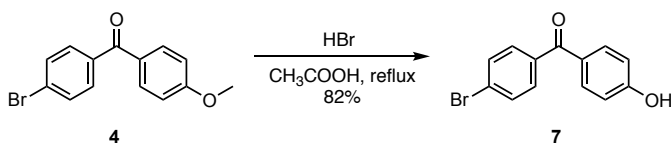
**(2-fluorophenyl)(4-hydroxyphenyl)methanone (6).** A flame-dried round bottom flask equipped with a stir bar was charged with **3** (1.027 g, 4.459 mmol) and dry DCM (6.5 mL). The flask was cooled in a bath of ice and salt, followed by the slow addition of BBr<sub>3</sub> (1 M in DCM, 22.0 mL, 22.0 mmol). The flask was allowed to warm to room temperature and stirred overnight, after which the crude mixture was poured over ice and partitioned between water and ethyl acetate. The organic layer was washed with water (40 mL) and brine (40 mL), then

dried over Na<sub>2</sub>SO<sub>4</sub>, filtered, and concentrated under reduced pressure. Purification by column chromatography (7–60% EtOAc/hexanes) afforded the title compound as a white solid (821 mg, 85%). *R<sub>f</sub>* = 0.42 (3:7 EtOAc/hexanes)

<sup>1</sup>H NMR (400 MHz, acetone-*d*<sub>6</sub>) δ: 9.41 (s, 1H), 7.77–7.71 (m, 2H), 7.61 (dddd, *J*<sub>HF</sub> = 5.3, *J*<sub>HH</sub> = 8.3, 7.3, 1.8 Hz, 1H), 7.51 (ddd, *J*<sub>HF</sub> = 7.3 Hz, *J*<sub>HH</sub> = 7.3, 1.8 Hz, 1H), 7.35 (ddd, *J* = 7.5, 7.5, 1.0 Hz, 1H), 7.27 (ddd, *J*<sub>HF</sub> = 9.6 Hz, *J*<sub>HH</sub> = 8.3, 1.0 Hz, 1H), 7.01–6.92 (m, 2H) ppm.

<sup>13</sup>C{<sup>1</sup>H} NMR (101 MHz, CDCl<sub>3</sub>) δ: 192.7, 161.2, 159.9 (d, *J*<sub>CF</sub> = 251.3 Hz), 132.90, 132.88 (d, *J*<sub>CF</sub> = 8.2 Hz), 130.6 (d, *J*<sub>CF</sub> = 3.0 Hz), 130.2, 127.4 (d, *J*<sub>CF</sub> = 15.4 Hz), 124.4 (d, *J*<sub>CF</sub> = 3.6 Hz), 116.4 (d, *J*<sub>CF</sub> = 21.8 Hz), 115.6 ppm.

HRMS (ESI, *m/z*): calcd for [C<sub>13</sub>H<sub>10</sub>FO<sub>2</sub>]<sup>+</sup> (M+H)<sup>+</sup>, 217.0659; found, 217.0667.

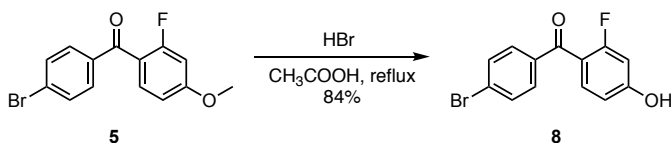


**(4-bromophenyl)(4-hydroxyphenyl)methanone (7).** A flame-dried round bottom flask equipped with a stir bar and reflux condenser was charged with **4** (5.012 g, 17.22 mmol), concentrated HBr (48% aqueous solution, 30.0 mL, 265 mmol), and glacial acetic acid (60.0 mL). After refluxing for 16 h, the reaction mixture was diluted with water (75 mL) and extracted with DCM (3 x 25 mL). The combined organic fractions were washed with water (25 mL) and brine (25 mL), dried over MgSO<sub>4</sub>, filtered, and concentrated under reduced pressure to afford the title compound as a peach solid (3.92 g, 82%). *R<sub>f</sub>* = 0.40 (3:7 EtOAc/hexanes)

<sup>1</sup>H NMR (400 MHz, acetone-*d*<sub>6</sub>) δ: 9.26 (br s, 1H), 7.73 (d, *J* = 8.8 Hz, 4H), 7.67 (d, *J* = 8.4 Hz, 2H), 6.98 (d, *J* = 7.7 Hz, 2H) ppm.

<sup>13</sup>C{<sup>1</sup>H} NMR (101 MHz, acetone-*d*<sub>6</sub>) δ: 194.2, 162.9, 138.6, 133.5, 132.4, 132.2, 129.7, 126.8, 116.2 ppm.

HRMS (ESI, *m/z*): calcd for [C<sub>13</sub>H<sub>10</sub>BrO<sub>2</sub>]<sup>+</sup> (M+H)<sup>+</sup>, 276.9859; found, 276.9860.

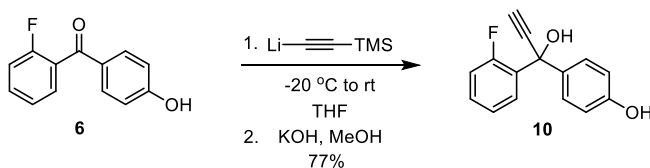


**(4-bromophenyl)(2-fluoro-4-hydroxyphenyl)methanone (8).** A round bottom flask equipped with a stir bar and reflux condenser was charged with **5** (579 mg, 1.87 mmol) and glacial acetic acid (8.5 mL). The flask was cooled to 0 °C in an ice bath, followed by the addition of HBr (48% aqueous solution, 3.6 mL, 32 mmol). The flask was then heated to reflux for 16 h, after which the reaction mixture was diluted with water (30 mL) and extracted with DCM (3 x 50 mL). The combined organic fractions were then washed with H<sub>2</sub>O (60 mL) and brine (50 mL), dried over Na<sub>2</sub>SO<sub>4</sub>, filtered, and concentrated under reduced pressure. Purification by column chromatography (6–50% EtOAc/hexanes) afforded the title compound as a white solid (465 mg, 84%). *R*<sub>f</sub> = 0.38 (1:4 EtOAc/hexanes)

<sup>1</sup>H NMR (400 MHz, acetone-*d*<sub>6</sub>) δ: 9.64 (br s, 1H), 7.76–7.68 (m, 4H), 7.53 (ddd, *J*<sub>HF</sub> = 8.5 Hz, *J*<sub>HH</sub> = 8.5, 1.5 Hz, 1H), 6.84 (dd, *J* = 8.6, 2.0 Hz, 1H), 6.70 (dd, *J*<sub>HF</sub> = 12.2 Hz, *J*<sub>HH</sub> = 1.4 Hz, 1H) ppm.

<sup>13</sup>C{<sup>1</sup>H} NMR (101 MHz, acetone-*d*<sub>6</sub>) δ: 191.7, 163.6 (d, *J*<sub>CF</sub> = 12.1 Hz), 162.9 (d, *J*<sub>CF</sub> = 251.7 Hz), 138.6, 133.7 (d, *J*<sub>CF</sub> = 4.5 Hz), 132.5, 131.9, 127.9, 118.7 (d, *J*<sub>CF</sub> = 13.6 Hz), 112.9 (d, *J*<sub>CF</sub> = 2.7 Hz), 104.0 (d, *J*<sub>CF</sub> = 24.7 Hz) ppm.

HRMS (FAB, *m/z*): calcd for [C<sub>13</sub>H<sub>9</sub>FO<sub>2</sub>Br]<sup>+</sup> (M+H)<sup>+</sup>, 294.9770; found, 294.9779.



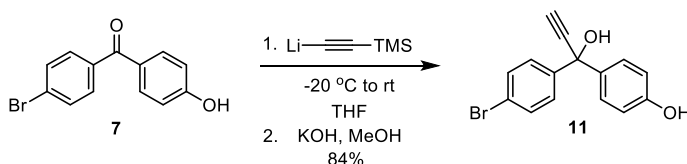
**4-(1-(2-fluorophenyl)-1-hydroxyprop-2-yn-1-yl)phenol (10).** A flame-dried round bottom flask equipped with a stir bar and rubber septum was charged with dry THF (30 mL) and trimethylsilylacetylene (1.55 mL, 11.2 mmol). The flask was cooled to –20 °C in a bath of ice and salt, followed by the slow addition of *n*-butyllithium (2.5 M in hexanes, 5.0 mL, 13 mmol). After stirring for 1 h, a solution of benzophenone **6** (1.025 g, 4.742 mmol) dissolved in dry THF (2 mL) was added dropwise to the cold lithium TMS-acetylide mixture. After complete addition, the reaction mixture was allowed to warm to room temperature. After stirring for 18 h, the flask was cooled to 0 °C in an ice bath and a solution of KOH (1.261 g, 22.47 mmol) in methanol (10 mL) was added via syringe. The mixture was warmed to room temperature and stirred for approximately 1 h. The flask was subsequently cooled to 0 °C in an ice bath and neutralized by the slow addition of acetic acid (1.5 mL). The crude mixture was concentrated under reduced pressure and partitioned between water and ethyl acetate. The aqueous layer was discarded and the organic phase was washed with water (40 mL) and

brine (40 mL), dried over Na<sub>2</sub>SO<sub>4</sub>, filtered, and concentrated under reduced pressure. The crude product was purified by column chromatography (10–60% EtOAc/hexanes) to yield the title compound as an off-white solid (0.88 g, 77%). *R<sub>f</sub>* = 0.69 (1:1 EtOAc/hexanes)

<sup>1</sup>H NMR (400 MHz, acetone-*d*<sub>6</sub>) δ: 8.37 (s, 1H), 7.92 (ddd, *J*<sub>HF</sub> = 8.0 Hz, *J*<sub>HH</sub> = 8.0, 1.8 Hz, 1H), 7.43–7.38 (m, 2H), 7.34 (dddd, *J*<sub>HF</sub> = 4.8 Hz, *J*<sub>HH</sub> = 7.9, 7.9, 1.8 Hz, 1H), 7.22 (ddd, *J* = 7.6, 7.6, 1.3 Hz, 1H), 6.99 (ddd, *J*<sub>HF</sub> = 11.5 Hz, *J*<sub>HH</sub> = 8.1, 1.3 Hz, 1H), 6.80–6.73 (m, 2H), 5.57 (s, 1H), 3.27 (s, 1H) ppm.

<sup>13</sup>C{<sup>1</sup>H} NMR (101 MHz, acetone-*d*<sub>6</sub>) δ: 160.2 (d, *J*<sub>CF</sub> = 249.4 Hz), 157.4, 136.0, 133.7 (d, *J*<sub>CF</sub> = 10.5 Hz), 130.0 (d, *J*<sub>CF</sub> = 8.2 Hz), 128.1, 127.4 (d, *J*<sub>CF</sub> = 2.9 Hz), 124.1 (d, *J*<sub>CF</sub> = 3.7 Hz), 116.4 (d, *J*<sub>CF</sub> = 21.7 Hz), 115.0, 86.2, 75.1 (d, *J*<sub>CF</sub> = 2.5 Hz), 70.8 ppm.

HRMS (ESI, *m/z*): calcd for [C<sub>15</sub>H<sub>10</sub>FO]<sup>+</sup> (M–OH)<sup>+</sup>, 225.0710; found, 225.0707.

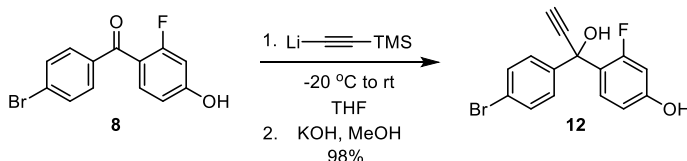


**4-(1-(4-bromophenyl)-1-hydroxyprop-2-yn-1-yl)phenol (11).** A flame-dried round bottom flask equipped with a stir bar and rubber septum was charged with dry THF (90 mL) and trimethylsilylacetylene (4.3 mL, 31.0 mmol). The flask was cooled to –20 °C in a bath of ice and salt, followed by the slow addition of n-butyllithium (2.5 M in hexanes, 13.0 mL, 32.5 mmol). After stirring for 1 h, a solution of benzophenone 7 (3.753 g, 13.54 mmol) in dry THF (12 mL) was added dropwise to the cold lithium TMS-acetylide mixture. After complete addition, the reaction mixture was allowed to warm to room temperature. After stirring overnight, the flask was cooled to 0 °C in an ice bath and a solution of KOH (3.86 g, 68.8 mmol) in methanol (20 mL) was added via syringe. The mixture was warmed to room temperature and stirred for approximately 1 h. The flask was subsequently cooled to 0 °C in an ice bath and neutralized by the slow addition of acetic acid (~ 6 mL). The crude mixture was concentrated under reduced pressure and partitioned between water and ethyl acetate. The aqueous layer was discarded and the organic phase was washed with water (100 mL) and brine (100 mL), dried over MgSO<sub>4</sub>, filtered, and concentrated under reduced pressure. Purification by column chromatography (7–60% EtOAc/hexanes) afforded the title compound as an off-white solid (3.5 g, 84%). *R<sub>f</sub>* = 0.27 (1:5 EtOAc/hexanes)

<sup>1</sup>H NMR (400 MHz, acetone-*d*<sub>6</sub>) δ: 8.34 (s, 1H), 7.57–7.46 (m, 4H), 7.44–7.38 (m, 2H), 6.82–6.73 (m, 2H), 5.63 (s, 1H), 3.35 (s, 1H) ppm.

$^{13}\text{C}\{^1\text{H}\}$  NMR (101 MHz, acetone- $d_6$ )  $\delta$ : 157.4, 146.6, 137.0, 131.5, 128.6, 127.9, 121.2, 115.3, 87.5, 76.0, 73.4 ppm.

HRMS (ESI,  $m/z$ ): calcd for  $[\text{C}_{15}\text{H}_{10}\text{BrO}]^+$  ( $\text{M}-\text{OH}$ ) $^+$ , 284.9910; found, 284.9910.

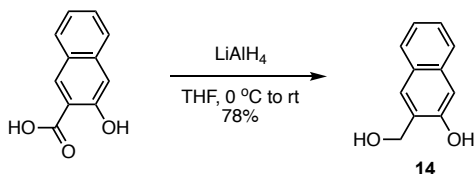


**4-(1-(4-bromophenyl)-1-hydroxyprop-2-yn-1-yl)-3-fluorophenol (12).** A flame-dried round bottom flask equipped with a stir bar and rubber septum was charged with dry THF (12 mL) and trimethylsilylacetylene (1.0 mL, 7.2 mmol). The flask was cooled to 0 °C in an ice bath, followed by the slow addition of *n*-butyllithium (2.5 M in hexanes, 2.8 mL, 7.0 mmol). After stirring for 1 h, a solution of **8** (865 mg, 2.93 mmol) in dry THF (13 mL) was added dropwise to the cold lithium TMS-acetylide mixture. After complete addition, the reaction mixture was allowed to warm to room temperature. After stirring for 18 h, the flask was cooled to 0 °C in an ice bath and a solution of KOH (850 mg, 15 mmol) in methanol (4 mL) was added via syringe. The mixture was warmed to room temperature and stirred for 3.5 h, then neutralized by the slow addition of hydrochloric acid (6 M). The crude material was then diluted in ethyl acetate (50 mL) and washed with water (2 x 50 mL) and brine (30 mL), dried over  $\text{Na}_2\text{SO}_4$ , filtered, and concentrated under reduced pressure to yield the title compound as a sticky brown solid (920 mg, 98%).  $R_f$  = 0.68 (1:1 EtOAc/hexanes)

$^1\text{H}$  NMR (400 MHz, acetone- $d_6$ )  $\delta$ : 8.81 (d,  $J_{\text{HF}}$  = 0.9 Hz, 1H), 7.73 (dd,  $J_{\text{HF}}$  = 9.4 Hz,  $J_{\text{HH}}$  = 8.6 Hz, 1H), 7.54–7.47 (m, 4H), 6.70 (ddd,  $J_{\text{HF}}$  = 0.8 Hz,  $J_{\text{HH}}$  = 8.6, 2.4 Hz, 1H), 6.48 (dd,  $J_{\text{HF}}$  = 12.8 Hz,  $J_{\text{HH}}$  = 2.4 Hz, 1H), 5.75 (s, 1H), 3.35 (s, 1H) ppm.

$^{13}\text{C}\{^1\text{H}\}$  NMR (101 MHz, acetone- $d_6$ )  $\delta$ : 161.1 (d,  $J_{\text{CF}}$  = 248.8 Hz), 159.7 (d,  $J_{\text{CF}}$  = 11.4 Hz), 145.4, 131.6, 129.0, 128.9 (d,  $J_{\text{CF}}$  = 4.7 Hz), 124.0 (d,  $J_{\text{CF}}$  = 11.3 Hz), 121.7, 111.2 (d,  $J_{\text{CF}}$  = 2.9 Hz), 104.3 (d,  $J_{\text{CF}}$  = 24.1 Hz), 86.2, 76.2 (d,  $J_{\text{CF}}$  = 2.1 Hz), 71.1 ppm.

HRMS (FAB,  $m/z$ ): calcd for  $[\text{C}_{15}\text{H}_{10}\text{FO}_2\text{Br}]^+$  ( $\text{M}$ ) $^+$ , 319.9848; found, 319.9835.

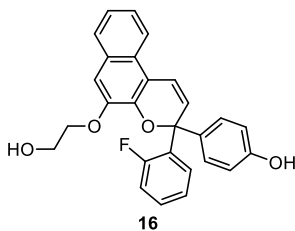


**3-(hydroxymethyl)naphthalen-2-ol (14).** A flame-dried round bottom flask equipped with a stir bar and rubber septum was cooled to 0 °C in an ice bath and charged with lithium aluminum hydride (3.5 M in THF, 34.5 mL, 121 mmol). A solution of 3-hydroxy-2-naphthoic acid (4.495 g, 23.89 mmol) in dry THF (20 mL) was added dropwise to the cold solution of LAH over 45 minutes. The flask was allowed to warm to room temperature and stirred for 16 h, after which the mixture was cooled to 0 °C in an ice bath and quenched by the slow, dropwise addition of ethyl acetate (40 mL), followed by a saturated aqueous solution of Rochelle's salt (150 mL). The crude mixture was stirred for 1 h, then warmed to room temperature and diluted with ethyl acetate (100 mL) and saturated Rochelle's salt (100 mL). Concentrated hydrochloric acid (6 M) was added to reach pH 5 and the solution was extracted with 1:1 DCM/ethyl acetate (900 mL). The organic phase was washed with water, saturated NaHCO<sub>3</sub>, and brine, then dried over Na<sub>2</sub>SO<sub>4</sub>, filtered, and concentrated under reduced pressure. Purification by column chromatography (12–100% EtOAc/hexanes) afforded the title compound as a beige powder (3.25 g, 78%).  $R_f$  = 0.50 (1:1 EtOAc/hexanes)

<sup>1</sup>H NMR (400 MHz, acetone-*d*<sub>6</sub>)  $\delta$ : 7.83 (d,  $J$  = 1.1 Hz, 1H), 7.76 (dd,  $J$  = 8.2, 1.2 Hz, 1H), 7.65 (dd,  $J$  = 8.4, 1.2 Hz, 1H), 7.35 (ddd,  $J$  = 8.2, 6.8, 1.3 Hz, 1H), 7.26 (ddd,  $J$  = 8.1, 6.8, 1.3 Hz, 1H), 7.19 (s, 1H), 4.89 (d,  $J$  = 1.2 Hz, 2H), 3.05 (br s, 1H) ppm.

<sup>13</sup>C{<sup>1</sup>H} NMR (101 MHz, acetone-*d*<sub>6</sub>)  $\delta$ : 154.4, 134.9, 131.5, 129.3, 128.3, 126.8, 126.5, 126.4, 123.7, 109.6, 61.5 ppm.

HRMS (ESI,  $m/z$ ): calcd for [C<sub>11</sub>H<sub>9</sub>O<sub>2</sub>]<sup>-</sup> (M-H)<sup>-</sup>, 173.0608; found 173.0605.

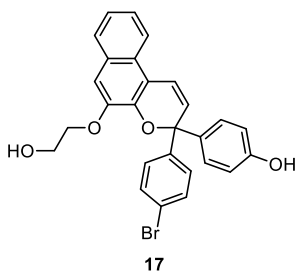


**5-(2-hydroxyethoxy)-3-(4-hydroxyphenyl)-3-(2-fluorophenyl)-3H-naphtho[2,1-b]pyran (16).** A two-neck round bottom flask equipped with a stir bar and reflux condenser was charged with **13**<sup>1</sup> (285 mg, 1.40 mmol), **10** (440 mg, 1.82 mmol), acidic alumina (1.095 g), and dry toluene (16.5 mL). After refluxing for 18 h, the mixture was removed from heat and filtered through a plug of silica, eluting with ethyl acetate, and the filtrate was concentrated under reduced pressure. Purification by column chromatography (52–67% EtOAc/hexanes) provided the title compound as a red foamy solid (246 mg, 41%).  $R_f$  = 0.38 (1:1 EtOAc/hexanes)

$^1\text{H}$  NMR (400 MHz, acetone- $d_6$ )  $\delta$ : 8.01–7.95 (m, 1H), 7.86 (ddd,  $J_{\text{HF}} = 8.0$  Hz,  $J_{\text{HH}} = 8.0$ , 1.8 Hz, 1H), 7.73–7.68 (m, 1H), 7.43 (d,  $J = 10.1$  Hz, 1H), 7.40–7.28 (m, 6H), 7.16 (ddd,  $J = 7.6$ , 7.6, 1.2 Hz, 1H), 7.08 (ddd,  $J_{\text{HF}} = 11.8$  Hz,  $J_{\text{HH}} = 8.2$ , 1.2 Hz, 1H), 6.83–6.77 (m, 2H), 6.59 (dd,  $J_{\text{HF}} = 5.5$  Hz,  $J_{\text{HH}} = 10.0$  Hz, 1H), 4.32–4.22 (m, 2H), 4.02–3.95 (m, 2H) ppm.

$^{13}\text{C}\{^1\text{H}\}$  NMR (101 MHz, acetone- $d_6$ )  $\delta$ : 160.1 (d,  $J_{\text{CF}} = 246.4$  Hz), 158.1, 149.1, 143.0, 135.3, 132.4 (d,  $J_{\text{CF}} = 11.3$  Hz), 130.7, 130.5 (d,  $J_{\text{CF}} = 8.4$  Hz), 129.3, 129.0 (d,  $J_{\text{CF}} = 3.6$  Hz), 128.5 (d,  $J_{\text{CF}} = 4.7$  Hz), 128.1, 125.9, 125.3, 125.1, 124.8 (d,  $J_{\text{CF}} = 3.4$  Hz), 122.1, 120.4, 117.0 (d,  $J_{\text{CF}} = 22.3$  Hz), 116.2, 115.6, 110.2, 81.6 (d,  $J_{\text{CF}} = 2.8$  Hz), 71.5, 61.3 ppm.

HRMS (ESI,  $m/z$ ): calcd for  $[\text{C}_{27}\text{H}_{21}\text{FO}_4\text{Na}]^+$  ( $\text{M}+\text{Na}$ ) $^+$ , 451.1316; found, 451.1324.



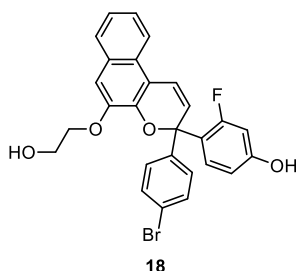
**5-(2-hydroxyethoxy)-3-(4-hydroxyphenyl)-3-(4-bromophenyl)-3H-naphtho[2,1-**

**b]pyran (17).** A two-neck round bottom flask equipped with a stir bar and reflux condenser was charged with **13**<sup>1</sup> (313 mg, 1.53 mmol), **11** (603 mg, 1.99 mmol), acidic alumina (1.200 g), and toluene (18 mL). After refluxing overnight, the mixture was removed from heat and filtered through a plug of celite, eluting with ethyl acetate, and the filtrate was concentrated under reduced pressure. Purification by column chromatography (20–100% EtOAc/hexanes) provided the title compound as a red foamy solid (548 mg, 73%).  $R_f = 0.40$  (1:1 EtOAc/hexanes)

$^1\text{H}$  NMR (400 MHz, acetone- $d_6$ )  $\delta$ : 8.41 (s, 1H), 7.97 (dd,  $J = 8.0$ , 1.3 Hz, 1H), 7.71–7.66 (m, 1H), 7.59–7.53 (m, 2H), 7.50–7.46 (m, 2H), 7.45 (d,  $J = 9.9$  Hz, 1H), 7.42–7.26 (m, 5H), 6.81–6.76 (m, 2H), 6.53 (d,  $J = 9.9$  Hz, 1H), 4.26 (dd,  $J = 5.9$ , 3.4 Hz, 2H), 4.05–3.97 (m, 3H) ppm.

$^{13}\text{C}\{^1\text{H}\}$  NMR (101 MHz, acetone- $d_6$ )  $\delta$ : 157.9, 149.3, 145.8, 143.4, 136.3, 131.9, 130.8, 129.9, 129.7, 129.2, 128.1, 126.0, 125.3, 125.2, 122.1, 121.8, 120.9, 116.7, 115.8, 110.3, 82.7, 71.6, 61.4 ppm.

HRMS (ESI,  $m/z$ ): calcd for  $[\text{C}_{27}\text{H}_{22}\text{BrO}_4]^+$  ( $\text{M}+\text{H}$ ) $^+$ , 489.0696; found, 489.0688.

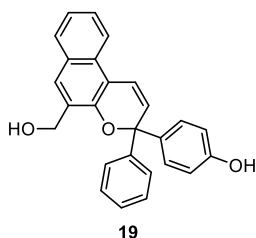


**5-(2-hydroxymethyl)-3-(2-fluoro-4-hydroxyphenyl)-3-(4-bromophenyl)-3H-naphtho[2,1-*b*]pyran (18).** A two-neck round bottom flask equipped with a stir bar and reflux condenser was charged with **12** (579 mg, 1.80 mmol), **13**<sup>1</sup> (582 mg, 2.85 mmol), acidic alumina (2.343 g), and toluene (18 mL). After refluxing overnight, the mixture was filtered through a plug of celite, eluting with ethyl acetate, and the filtrate was concentrated under reduced pressure. Purification by column chromatography (20–100% EtOAc/hexanes) afforded the title product as a foamy red-orange solid (437 mg, 48%).  $R_f = 0.25$  (1:1 EtOAc/hexanes)

<sup>1</sup>H NMR (400 MHz, acetone-*d*<sub>6</sub>)  $\delta$ : 8.86 (s, 1H), 8.02–7.95 (m, 1H), 7.73–7.67 (m, 1H), 7.59–7.48 (m, 5H), 7.44 (d,  $J = 10.0$  Hz, 1H), 7.38–7.28 (m, 3H), 6.64 (ddd,  $J_{HF} = 0.6$  Hz,  $J_{HH} = 8.6, 2.4$  Hz, 1H), 6.57 (dd,  $J_{HF} = 13.2$  Hz,  $J_{HH} = 2.4$  Hz, 1H), 6.52 (dd,  $J_{HF} = 4.5$  Hz,  $J_{HH} = 10.0$  Hz, 1H), 4.31–4.22 (m, 2H), 4.02–3.93 (m, 3H) ppm.

<sup>13</sup>C{<sup>1</sup>H} NMR (101 MHz, acetone-*d*<sub>6</sub>)  $\delta$ : 161.0 (d,  $J_{CF} = 246.7$  Hz), 159.8 (d,  $J_{CF} = 12.2$  Hz), 149.0, 144.4, 142.8, 131.9, 130.7, 129.8 (d,  $J_{CF} = 5.3$  Hz), 129.7, 128.2 (d,  $J_{CF} = 3.7$  Hz), 128.1, 125.8, 125.3, 125.2, 122.4 (d,  $J_{CF} = 11.5$  Hz), 122.1, 120.6, 120.5, 116.4, 111.7 (d,  $J_{CF} = 2.9$  Hz), 110.3, 104.5 (d,  $J_{CF} = 24.7$  Hz), 81.1 (d,  $J_{CF} = 2.5$  Hz), 71.5, 61.3 ppm.

HRMS (FAB,  $m/z$ ): calcd for [C<sub>27</sub>H<sub>20</sub>FO<sub>4</sub>Br]<sup>+</sup> (M)<sup>+</sup>, 506.0529; found, 506.0540.



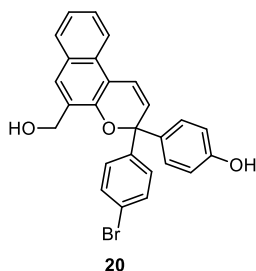
**5-(2-hydroxymethyl)-3-(4-hydroxyphenyl)-3-phenyl-3H-naphtho[2,1-*b*]pyran (19).** A two-neck round bottom flask equipped with a stir bar and reflux condenser was charged with **14** (0.503 g, 2.89 mmol), **9**<sup>1</sup> (0.843 g, 3.76 mmol), acidic alumina (1.932 g), and dry toluene (34 mL). After refluxing 13 h, the mixture was removed from heat and filtered through a plug of silica, eluting with ethyl acetate, and the filtrate was concentrated under reduced

pressure. Purification by column chromatography (7–60% EtOAc/hexanes) afforded the title product as a foamy red-orange solid (882 mg, 80%).  $R_f = 0.54$  (1:1 EtOAc/hexanes)

$^1\text{H NMR}$  (400 MHz, acetone- $d_6$ )  $\delta$ : 8.06 (dd,  $J = 8.5, 1.0$  Hz, 1H), 7.86 (d,  $J = 1.3$  Hz, 1H), 7.80–7.75 (m, 1H), 7.57–7.51 (m, 2H), 7.49–7.43 (m, 2H), 7.38–7.30 (m, 5H), 7.27–7.21 (m, 1H), 6.81–6.75 (m, 2H), 6.37 (d,  $J = 10.0$  Hz, 1H), 5.00–4.90 (m, 2H) ppm.

$^{13}\text{C}\{^1\text{H}\}$  NMR (101 MHz, acetone- $d_6$ )  $\delta$ : 157.7, 149.0, 146.6, 136.8, 132.1, 130.0, 129.9, 129.13, 129.07, 128.9, 128.0, 127.3, 127.1, 127.0, 124.6, 122.1, 120.4, 115.6, 114.6, 83.1, 60.1 ppm.

HRMS (ESI,  $m/z$ ): calcd for  $[\text{C}_{26}\text{H}_{21}\text{O}_3]^+$  (M+H) $^+$ , 381.1485; found, 381.1488.

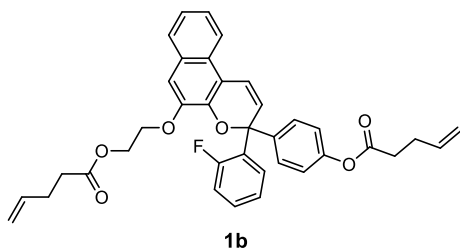


**5-(2-hydroxymethyl)-3-(4-hydroxyphenyl)-3-(4-bromophenyl)-3H-naphtho[2,1-b]pyran (20).** A two-neck round bottom flask equipped with a stir bar and reflux condenser was charged with **14** (0.507 g, 2.91 mmol), **11** (1.148 g, 3.79 mmol), acidic alumina (1.947 g), and dry toluene (35 mL). After refluxing overnight, the mixture was removed from heat, filtered through a plug of celite, eluting with ethyl acetate, and the filtrate was concentrated under reduced pressure. Purification by column chromatography (7–60% EtOAc/hexanes) afforded the title product as a foamy red-orange solid (1.09 g, 81%).  $R_f = 0.50$  (1:1 EtOAc/hexanes)

$^1\text{H NMR}$  (400 MHz, acetone- $d_6$ )  $\delta$ : 8.42 (s, 1H), 8.06 (dd,  $J = 8.6, 1.1$  Hz, 1H), 7.87 (d,  $J = 1.2$  Hz, 1H), 7.80–7.76 (m, 1H), 7.54–7.43 (m, 6H), 7.38–7.31 (m, 3H), 6.82–6.77 (m, 2H), 6.36 (d,  $J = 10.0$  Hz, 1H), 5.01–4.87 (m, 2H), 4.29 (t,  $J = 5.7$  Hz, 1H) ppm.

$^{13}\text{C}\{^1\text{H}\}$  NMR (101 MHz, acetone- $d_6$ )  $\delta$ : 157.8, 148.8, 145.9, 136.2, 131.92, 131.90, 130.0, 129.8, 129.5, 129.1, 129.0, 128.3, 127.4, 127.1, 124.7, 122.1, 121.7, 120.8, 115.8, 114.5, 82.7, 60.1 ppm.

HRMS (ESI,  $m/z$ ): calcd for  $[\text{C}_{26}\text{H}_{20}\text{BrO}_3]^+$  (M+H) $^+$ , 459.0590; found, 459.0578.

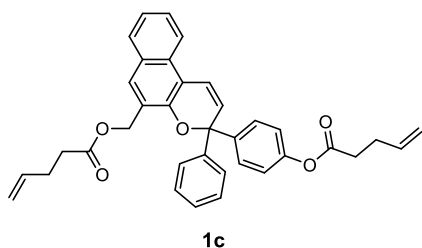


**5-(2-(pent-4-enyloxy)ethoxy)-3-(4-(pent-4-enyloxy)phenyl)-3-(2-fluorophenyl)-3H-naphtho[2,1-*b*]pyran (**1b**).** A flame-dried round bottom flask equipped with a stir bar and rubber septum was charged with **16** (142 mg, 0.331 mmol) and DMAP (11 mg, 0.090 mmol). Dry THF (3.2 mL), triethylamine (105  $\mu$ L, 0.753 mmol), and 4-pentenoic anhydride (155  $\mu$ L, 0.848 mmol) were then added sequentially. After stirring overnight, THF was removed under reduced pressure and the crude reaction mixture was partitioned between ethyl acetate (12 mL) and water (6 mL). The aqueous layer was discarded and the organic layer was washed with 10% aqueous NaHSO<sub>4</sub> (6 mL), 10% aqueous NaHCO<sub>3</sub> (6 mL), and brine (6 mL), dried over Na<sub>2</sub>SO<sub>4</sub>, filtered, and concentrated under reduced pressure. The crude mixture was purified by column chromatography (5–30% EtOAc/hexanes) to afford the title compound as a red oil (127 mg, 62%).  $R_f$  = 0.62 (3:7 EtOAc/hexanes)

$^1\text{H NMR}$  (400 MHz, acetone- $d_6$ )  $\delta$ : 7.99 (dd,  $J_{\text{HF}} = 1.4$  Hz,  $J_{\text{HH}} = 8.2$  Hz, 1H), 7.86 (ddd,  $J_{\text{HF}} = 8.0$  Hz,  $J_{\text{HH}} = 8.0, 1.8$  Hz, 1H), 7.75–7.68 (m, 1H), 7.67–7.59 (m, 2H), 7.48 (d,  $J = 10.1$  Hz, 1H), 7.40–7.29 (m, 4H), 7.20 (ddd,  $J_{\text{HF}} = 1.2$  Hz,  $J_{\text{HH}} = 7.6, 7.6$  Hz, 1H), 7.15–7.06 (m, 3H), 6.65 (dd,  $J_{\text{HF}} = 5.0$  Hz,  $J_{\text{HH}} = 10.0$  Hz, 1H), 5.96–5.76 (m, 2H), 5.14–4.89 (m, 4H), 4.56 (t,  $J = 4.6$  Hz, 2H), 4.49–4.36 (m, 2H), 2.65 (t,  $J = 7.3$  Hz, 2H), 2.49–2.39 (m, 4H), 2.38–2.30 (m, 2H) ppm.

$^{13}\text{C}\{^1\text{H}\}$  NMR (101 MHz, acetone- $d_6$ )  $\delta$ : 173.1, 171.7, 160.1 (d,  $J_{\text{CF}} = 246.9$  Hz), 151.6, 148.5, 142.7, 141.8, 137.9, 137.7, 132.1 (d,  $J_{\text{CF}} = 11.0$  Hz), 130.9 (d,  $J_{\text{CF}} = 8.5$  Hz), 130.7, 128.8, 128.7 (d,  $J_{\text{CF}} = 3.4$  Hz), 128.2, 127.7 (d,  $J_{\text{CF}} = 4.8$  Hz), 126.0, 125.6, 125.4, 125.0 (d,  $J_{\text{CF}} = 3.4$  Hz), 122.3, 122.2, 120.9, 117.3 (d,  $J_{\text{CF}} = 22.1$  Hz), 116.4, 116.0, 115.8, 110.5, 81.3 (d,  $J_{\text{CF}} = 2.7$  Hz), 67.8, 63.3, 34.0, 29.63, 29.55 ppm.

HRMS (ESI,  $m/z$ ): calcd for  $[\text{C}_{37}\text{H}_{37}\text{FO}_6\text{N}]^+$  ( $\text{M}+\text{NH}_4$ )<sup>+</sup>, 610.2599; found, 610.2599.

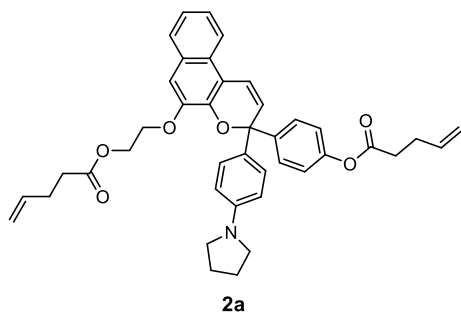


**5-(2-(pent-4-enyloxy)methyl)-3-(4-(pent-4-enyloxy)phenyl)-3-phenyl-3H-naphtho[2,1-b]pyran (1c).** A flame-dried round bottom flask equipped with a stir bar was charged with **19** (401 mg, 1.06 mmol) and DMAP (36 mg, 0.28 mmol). THF (10.2 mL), triethylamine (0.34 mL, 2.4 mmol), and 4-pentenoic anhydride (0.49 mL, 2.7 mmol) were added sequentially. After stirring at room temperature 10 h, THF was removed under reduced pressure. The crude reaction mixture was then partitioned between ethyl acetate (10 mL) and water (5 mL). The aqueous layer was discarded, and the organic layer washed with 10% aqueous NaHSO<sub>4</sub> (2 x 5 mL), 10% aqueous NaHCO<sub>3</sub> (5 mL) and brine (5 mL), dried over Na<sub>2</sub>SO<sub>4</sub>, and concentrated under reduced pressure. Purification by column chromatography (5–30% EtOAc/hexanes) afforded the title compound as an orange oil (0.49 g, 85%). *R<sub>f</sub>* = 0.70 (3:7 EtOAc/hexanes)

<sup>1</sup>H NMR (400 MHz, acetone-*d*<sub>6</sub>) δ: 8.10 (dd, *J* = 8.7, 1.1 Hz, 1H), 7.86–7.79 (m, 2H), 7.62–7.48 (m, 6H), 7.41–7.33 (m, 3H), 7.30–7.24 (m, 1H), 7.13–7.08 (m, 2H), 6.49 (d, *J* = 10.0 Hz, 1H), 5.96–5.82 (m, 2H), 5.42 (d, *J* = 0.8 Hz, 2H), 5.15–4.94 (m, 4H), 2.65 (t, *J* = 7.3 Hz, 2H), 2.55–2.47 (m, 2H), 2.47–2.34 (m, 4H) ppm.

<sup>13</sup>C{<sup>1</sup>H} NMR (101 MHz, acetone-*d*<sub>6</sub>) δ: 172.0, 170.8, 150.4, 148.5, 144.9, 142.4, 137.1, 136.8, 129.79, 129.77, 128.8, 128.5, 128.2, 127.8, 127.8, 127.6, 127.1, 126.6, 125.0, 124.2, 121.5, 121.4, 119.7, 115.1, 114.9, 114.2, 82.4, 61.3, 33.2, 33.1, 28.74, 28.66 ppm.

HRMS (ESI, *m/z*): calcd for [C<sub>36</sub>H<sub>36</sub>O<sub>5</sub>N]<sup>+</sup> (M+NH<sub>4</sub>)<sup>+</sup>, 562.2588; found 562.2589.



**5-(2-(pent-4-enyloxy)ethoxy)-3-(4-(pent-4-enyloxy)phenyl)-3-(4-pyrrolidinophenyl)-3H-naphtho[2,1-b]pyran (2a).** A scintillation vial equipped with a stir bar was charged with **17** (256 mg, 0.524 mmol), RuPhosPd G2 (33 mg, 0.043 mmol), and RuPhos (19 mg, 0.043

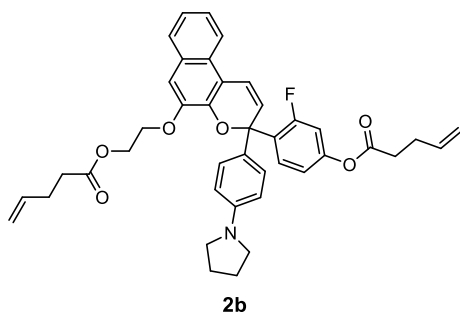
mmol) under nitrogen and sealed with a rubber septum. Pyrrolidine (62  $\mu$ L, 0.75 mmol), LHMDS (1.5 M in THF, 1.4 mL, 2.1 mmol), and THF (2 mL) were then added sequentially under nitrogen and the mixture was stirred at 55 °C. After 14 h, THF was removed under reduced pressure and the reaction mixture was resuspended in a mixture of ethyl acetate (3 mL) and DMF (3 mL). After stirring at room temperature 5 minutes, the mixture was diluted with ethyl acetate (150 mL) and methanol (5 mL) and washed with saturated aqueous ammonium chloride (60 mL), water (3 x 50 mL), and brine (50 mL). The aqueous layers were extracted with ethyl acetate (2 x 50 mL) and the combined organic fractions were dried over Na<sub>2</sub>SO<sub>4</sub>, eluted through a plug of celite with ethyl acetate, and the filtrate was concentrated under reduced pressure to afford the crude diol, which was carried forward in the next step without further purification.

A flame-dried round-bottom flask equipped with a stir bar and rubber septum was charged with the crude diol and DMAP (32 mg, 0.26 mmol). Dry THF (5.1 mL), triethylamine (0.35 mL, 2.5 mmol), and 4-pentenoic anhydride (0.45 mL, 2.5 mmol) were then added sequentially and the mixture was stirred at room temperature. After 15 h, THF was removed under reduced pressure and the crude reaction mixture was dissolved in ethyl acetate (30 mL) and washed with water (2 x 30 mL), dried over Na<sub>2</sub>SO<sub>4</sub>, filtered through a plug of basic alumina, and concentrated under reduced pressure. Purification by column chromatography (5–30% EtOAc/hexanes) afforded the title compound as a blue oil (65 mg, 19% over 2 steps).  $R_f$  = 0.44 (1:5 EtOAc/hexanes)

<sup>1</sup>H NMR (400 MHz, acetone-*d*<sub>6</sub>)  $\delta$ : 7.97 (d,  $J$  = 8.1 Hz, 1H), 7.70–7.66 (m, 1H), 7.62–7.58 (m, 2H), 7.42 (d,  $J$  = 10.0 Hz, 1H), 7.38–7.27 (m, 5H), 7.09–7.03 (m, 2H), 6.53 (d,  $J$  = 9.9 Hz, 1H), 6.48–6.43 (m, 2H), 5.97–5.75 (m, 2H), 5.15–4.89 (m, 4H), 4.57–4.52 (m, 2H), 4.43–4.38 (m, 2H), 3.23–3.17 (m, 4H), 2.64 (t,  $J$  = 7.2 Hz, 2H), 2.49–2.39 (m, 4H), 2.37–2.30 (m, 2H), 1.98–1.92 (m, 4H) ppm.

<sup>13</sup>C{<sup>1</sup>H} NMR (101 MHz, acetone-*d*<sub>6</sub>)  $\delta$ : 173.0, 171.7, 150.8, 148.8, 148.2, 144.2, 143.5, 137.8, 137.6, 131.6, 130.4, 130.2, 128.5, 128.3, 128.0, 126.1, 125.3, 125.0, 122.0, 121.9, 120.2, 116.7, 115.9, 115.7, 111.8, 110.2, 82.9, 67.7, 63.3, 48.0, 33.9, 29.64, 29.59, 25.9 ppm.

HRMS (ESI,  $m/z$ ): calcd for [C<sub>41</sub>H<sub>42</sub>NO<sub>6</sub>]<sup>+</sup> (M+H)<sup>+</sup>, 644.3007; found, 644.2987.



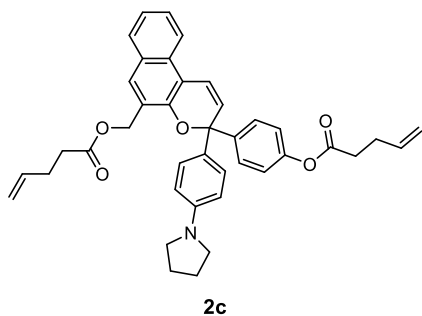
**5-(2-(pent-4-enyloxy)ethoxy)-3-(2-fluoro-4-(pent-4-enyloxy)phenyl)-3-(4-pyrrolidinophenyl)-3*H*-naphtho[2,1-*b*]pyran (2b).** A scintillation vial equipped with a stir bar was charged with **18** (449 mg, 0.885 mmol), RuPhosPd G2 (44.8 mg, 0.0577 mmol), and RuPhos (31.0 mg, 0.0664 mmol) under nitrogen and sealed with a rubber septum. Pyrrolidine (110  $\mu$ L, 1.3 mmol) and LHMDS (1.5 M in THF, 2.5 mL, 3.8 mmol) were then added sequentially under nitrogen and the mixture was stirred at 65  $^{\circ}$ C. After 22 h, the reaction was diluted with a mixture of ethyl acetate, DCM, and methanol. The organic phase was washed with saturated aqueous  $\text{NH}_4\text{Cl}$  (2 x 100 mL) and concentrated under reduced pressure. The crude product was then taken up in a mixture of DMF (3 mL) and DCM (10 mL). After stirring for 10 min, the solution was diluted with ethyl acetate (50 mL), washed with  $\text{H}_2\text{O}$  (2 x 50 mL) and brine (50 mL), dried over  $\text{Na}_2\text{SO}_4$ , filtered, and concentrated under reduced pressure to afford the crude diol, which was carried forward in the next step without further purification.

A round-bottom flask equipped with a stir bar and rubber septum was charged with the crude diol and DMAP (60.1 mg, 0.492 mmol). Dry THF (20 mL), triethylamine (0.60 mL, 4.3 mmol), and 4-pentenoic anhydride (0.75 mL, 4.1 mmol) were then added sequentially and the mixture was stirred at room temperature. After 15 h, the crude reaction mixture was diluted with ethyl acetate (100 mL) and washed with saturated aqueous  $\text{NH}_4\text{Cl}$  (150 mL), saturated aqueous  $\text{NaHCO}_3$  (100 mL), and brine (50 mL). The organic layer was dried over  $\text{Na}_2\text{SO}_4$ , filtered through a plug of basic alumina, and concentrated under reduced pressure. Purification by column chromatography (3–30% EtOAc/hexanes) afforded the title compound as a blue oil (245 mg, 42% over 2 steps).  $R_f$  = 0.34 (1:5 EtOAc/hexanes)

$^1\text{H NMR}$  (400 MHz, acetone- $d_6$ )  $\delta$ : 7.99 (d,  $J$  = 8.2 Hz, 1H), 7.84 (t,  $J$  = 8.9 Hz, 1H), 7.72–7.68 (m, 1H), 7.44 (d,  $J$  = 10.1 Hz, 1H), 7.39–7.28 (m, 5H), 6.99–6.92 (m, 2H), 6.59 (dd,  $J_{\text{HF}}$  = 5.1 Hz,  $J_{\text{HH}}$  = 10.0 Hz, 1H), 6.50–6.44 (m, 2H), 5.96–5.77 (m, 2H), 5.15–4.89 (m, 4H), 4.59–4.49 (m, 2H), 4.47–4.36 (m, 2H), 3.26–3.16 (m, 4H), 2.66 (t,  $J$  = 7.3 Hz, 2H), 2.48–2.39 (m, 4H), 2.38–2.29 (m, 2H), 2.00–1.92 (m, 4H) ppm.

$^{13}\text{C}\{^1\text{H}\}$  NMR (101 MHz, acetone- $d_6$ )  $\delta$ : 173.1, 171.6, 159.9 (d,  $J_{\text{CF}} = 248.3$  Hz), 152.3 (d,  $J_{\text{CF}} = 11.0$  Hz), 148.7, 143.1, 138.0, 137.7, 130.7, 130.5 (d,  $J_{\text{CF}} = 11.3$  Hz), 130.2, 129.2 (d,  $J_{\text{CF}} = 4.8$  Hz), 128.9, 128.5 (d,  $J_{\text{CF}} = 4.6$  Hz), 128.2, 126.2, 125.5, 125.3, 122.2, 120.6, 118.1 (d,  $J_{\text{CF}} = 3.4$  Hz), 116.6, 116.2, 115.9, 111.9, 111.4 (d,  $J_{\text{CF}} = 25.4$  Hz), 110.4, 81.7 (d,  $J_{\text{CF}} = 3.0$  Hz), 67.9, 63.4, 48.2, 34.1, 34.0, 29.7, 29.6, 26.1 ppm.

**HRMS (ESI,  $m/z$ ):** calcd for  $[\text{C}_{41}\text{H}_{41}\text{FNO}_6]^+$  (M+H) $^+$ , 662.2912; found, 662.2902.



**5-(2-(pent-4-enoyloxy)methyl)-3-(4-(pent-4-enoyloxy)phenyl)-3-(4-pyrrolidinophenyl)-3H-naphtho[2,1-b]pyran (2c).** A scintillation vial equipped with a stir bar was charged with **20** (298 mg, 0.649 mmol), RuPhosPd G2 (39 mg, 0.050 mmol), and RuPhos (23 mg, 0.049 mmol) under nitrogen and sealed with a rubber septum. Pyrrolidine (75  $\mu\text{L}$ , 0.91 mmol), LHMDS (1.5 M in THF, 1.8 mL, 2.7 mmol), and THF (2 mL) were then added sequentially. After stirring at 55  $^\circ\text{C}$  overnight, THF was removed under reduced pressure and the reaction mixture was resuspended in a mixture of ethyl acetate (5 mL) and DMF (3 mL). After stirring for 5 minutes, the mixture was diluted with ethyl acetate (150 mL) and methanol (5 mL) and washed with saturated aqueous ammonium chloride (2 x 50 mL), water (2 x 50 mL), and brine (50 mL). The organic phase was dried over  $\text{Na}_2\text{SO}_4$  and passed through a plug of celite, eluting with ethyl acetate, and then concentrated under reduced pressure to afford the crude diol, which was carried forward in the next step without further purification.

A flame-dried round-bottom flask equipped with a stir bar and rubber septum was charged with the crude diol and DMAP (42 mg, 0.36 mmol). Dry THF (6.3 mL), triethylamine (0.40 mL, 2.9 mmol), and 4-pentenoic anhydride (0.56 mL, 3.1 mmol) were then added sequentially and the mixture was stirred at room temperature. After 15 h, THF was removed under reduced pressure and the crude reaction mixture was dissolved in ethyl acetate (30 mL) and washed with water (2 x 30 mL), dried over  $\text{Na}_2\text{SO}_4$ , filtered through a plug of basic alumina, and concentrated under reduced pressure. Purification by column chromatography (5–30% EtOAc/hexanes) yielded the title compound as a blue oil (110 mg, 27% over 2 steps).  $R_f = 0.33$  (1:5 EtOAc/hexanes)

$^1\text{H}$  NMR (400 MHz, acetone- $d_6$ )  $\delta$ : 8.09 (dd,  $J = 8.6, 1.0$  Hz, 1H), 7.82–7.77 (m, 2H), 7.58–7.53 (m, 2H), 7.50 (ddd,  $J = 8.4, 6.9, 1.3$  Hz, 1H), 7.46 (d,  $J = 10.1$  Hz, 1H), 7.35 (ddd,  $J = 8.1, 6.8, 1.1$  Hz, 1H), 7.33–7.28 (m, 2H), 7.12–7.07 (m, 2H), 6.49–6.45 (m, 2H), 6.37 (d,  $J = 9.9$  Hz, 1H), 5.97–5.82 (m, 2H), 5.43–5.33 (m, 2H), 5.16–4.94 (m, 4H), 3.24–3.15 (m, 4H), 2.66 (t,  $J = 7.3$  Hz, 2H), 2.54–2.33 (m, 6H), 1.99–1.91 (m, 4H) ppm.

$^{13}\text{C}\{^1\text{H}\}$  NMR (101 MHz, acetone- $d_6$ )  $\delta$ : 173.0, 171.9, 151.1, 149.7, 148.5, 144.4, 138.1, 137.8, 131.6, 130.8, 130.4, 129.8, 129.49, 129.46, 129.0, 128.6, 127.9, 126.1, 125.0, 122.34, 122.26, 120.1, 116.1, 115.8, 115.3, 112.0, 83.8, 62.4, 48.2, 34.13, 34.11, 29.74, 29.69, 26.1 ppm.

HRMS (ESI,  $m/z$ ): calcd for  $[\text{C}_{40}\text{H}_{40}\text{NO}_5]^+$  ( $\text{M}+\text{H}$ ) $^+$ , 614.2901; found 614.2910.

### III. Preparation of PDMS Materials

PDMS materials incorporating mechanophore crosslinkers (1.5 wt %) were prepared following previously reported procedures using the two-part Sylgard<sup>®</sup> 184 elastomer kit (Dow Corning).<sup>1,3</sup> PDMS films were cut into 25 mm x 3 mm strips for testing.

**General procedure for preparation of PDMS strips.** A representative procedure is provided for the preparation of PDMS containing a 1:1 mixture of mechanophores **1c** and **SP**. Naphthopyran **1c** (22 mg) and spiropyran crosslinker **SP**<sup>2</sup> (17 mg) were dissolved in 0.1 mL xylene in a 20 mL scintillation vial. Sylgard<sup>®</sup> 184 prepolymer base (2.083 g) and 0.1 mL xylene were added and the contents were thoroughly mixed in a vortex mixer with intermittent gentle heating to form a homogeneous, pale orange dispersion. Sylgard<sup>®</sup> 184 curing agent (0.208 g) was added and the contents were mixed thoroughly using a vortex mixer. The mixture was pipetted onto a clean 5 cm x 5 cm delrin plate, which was placed inside a vacuum chamber and evacuated under high vacuum (~30 mTorr) for 3 h. The delrin plate was then transferred to an oven and cured at 80 °C overnight. After curing, the plate was removed from the oven and the PDMS film was peeled off and cut into strips with a razor blade.

### IV. DFT Calculations

CoGEF calculations were performed using Spartan '18 according to previously reported methods.<sup>4</sup> Ground state energies were calculated using DFT at the B3LYP/6-31G\* level of theory. Starting from the equilibrium geometry of the unconstrained molecule (relative energy = 0 kJ/mol), the distance between the terminal methyl groups of the truncated

structure was increased in increments of 0.05 Å and the energy was minimized at each step. The maximum force associated with the transformation was calculated from the slope of the energy–displacement curve immediately prior to bond cleavage. All naphthopyrans examined in this study are predicted to undergo cleavage of the C–O pyran bond, resulting in generation of the merocyanine product *via* a  $6\pi$  electrocyclic ring-opening reaction. The CoGEF results for each naphthopyran mechanophore are illustrated below in Figures A.1–A.5.

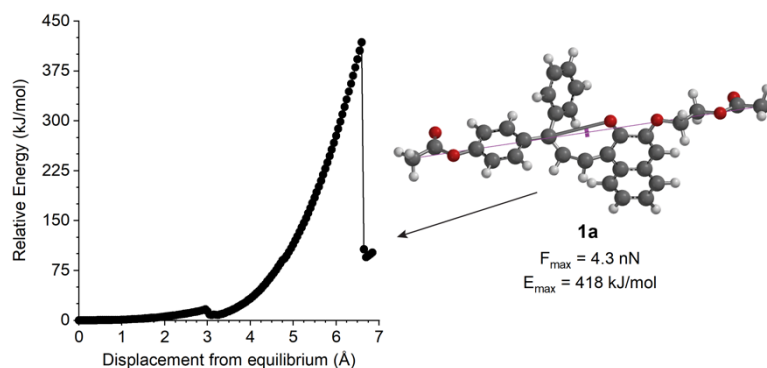


**Figure A.1** CoGEF plot of relative energy vs. displacement and the calculated structure immediately after the ring-opening reaction for naphthopyran **1a**.

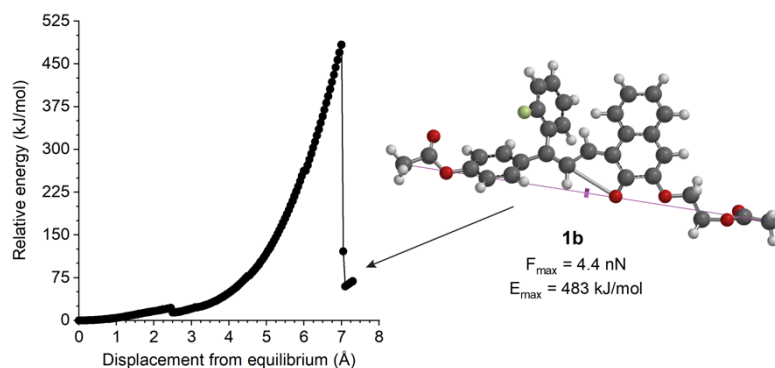


**Figure A.2** CoGEF plot of relative energy vs. displacement and the calculated structure immediately after the ring-opening reaction for naphthopyran **1b**.

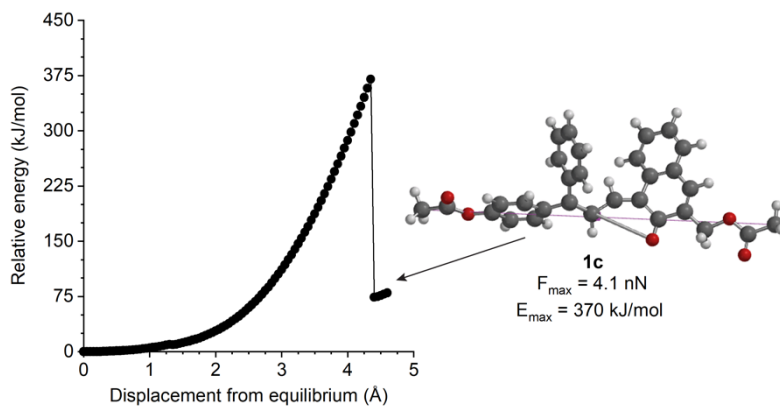


**Figure A.3** CoGEF plot of relative energy vs. displacement and the calculated structure immediately after the ring-opening reaction for naphthopyran **1c**.

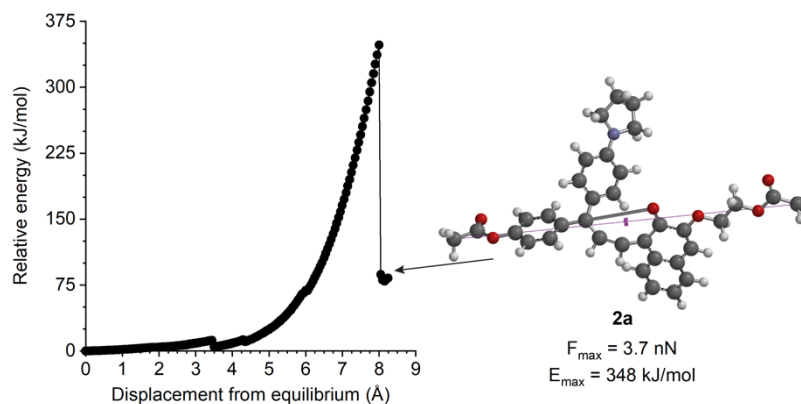


**Figure A.4** CoGEF plot of relative energy vs. displacement and the calculated structure immediately after the ring-opening reaction for naphthopyran **2a**.

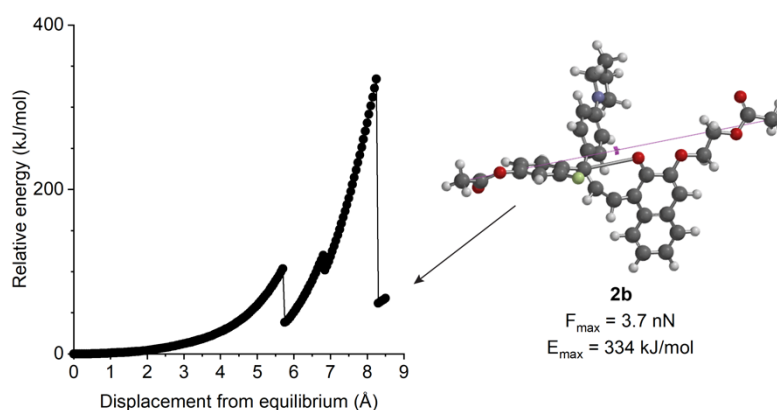


**Figure A.5** CoGEF plot of relative energy vs. displacement and the calculated structure immediately after the ring-opening reaction for naphthopyran **2b**.

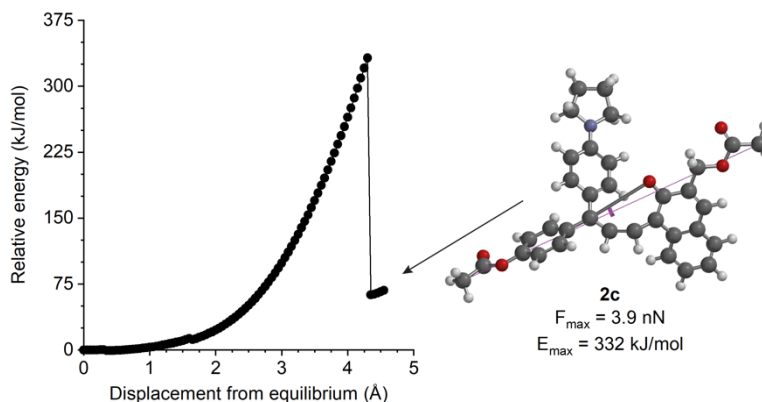


**Figure A.7** CoGEF plot of relative energy vs. displacement and the calculated structure immediately after the ring-opening reaction for naphthopyran **2c**.

## V. Characterization of Thermal Reversion Kinetics

**Characterization of merocyanine electrocyclization in solution.** The kinetics of thermal ring-closure for each merocyanine was evaluated in solution after photoirradiation of the naphthopyran at room temperature in the dark. Solutions of each naphthopyran (**1a–2b**) in THF (non-stabilized) were irradiated with UV light ( $\lambda = 311$  nm, 30 s) in a quartz cuvette and immediately transferred to a spectrophotometer. Concentrations were 0.1 mM (**1a**, **1c**, **2b**), 0.01 mM (**1b**), and 0.25 mM (**2a**). The time-dependent absorbance was monitored at the  $\lambda_{\max}$  corresponding to each merocyanine and the data were fit to first-order exponential decay using OriginPro 2020, given by eq 1:

$$A(t) = Ae^{-k_r t} + c \quad (1)$$

where  $A(t)$  is the absorbance at  $\lambda_{\max}$  at time  $t$ ,  $c$  is the residual absorbance,  $A$  is the pre-exponential factor, and  $k_r$  is the rate constant for the thermal ring-closing reaction. Rate constants are reported in  $\text{s}^{-1}$  as an average of three separate trials (error is reported as standard deviation). Representative plots are displayed in Figure 1.2 and a summary of the determined parameters and fit statistics for all trials are reported below in Table A1. Electrocyclization of the merocyanine derived from **2c** was too rapid for the initial fading rate to be measured under these conditions, although a persistent merocyanine isomer fraction remains after an extended period of time post-irradiation enabling characterization of the absorption spectrum of the merocyanine species. The persistent color observed after photoactivation of some naphthopyrans has been attributed to the relative thermal stability of the merocyanine isomer with *trans* configuration of the exocyclic double bond, which isomerizes slowly in the dark to the *cis* isomer prior to ring-closure.<sup>5–7</sup> The isomerization is promoted efficiently, however, with visible light. Irradiation of the solution containing **2c** and the persistent merocyanine

isomer with a fluorescent white light source for 1 min results in complete attenuation of the visible absorption peak and recovery of the original absorption spectrum (prior to UV irradiation), indicating full conversion of the merocyanine back to the ring-closed naphthopyran (Figure A.6).

	<b>Trial</b>	<i>A</i>	<i>k<sub>r,soln</sub></i> (s <sup>-1</sup> )	<i>c</i>	Reduced $\chi^2$	R <sup>2</sup> (COD)
<b>1a</b>	1	0.72	0.033	0.068	8.13E-06	1.00
	2	0.51	0.033	0.053	2.07E-06	1.00
	3	0.48	0.033	0.058	9.37E-07	1.00
	<i>Average</i>	<i>0.57 ± 0.1</i>	<i>0.033</i>	<i>0.060 ± 0.008</i>		
<b>1b</b>	1	0.12	0.0022	0.028	3.44E-06	0.995
	2	0.13	0.0024	0.032	3.57E-06	0.995
	3	0.13	0.0024	0.030	4.05E-06	0.994
	<i>Average</i>	<i>0.13 ± 0.006</i>	<i>0.0023 ± 0.0001</i>	<i>0.030 ± 0.002</i>		
<b>1c</b>	1	0.39	0.073	0.051	6.84E-06	0.999
	2	0.47	0.075	0.064	7.89E-06	0.999
	3	0.37	0.076	0.052	5.29E-06	0.999
	<i>Average</i>	<i>0.41 ± 0.05</i>	<i>0.075 ± 0.002</i>	<i>0.056 ± 0.007</i>		
<b>2a</b>	1	0.040	0.21	0.070	9.18E-08	0.999
	2	0.057	0.17	0.072	9.63E-08	1.00
	3	0.050	0.19	0.082	2.33E-08	1.00
	<i>Average</i>	<i>0.049 ± 0.009</i>	<i>0.19 ± 0.02</i>	<i>0.075 ± 0.006</i>		
<b>2b</b>	1	1.19	0.010	0.11	1.22E-05	1.00
	2	1.08	0.010	0.10	1.33E-05	1.00
	3	1.31	0.010	0.12	2.54E-05	0.999
	<i>Average</i>	<i>1.19 ± 0.1</i>	<i>0.010</i>	<i>0.11 ± 0.01</i>		

<sup>a</sup>Error is reported as standard deviation.

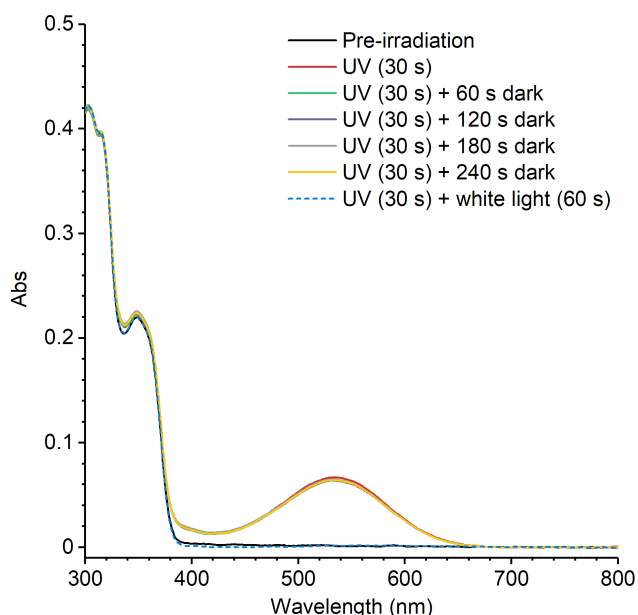


**Figure A.6** Photochemical activation of naphthopyran **2c** results in a persistent merocyanine species that can be efficiently reverted upon irradiation with visible light. A solution of **2c** in THF (0.1 mM) was irradiated with UV light ( $\lambda = 311$  nm, 30 s) and absorbance spectra were subsequently collected over 240 s, demonstrating negligible changes over that time period in the dark. After irradiating the solution with fluorescent white light for 60 s, the visible absorption peak is completely attenuated and the original absorption spectrum is returned, indicating full conversion of the merocyanine species back to the naphthopyran.

**Characterization of merocyanine electrocyclization in PDMS materials.** PDMS strips were activated mechanically by hand in tension or photochemically by irradiation with UV light ( $\lambda = 311$  nm, 90 s). Digital images were acquired with a Canon EOS 5D Mark IV DSLR camera equipped with a Canon 24-70 f/4 lens and a Canon Speedlite flash. Images were standardized to a white balance of 6500 K in Adobe Lightroom, then straightened and cropped in Adobe Photoshop. For Figure 2 and Figure 3 in the main text, images were also individually adjusted to achieve equal exposure levels using the exposure adjustment tool in Adobe Photoshop.

To determine approximate rates of thermal reversion of the merocyanine dyes in PDMS materials, samples were uniformly irradiated with UV light ( $\lambda = 311$  nm, 90 s) and photographs were subsequently acquired at regular time intervals. After correcting white balance, straightening, and cropping, average intensity values of the red and green channels over a 1000 x 80 pixel area at the center of each film were extracted from the RGB histogram in Adobe Photoshop. Ratios of the red and green channel intensities were then plotted as a function of time for each PDMS sample and the data were fit to a model of biexponential decay in OriginPro 2020, given by eq S2:

$$A(t) = A_1 e^{-k_{r1}t} + A_2 e^{-k_{r2}t} + c \quad (2)$$

where  $A(t)$  is the absorbance at  $\lambda_{\text{max}}$  at time  $t$ ,  $c$  is the residual ratio,  $A_1$  and  $A_2$  are pre-exponential factors, and  $k_{r1}$  and  $k_{r2}$  are the rate constants that describe the thermal electrocyclization reaction. Terms  $A_1$  and  $A_2$  express the relative contributions of  $k_{1,\text{solid}}$  and  $k_{2,\text{solid}}$  to the observed fading behavior, respectively. The data are displayed in Figure 1.4 and a summary of the determined parameters and fit statistics are reported below in Table S2. For the PDMS material incorporating naphthopyran **1a**, the fit-determined values of  $k_{r1}$  and  $k_{r2}$  are equivalent, as are the values of  $A_1$  and  $A_2$  (0.09). Thus, the thermal reversion data for sample **1a** were fit to the simpler monoexponential eq 1.

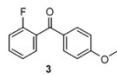
	$A_{1,\text{solid}}$	$A_{2,\text{solid}}$	$k_{1,\text{solid}} \text{ (s}^{-1}\text{)}$	$k_{2,\text{solid}} \text{ (s}^{-1}\text{)}$	$c$	Reduced $\chi^2$	$R^2$ (COD)
<b>1a</b> <sup>a</sup>	0.2	-	0.02	-	0.8	2.71E-05	0.994
<b>1b</b>	0.2	0.04	0.002	0.02	0.7	1.63E-05	0.998
<b>1c</b>	0.07	0.03	0.02	0.09	0.9	5.89E-06	0.996
<b>2a</b>	0.04	0.03	0.01	0.1	0.9	8.11E-06	0.988
<b>2b</b>	0.2	0.1	0.01	0.002	0.6	1.55E-05	0.999
<b>2c</b>	0.04	0.02	0.02	0.1	0.9	3.99E-06	0.993

<sup>a</sup>Thermal reversion data were fit to monoexponential eq. 1.

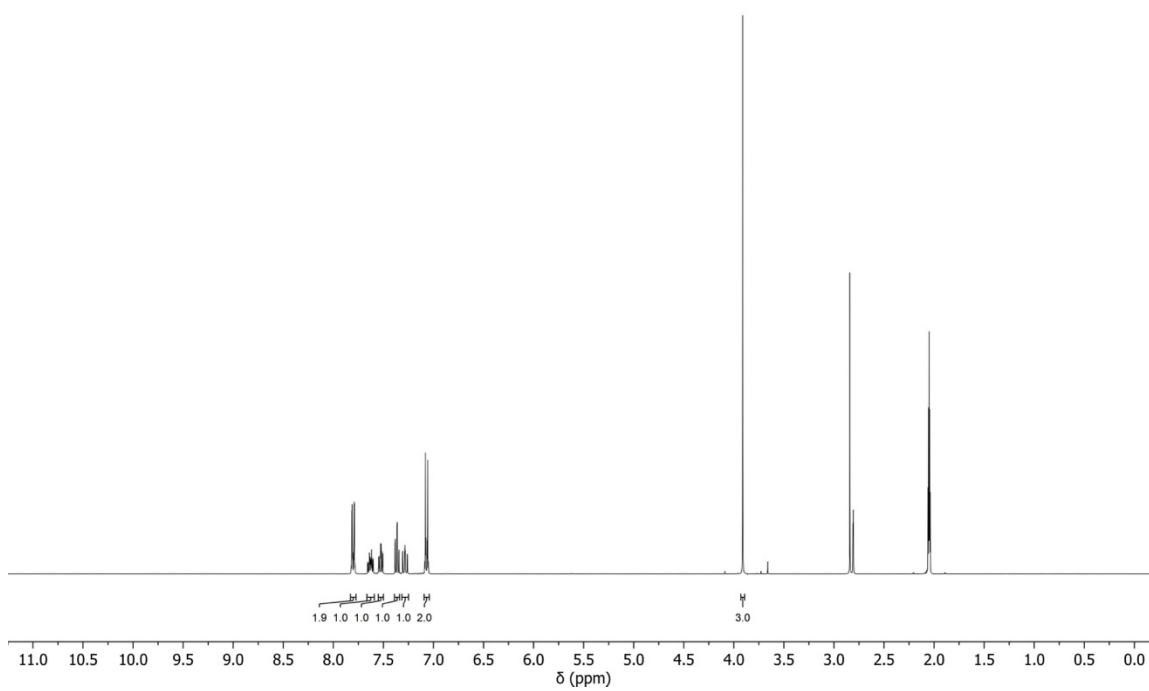
## VI. References

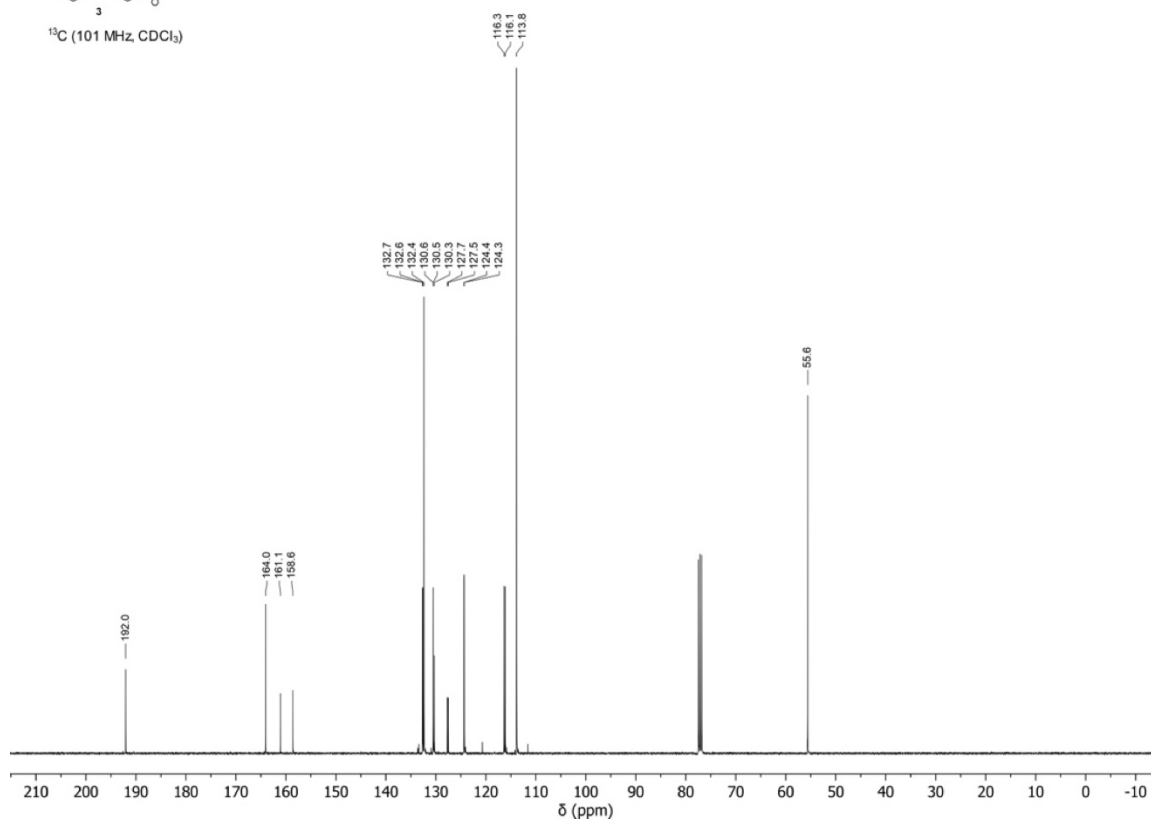
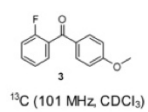
1. Robb, M. J.; Kim, T. A.; Halmes, A. J.; White, S. R.; Sottos, N. R.; Moore, J. S. Regioisomer-Specific Mechanochromism of Naphthopyran in Polymeric Materials. *J. Am. Chem. Soc.* **2016**, *138*, 12328–12331
2. Barbee, M. H.; Mondal, K.; Deng, J. Z.; Bharambe, V.; Neumann, T. V.; Adams, J. J.; Boechler, N.; Dickey, M. D.; Craig, S. L. Mechanochromic Stretchable Electronics. *ACS Appl. Mater. Interfaces* **2018**, *10*, 29918–29924.
3. Gossweiler, G. R.; Hewage, G. B.; Soriano, G.; Wang, Q.; Welshofer, G. W.; Zhao, X.; Craig, S. L. Mechanochemical Activation of Covalent Bonds in Polymers with Full and Repeatable Macroscopic Shape Recovery. *ACS Macro Lett.* **2014**, *3*, 216–219
4. Beyer, M. K. The mechanical strength of a covalent bond calculated by density functional theory. *J. Chem. Phys.* **2000**, *112*, 7307–7312.

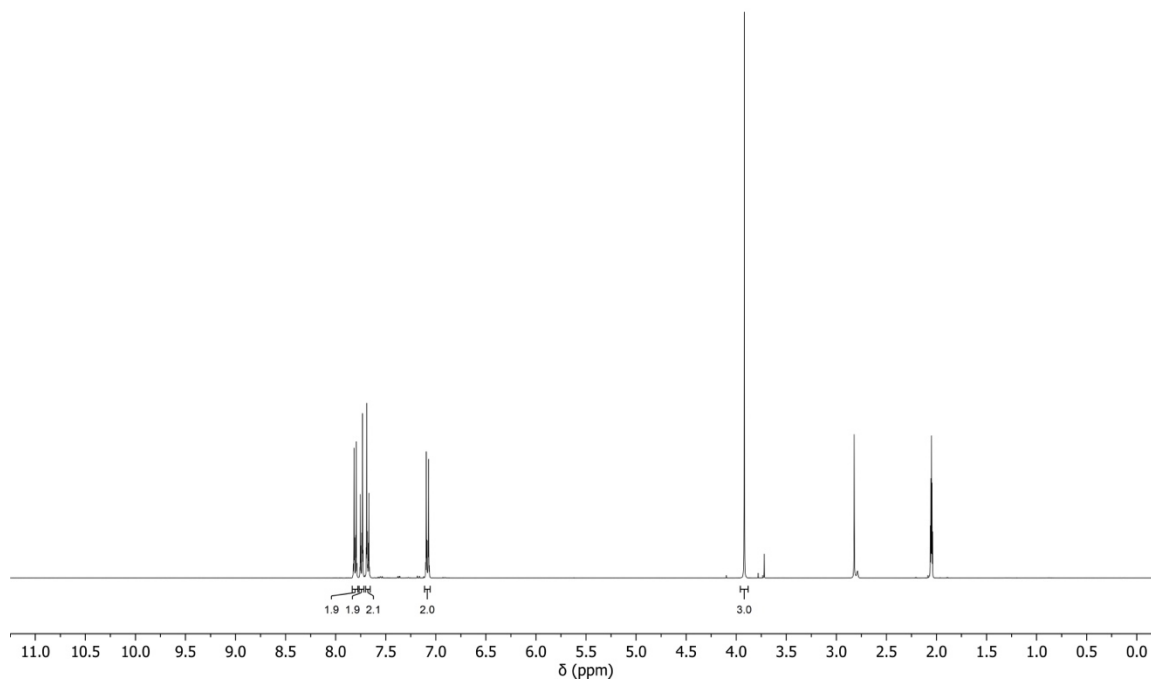
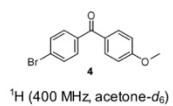
5. Ottavi, G.; Favaro, G.; Malatesta, V. Spectrokinetic study of 2,2-diphenyl-5,6-benzo(2H)chromene: a thermoreversible and photoreversible photochromic system. *J. Photochem. Photobiol. A* **1998**, *115*, 123–128.
6. Delbaere, S.; Luccioni-Houze, B.; Bochu, C.; Teral, Y.; Campredon, M.; Vermeersch, G. Kinetic and structural studies of the photochromic process of 3 H -naphthopyrans by UV and NMR spectroscopy. *J. Chem. Soc. Perkin Trans. 2* **1998**, 1153–1158.
7. Delbaere, S.; Micheau, J.-C.; Teral, Y.; Bochu, C.; Campredon, M.; Vermeersch, G. NMR Structural and Kinetic Assignment of Fluoro-3H-naphthopyran Photomerocyanines. *Photochem. Photobiol.* **2001**, *74*, 694–699.

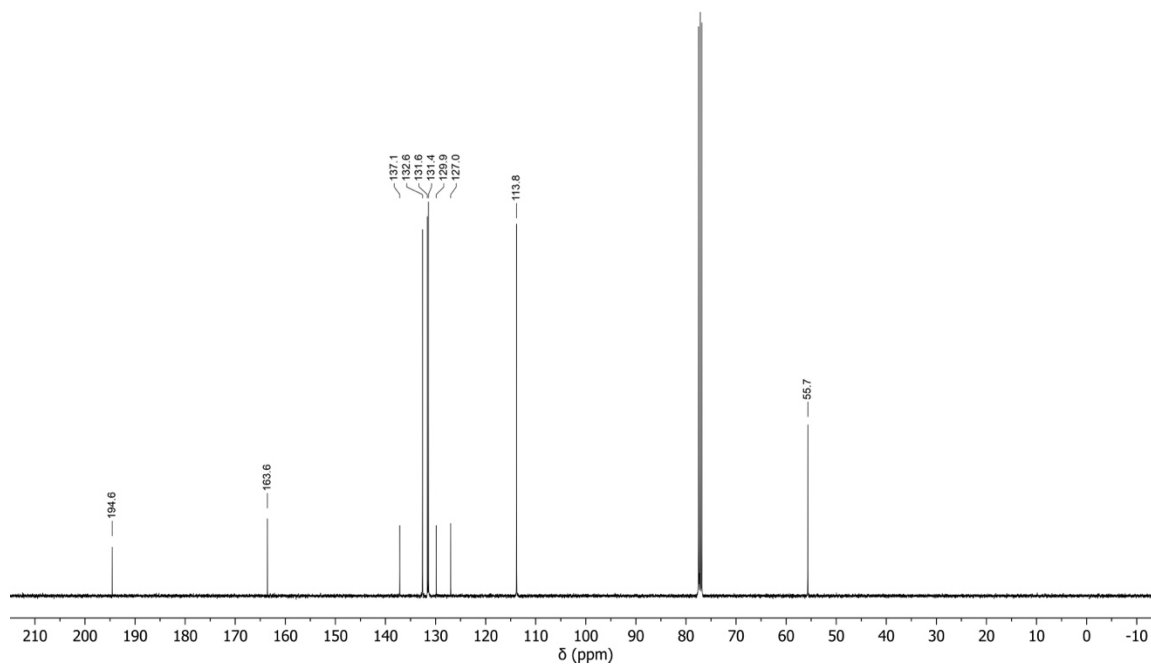
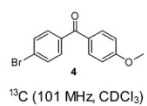
VII.  $^1\text{H}$  and  $^{13}\text{C}$  NMR Spectra

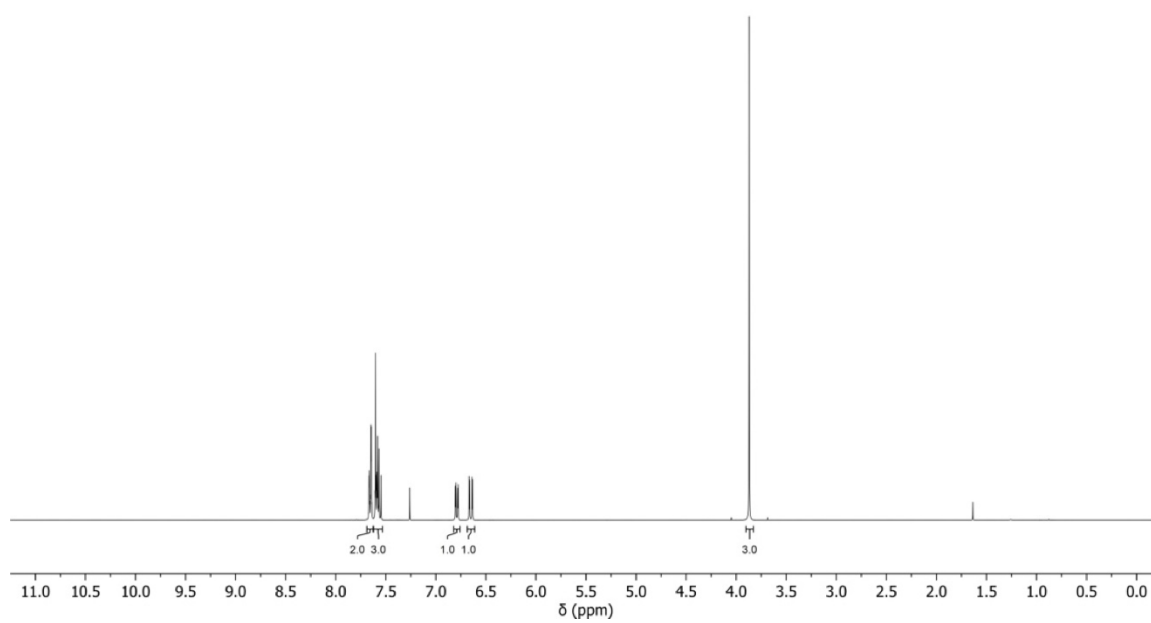
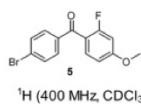
$^1\text{H}$  (400 MHz, acetone- $d_6$ )

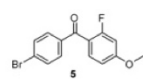




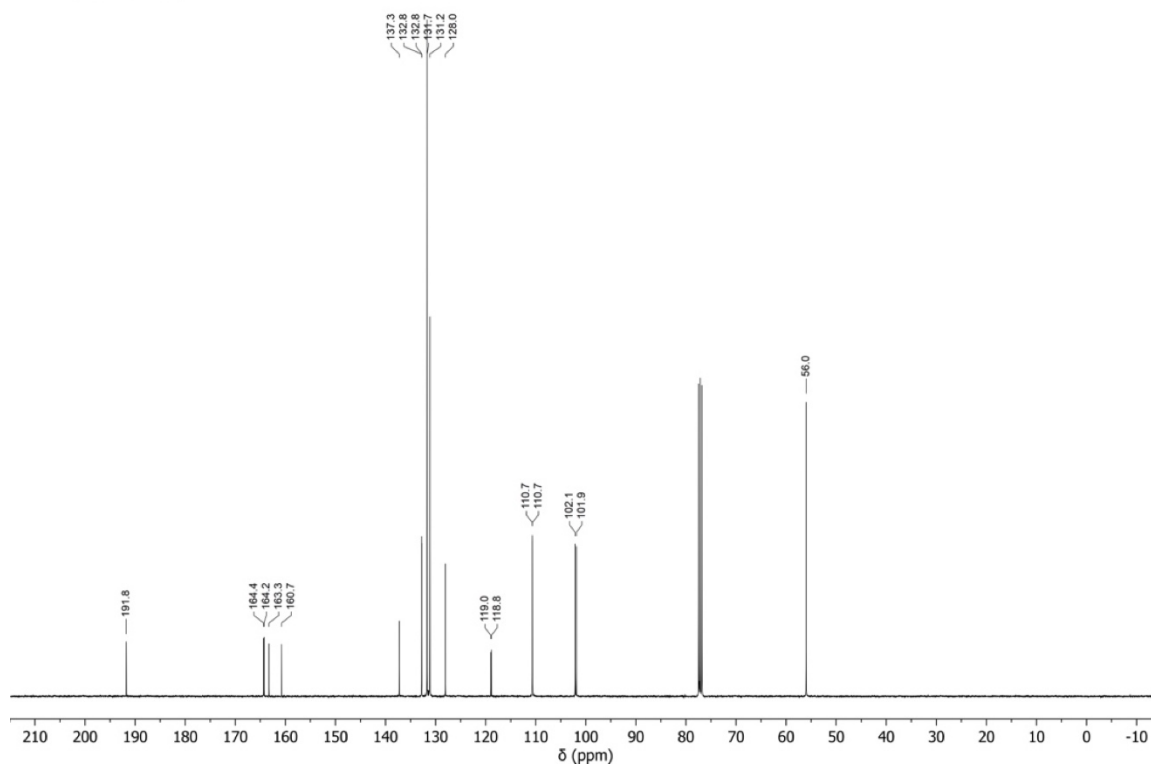


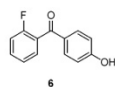




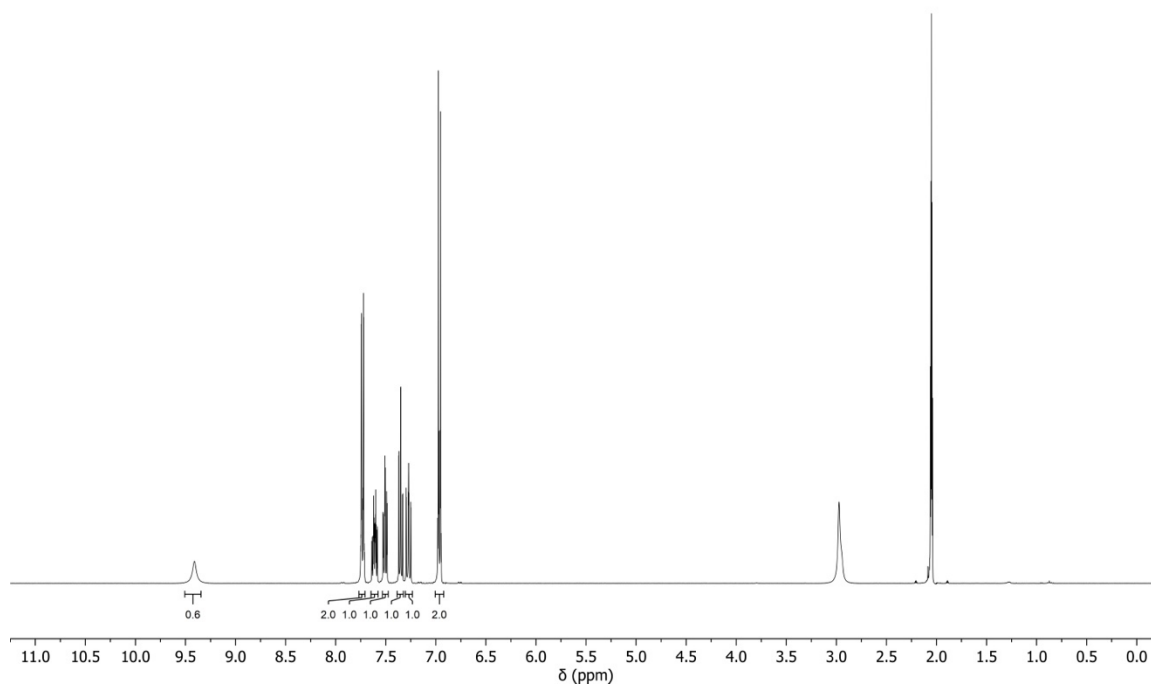


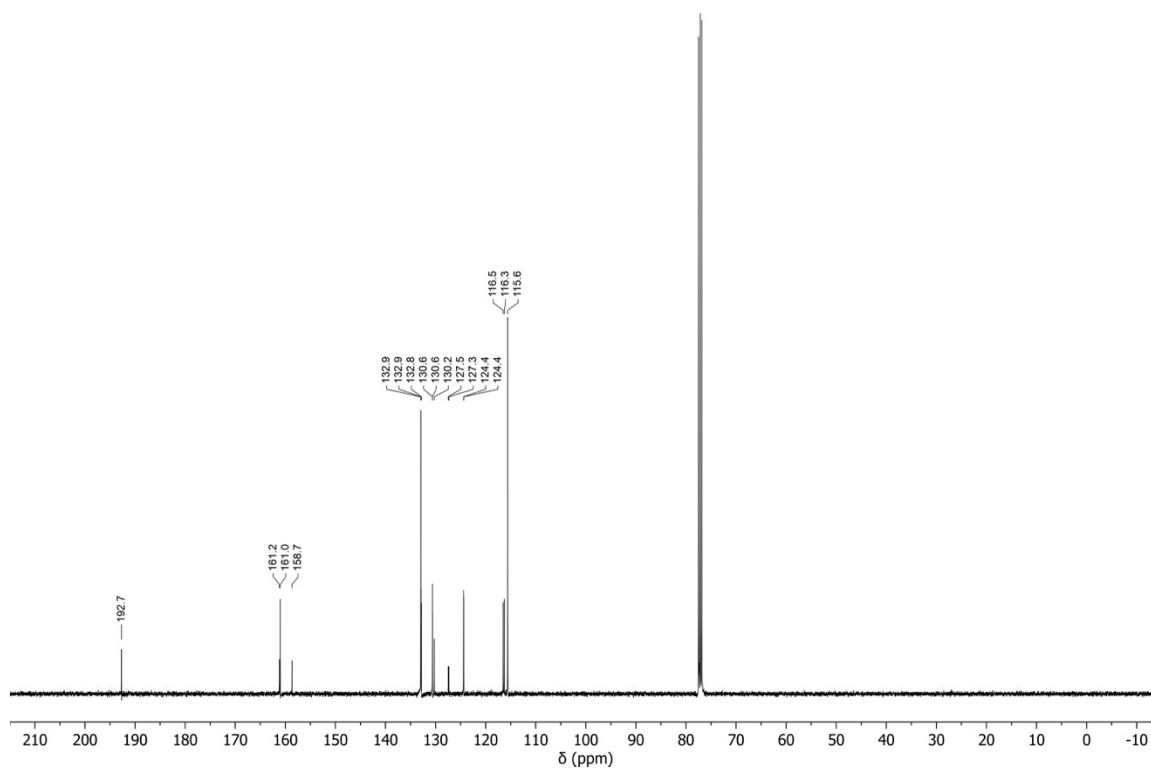
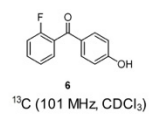
$^{13}\text{C}$  (101 MHz,  $\text{CDCl}_3$ )

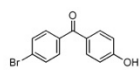




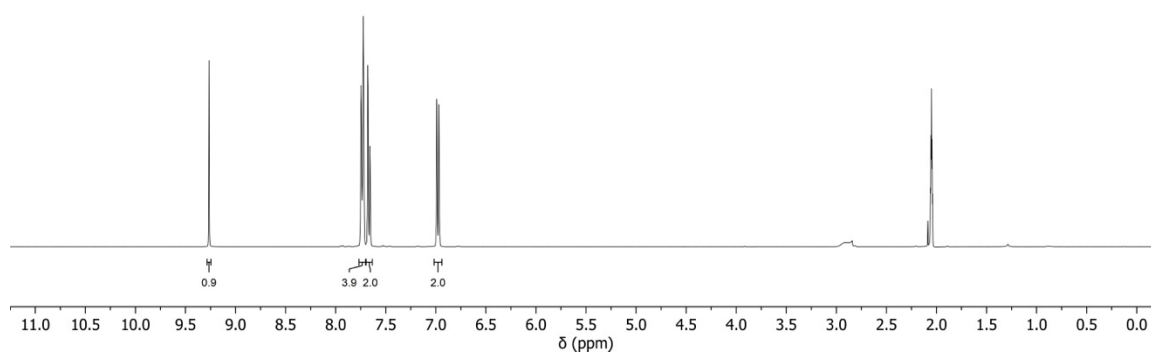
$^1\text{H}$  (400 MHz, acetone- $d_6$ )

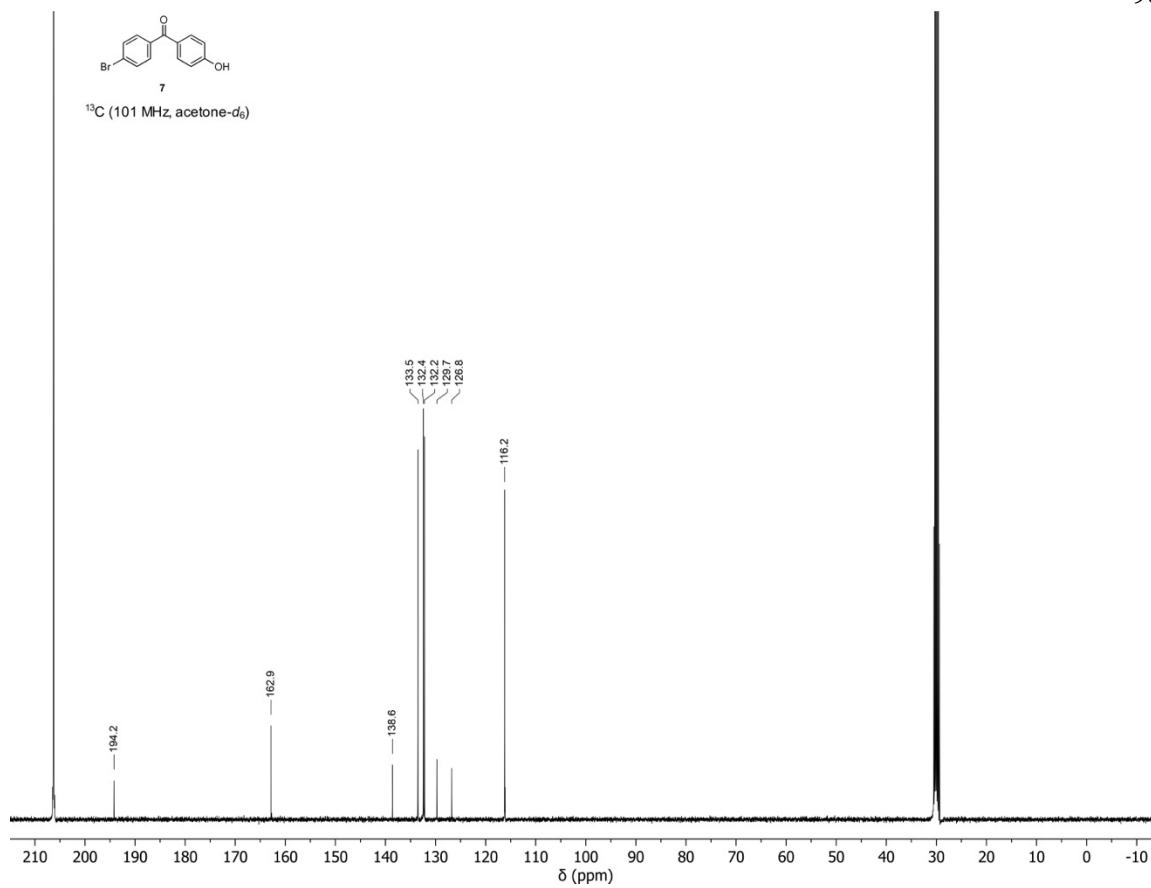


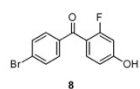




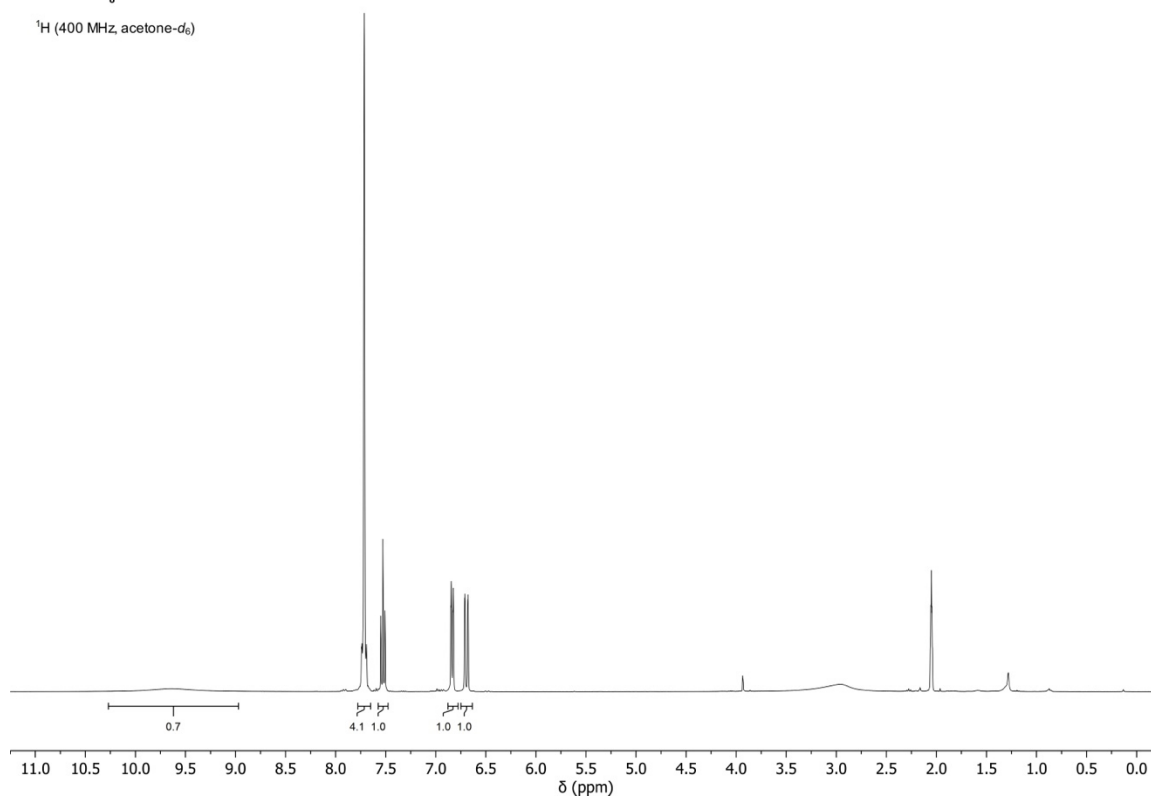
7

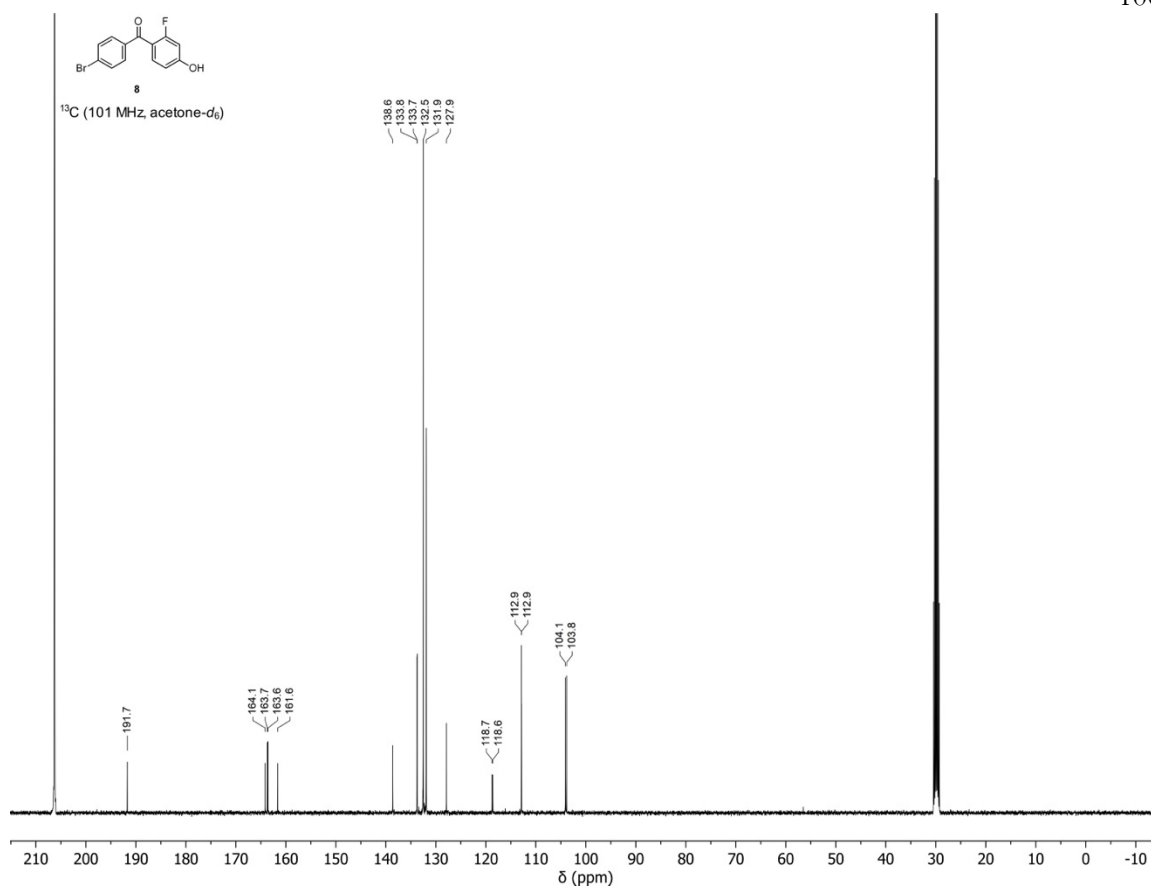
 $^1\text{H}$  (400 MHz, acetone- $d_6$ )

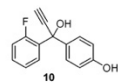




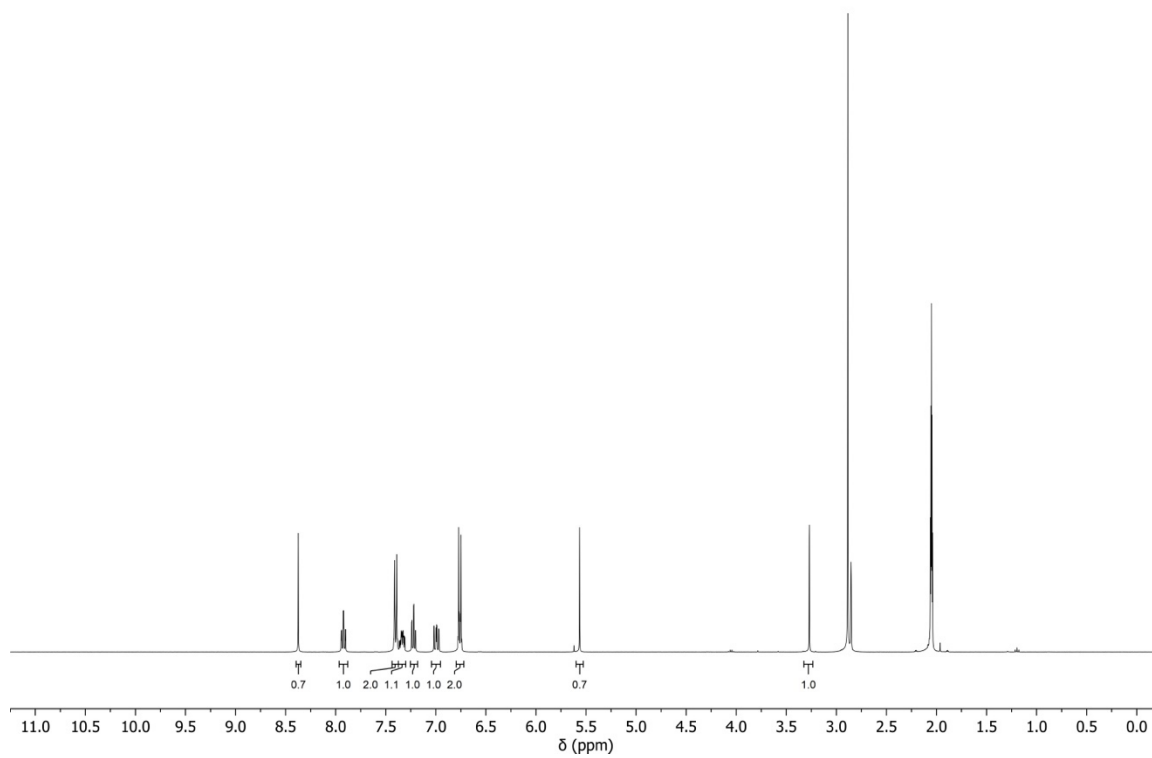
$^1\text{H}$  (400 MHz, acetone- $d_6$ )

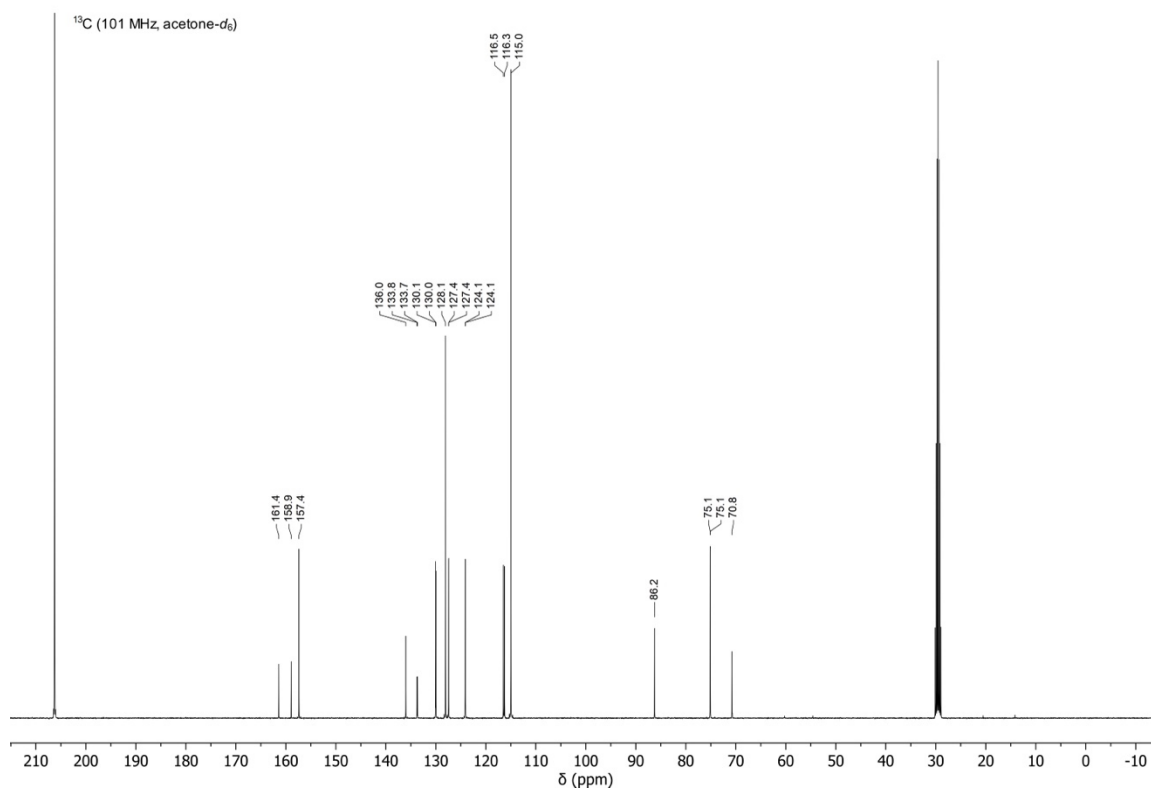
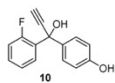


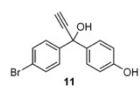




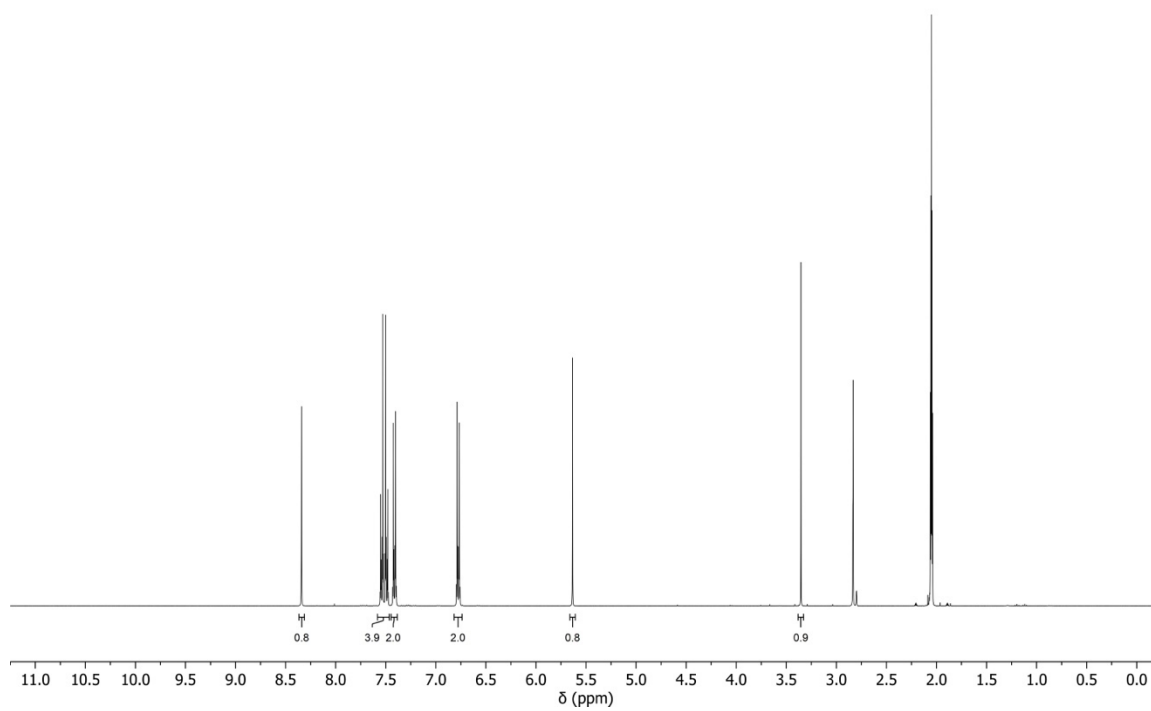
$^1\text{H}$  (400 MHz, acetone- $d_6$ )

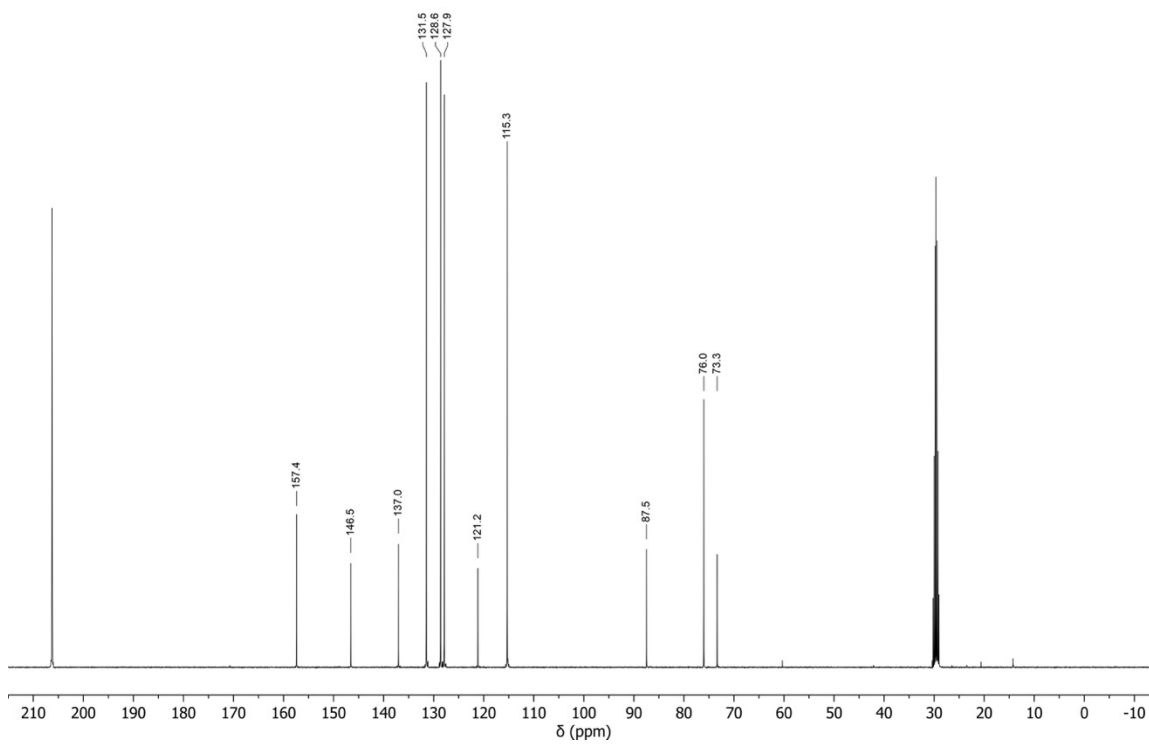
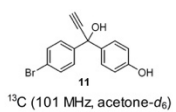


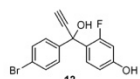




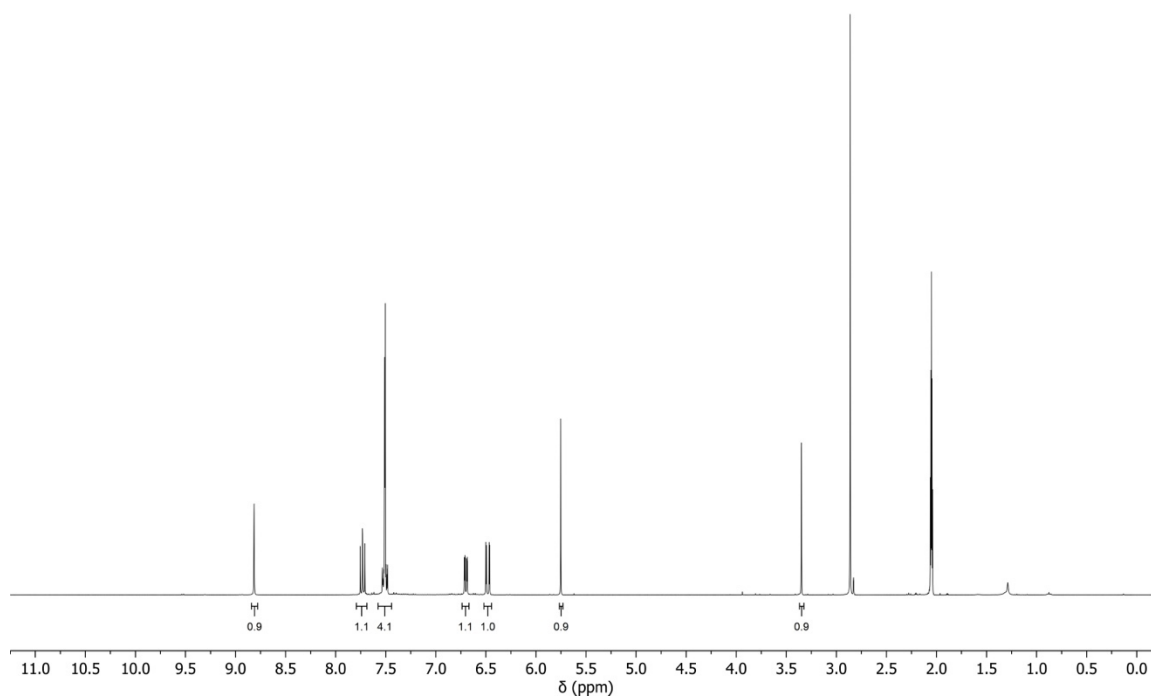
$^1\text{H}$  (400 MHz, acetone- $d_6$ )

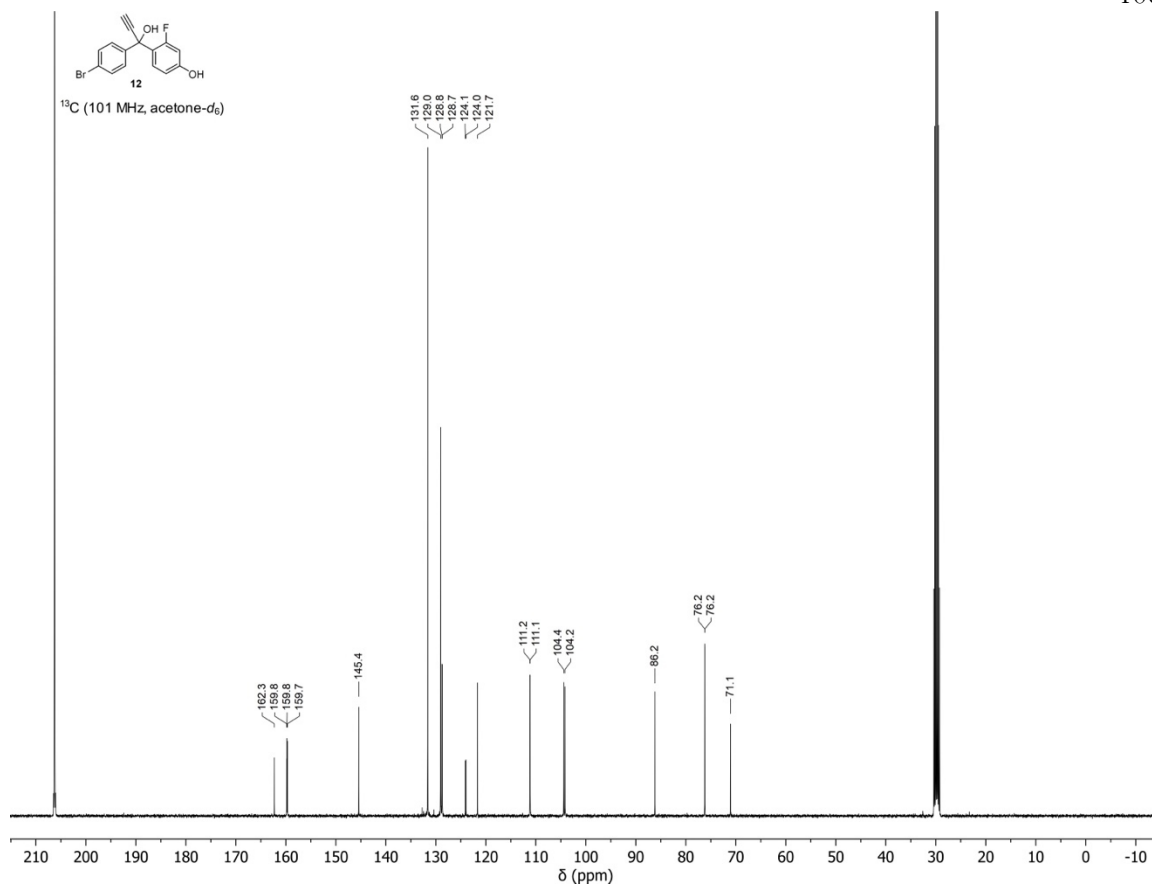


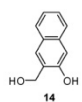




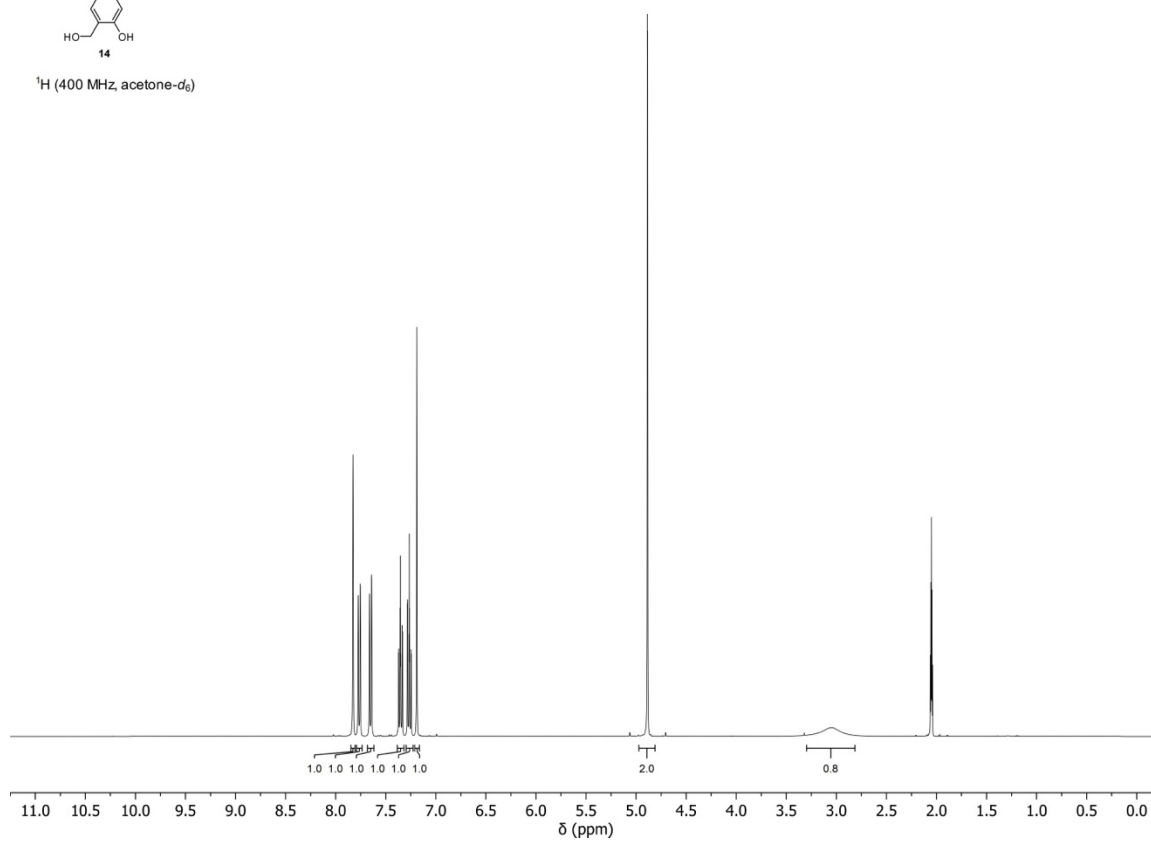
<sup>1</sup>H (400 MHz, acetone-d<sub>6</sub>)

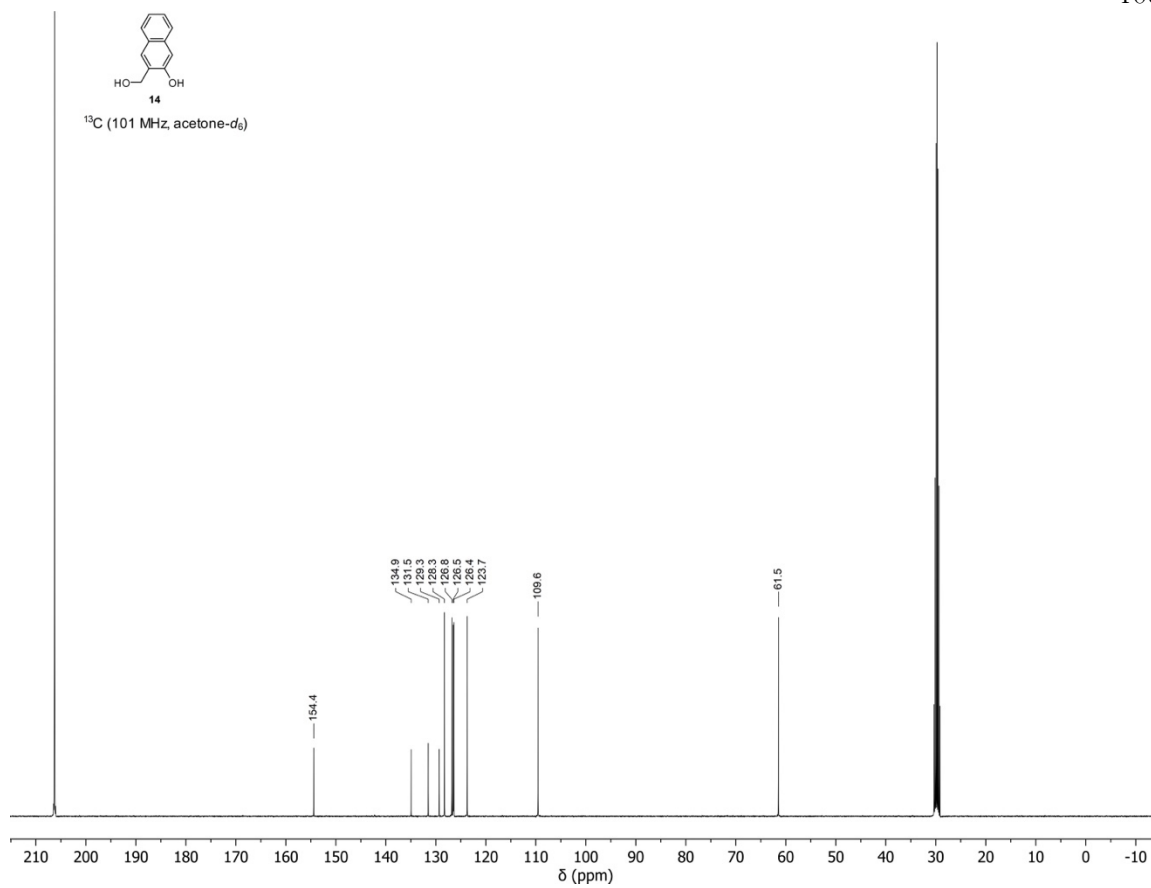


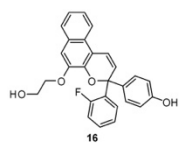




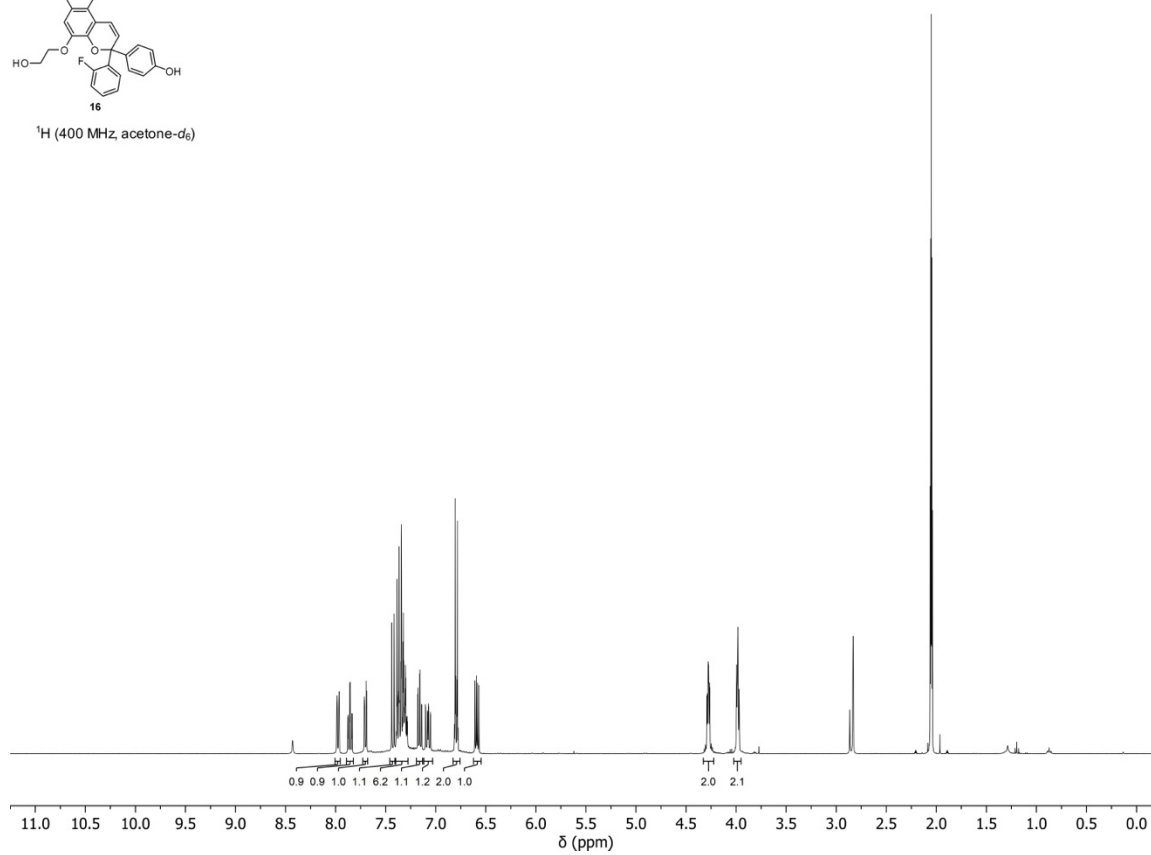
$^1\text{H}$  (400 MHz, acetone- $d_6$ )

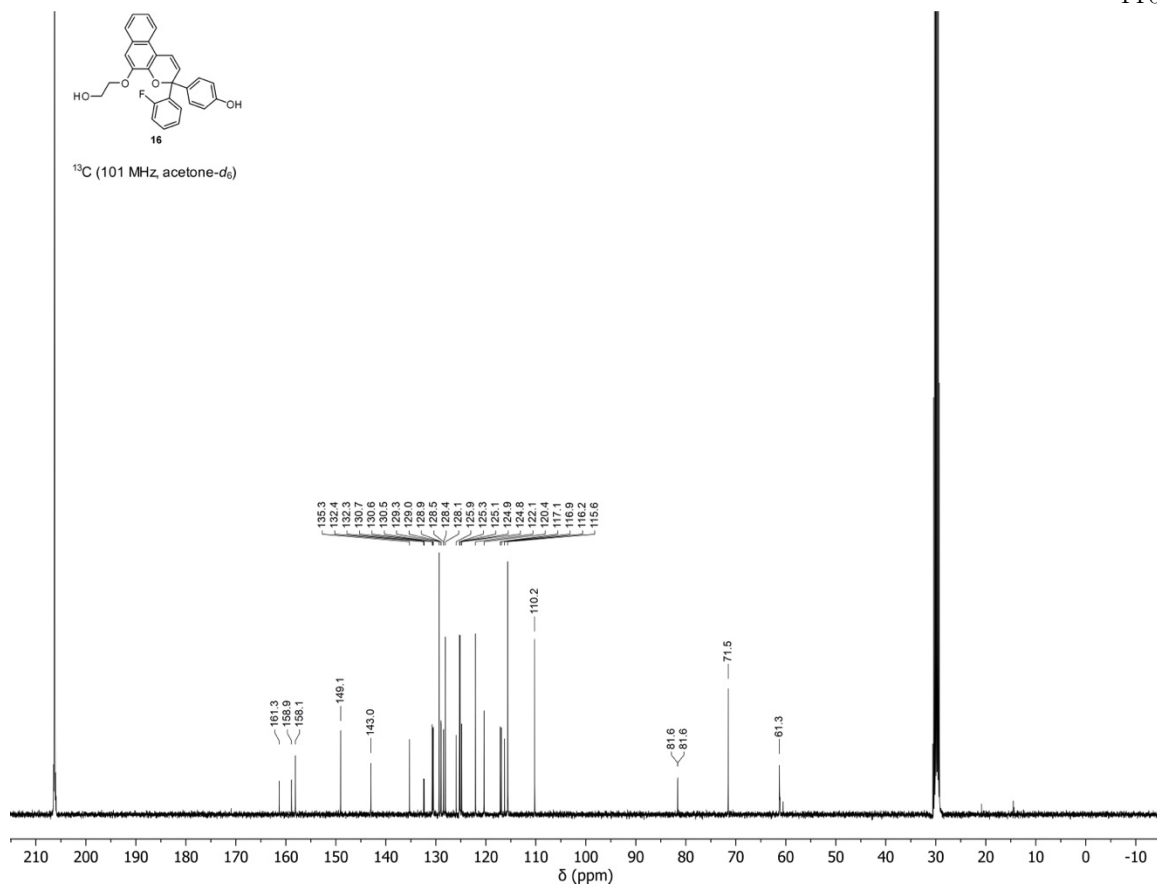


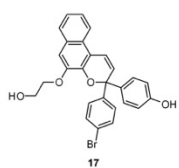
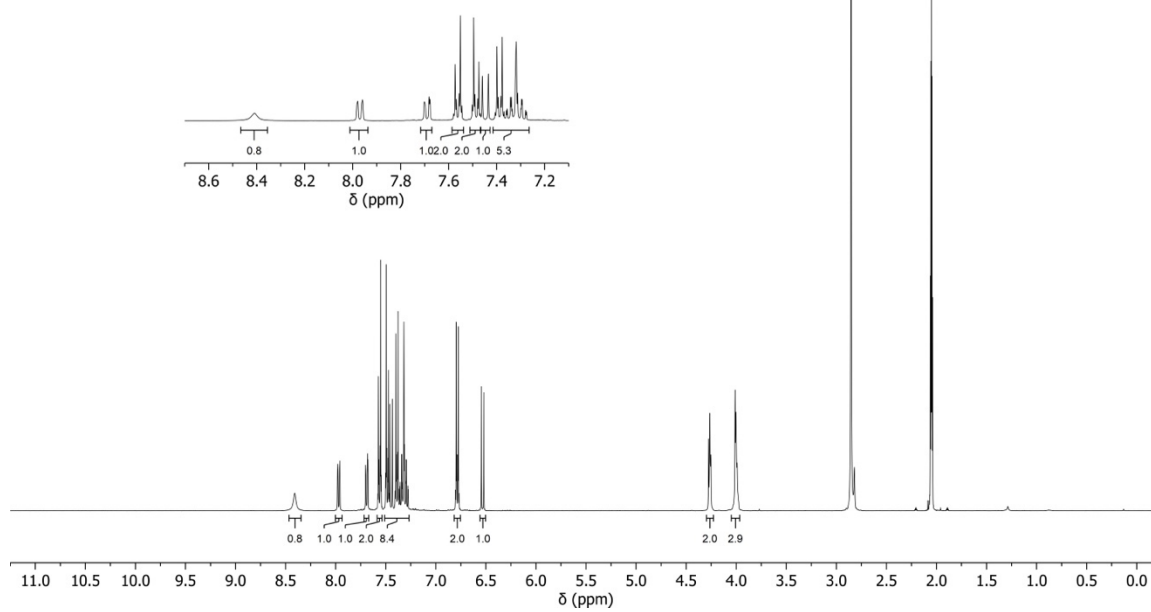


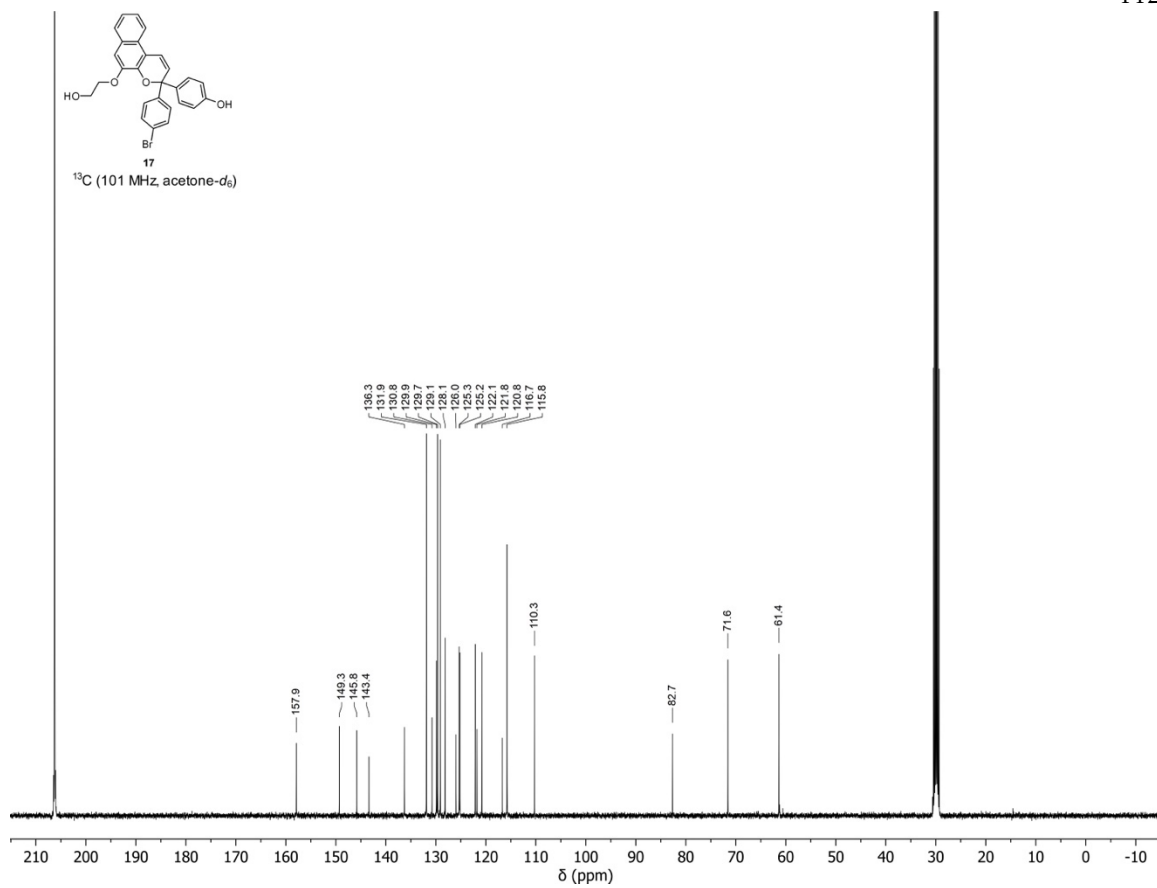


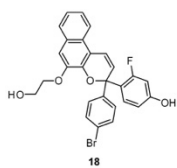
<sup>1</sup>H (400 MHz, acetone-d<sub>6</sub>)



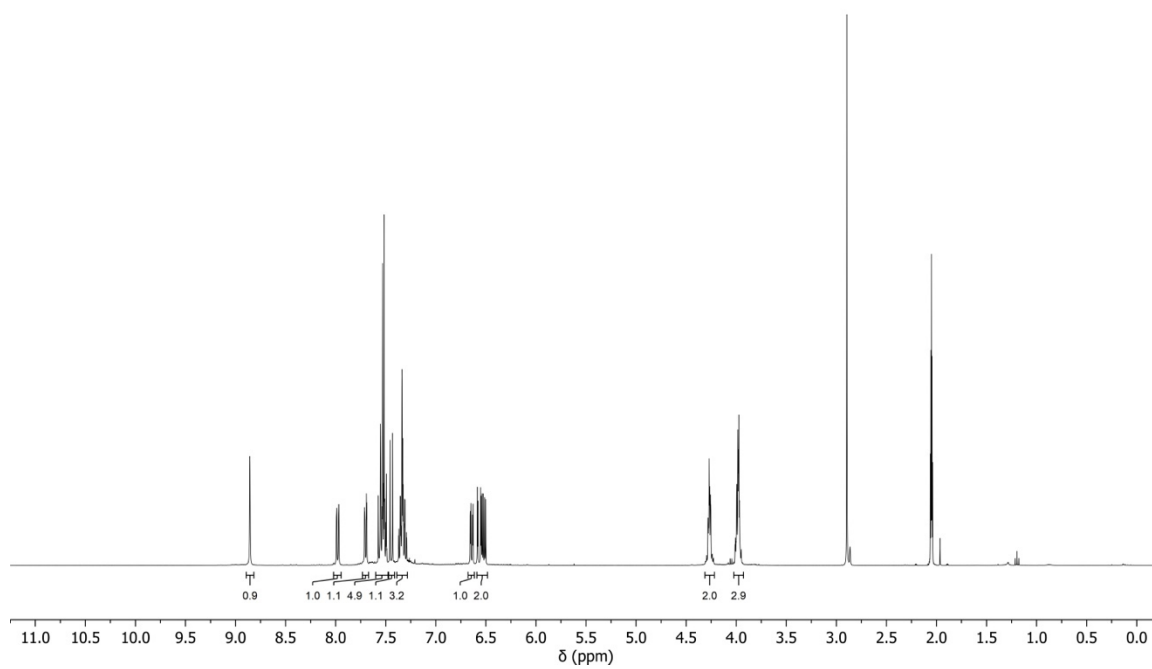


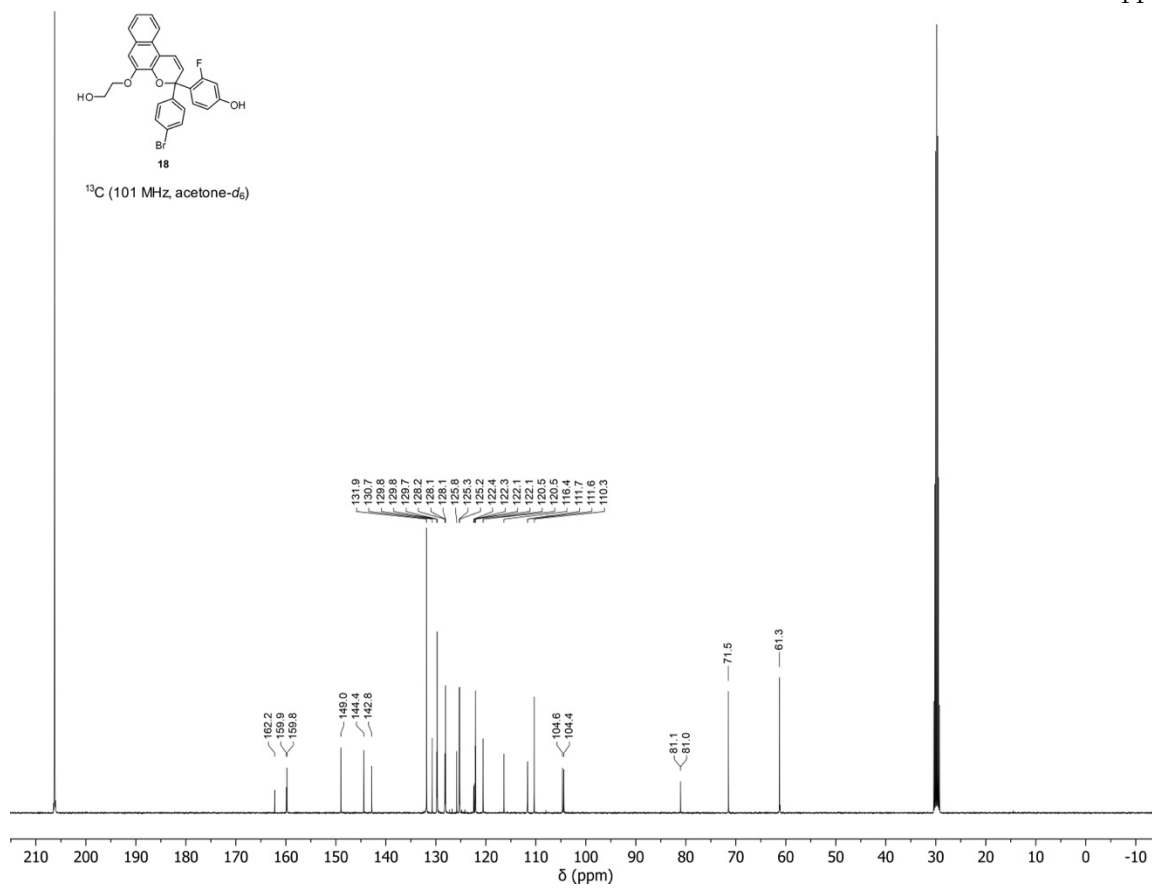
<sup>1</sup>H (400 MHz, acetone-*d*<sub>6</sub>)

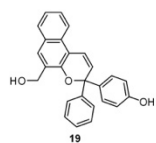




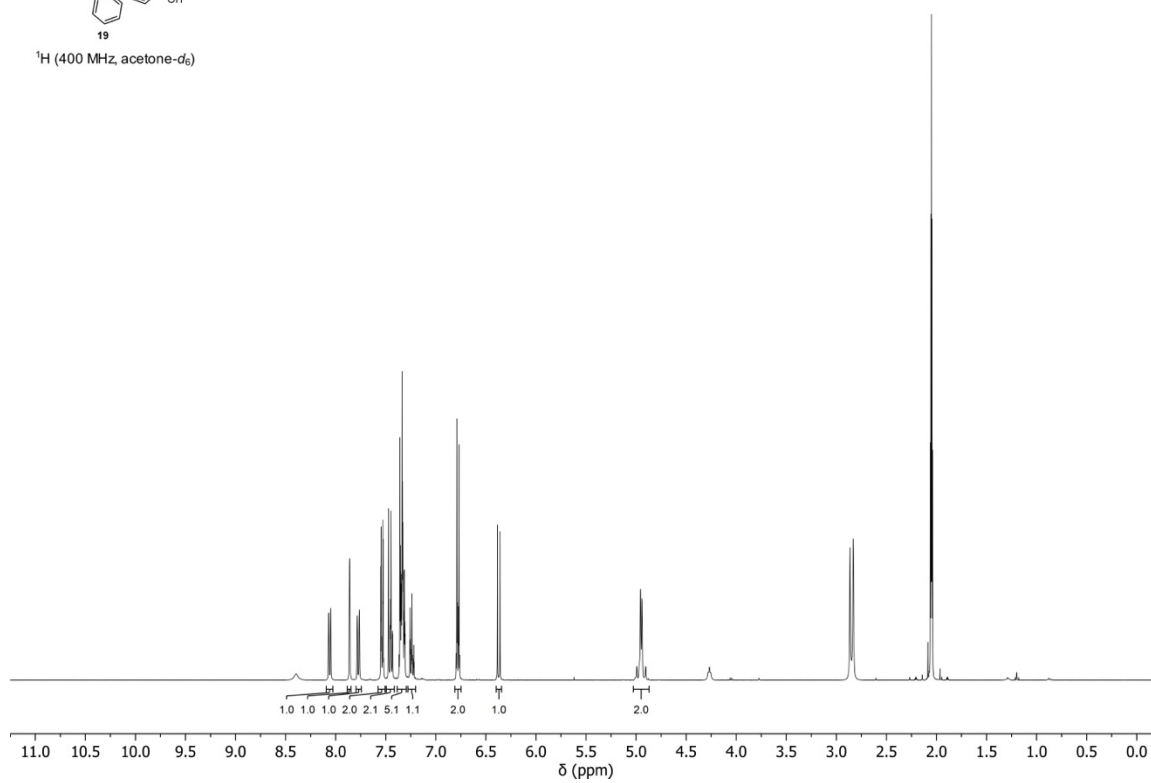
<sup>1</sup>H (400 MHz, acetone-*d*<sub>6</sub>)

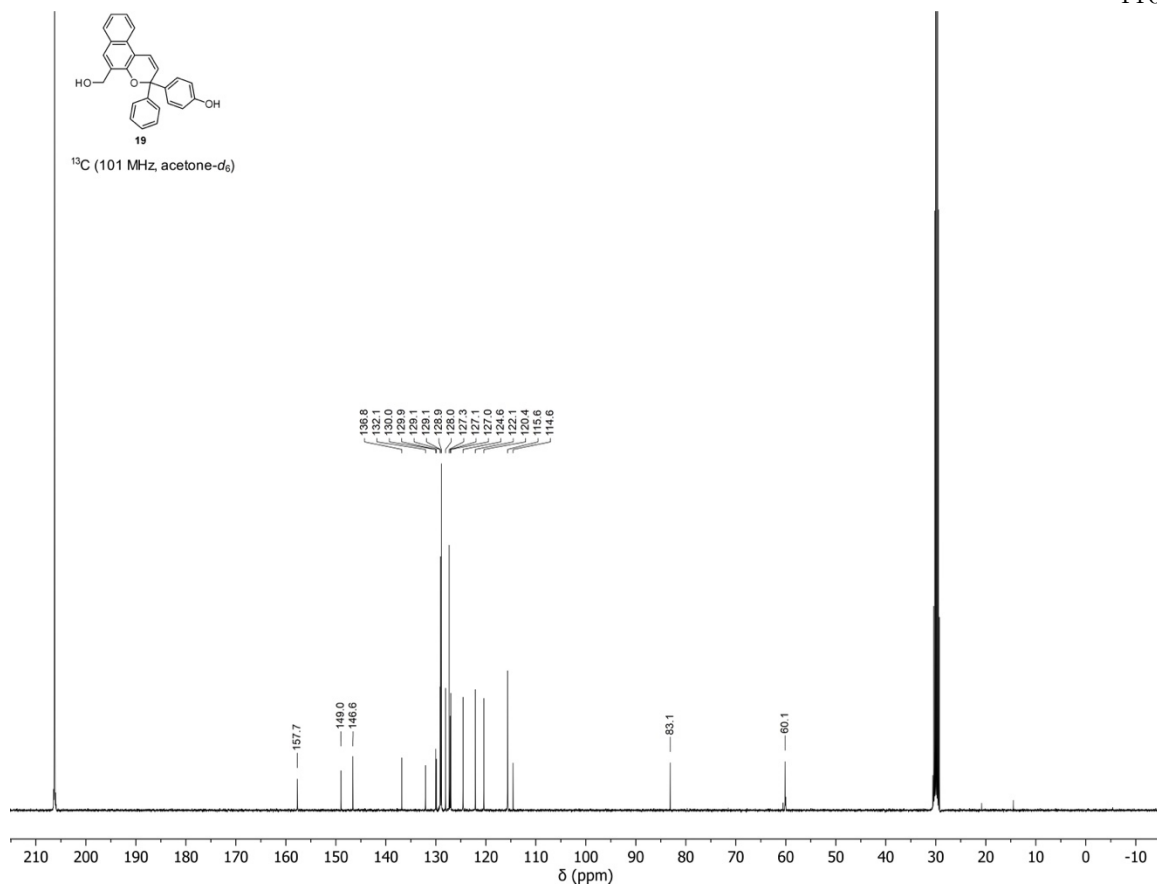


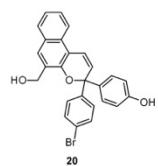




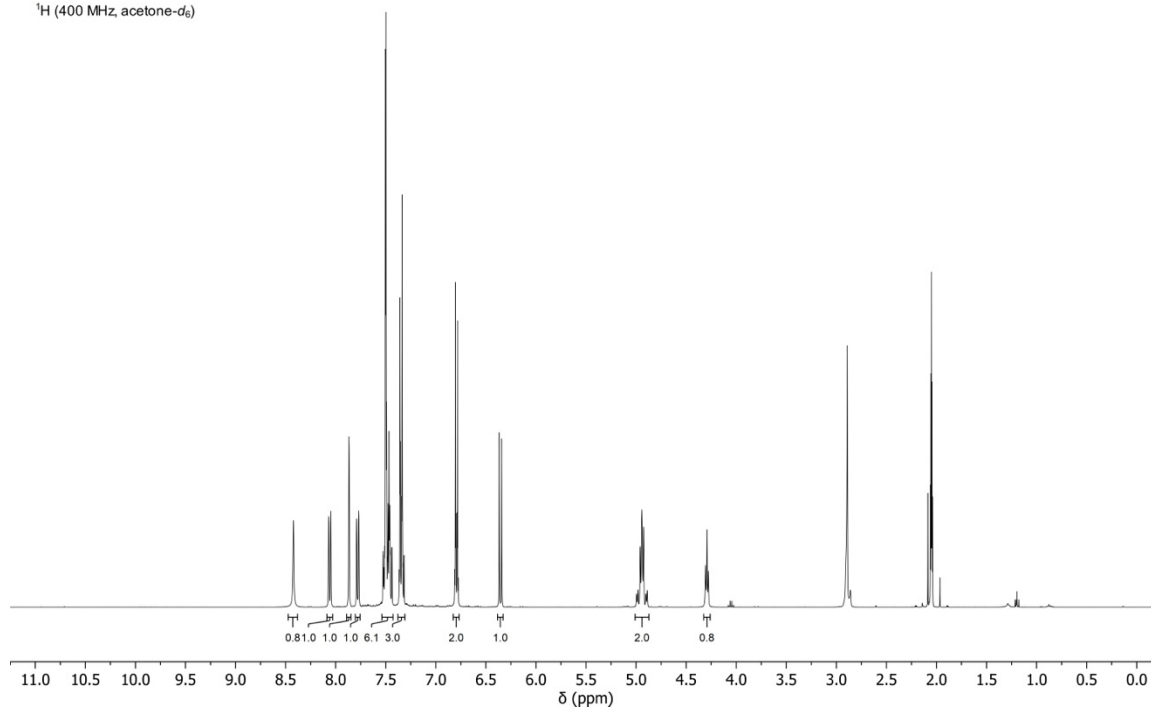
<sup>1</sup>H (400 MHz, acetone-d<sub>6</sub>)

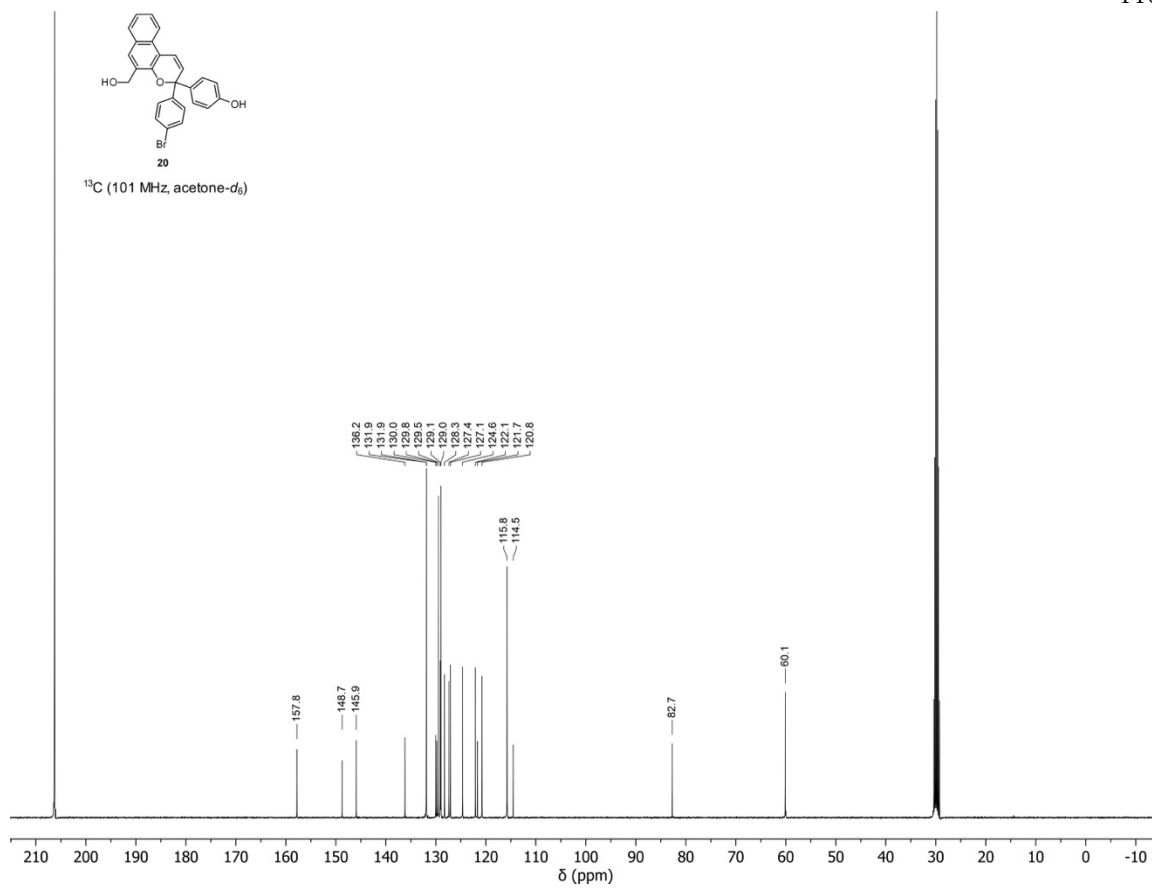


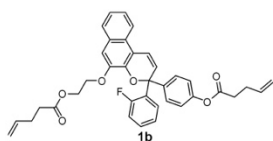




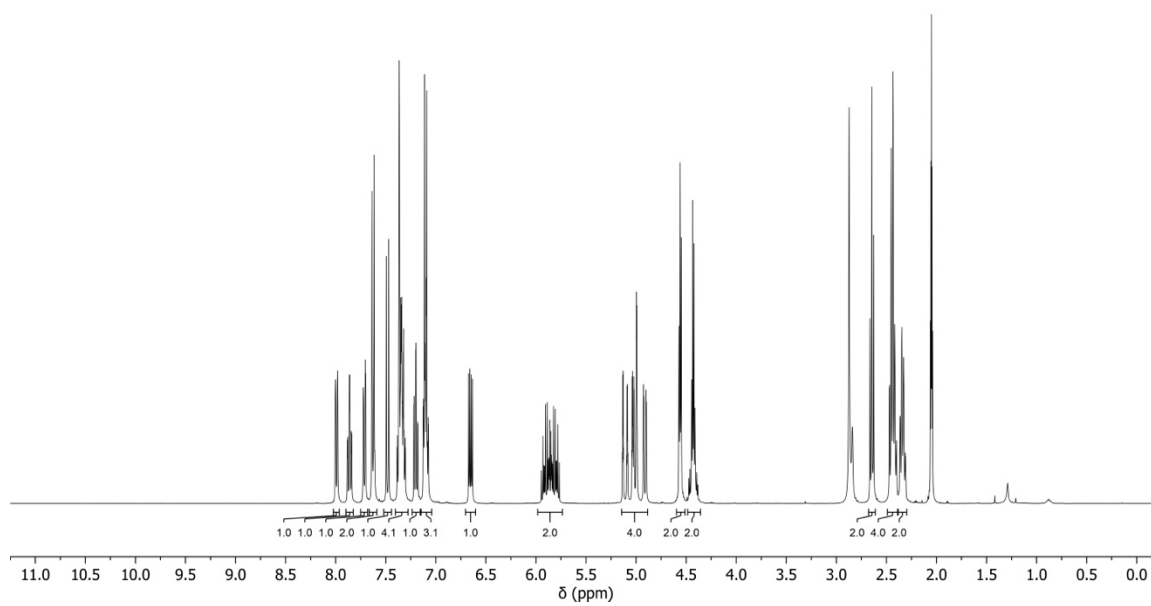
<sup>1</sup>H (400 MHz, acetone-*d*<sub>6</sub>)

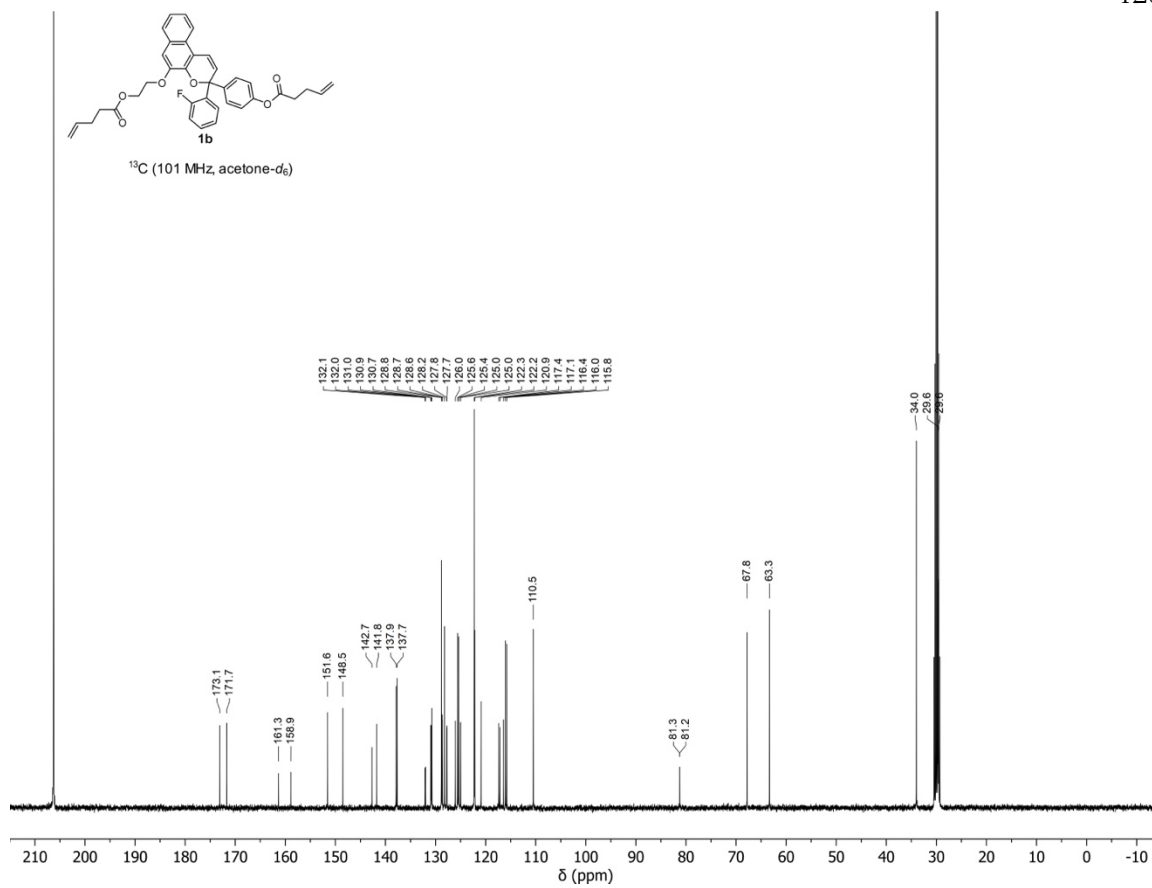


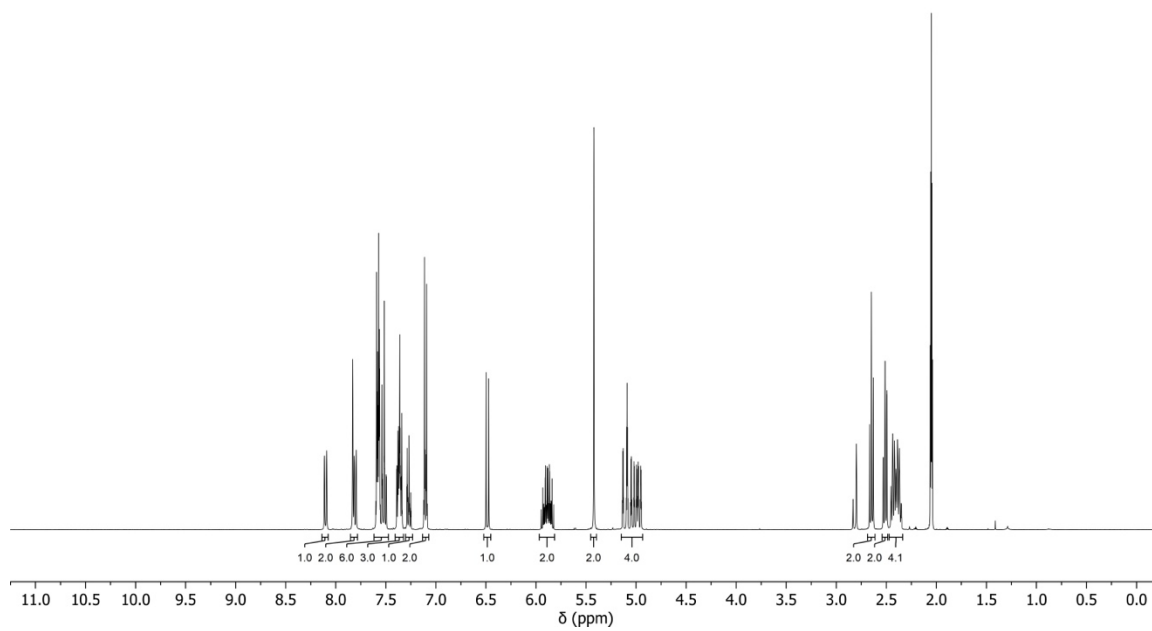
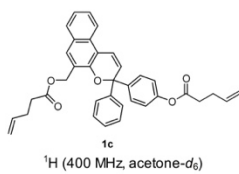




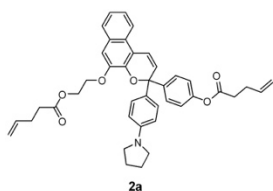
$^1\text{H}$  (400 MHz, acetone- $d_6$ )



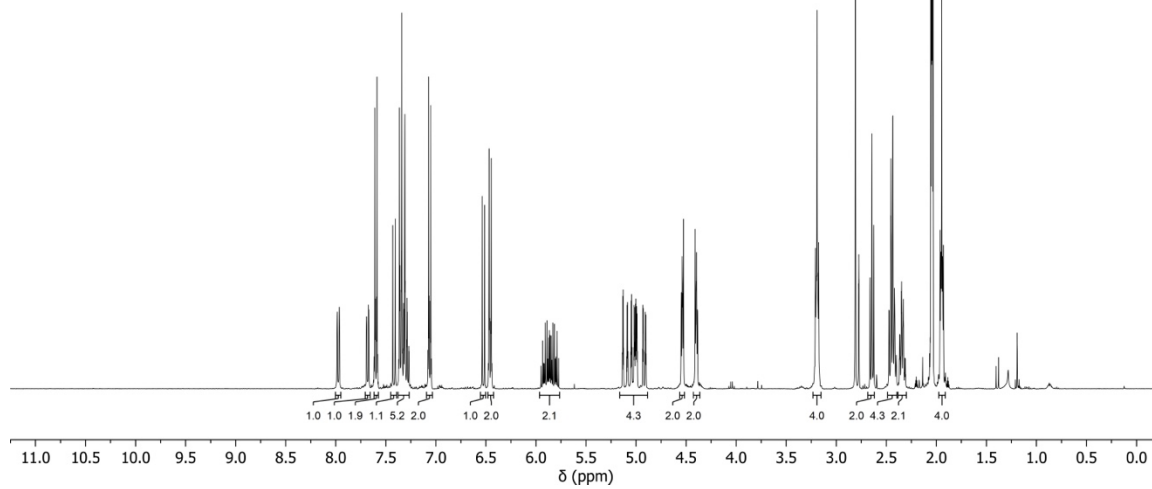


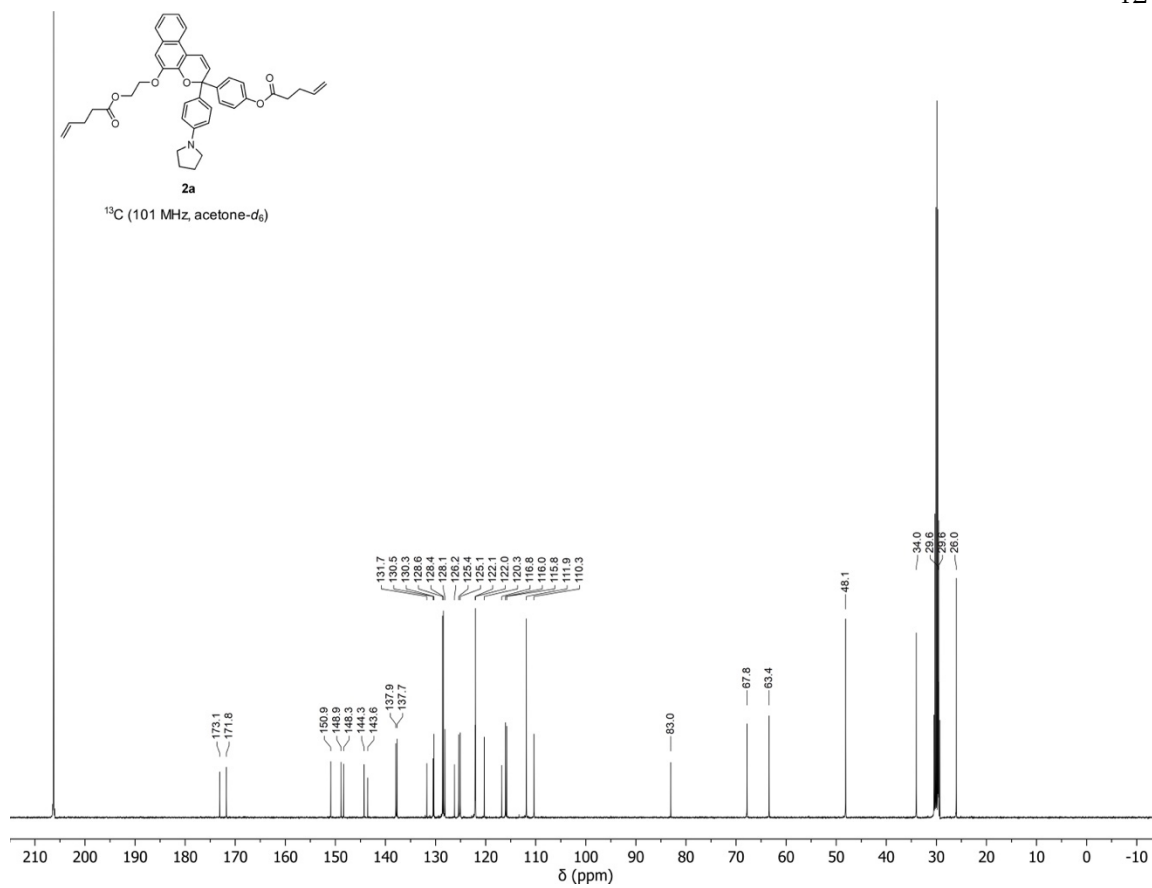


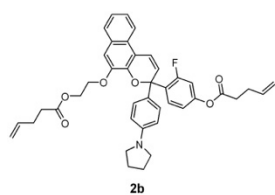




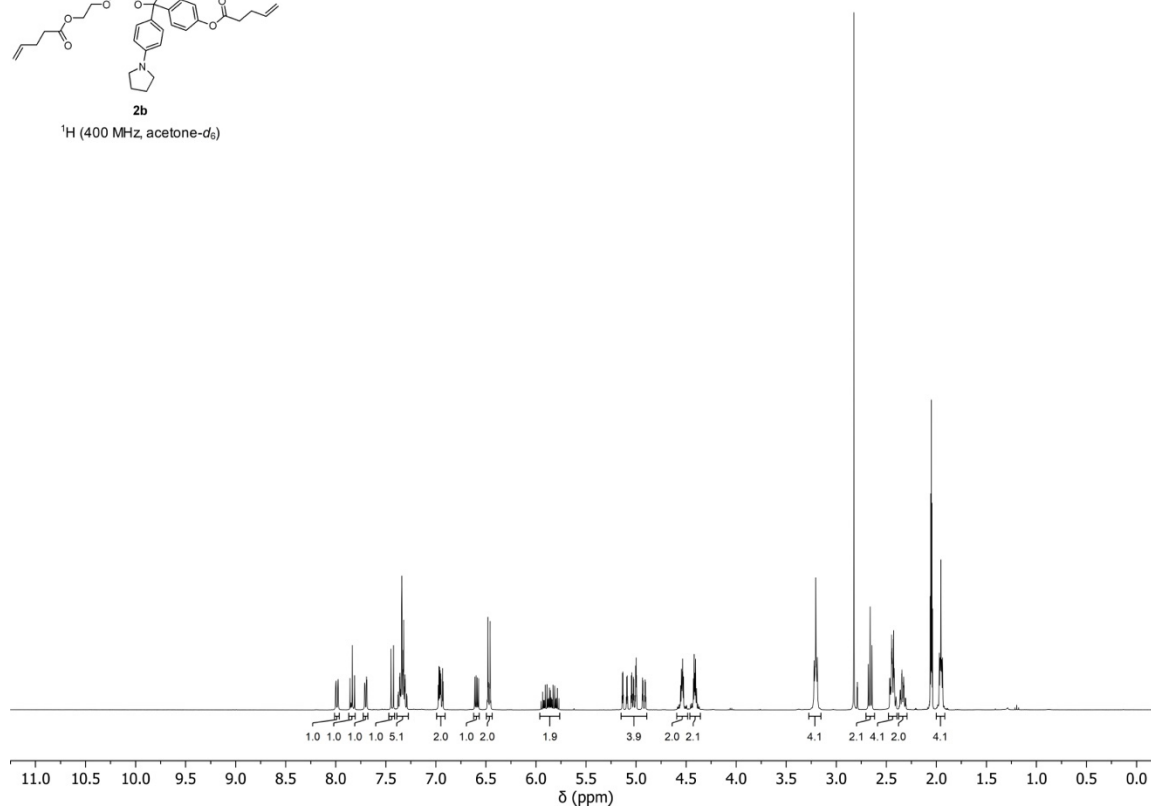
**2a**  
 $^1\text{H}$  (400 MHz, acetone- $d_6$ )

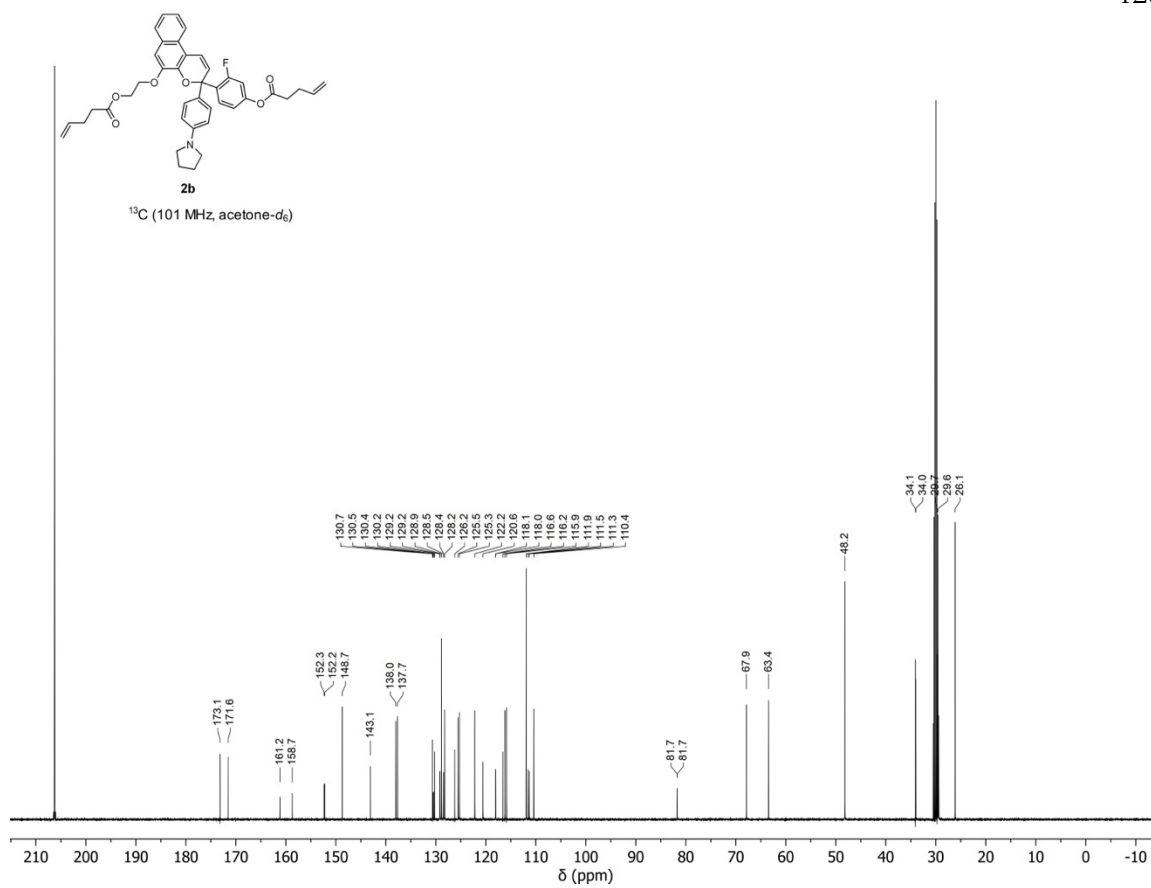


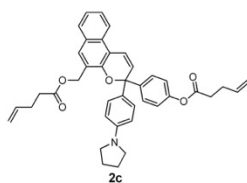




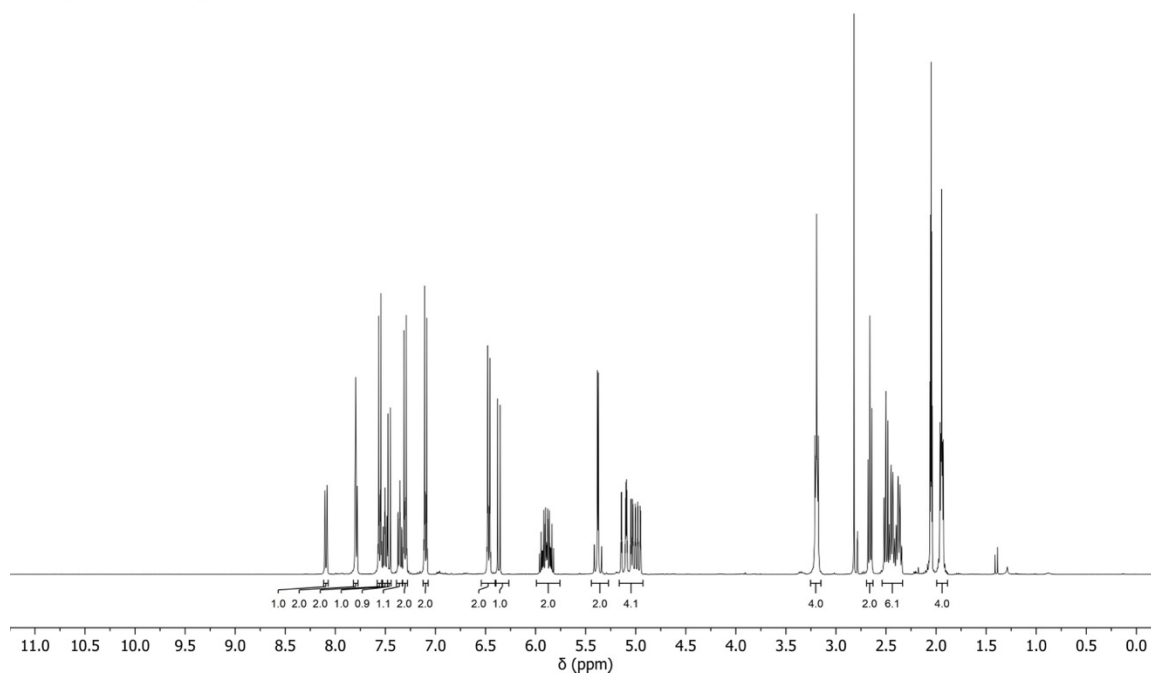
**2b**  
 $^1\text{H}$  (400 MHz, acetone- $d_6$ )

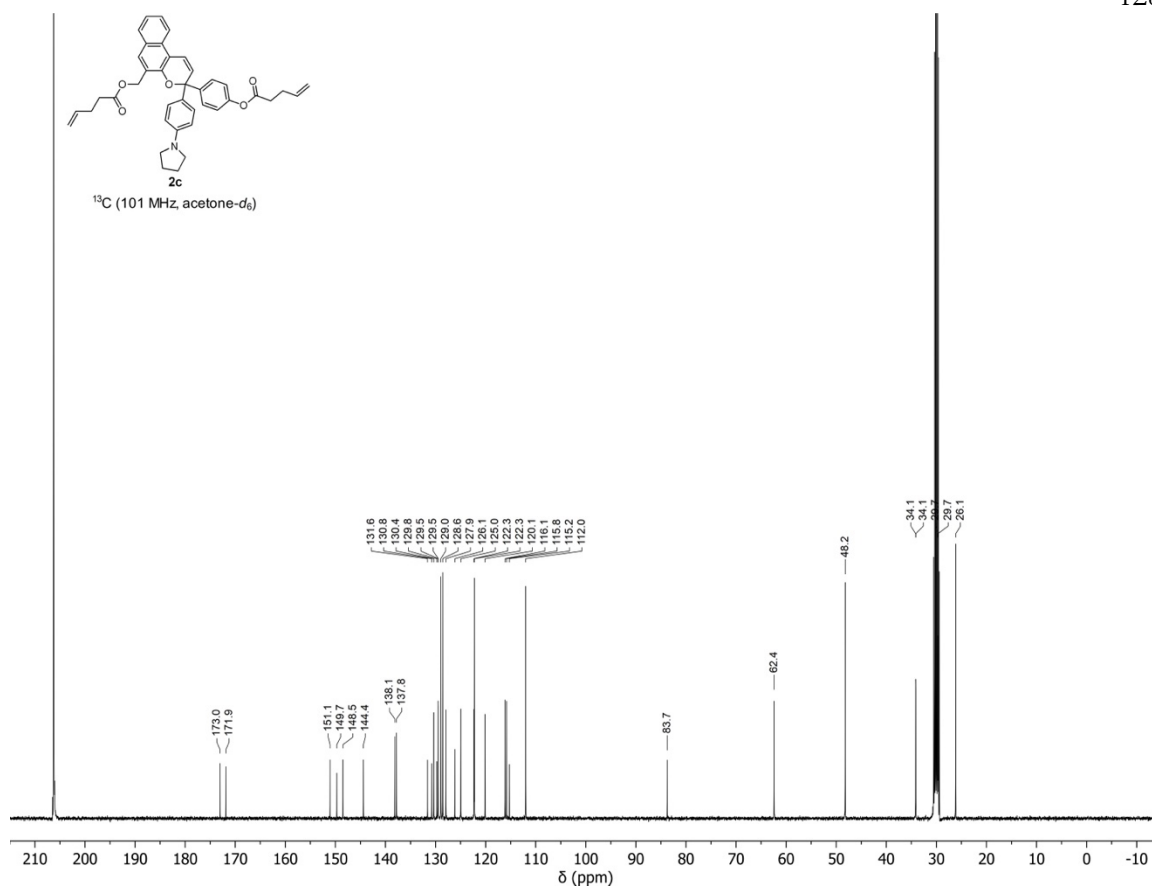






<sup>1</sup>H (400 MHz, acetone-*d*<sub>6</sub>)





*APPENDIX B:*  
*SUPPORTING INFORMATION FOR CHAPTER 3*

### **I. General Experimental Methods**

Reagents from commercial sources were used without further purification unless otherwise stated. Methyl acrylate was passed through a short plug of basic alumina to remove inhibitor immediately prior to use. Copper wire was cleaned prior to use by soaking in 1 M HCl for 5 min, and rinsed consecutively with deionized water, acetone, and DCM and then dried. Dry THF, DCM, and MeCN were obtained from a Pure Process Technology solvent purification system. All reactions were performed under a N<sub>2</sub> atmosphere unless specified otherwise. Silica column chromatography was performed on a Biotage Isolera system using SiliCycle SiliaSep HP flash cartridges.

NMR spectra were recorded using a 400 MHz Bruker Avance III HD with Prodigy Cryoprobe, a 400 MHz Bruker Avance Neo, Varian Inova 500 MHz, or Varian Inova 600 MHz spectrometers. All <sup>1</sup>H NMR spectra are reported in parts per million (ppm) and were measured relative to the signals for residual chloroform (7.26 ppm), 1,2-dichlorobenzene (6.93 ppm), or acetonitrile (1.94 ppm) in deuterated solvent. All <sup>13</sup>C NMR spectra were measured in deuterated solvents and are reported in ppm relative to the signals for CDCl<sub>3</sub> (77.16 ppm) or DCM-*d*<sub>2</sub> (54.00 ppm). Multiplicity and qualifier abbreviations are as follows: s = singlet, d = doublet, t = triplet, q = quartet, dd = doublet of doublets, ddd = doublet of doublet of doublets, td = triplet of doublets, tt = triplet of triplets, p = pentet, m = multiplet, br = broad.

High resolution mass spectra (HRMS) were obtained from an Agilent 6230 series time-of-flight mass spectrometer equipped with an Agilent G1958 Jet Stream electrospray ionization source or a Waters LCT Premier XE time-of-flight mass spectrometer equipped with a direct infusion electrospray ionization source. Matrix-assisted laser desorption ionization (MALDI) mass spectra were obtained from a Bruker Autoflex Speed MALDI-TOF mass spectrometer equipped with a MALDIAnalyzer source and calibrated with Protein Standard I (Bruker). All samples analyzed by MALDI were prepared as solutions in THF with trans-2-[3-(4-tert-Butylphenyl)-2-methyl-2-propenylidene]malononitrile (DCTB) as matrix. Laser power was adjusted to 10% over the ionization threshold with 25% attenuation. Spectra for **DA-PMA** postheat, **Me-PMA**, and **hDA-PMA** pre- and postheat were recorded in linear mode. The

spectrum for **DA-PMA** preheat was recorded in reflectron mode. All expected masses are average masses calculated using Mass Mountaineer software (Chip Cody).

Analytical gel permeation chromatography (GPC) was performed using an Agilent 1260 series pump equipped with two Agilent PLgel MIXED-B columns (7.5 x 300 mm), an Agilent 1200 series diode array detector, a Wyatt 18-angle DAWN HELEOS light scattering detector, and an Optilab rEX differential refractive index detector. The mobile phase was THF at a flow rate of 1 mL/min. Molecular weights and molecular weight distributions were calculated relative to a universal calibration curve of poly(methyl acrylate) standards.

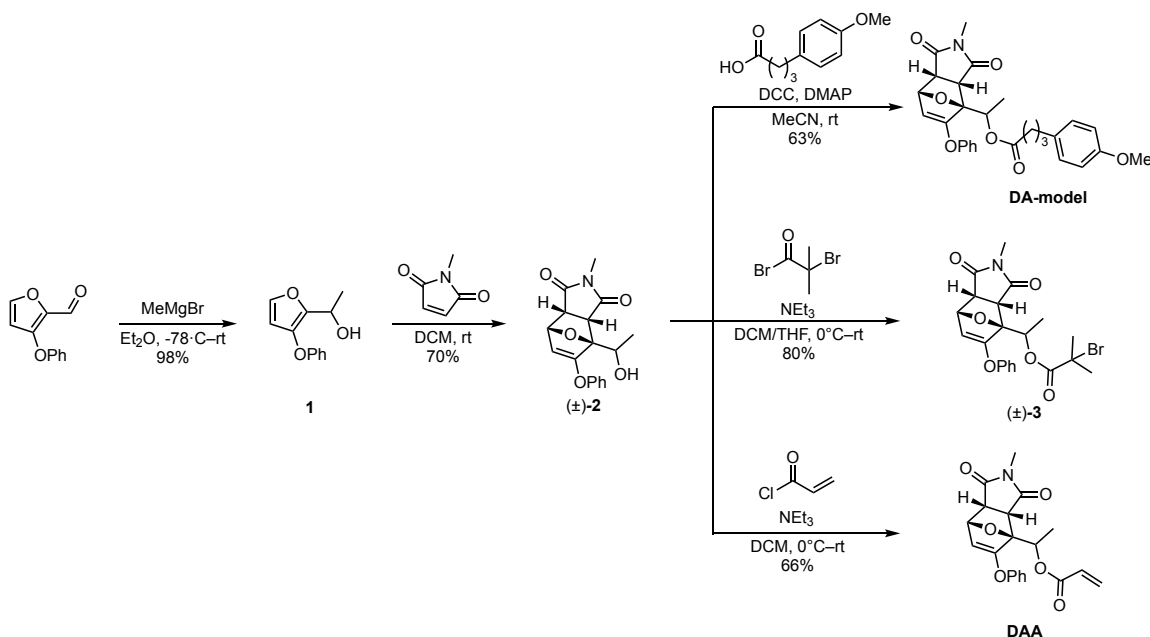
3-phenoxyfurfural<sup>1</sup> and compound **4**<sup>2</sup> were prepared according to the literature.

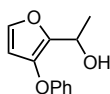
### Safety statement

Heating experiments were performed in Biotage microwave reaction vials sealed with crimped aluminum septum caps. All heating experiments were performed behind a blast shield.

## II. Synthetic Details

**Scheme B.1** Synthesis of model compound **DA-model**, polymerization initiator ( $\pm$ )-**3**, and acrylate monomer **DAA**.





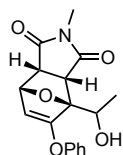
1

**1-(3-phenoxyfuran-2-yl)ethan-1-ol (1).** A flame-dried 250 mL round-bottom flask equipped with a stir bar was charged with 3-phenoxyfurfural<sup>1</sup> (2.040 g, 10.84 mmol) and diethyl ether (54 mL). The solution was cooled to  $-78^{\circ}\text{C}$  with a dry ice/acetone bath before adding methyl magnesium bromide (3 M in diethyl ether, 5.5 mL, 17 mmol) dropwise via syringe. The reaction mixture was warmed to room temperature and allowed to stir for 1 h before quenching by the slow addition of 10%  $\text{NH}_4\text{Cl}$  (100 mL). The mixture was then diluted with diethyl ether (50 mL) and partitioned. The aqueous layer was extracted once with diethyl ether (50 mL), and the combined organic extracts were washed with brine (100 mL). The organic layer was dried over  $\text{MgSO}_4$ , filtered, and concentrated under reduced pressure. The crude product was isolated as an orange oil and used without further purification (2.17 g, 98%). This compound is not stable to thin layer chromatography.

HRMS (ESI,  $m/z$ ): calcd for  $[\text{C}_{12}\text{H}_{12}\text{O}_2]^+$  (M-OH)<sup>+</sup>, 188.0837; found, 187.0752.

$^1\text{H}$  NMR (500 MHz,  $\text{CDCl}_3$ )  $\delta$ : 7.30 (m, 3H), 7.05 (t,  $J = 7.4$  Hz, 1H), 7.00 (d,  $J = 7.5$  Hz, 2H), 6.23 (d,  $J = 2.1$  Hz, 1H), 4.96 (q,  $J = 6.7$  Hz, 1H), 1.94 (s, 1H), 1.56 (d,  $J = 6.7$  Hz, 3H) ppm.

$^{13}\text{C}\{^1\text{H}\}$  NMR (126 MHz,  $\text{CDCl}_3$ )  $\delta$ : 158.2, 144.7, 141.0, 138.5, 129.7, 129.7, 122.7, 122.7, 116.3, 106.7, 61.3, 20.7 ppm.



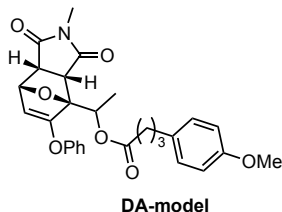
(±)-2

**(3a*S*,4*S*,7*R*,7a*R*)-4-(1-hydroxyethyl)-2-methyl-5-phenoxy-3a,4,7,7a-tetrahydro-1*H*-4,7-epoxyisoindole-1,3(2*H*)-dione ((±)-2).** A 20 mL vial equipped with a stir bar was charged with compound **1** (2.161 g, 10.58 mmol), *N*-methyl maleimide (1.654 g, 14.89 mmol) and DCM (2.9 mL). The solution was allowed to stir at room temperature overnight, then concentrated under reduced pressure. The 4 diastereomeric products were separated by column chromatography (15–100% EtOAc/hexanes) to yield the desired *endo* isomer as a white solid (1.048 g, 70%).  $R_f = 0.20$  (50% EtOAc/hexanes).

HRMS (ESI,  $m/z$ ): calcd for  $[\text{C}_{16}\text{H}_{15}\text{NO}_4]^+$  (M- $\text{H}_2\text{O}$ )<sup>+</sup>, 297.1001; found, 297.0820.

$^1\text{H}$  NMR (400 MHz,  $\text{CDCl}_3$ )  $\delta$ : 7.33 (m, 2H), 7.20 (t,  $J = 7.4$  Hz, 1H), 5.96 (d,  $J = 7.9$  Hz, 2H), 5.18 (dd,  $J = 5.2, 2.0$  Hz, 1H), 4.92 (d,  $J = 2.0$  Hz, 1H), 4.62 (p,  $J = 6.5$  Hz, 1H), 3.86 (d,  $J = 7.7$  Hz, 1H), 3.70 (dd,  $J = 7.7, 5.1$  Hz, 1H), 2.83 (s, 3H), 2.08 (d,  $J = 7.1$  Hz, 1H), 1.54 (d,  $J = 6.6$  Hz, 3H) ppm.

$^{13}\text{C}\{^1\text{H}\}$  NMR (101 MHz,  $\text{CDCl}_3$ )  $\delta$ : 175.3, 174.6, 163.4, 155.0, 130.1, 126.0, 120.2, 100.5, 92.0, 78.4, 64.9, 50.8, 45.9, 24.8, 19.0 ppm.

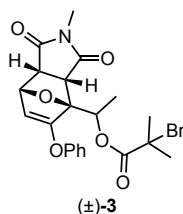


**1-((3*aS*,4*S*,7*R*,7*aR*)-2-methyl-1,3-dioxo-5-phenoxy-1,2,3,3*a*,7,7*a*-hexahydro-4*H*-4,7-epoxyisoindol-4-yl)ethyl 4-(4-methoxyphenyl)butanoate (DA-model).** A flame-dried 25 mL two-neck flask equipped with a stir bar was charged with compound ( $\pm$ )-**3** (48.3 mg, 0.153 mmol), 4-(4-methoxyphenyl)butanoic acid (61.5 mg, 0.317 mmol), DMAP (10.6 mg, 0.087 mmol), and MeCN (4 mL). DCC (60.9 mg, 0.316 mmol) was then added in one portion. The reaction mixture was stirred at room temperature until full conversion was achieved by crude NMR. The crude reaction mixture was then filtered, diluted with DCM (10 mL), and washed consecutively with sat.  $\text{NH}_4\text{Cl}$  (10 mL) and brine (10 mL). The organic layer was then dried with  $\text{MgSO}_4$ , filtered, and concentrated under reduced pressure. The crude product was purified by column chromatography (10–100% EtOAc/hexanes) to yield the title compound as a colorless oil (47.2 mg, 63%).  $R_f = 0.60$  (50% EtOAc/hexanes).

**HRMS (ESI,  $m/z$ ):** calcd for  $[\text{C}_{28}\text{H}_{29}\text{Br}_2\text{NO}_7\text{Na}]^+$  ( $\text{M}+\text{Na}$ ) $^+$ , 514.1842; found, 514.1839.

$^1\text{H}$  NMR (400 MHz,  $\text{CD}_2\text{Cl}_2$ )  $\delta$ : 7.33 (m, 2H), 7.20 (tt,  $J = 7.4, 1.2$  Hz, 1H), 7.10 (m, 2H), 6.96 (m, 2H), 6.82 (m, 2H), 5.76 (q,  $J = 6.5$  Hz, 1H), 5.20 (dd,  $J = 5.1, 2.0$  Hz, 1H), 4.95 (d,  $J = 2.0$  Hz), 3.78 (s, 3H), 3.71 (dd,  $J = 7.7, 5.1$  Hz, 1H), 3.55 (d,  $J = 7.7$  Hz, 1H), 2.82 (s, 3H), 2.63 (t,  $J = 7.5$  Hz, 2H), 2.42 (t,  $J = 7.5$  Hz, 2H), 1.98 (p,  $J = 7.4$  Hz, 2H), 1.56 (d,  $J = 6.6$  Hz, 3H) ppm.

$^{13}\text{C}\{^1\text{H}\}$  NMR (101 MHz,  $\text{CDCl}_3$ )  $\delta$ : 174.9, 173.5, 172.3, 162.7, 157.9, 154.8, 133.4, 130.0, 129.9, 129.5, 126.0, 120.0, 113.8, 100.4, 90.6, 78.3, 66.8, 55.3, 50.7, 46.1, 34.1, 33.6, 26.8, 24.7, 16.0 ppm.

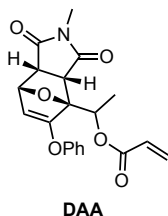


**1-((3a*S*,4*S*,7*R*,7a*R*)-2-methyl-1,3-dioxo-5-phenoxy-1,2,3,3a,7,7a-hexahydro-4*H*-4,7-epoxyisoindol-4-yl)ethyl 2-bromo-2-methylpropanoate ((±)-3).** A flame-dried 5 mL round-bottom flask equipped with a stir bar was charged with adduct (±)-2 (74.6 mg, 0.237 mmol), triethylamine (68  $\mu$ L, 0.49 mmol), DCM (1.2 mL), and THF (1 mL). The mixture was cooled to 0°C in an ice bath before adding bromosioobutyryl bromide (60  $\mu$ L, 0.49 mmol) dropwise. The mixture was warmed to room temperature and allowed to stir until full conversion was achieved by crude NMR, then quenched by the slow addition of sat.  $\text{NH}_4\text{Cl}$  (5 mL). The aqueous layer was extracted with diethyl ether (1 x 10 mL, 2 x 5 mL). The combined organic extracts were then washed with brine (10 mL), dried with  $\text{MgSO}_4$ , and concentrated under reduced pressure. The crude product was purified by column chromatography (10–100% EtOAc/hexanes) to yield the title product as a foamy white solid (88 mg, 80%).  $R_f = 0.14$  (20% EtOAc/hexanes).

HRMS (ESI,  $m/z$ ): calcd for  $[\text{C}_{21}\text{H}_{22}\text{NO}_6\text{Br}]^+$  (M)<sup>+</sup>, 463.0631; found, 463.0651.

$^1\text{H}$  NMR (400 MHz,  $\text{CDCl}_3$ )  $\delta$ : 7.34 (m, 2H), 7.21 (tt,  $J = 7.4, 1.2$  Hz, 1H), 6.97 (m, 2H), 5.78 (q,  $J = 6.6$  Hz, 1H), 5.21 (m, 1H), 4.95 (d,  $J = 2.1$  Hz, 1H), 3.74 (m, 2H), 2.83 (s, 3H), 1.99 (d,  $J = 4.7$  Hz, 6H), 1.60 (d,  $J = 6.6$  Hz, 3H) ppm.

$^{13}\text{C}$  { $^1\text{H}$ } NMR (101 MHz,  $\text{CDCl}_3$ )  $\delta$ : 175.1, 173.6, 170.6, 162.8, 154.9, 130.1, 126.1, 120.1, 100.5, 90.7, 78.4, 68.6, 56.0, 50.8, 46.2, 30.9, 30.8, 24.8, 15.6 ppm.



**1-((3a*S*,4*S*,7*R*,7a*R*)-2-methyl-1,3-dioxo-5-phenoxy-1,2,3,3a,7,7a-hexahydro-4*H*-4,7-epoxyisoindol-4-yl)ethyl acrylate DAA).** A flame-dried 25 mL round-bottom flask equipped with a stir bar was charged with Diels–Alder adduct (±)-3 (91.0 mg, .289 mmol), triethylamine (0.12 mL, 0.86 mmol), and DCM (5.75 mL). The mixture was cooled to 0°C in an ice bath before adding acryloyl chloride (58  $\mu$ L, 0.72 mmol) dropwise. Upon reaching full conversion by crude NMR, the crude mixture was diluted with DCM (25 mL) and

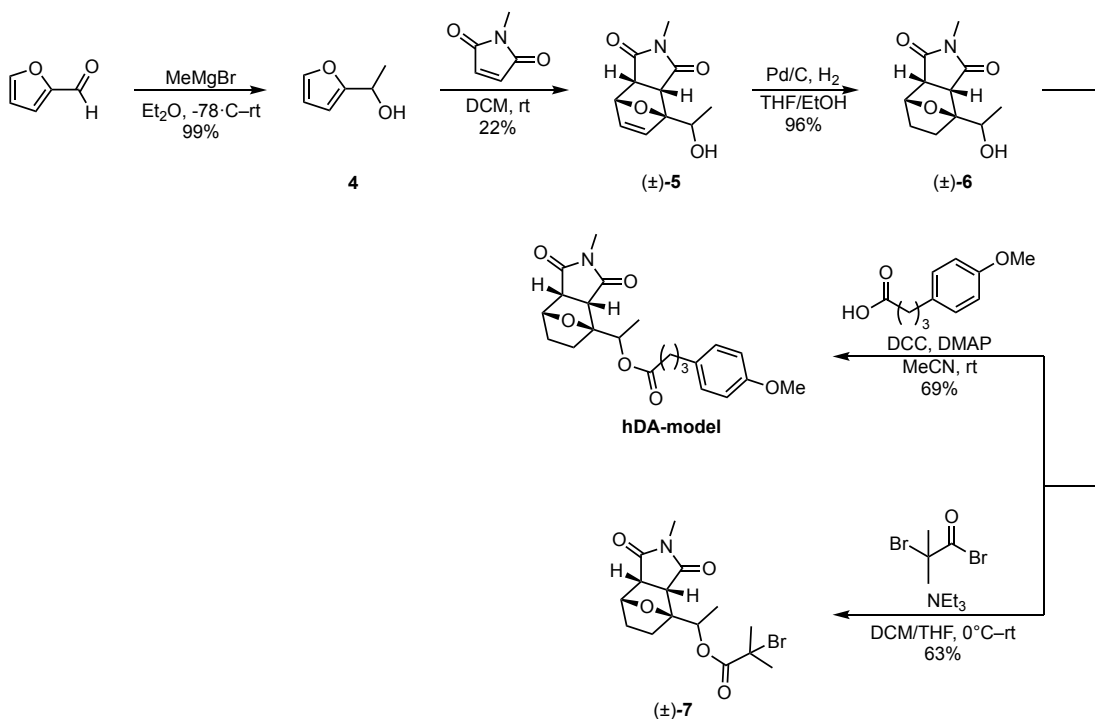
washed consecutively with sat.  $\text{NaHCO}_3$  (2 x 10 mL) and brine (10 mL). The organic layer was then dried with  $\text{MgSO}_4$ , filtered, and concentrated under reduced pressure. The crude product was purified by column chromatography (10–100% EtOAc/hexanes) to yield the title compound as a foamy white solid (69 mg, 66% yield). ( $\pm$ )-**4** was stored and characterized with added MEHQ to prevent autopolymerization.  $R_f = 0.60$  (50% EtOAc/hexanes).

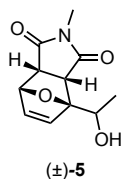
**HRMS (ESI,  $m/z$ ):** calcd for  $[\text{C}_{20}\text{H}_{21}\text{NO}_6]^+$  ( $\text{M}+\text{H}$ ) $^+$ , 370.1291; found, 370.1276.

**$^1\text{H}$  NMR (400 MHz,  $\text{CDCl}_3$ )  $\delta$ :** 7.34 (m, 2H), 7.20 (tt,  $J = 7.4, 1.2$  Hz, 1H), 6.97 (m, 2H), 6.53 (dd,  $J = 17.3, 1.4$  Hz, 1H), 6.23 (dd,  $J = 17.3, 10.4$  Hz, 1H), 5.88 (m, 2H), 5.21 (dd,  $J = 5.1, 2.0$  Hz, 1H), 4.96 (d,  $J = 2.0$  Hz, 1H), 3.74 (m, 1H), 3.60 (d,  $J = 7.7$  Hz, 1H), 2.82 (s, 3H), 1.60 (d,  $J = 6.6$  Hz, 3H) ppm.

**$^{13}\text{C}\{^1\text{H}\}$  NMR (101 MHz,  $\text{CDCl}_3$ )  $\delta$ :** 175.1, 173.6, 165.2, 162.8, 154.9, 131.9, 130.1, 128.2, 126.1, 120.1, 100.6, 90.7, 78.4, 67.1, 50.8, 46.2, 24.8, 16.1 ppm.

**Scheme B.2** Synthesis of model compound **hDA-model** and polymerization initiator ( $\pm$ )-**8**



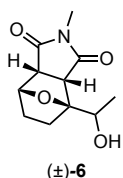


**(3a*S*,4*S*,7*R*,7a*R*)-4-(1-hydroxyethyl)-2-methyl-3a,4,7,7a-tetrahydro-1*H*-4,7-epoxyisoindole-1,3(2*H*)-dione ((±)-5).** A 20 mL vial equipped with a stir bar was charged with **4<sup>2</sup>** (2.399 g, 21.40 mmol), *N*-methyl maleimide (3.303 g, 30.00 mmol), and CHCl<sub>3</sub> (3.0 mL). The solution was allowed to stir at room temperature overnight, then concentrated under reduced pressure. The crude mixture of diastereomers was purified by column chromatography (10-80% EtOAc/hexanes, then 40-100% EtOAc/hexanes) to provide the desired *endo* isomer as a powdery white solid (0.904 g, 19%). *R<sub>f</sub>* = 0.30 (50% EtOAc/hexanes).

HRMS (ESI, *m/z*): calcd for [C<sub>11</sub>H<sub>14</sub>NO<sub>4</sub>]<sup>+</sup> (M+H)<sup>+</sup>, 224.0923; found, 224.09065.

<sup>1</sup>H NMR (500 MHz, CDCl<sub>3</sub>) δ: 6.46 (dd, *J* = 5.8, 1.7 Hz, 1H), 6.35 (d, *J* = 5.7 Hz, 1H), 5.31 (dd, *J* = 5.5, 1.7 Hz, 1H), 4.30 (d, *J* = 12.5 Hz), 4.19 (dd, *J* = 12.4, 4.6 Hz, 1H), 3.67 (dd, *J* = 7.7, 5.5 Hz, 1H), 3.44 (d, *J* = 7.6 Hz, 1H), 2.84 (s, 3H), 2.05 (s, 1H) ppm.

<sup>13</sup>C {<sup>1</sup>H} NMR (101 MHz, CDCl<sub>3</sub>) δ: 175.4, 175.0, 135.8, 134.9, 92.0, 79.6, 61.8, 48.4, 46.6, 24.8 ppm.

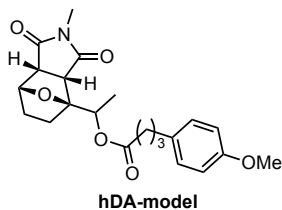


**(3a*S*,4*S*,7*R*,7a*R*)-4-(1-hydroxyethyl)-2-methylhexahydro-1*H*-4,7-epoxyisoindole-1,3(2*H*)-dione ((±)-6).** A flame-dried 25 mL round-bottom flask equipped with a stir bar was charged with Pd/C (10% by weight, 27.5 mg) and a solution of adduct (±)-5 (255.5 mg, 1.145 mmol) in ethanol (11 mL) and THF (3 mL). The mixture was stirred under a H<sub>2</sub> atmosphere (by balloon) until full conversion was achieved by crude NMR. The mixture was then filtered over Celite to remove residual Pd/C and concentrated under reduced pressure. The crude product was purified further by column chromatography (15-100% EtOAc/hexanes) to provide the title compound as a powdery white solid (242.1 mg, 96%). *R<sub>f</sub>* = 0.60 (50% EtOAc/hexanes).

HRMS (ESI,  $m/z$ ): calcd for  $[C_{11}H_{13}NO_3]^+$  (M-H<sub>2</sub>O)<sup>+</sup>, 207.0895; found, 207.0988.

<sup>1</sup>H NMR (500 MHz, CDCl<sub>3</sub>)  $\delta$ : 4.85 (t,  $J$  = 5.4 Hz, 1H), 4.19 (dt,  $J$  = 10.5, 5.5 Hz, 1H), 3.57 (dd,  $J$  = 9.7, 6.1 Hz), 3.28 (d,  $J$  = 9.6 Hz, 1H), 2.99 (s, 3H), 2.26 (d,  $J$  = 4.4 Hz, 1H), 1.91 (m, 2H), 1.50 (m, 1H), 1.41 (d,  $J$  = 5.5 Hz) ppm.

<sup>13</sup>C{<sup>1</sup>H} NMR (125 MHz, CDCl<sub>3</sub>)  $\delta$ : 175.8, 175.6, 92.2, 77.5, 69.0, 53.3, 52.5, 27.2, 25.2, 25.0, 18.0 ppm.

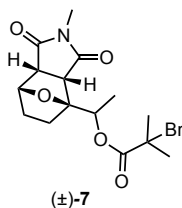


**1-((3*a*S,4*S*,7*R*,7*a*R)-2-methyl-1,3-dioxooctahydro-4*H*-4,7-epoxyisoindol-4-yl)ethyl 4-(4-methoxyphenyl)butanoate (hDA-model).** A flame-dried 10 mL round-bottom flask equipped with a stir bar was charged with ( $\pm$ )-**6** (49.8 mg, 0.221 mmol), 4-(4-methoxyphenyl)butanoic acid (92.6 mg, 0.477 mmol), DMAP (18.6 mg, 0.152 mmol), and MeCN (4.4 mL). DCC (91.1 mg, 0.472 mmol) was then added in one portion. The reaction mixture was stirred at room temperature until full conversion was achieved by crude NMR. The crude reaction mixture was then filtered, diluted with dichloromethane (12 mL) and washed consecutively with sat. NH<sub>4</sub>Cl (2 x 6 mL) and brine (6 mL). The organic layer was dried with MgSO<sub>4</sub> and concentrated under reduced pressure, then purified by column chromatography (10–100% EtOAc/hexanes) to afford the title product as a waxy yellow solid (61.7 mg, 69%).  $R_f$  = 0.14 (20% EtOAc/hexanes).

HRMS (ESI,  $m/z$ ): calcd for  $[C_{22}H_{27}NO_6Na]^+$  (M+Na)<sup>+</sup>, 424.1736; found, 424.1729

<sup>1</sup>H NMR (400 MHz, CDCl<sub>3</sub>)  $\delta$ : 7.09, (m, 2H), 6.92 (m, 2H), 5.42 (q,  $J$  = 6.6 Hz, 1H), 4.84 (t,  $J$  = 5.3 Hz, 1H), 3.78 (s, 3H), 3.57 (ddd,  $J$  = 9.9, 6.1, 1.4 Hz, 1H), 3.27 (dd,  $J$  = 9.7, 1.8 Hz, 1H), 2.98 (s, 3H), 2.60 (dd,  $J$  = 8.3, 6.8 Hz, 2H), 2.36 (td,  $J$  = 7.3, 1.6 Hz, 2H), 1.91 (m, 4H), 1.58 (m, 4H), 1.45 (d,  $J$  = 6.6 Hz, 3H) ppm

<sup>13</sup>C{<sup>1</sup>H} NMR (101 MHz, CDCl<sub>3</sub>)  $\delta$ : 175.3, 175.1, 172.7, 158.0, 133.6, 129.5, 113.9, 90.4, 69.5, 55.4, 53.1, 52.7, 34.2, 33.8, 26.9, 26.3, 25.0, 16.0 ppm.



**1-((3a*S*,4*S*,7*R*,7a*R*)-2-methyl-1,3-dioxooctahydro-4*H*-4,7-epoxyisoindol-4-yl)ethyl 2-bromo-2-methylpropanoate ((±)-7).** A flame-dried 5 mL round-bottom flask equipped with a stir bar was charged with adduct (±)-5 (135.1 mg, 0.600 mmol), triethylamine (0.68 mL, 4.9 mmol), and THF (2.5 mL). The mixture was cooled to 0°C in an ice bath before adding bromoisobutyryl bromide (0.60 mL, 4.9 mmol) dropwise. The mixture was warmed to room temperature and allowed to stir until full conversion was achieved by crude NMR, then quenched by the slow addition of sat. NH<sub>4</sub>Cl (10 mL). The aqueous layer was extracted with diethyl ether (1 x 10 mL, 2 x 5 mL). The combined organic extracts were then washed with brine (10 mL), dried with MgSO<sub>4</sub>, and concentrated under reduced pressure. The crude product was purified by column chromatography (10–80% EtOAc/hexanes) to yield the title product as a waxy brown solid (140 mg, 63%). *R<sub>f</sub>* = 0.14 (20% EtOAc/hexanes).

**HRMS (ESI, *m/z*):** calcd for [C<sub>15</sub>H<sub>21</sub>BrNO<sub>5</sub>]<sup>+</sup> (M+H)<sup>+</sup>, 374.0603; found, 374.0573.

**<sup>1</sup>H NMR (400 MHz, CDCl<sub>3</sub>) δ:** 5.43 (q, *J* = 6.7 Hz, 1H), 4.85 (m, 1H), 3.58 (ddd, *J* = 9.8, 6.1, 2.1 Hz), 3.33 (dd, *J* = 9.8, 1.7 Hz), 2.98 (s, 3H), 1.95 (d, *J* = 4.7 Hz, 6H), 1.91 (m, 2H), 1.61 (m, 2H), 1.50 (d, *J* = 6.6 Hz) ppm.

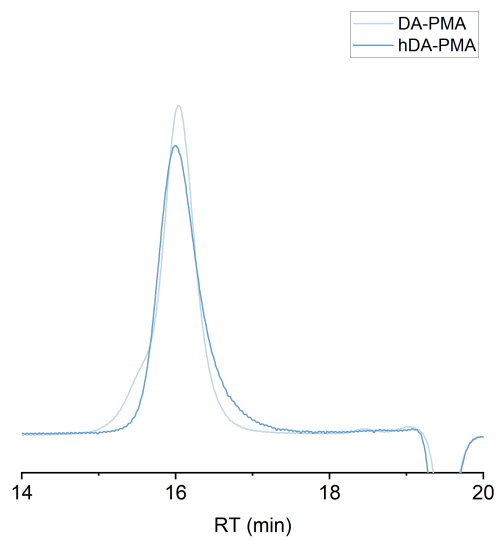
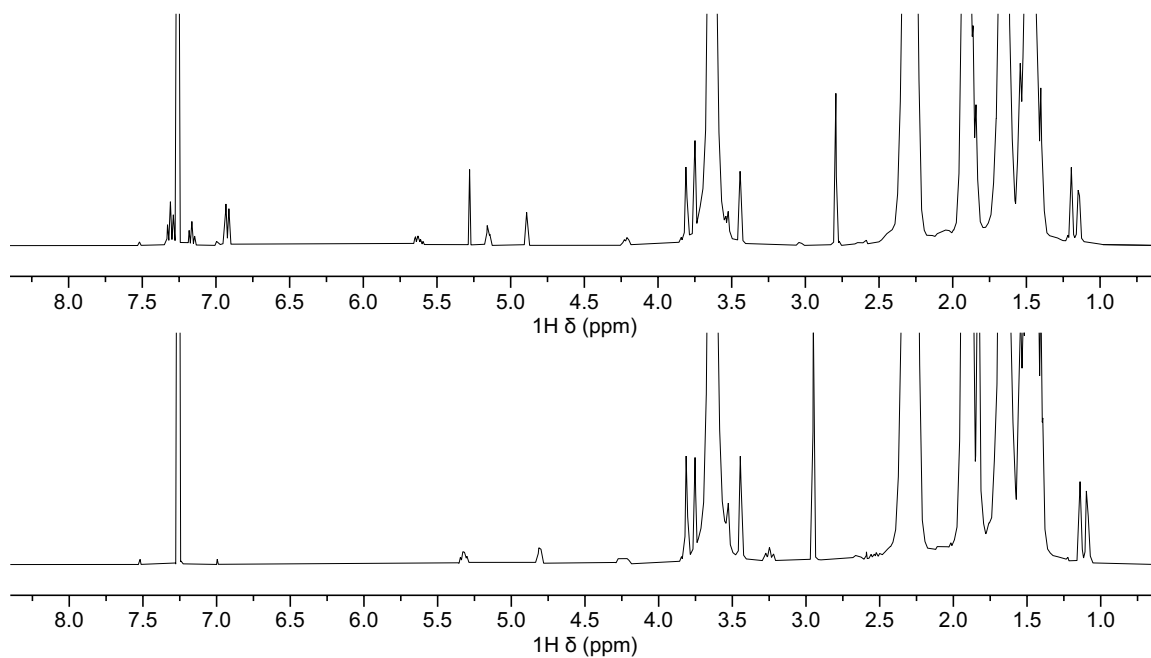
**<sup>13</sup>C{<sup>1</sup>H} NMR (101 MHz, CDCl<sub>3</sub>) δ:** 175.3, 175.0, 170.8, 90.4, 71.4, 56.1, 53.1, 52.6, 30.9, 30.8, 26.9, 26.3, 25.0, 15.5 ppm.

### General procedure for the synthesis of α-masked poly(methylacrylate)s DA-PMA and hDA-PMA

A 25 mL Schlenk flask equipped with a stir bar was charged with initiator (1 equiv), copper wire (1 cm length, 20 gauge), methyl acrylate (180 equiv.), and DMSO (equal volume to methyl acrylate). The flask was sealed and the contents deoxygenated with five freeze-pump-thaw cycles. The flask was then backfilled with nitrogen and warmed to rt before adding Me<sub>6</sub>TREN (2 equiv) via microsyringe. After stirring at rt for 2.5 h, the flask was opened to air and the contents diluted with DCM. The polymer solution was then precipitated into cold methanol (x3) and dried under vacuum. Molecular weight characterization data for the polymers in this study are reported below in Table B.1.

**Table B.1** Molecular weight characterization of **DA-PMA** and **hDA-PMA**

	$M_n$ , NMR (kDa)	$M_n$ , GPC (kDa)	$\bar{D}$
<b>DA-PMA</b>	16.6	16.1	1.20
<b>hDA-PMA</b>	16.6	14.8	1.16

**Figure B.1** GPC chromatogram (refractive index response) for poly(methylacrylate)s **DA-PMA** and **hDA-PMA**.**Figure B.2**  $^1\text{H}$  NMR spectra (400 MHz,  $\text{CDCl}_3$ ) of  $\alpha$ -masked polymers **DA-PMA** (upper) and **hDA-PMA** (lower).

### Synthesis of Me-PMA by Fischer esterification of thermally unmasked DA-PMA

A 4 mL vial equipped with a stir bar was charged with unmasked (post-heat) **DA-PMA** (98.3 mg, 5.70  $\mu\text{mol}$ ), anhydrous methanol (0.25 mL, 6.2 mmol), sulfuric acid (3 drops), and THF (0.75 mL). After stirring at room temperature overnight, the contents were concentrated. The polymer solution was then precipitated into cold methanol (x3) and dried under vacuum to afford **Me-PMA** as a fluffy white solid (59 mg, 60%).  $M_{n, \text{NMR}} = 17.6 \text{ kDa}$ ,  $M_{n, \text{GPC}} = 16.1 \text{ kDa}$ ,  $\text{Đ} = 1.20$

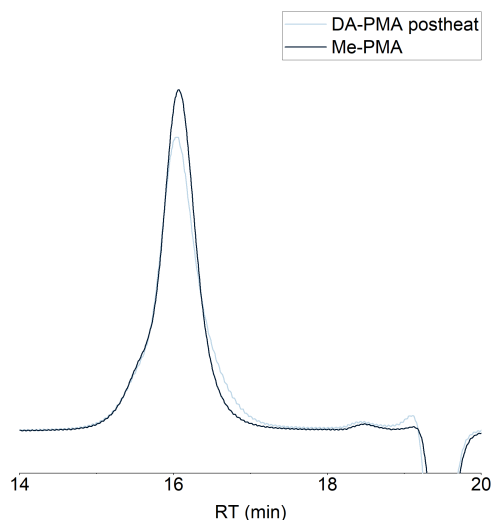


**Figure B.3** GPC chromatograms (refractive index response) for **DA-PMA** after heating and after Fischer esterification to **Me-PMA**.

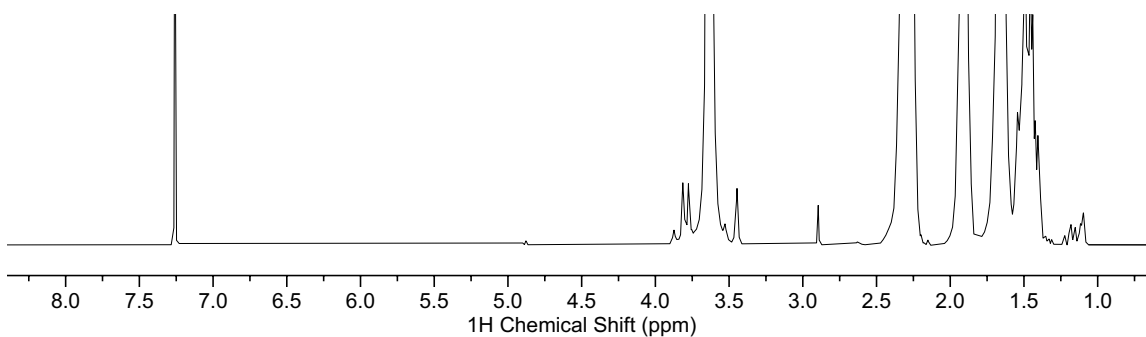


**Figure B.4**  $^1\text{H}$  NMR spectrum (400 MHz,  $\text{CDCl}_3$ ) of **Me-PMA**.

### Synthesis of poly(DAA-co-PMA)

A 10 mL Schlenk flask equipped with a stir bar was charged with ethyl  $\alpha$ -bromoisobutyrate (6.3  $\mu\text{L}$ , 0.043 mmol), copper wire (1 cm length, 20 gauge), **DAA** (144.3 mg, 0.3907 mmol),

methyl acrylate (0.67 mL, 7.4 mmol), and DMSO (equal volume to methyl acrylate). The flask was sealed and the contents deoxygenated with four freeze-pump-thaw cycles. The flask was then backfilled with nitrogen and warmed to rt before adding Me<sub>6</sub>TREN (23.5 μL, 0.0879 mmol) via microsyringe. After stirring at room temperature for 2.5 h, the flask was opened to air and the contents diluted with DCM. The polymer solution was then precipitated into cold methanol (x3) and dried under vacuum to afford the polymer as a fluffy solid (406 mg, 52%).  $M_{n, \text{NMR}} = 17.9 \text{ kDa}$ ,  $M_{n, \text{GPC}} = 19.4 \text{ kDa}$ ,  $\bar{D} = 1.83$

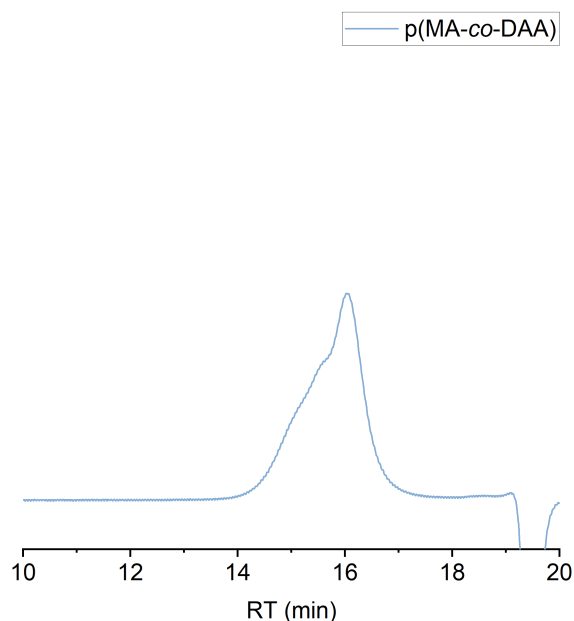


**Figure B.5** GPC trace (refractive index response) for copolymer **p(MA-co-DAA)**.

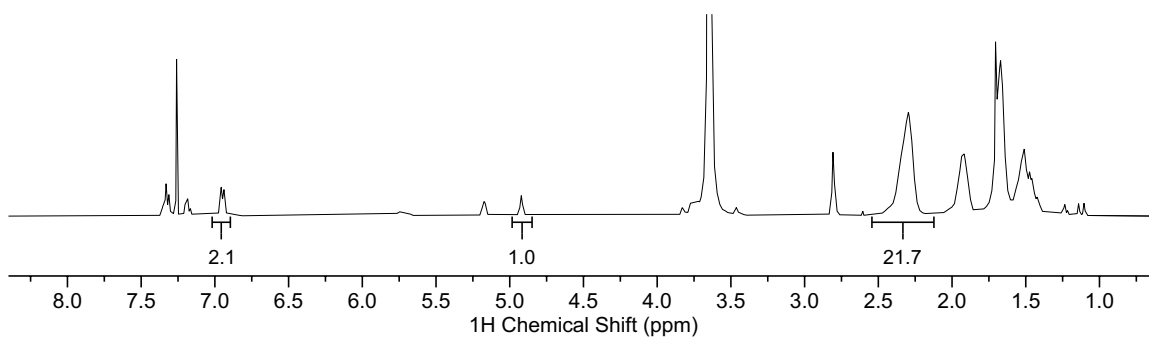


**Figure B.6** <sup>1</sup>H NMR spectrum (400 MHz, CDCl<sub>3</sub>) of **p(MA-co-DAA)**. Integral ratios indicate monomer incorporation of 22:1 MA:DAA.

### III. General Procedure for Thermal Unmasking of Model Latent Furfuryl Esters

Microwave vials equipped with stir bars were charged with a solution of **FM-model** or **ctrl-model** in MeCN-*d*<sub>3</sub>/H<sub>2</sub>O (9:1 v/v, 10 mM, 0.5 mL/vial) containing 10 mM trimethoxybenzene as an internal standard. Vials were sealed using crimped caps, then lowered into a preheated bath and stirred at 100°C. One-vial aliquots were cooled to room temperature and analyzed by <sup>1</sup>H NMR at regular time intervals.

### IV. Thermal Unmasking of Polymer-bound Latent Furfuryl Esters

**General procedure:** A microwave vial equipped with a stir bar was charged with a solution of polymer in MeCN/H<sub>2</sub>O (9:1 v/v, 50 mg/mL). The vial was sealed using a crimped cap, then lowered into a preheated bath and stirred at 100°C for 24 h. The solution was then cooled to room temperature and dried under vacuum before redissolving in DCM and precipitating into cold methanol.

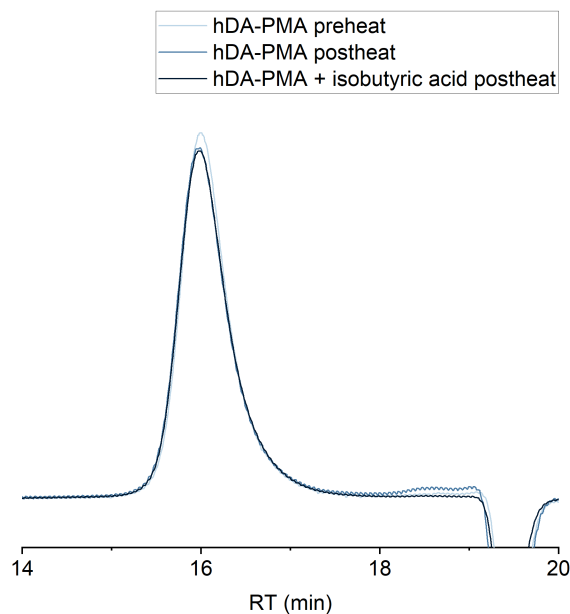


**Figure B.7** GPC chromatograms (RI response) of **hDA-PMA** before and after heating (with or without added acid) show minimal changes in molecular weight distribution.

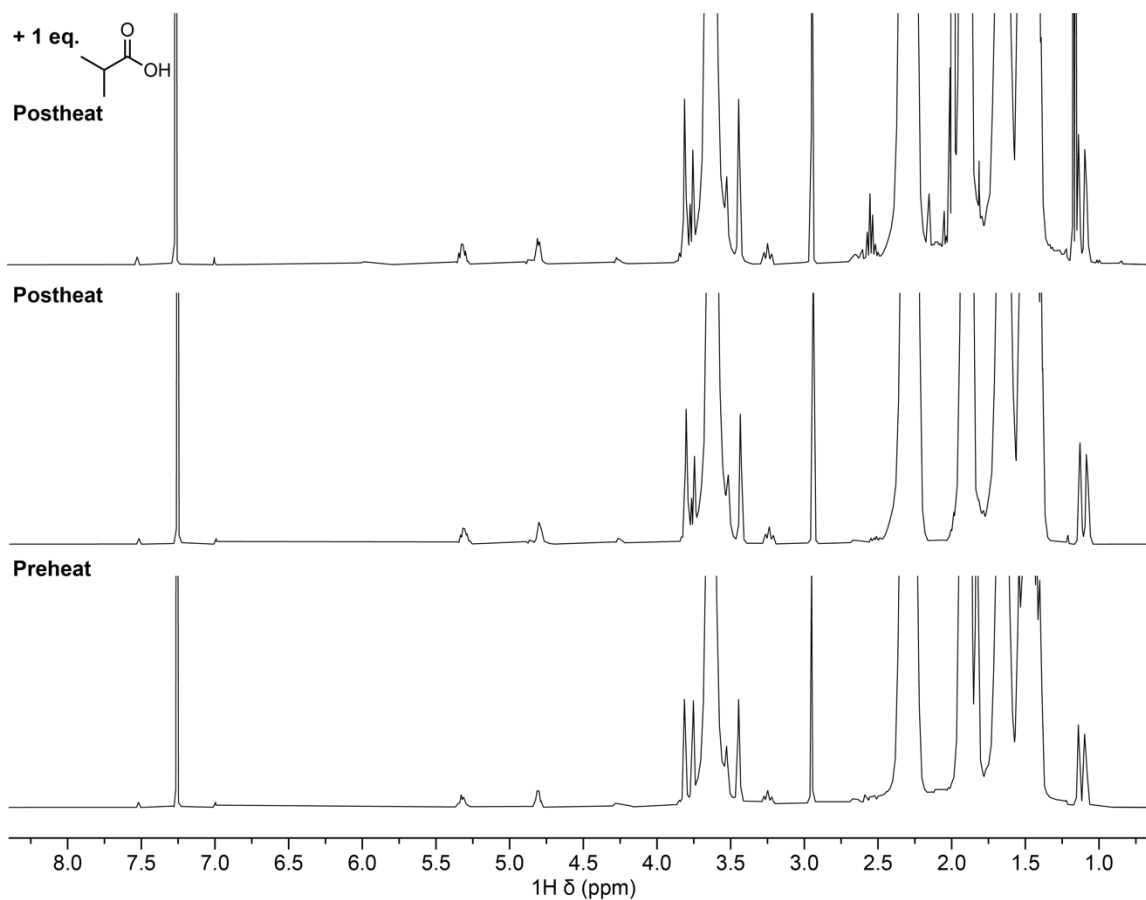


**Figure B.8** Partial  $^1\text{H}$  NMR spectra (400 MHz,  $\text{CDCl}_3$ ) of control polymer **hDA-PMA** before and after heating at  $100^\circ\text{C}$  for 24 h, either with or without 1 eq. isobutyric acid.

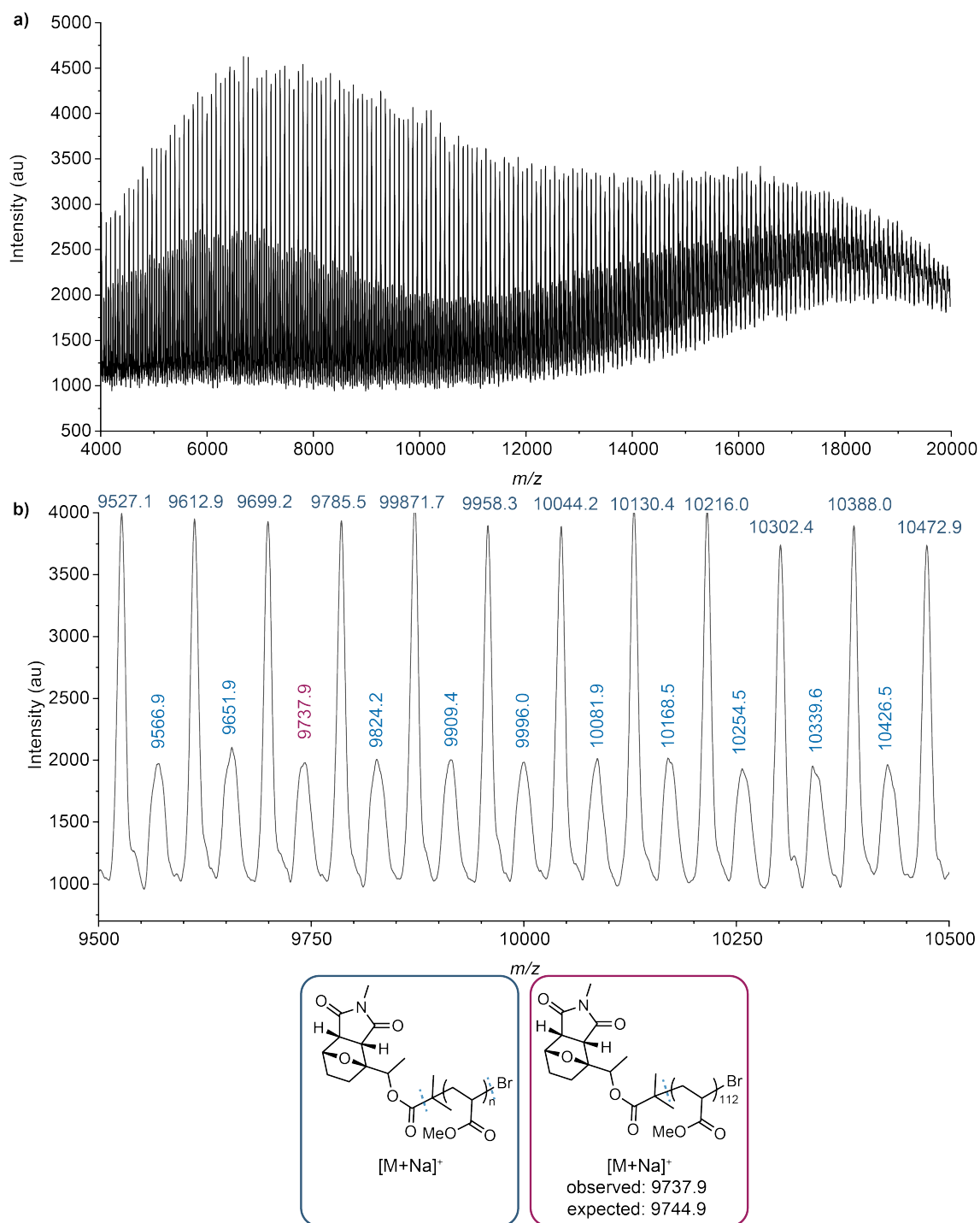


**Figure B.9** Complete (a) and close-up (b) MALDI-TOF mass spectra of pristine hDA-PMA.

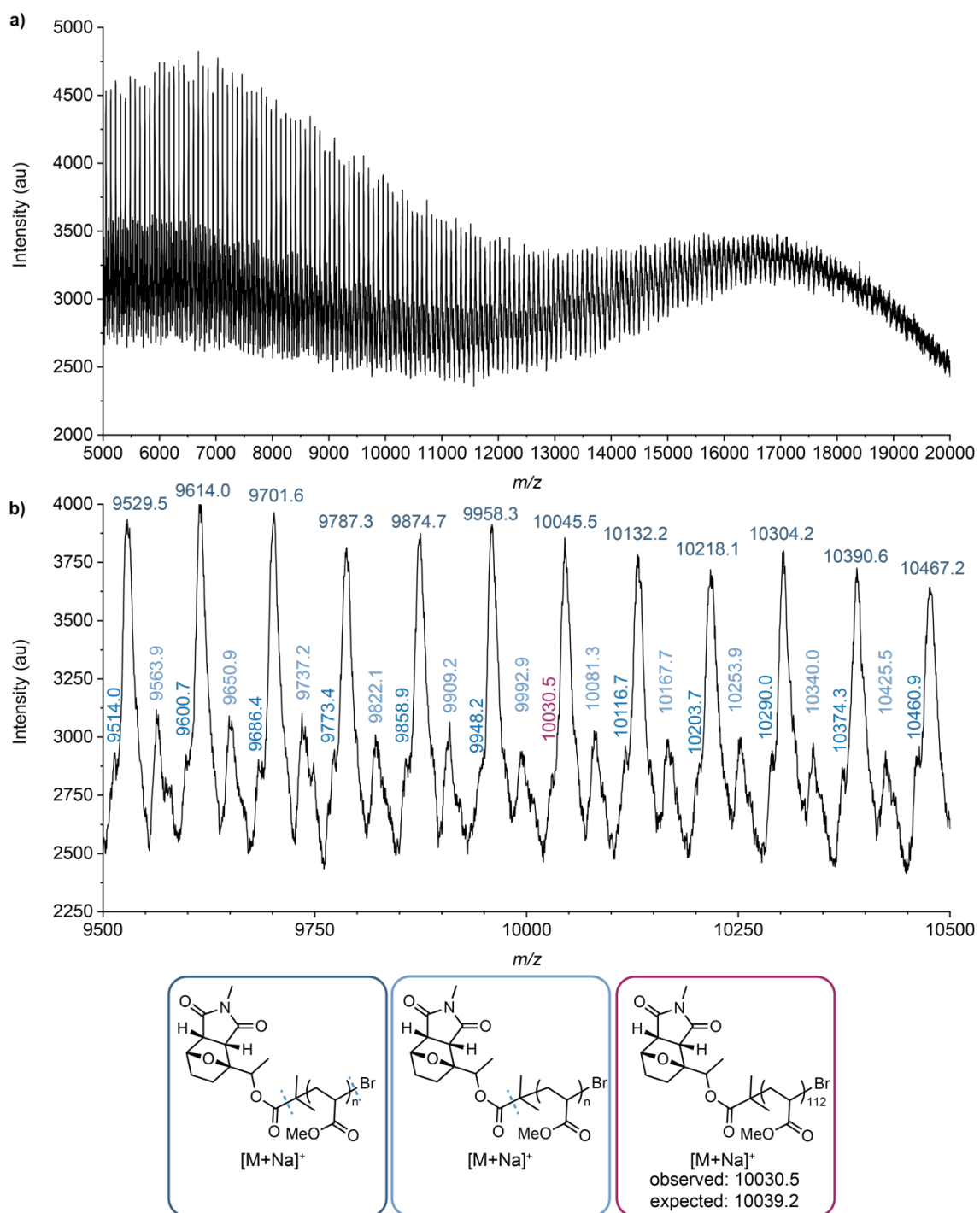
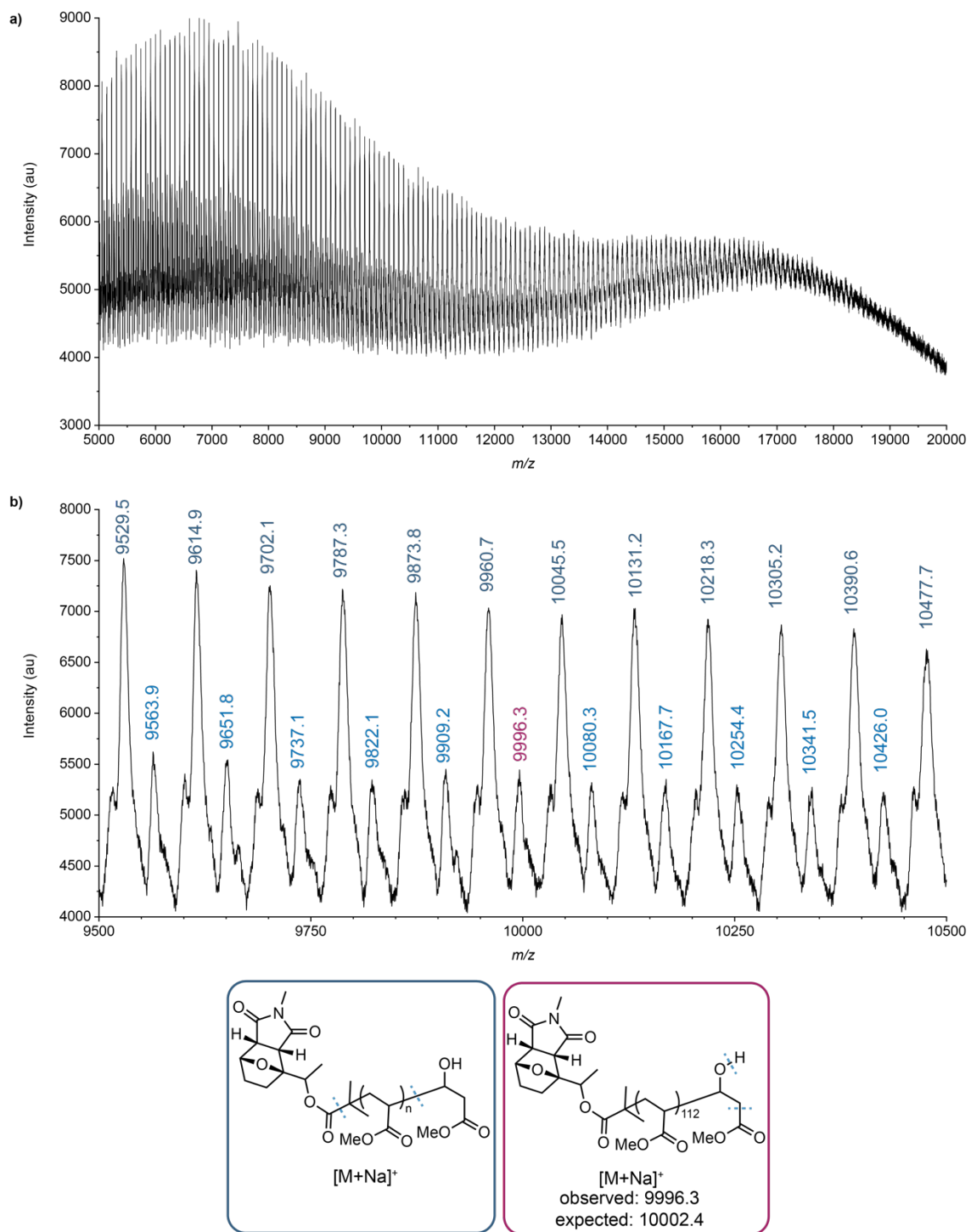


Figure B.10 Complete (a) and close-up (b) MALDI-TOF mass spectra of hDA-PMA after heating.



**Figure B.11** Complete (a) and close-up (b) MALDI-TOF mass spectra of **hDA-PMA** after heating in the presence of 1 equivalent isobutyric acid.

## V. References

1. Hu, X.; Zeng, T.; Husic, C. C.; Robb, M. J. Mechanically Triggered Release of Functionally Diverse Molecular Payloads from Masked 2-Furylcarbinol Derivatives. *ACS Cent. Sci.* **2021**, *7*, 1216–1224.
2. Nunes, J. P. M.; Veiros, L. F.; Vaz, P. D.; Afonso, C. A. M.; Caddick, S. Asymmetric synthesis of trans-4,5-dioxygenated cyclopentenone derivatives by organocatalyzed rearrangement of pyranones and enzymatic dynamic kinetic resolution. *Tetrahedron* **2011**, *67*, 2779–2787.

VI.  $^1\text{H}$  and  $^{13}\text{C}$  NMR Spectra